



THE UNIVERSITY OF HULL

An investigation of the regulatory mechanisms of cellular
homeostasis and haemostasis initiated by tissue factor

Thesis submitted to the University of Hull towards the degree of
Doctor of Philosophy

by

Mohammad Abdullah Mohammad

November 2020

Abstract

The signalling arising from tissue factor (TF) has been associated with cellular homeostasis as well as haemostasis and, is particularly pertinent in carcinogenesis and cancer progression. The formation of the TF-FVIIa complex is known to activate protease activated receptor 2 (PAR2) and initiates multiple signalling pathways which can determine the fate of the cell. Among these mechanisms PI3K-Akt is known as a major promoter of cell survival and proliferation. The regulation of Akt is mediated by PTEN, a tumour suppressor that negatively regulates the PI3K-Akt pathway resulting in the loss of downstream proliferative and pro-survival signalling. In this study, seven tumour cell lines from different tissues were activated with PAR2-activating peptide (SLIGKV), or incubated with a range of concentrations of rec-TF (65-1300 pg/ml). The outcome on the phosphorylation state and the lipid-phosphatase activity of PTEN, and also Akt activity was assessed. Incubation of cells with rec-TF (65 pg/ml) resulted in de-phosphorylation of PTEN in all the cell lines tested which was concurrent with increased PTEN activity and reduced Akt activity. Moreover, activation of PAR2 reduced PTEN phosphorylation and Akt activity in the majority, but not all of the cell lines tested. However, prolonged exposure of cells to rec-TF over 5 days, resulted in decreased PTEN antigen levels together with enhanced Akt activity and increased cell proliferation in the cell lines tested. To explore the mechanism of regulation of PTEN by PAR2, the association of membrane-associated guanylate kinase-with inverted configuration (MAGI)1-3 proteins with PTEN was assessed by the proximity ligation assay (PLA) and co-IP. The interaction of PTEN with all three MAGI proteins was reduced following PAR2 activation and explains the alterations in PTEN activity and stability. The structure of MAGI proteins contains a guanylate kinase-like (GK) domain, two WW domains and six PDZ domains. This structure allows MAGI to restrain proteins at the cell junction, regulating the activity of the proteins and stabilising cell-cell contacts. In the second part of the study, analysis of a motif within the cytoplasmic domain of

TF (ENSPL) indicated the possible interaction with MAGI proteins. PLA and co-IP studies showed that TF may be restrained at the tight junctions through interaction with MAGI-1. Interestingly the activation of PAR2 transiently dissociated TF from MAGI-1. By expressing the individual PDZ domains as tagged-hybrid proteins, the first PDZ domain was identified to be capable of binding TF and competing with MAGI-1. The expression of this hybrid protein also resulted in augmented TF activity, similar to that following PAR2 activation. Analysis of the interactions of the N-terminal region of MAGI-1 with or without PDZ1 further confirmed the role of PDZ1 in the constraint of TF and regulation of its procoagulant activity. In conclusion, this study has demonstrated that PAR2 activation promotes increased PTEN activity in the short term, allowing for the elimination of severely injured cells. However, prolonged exposure TF reduces the cellular PTEN antigen levels allowing aberrant cell survival and proliferation, through increased Akt activity. This study also demonstrated the interaction of TF with the PDZ1 domain of MAGI-1, suggesting a mechanism for restraining cell-surface TF from contact with the surrounding fluid, and may explain the regulation of both coagulation and signalling mechanisms.

Acknowledgment

First of all, I would like to thank Dr. Camille Ettelaie for welcoming me in her lab and the stimulating environment she created for everyone. I thank her for the time, supervision, guidance, patience and continuous support she provided me during the course of my PhD, I'm forever grateful. Also, I would like to thank my second supervisor Professor. John Greenman for his support, advice, help and being there for me during harsh times. Again, I would like to thank Professor. Anthony Maraveyas and Dr. Mary Collier for sharing their knowledge and input in this research. The ultimate gratitude goes to my Mother, Father, Nada, Najla, Nahed, Ahmed, Shahad for their endless love, support, inspiration and encouragement. They have always been the largest driving force in my life. I give thanks to the Ministry of Higher Education and the Saudi Cultural Bureau in London for financially supporting my education and this research. My PhD would not be possible if it was not for the help I received specially from Sophie, also from Yahya, Ali and other lab members.

Publication and presentation

Papers

Mohammad, M. Maraveyas, A. Greenman, J and Ettelaie, C. (2020) Activation of PAR2 by tissue factor induces the release of the PTEN from MAGI proteins and regulates PTEN and Akt activities. *Scientific Reports* (10) 20908.

Ethab, A. Mohammad, M. Madkhali, Y. Featherby, S. Maraveyas, A. Greenman, J. and Ettelaie, C. (2020) Accumulation of tissue factor in endothelial cells promotes cellular apoptosis through over-activation of Src1 and involves β 1-integrin signalling. *Apoptosis* 25 (1), 29-41.

Mohammad, M. Featherby, S. Collier, M. Maraveyas, A. Greenman, J and Ettelaie, C. Tissue factor is restrained to the cell junction by interacting with the first PDZ domain of MAGI1 and is released following PAR2 activation (article under review).

Poster presentations

Mohammad, M. Greenman, J. Maraveyas, A and Ettelaie, C (2017) Tissue factor attenuates PI3K/AKT pathway through upregulation of PTEN (poster). Presented at the British Society for Haemostasis and Thrombosis (BSHT) Annual Scientific Meeting. University of Warwick, UK.

Mohammad, M. Greenman, J. Maraveyas, A and Ettelaie, C (2018) Tissue factor attenuates PI3K/AKT pathway through upregulation of PTEN (poster). Presented at the North of England Cell Biology Forum, University of Huddersfield, UK.

Mohammad, M. Greenman, J. Maraveyas, A and Ettelaie, C (2018) Long term exposure to tissue factor induce cell proliferation by lowering PTEN protein levels (poster). Presented at the BSHT Annual Scientific Meeting. University of Warwick, UK.

Mohammad, M. Featherby, S. Mary, C. Maraveyas, A. Greenman, J. and Ettelaie, C The cellular localisation of tissue factor is constrained by MAGI-1 and is released by PAR2 activation (poster). Presented at the BSHT Annual Scientific Meeting. University of Warwick, UK.

Mohammad, M. Maraveyas A, Greenman J, Ettelaie C (2019) Long term exposure to tissue factor induce cell proliferation by lowering PTEN protein levels (poster). Presented at the congress of the international society on thrombosis and haemostasis (ISTH). Melbourne, Australia.

Mohammad, M. Featherby, S. Maraveyas A, Greenman J, Ettelaie C (2019) The cellular location of tissue factor is constrained by MAGI-1 and is released by PAR2 activation (poster). Presented at the ISTH. Melbourne, Australia.

Mohammad, M. Featherby, S. Maraveyas A, Greenman J, Ettelaie (2019) Tissue factor is constrained by interaction with the PDZ-1 domain of MAGI-1 protein (poster). Presented at the European Congress on Thrombosis and Haemostasis (ECTH). Glasgow, UK.

To My Family,

Thank you

Table of content

Abstract	ii
Acknowledgment	iv
Publication and presentation	v
Table of content	viii
Table of figures	xiv
Table of tables.....	xvii
List of Symbols and Abbreviations.....	xviii
Chapter 1 General introduction.....	1
1.1 Introduction	2
1.1.2 Tissue factor	3
1.1.3 The role of TF in the initiation of the coagulation cascade.....	3
1.1.4 The structure of TF protein	6
1.1.5 The role of TF as a signalling receptor	6
1.1.6 Protease-activated receptors (PARs).....	8
1.1.7 Mechanisms and outcomes of TF signalling in cancer	11
1.2 PTEN	12
1.2.1 Structure of PTEN protein.....	12
1.2.2 Association of PTEN with the phospholipid membrane.....	14
1.2.3 PTEN activation	16
1.2.4 The association of PTEN with the PI3K-Akt pathway	18
1.2.4.1 The PI3K-Akt pathway	18
1.2.5 The regulation of PTEN activity	21
1.3 Membrane-associated guanylate kinase with inverted orientation (MAGI).....	21
1.3.1 The role of MAGIs in the regulation of PTEN	23
1.3.1.1 MAGI-1	23

1.3.1.2 MAGI-2.....	24
1.3.1.3 MAGI-3.....	24
1.4 Aims	25
Chapter 2 Materials and methods.....	27
2.1 Materials.....	28
2.2 Methods.....	33
2.2.1 Cell culture	33
2.2.2 Harvesting, subculturing and counting of cells	33
2.2.3 Cryopreservation and cell recovery.....	34
2.2.4 Activation of cells with rec-TF or PAR2-AP	34
2.3 Molecular biology techniques	35
2.3.1 SDS-polyacrylamide gel electrophoresis (SDS-PAGE)	35
2.3.2 Western blot analysis	36
2.3.3 Examination of cell proliferation using the crystal violet assay	38
2.3.4 Estimation of protein concentration using the Bradford assay	38
2.3.5 <i>In situ</i> examination of protein interaction using the proximity ligation assay (PLA)	39
2.3.6 Examination of protein interaction by co-immunoprecipitation	42
2.4 Bacterial cell culture and plasmid isolation	43
2.4.1 Agar selection plates preparation	43
2.4.2 Bacterial cell culture.....	44
2.4.3 Cryopreservation of bacterial cell	44
2.4.4 Isolation of plasmid DNA using the Monarch plasmid Miniprep kit	44
2.4.5 Isolation of plasmid DNA using the Wizard plus Midiprep kit.....	45
2.4.6 Examination of the plasmid DNA by agarose gel electrophoresis.....	46
2.4.7 Ethanol precipitation of DNA	46
2.4.8 Determination of plasmid DNA concentration and purity	46

2.4.9 Statistical analysis	47
Chapter 3 Activation of PAR2 by tissue factor regulates PTEN and Akt activities by inducing the release of PTEN from MAGI proteins	48
3.1 Introduction	49
3.1.1 Aims	50
3.2 Methods	51
3.2.1 Activation of cells and preparation of cell lysate	51
3.2.2 Determination of PTEN phosphorylation using western blot analysis	52
3.2.3 Determination of PTEN lipid-phosphatase activity using an ELISA-based kit.....	52
3.2.4 Measurement of Akt kinase activity by ELISA	55
3.2.5 Analysis of cellular PTEN antigen by ELISA	56
3.2.6 Examination of the association of PTEN with MAGI proteins using the proximity ligation assay (PLA).....	59
3.2.7 Examination of the interaction of PTEN and MAGI-2 using co-immunoprecipitation	59
3.3 Results	61
3.3.1 Assessment of the expression of PTEN in the cell lines	61
3.3.2 The influence of rec-TF on PTEN phosphorylation	61
3.3.3 The influence of PAR2 activation on PTEN phosphorylation.....	66
3.3.4 Short-term exposure of cells to TF induces the activity of PTEN	66
3.3.5 PAR2 activation increases the lipid-phosphatase activity of PTEN	66
3.3.6 Short-term exposure of cells to TF reduces the kinase activity of Akt	70
3.3.7 PAR2 activation reduces the kinase activity of Akt.....	70
3.3.8 Prolonged exposure of cells to rec-TF increases the rate of cell proliferation.....	70
3.3.9 Prolonged exposure of cells to rec-TF reduces total PTEN protein.....	73
3.3.10 Prolonged exposure of cells to rec-TF increases Akt kinase activity	73

3.3.11 Activation of PAR2 releases PTEN from MAGI complexes.....	78
3.3.12 Confirmation of the interaction between MAGI-2 and PTEN by co-immunoprecipitation	84
3.3.13 Confirmation of the interaction between PTEN and MAGI-2 by co-immunoprecipitation	84
3.4 Discussion	87
Chapter 4 Investigation of the regulation of TF localisation by interaction with MAGI proteins	91
4.1 Introduction	92
4.1.1 MAGI proteins	93
4.1.2 Aims	94
4.2 Methods.....	97
4.2.1 Examination of the association of TF with MAGI proteins using the PLA.....	97
4.2.2 Examination of the interaction between TF and MAGI-1 by co-immunoprecipitation	98
4.2.3 Examination of the association of TF with tight junction proteins JAM-A and MAGI-1	99
4.2.4 Examination of the influence of PAR2 activation on the localisation of TF within the cell junction.....	99
4.3 Results.....	100
4.3.1 Prediction of the interacting motifs between TF and MAGI proteins using the POW software	100
4.3.2 Examination of the association of TF with MAGI-(1-3) proteins using the PLA	102
4.3.3 Activation of PAR2 reduces the association between TF and MAGI-1	102
4.3.4 Examination the influence of PAR2 activation on the interaction between TF and MAGI-1 by co-immunoprecipitation	109
4.3.5 The association of TF with tight junction MAGI-1 and JAM-A proteins	112

4.3.6 The localisation of TF within intercellular regions is disrupted following PAR2 activation	112
4.4 Discussion	116
Chapter 5 Characterisation of the interaction between TF and PDZ domains of MAGI-1	121
5.1 Introduction	122
5.1.1 PDZ domains	124
5.1.2 Aims	126
5.2 Methods	127
5.2.1 Design of primers and PCR amplification of MAGI-1 cDNA, the individual PDZ domains and the N-terminal regions including or excluding the PDZ1 domain.....	127
5.2.2 Amplification of MAGI-1 cDNA, PDZ sequences and the N-terminal sequences of MAGI-1	130
5.2.3 Restriction digestion of the DNA inserts and the FLAG-HA-pcDNA3.1 vector	130
5.2.4 Purification of the digested DNA using the Monarch DNA Clean-up kit	132
5.2.5 Ligation of the digested MAGI-1 DNA and the PDZ DNA fragments into the FLAG-HA-pcDNA3.1 expression vector	132
5.2.6 Bacterial transformation	133
5.2.7 Confirmation of sub-cloning by restriction digestion	133
5.2.8 Confirmation of sub-cloning by DNA sequencing	134
5.2.9 Determination of the optimal incubation time for the expression of FLAG-HA tagged PDZ proteins in MDA-MB-231 cells.....	134
5.2.10 Confirmation of protein expression using dot blot.....	135
5.2.11 Examination of the association of TF with FLAG-HA-dual tagged PDZ proteins using the PLA.....	135
5.2.12 Examination of the interaction between TF and Flag-HA-dual tagged PDZ proteins using co-immunoprecipitation.....	136
5.2.13 Measurement of cell surface TF activity using the thrombin generation assay	137
5.3 Results	139

5.3.1 Optimisation of digestion of MAGI-1 cDNA with <i>BamHI</i> and <i>HindIII</i> restriction enzymes	139
5.3.2 PCR amplification of MAGI-1 cDNA and the PDZ domains	139
5.3.3 Verification of MAGI-1 DNA sub-cloning using restriction digestion	142
5.3.4 Verification of sub-cloning of PDZ domains using restriction digestion	142
5.3.5 Verification of DNA sub-cloning by sequencing.....	142
5.3.6 Determination the optimal duration for protein expression	145
5.3.7 Analysis of the interaction of the PDZ domains with TF by PLA, using the FLAG-tag antibody	145
5.3.8 Analysis of the interaction of the PDZ domains with TF by PLA, using the HA-tag antibody	145
5.3.9 Examination of the association of TF with the N-terminal regions of MAGI-1	149
5.3.10 Analysis of the interaction between TF and the N-terminal regions of MAGI-1 by co-immunoprecipitation	149
5.3.11 Measurement of the activity of TF on the cell surface.....	155
5.4 Discussion	158
Chapter 6 Discussion	161
Appendix	175
Chapter 7 References	185

Table of figures

Figure 1.1 The cascade pathways of the coagulation mechanism	4
Figure 1. 2 Schematic representation of the structural domains of TF	7
Figure 1. 3 Cellular signalling mechanisms initiated by the TF-FVIIa-PAR2 complex	9
Figure 1. 4 Schematic representation of PTEN protein	13
Figure 1. 5 The structure of phosphoinositides.....	15
Figure 1. 6 The activation mechanism of PTEN.....	17
Figure 1. 7 The PI3K-Akt signalling pathway.....	19
Figure 1. 8 Schematic representation of the structural domains of MAGI proteins	22
Figure 2. 1 Representative standard curve for Bradford assay	40
Figure 2. 2 Schematic diagram of a PLA reaction.....	41
Figure 3. 1 Standard curve for PTEN activity.	54
Figure 3. 2 Standard curve for Akt kinase activity..	57
Figure 3. 3 Standard curve for PTEN protein.	58
Figure 3. 4 The influence of rec-TF and PAR2 activation on the expression levels of PTEN and P-PTEN in cancer cells.	63
Figure 3. 5 The influence of high concentration rec-TF on PTEN phosphorylation state.....	64
Figure 3. 6 The influence of low concentration rec-TF on PTEN phosphorylation state.....	65
Figure 3. 7 The influence of PAR2 activation on PTEN phosphorylation state.....	67
Figure 3. 8 The influence of low rec-TF on the lipid-phosphatase activity of PTEN.	68
Figure 3. 9 The influence of PAR2-activation on the lipid-phosphatase activity of PTEN. ...	69
Figure 3. 10 The influence of rec-TF on the cellular activity of Akt.....	71
Figure 3. 11 The influence of PAR2 activation on the cellular activity of Akt.....	72
Figure 3. 12 The influence of prolonged exposure of cells to rec-TF on the cell number..	75
Figure 3. 13 The influence of prolonged exposure of cells to rec-TF on the cellular levels of PTEN antigen.....	76
Figure 3. 14 The influence of prolonged exposure of cells to rec-TF on the cellular levels of Akt activity.....	77
Figure 3. 15 Analysis of the influence of PAR2 activation on the association of PTEN with MAGI-1 by PLA.....	80
Figure 3. 16 Analysis of the influence of PAR2 activation on the association of PTEN with MAGI-2 by PLA.....	82

Figure 3. 17 Analysis of the influence of PAR2 activation on the association of PTEN with MAGI-3 by PLA.....	83
Figure 3. 18 Analysis of the interaction between PTEN and MAGI-2 using co-immunoprecipitation.....	85
Figure 3. 19 Analysis of the interaction between MAGI-2 and PTEN using co-immunoprecipitation.....	86
Figure 3. 20 The proposed role of TF on the regulation of PTEN.....	90
Figure 4. 1 The proposed study by which MAGI proteins may restrain TF at the cellular junctions.....	96
Figure 4. 2 Examination of the association between TF and MAGI (1-3) proteins using PLA.....	104
Figure 4. 3 Examination the influence of PAR2 activation on the association of TF with MAGI-1 by PLA assay.....	106
Figure 4. 4 Examination the influence of PAR2 activation on the association of TF with MAGI-2 by PLA.....	107
Figure 4. 5 Examination the influence of PAR2 activation on the association of TF with MAGI-3 by PLA assay.....	108
Figure 4. 6 Analysis of PAR2 activation on the interaction of TF with MAGI-1 by co-immunoprecipitation.....	110
Figure 4. 7 Examination the influence of PAR2 activation on the interaction of MAGI-1 with TF by co-immunoprecipitation.....	111
Figure 4. 8 Co-localisation patterns of TF with JAM-A protein.....	113
Figure 4. 9 Co-localisation patterns of TF with MAGI-1 protein.....	114
Figure 4. 10 Localisation of TF in PAR2 activated confluent MDA-MB-231 cells.....	115
Figure 5. 1 The PDZ domain structure.....	125
Figure 5. 2 Vector map of FLAG-HA-pcDNA3.1 expression plasmid.....	129
Figure 5. 3 The standard curve for TF activity.....	138
Figure 5. 4 Optimisation of the digestion of MAGI-1 cDNA with <i>BamHI</i> and <i>HindIII</i> restriction enzymes.....	140
Figure 5. 5 Agarose gel electrophoresis of the amplified DNA.....	141
Figure 5. 6 Agarose gel electrophoresis of purified MAGI-1- FLAG-HA-pcDNA3.1 construct DNA. MAGI-1 DNA was digested, ligated into FLAG-HA-pcDNA3.1 expression plasmid and transformed into competent 5-alpha <i>E. coli</i>	143

Figure 5. 7 Analysis of the sub-cloning of the amplified DNA by restriction digestion. The recombinant plasmids containing the sub-cloned DNA were digested using <i>Bam</i> HI and <i>Hind</i> III restriction enzymes	144
Figure 5. 8 Confirmation of the expression of FLAG-HA-tagged PDZ proteins in MDA-MB-231 cells by dot-blot.....	146
Figure 5. 9 Analysis of the association of TF with MAGI-1-PDZ domains by PLA using the FLAG-tag antibody.....	148
Figure 5. 10 Analysis of the association of TF with MAGI-1-PDZ domains by PLA using the HA-tag antibody.....	151
Figure 5. 11 Analysis of the association between TF and the N-terminal regions of MAGI-1 using PLA	153
Figure 5. 12 Analysis of the interaction of TF with the N-terminal region of MAGI-1 using co-immunoprecipitation	154
Figure 5. 13 Examination the influence of expressing the PDZ1 and PDZ2 domains on TF activity by a modified thrombin generation assay	156
Figure 5. 14 Examination the influence of the expression of the N-terminal regions of MAGI-1 on TF activity by thrombin generation assay.....	157
Figure 6. 1 The proposed mechanism for TF signalling and the regulation of its TF procoagulant activity	174
Figure A- 1 Optimisation of cell permeabilising reagents.....	178
Figure A- 2 Optimisation of the concentration of primary antibodies.....	180
Figure A- 3 Sequence alignment of DNA regions coding for the PDZ domains within MGAI-1 compared to the published MAGI-1 cDNA sequence..	184

Table of tables

Table 2. 1 Primary and secondary antibody dilutions used in the western blot and co-immunoprecipitation procedures	37
Table 4. 1 Sequences and scores for the predicted PDZ domains capable of interacting with TF peptides	101
Table 5. 1 The sequences of forward and reverse primers used for PCR.....	128
Table 5. 2 PCR conditions for DNA amplification.....	131

List of Symbols and Abbreviations

α	Alpha
β	Beta
γ	Gamma
$^{\circ}\text{C}$	Degrees centigrade
μ	Micro
%	Percentage
APS	Ammonium persulphate
ATP	Adenosine triphosphate
ADP	Adenosine diphosphate
bp	Base pair
BSA	Bovine serum albumin
Ct	Threshold cycle
Ca ⁺²	Calcium
CaCl ₂	Calcium chloride
cDNA	Complementary deoxyribonucleic acid
CO ₂	Carbon dioxide
DAPI	4',6-Diamidino-2-phenylindole dihydrochloride
dH ₂ O	Distilled water
DMEM	Dulbecco's modified essential medium
DMSO	Dimethyl sulphoxide
DNA	Deoxyribonucleic acid
dNTP	Deoxynucleotide triphosphate
EGF	Epidermal growth factor
ELISA	Enzyme-linked immunosorbent assay
ERK1/2	Extracellular signal-regulated kinases 1/2
<i>E. coli</i>	Escherichia coli
EDTA	Ethylenediaminetetraacetic acid
FCS	Foetal calf serum
FICT	Fluorescein isothiocyanate
FVII	Factor VII
FVIIa	Activated factor VII
FX	Factor X
F	Phenylalanine
FXa	Activated factor FX
g	Gram
<i>g</i>	Gravity
G	Guanine
GAPDH	Glyceraldehyde-3-phosphate dehydrogenase
GPCR	G-protein coupled receptor
Gly	Glycine
GTP	Guanosine-5'-triphosphate

h	Hour
HCL	Hydrochloric acid
HRP	Horseradish peroxidase
IgG	Immunoglobulin G
IL	Interleukin
JNK	c-Jun N-Terminal Kinase
Kb	Kilo base
L	Litre
LB	Luria Bertani medium
L	Leucine
Log	Logarithm
M	Molar
m	Milli
MAPK	Mitogen-activated protein kinase
MAGI	Membrane-associated guanylate kinase with inverted orientation
min	Minute
mol	Mole
mRNA	Messenger ribonucleic acid
n	Nano
NaCl	Sodium chloride
NO	Nitric oxide
p38	Protein 38
PAR	Protease activated receptor
PAR2-AP	Protease activated receptor2-activating peptide
PIP3	Phosphatidylinositol (3,4,5)-trisphosphate
PIP2	Phosphatidylinositol 4,5-bisphosphate
PtdIns3P/PI	Phosphatidylinositol 3-phosphate
PI3K	Phosphoinositide 3-kinase
PBS	Phosphate buffered saline
PCR	Polymerase chain reaction
PLA	Proximity ligation assay
PS	Phosphatidylserine
RNA	Ribonucleic acid
RNase	Ribonuclease
rpm	Revolutions per minute
s	Second
SD	Standard deviation
SDS	Sodium dodecyl sulphate
SDS-PAGE	Sodium dodecyl sulphate polyacrylamide gel electrophoresis
SEM	Standard error of mean
siRNA	Short interfering RNA
TBE	Tris borate-EDTA

TBST	Tris buffered saline tween 20
TEMED	N,N,N',N'-Tetramethylethylenediamine
TF	Tissue factor
TMB	3,3',5,5'-Tetramethylbenzidine
TNF	Tumour necrosis factor
UV	Ultra violet
U	Unit
V	Volt
v/v	Volume to volume
w/v	Weight to volume

Chapter 1

General introduction

1.1 Introduction

Following injury to vascular tissue, tissue factor (TF) is exposed to the blood and binds to circulating FVIIa which initiates the extrinsic pathway of coagulation to prevent excessive blood loss. However, the formation of the TF-FVIIa complex on the cell surface also induces the signalling functions of TF through the activation of protease activated receptor (PAR2). This results in the activation of several downstream signal transduction pathways involved in inflammation, cell proliferation, migration and survival (Ruf *et al* 2011; Han *et al* 2014; Rondon *et al* 2019). To prevent inappropriate coagulation, the activity of TF at the cell surface is regulated through mechanisms known as the encryption and decryption of TF (Chen *et al* 2006). Within the intravascular compartment TF is present on resting cells in the encrypted form. However, damage in the endothelial barrier promotes the decryption of TF into an active form (Chen and Hogg 2013). In addition, aberrant expression of TF has been shown to cause an imbalance in the procoagulant activity of TF which has been associated with pathological conditions such as thrombosis and cancer (Palta *et al* 2014). Therefore, the regulation of TF activity is critical in the maintenance of the haemostatic balance within the vasculature. As stated above, it has also been documented that several signalling pathways are activated as a result of the formation of TF-FVIIa-PAR2 complex on the cell surface (Ruf 2011). The activation of PI3K-Akt pathway is one of the principal pathways which are induced from the TF-dependent mechanism and is well documented for conferring enhanced cell survival and proliferation, as well as being involved in uncontrolled cell growth in disease conditions (Arderiu *et al* 2012). This study investigates the mechanisms by which TF induces cell proliferation particularly observed in cancer cells. Additionally, this study attempts to identify a novel mechanism by which the encryption of TF activity may be achieved on the cell membrane.

1.1.2 Tissue factor

The role of TF in blood coagulation is well established (Hoffman and Monroe 2001; Palta *et al* 2014). In addition, it has been documented that TF has a non-haemostatic function in the body such as vascular development during embryogenesis (Carmeliet *et al* 1996; Mackman 2004; Chu 2011). TF is also known as CD142, factor III and thromboplastin and is predominantly expressed in extravascular tissues. Under physiological conditions, TF is strictly expressed in subendothelial cells including fibroblasts, smooth muscle cells, epithelial cells and pericytes but is absent from endothelial cells which are in direct contact with the blood (Butenas 2012; Palta *et al* 2014). However, the strict regulation of TF expression is often disrupted during inflammatory pathological conditions such as cardiovascular diseases and cancer (Bluff *et al* 2008). In addition, several reports have documented the release of TF as cell-derived microvesicles which are small cell-derived fragments that are enclosed by a phospholipid bilayer derived from a number of cell types (Palta *et al* 2014). Circulating TF-containing microvesicles are not normally detected within blood circulation (Breitenstein *et al* 2009). However, cells can produce and release TF-expressing microvesicles following trauma or injury (Yau *et al* 2015). Also, TF-expressing microvesicles can be detected in the circulation during many pathological conditions and have also been linked with the increased generation of thrombin and the activation of the coagulation system (Butenas *et al* 2009; Thaler *et al* 2012; Geddings and Mackman 2013).

1.1.3 The role of TF in the initiation of the coagulation cascade

The coagulation system, together with the platelets, the vasculature and the fibrinolytic system form the components of haemostasis. The coagulation mechanism is made up of three pathways called the intrinsic pathway, the extrinsic pathway and the common pathway (Figure 1.1). The extrinsic pathway is activated following damage and/or trauma to the vascular tissue which results in the exposure of TF to the bloodstream. TF binds to the

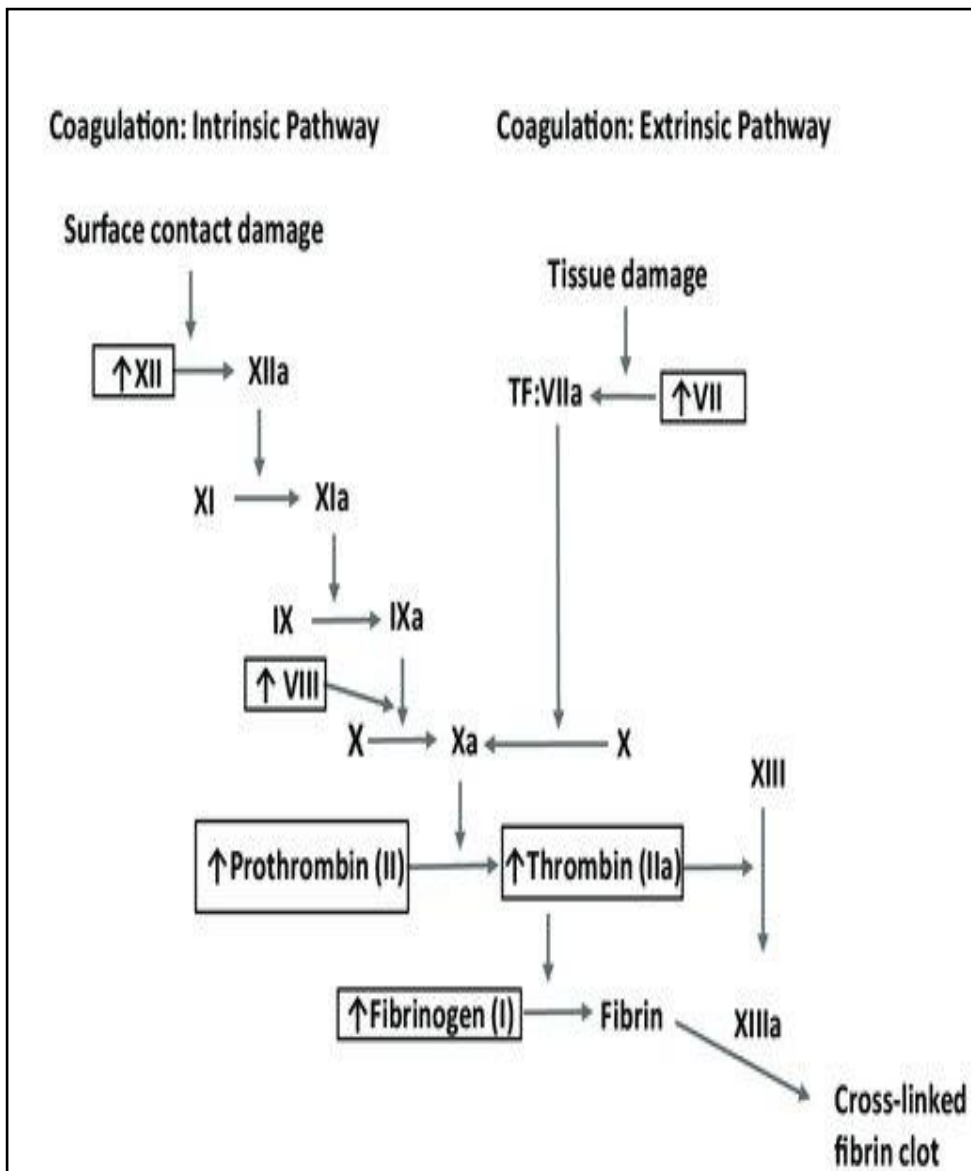


Figure 1.1 The cascade pathways of the coagulation mechanism. The coagulation mechanism is composed of three separate pathways known as the intrinsic, extrinsic and common pathways. Following injury, TF binds FVIIa and subsequently activates the extrinsic pathway. The exposure of FXIIa to negatively charged surfaces initiates the intrinsic pathway which subsequently triggers the activation of FXIa and then FIXa. The common pathway is activated by both extrinsic and intrinsic pathways which lead to the activation of FXa which activates prothrombin to thrombin and ultimately results in the production of a fibrin clot (Adapted from Heavner *et al* 2017).

circulating FVII promoting the formation of a complex and the activation of FVIIa (Figure 1.1). It has been reported that once TF is exposed to the cell surface it adapts a curved-like shape upon complex formation with FVIIa which permits TF to undergo conformational change at residues Lys165 and Lys166 which are required for the subsequent proteolytic activation of FX and FIX (Ohkubo *et al* 2010; Grover and Mackman 2018; Ansari *et al* 2019). The formation of TF-FVIIa complex activates the zymogen FX to the active form FXa, as well as FIX to the active form FIXa (Butenas 2012). FXa in turn catalyses the conversion of prothrombin (FII) into thrombin (FIIa). Thrombin converts fibrinogen into fibrin monomers which aggregate and is further cross-linked by a transglutaminase, FXIIIa to produce the fibrin clot (Malý *et al* 2007). Thrombin also feeds back into the coagulation cascade and activates coagulation factors V, VIII and XI to amplify clot generation. In particular, the activation of FV to FVa by thrombin allows the binding of FVa to FXa creating the prothrombinase complex. The formation of the prothrombinase complex accelerates the conversion of prothrombin to thrombin on the surface of cells or platelets (Palta *et al* 2014). Thrombin also acts as an agonist promoting the activation of platelets which leads to platelet aggregation. The fibrin aggregates together with the adhered platelets to form a haemostatic plug to prevent further loss of blood, and to preserves the vascular integrity (Mackman 2004). The intrinsic pathway is initiated through the activation of FXII following contact between the blood and the negatively charged surfaces, such as the sub-endothelial collagen or exposed on the plasma membrane of activated platelets (Bendapudi *et al* 2016; Grover and Mackman 2019). FXIIa catalysis the activation of FXI to FXIa which in turn activates FIX to FIXa. Activated FIXa forms a complex with FVIIIa promoting the activation of FXa. The intrinsic and common pathways are linked to activate prothrombin (FII) to thrombin (FIIa) which subsequently result in the formation of fibrin clot (Mann *et al* 2006; Chu 2011).

1.1.4 The structure of TF protein

The TF gene is located at locus 1p22-23 on chromosome 1 (Mackman *et al* 1989). TF is a transmembrane glycoprotein with a molecular mass of 47kDa. The protein consists of 263 amino acid and made up of three distinct domains (Figure 1.2). The extracellular domain (219 aa) is responsible for binding to FVIIa which is essential for its procoagulant activity. This domain contains 4 cysteine residues that form two disulphide bonds (Cys⁴⁹-Cys⁵⁷ and Cys¹⁸⁶-Cys²⁰⁹) which have been suggested to be essential for the regulation of TF activity (Schmidt *et al* 2006). The transmembrane domain (23 aa) is essential for anchoring TF to the cell membrane (Ohkubo *et al* 2010). The cytoplasmic domain (21 aa) does not influence the procoagulant function but permits TF to act as a signalling protein (Mueller and Ruf 1998; Dorfleutner and Ruf 2003). The cytoplasmic domain of TF contains three serine residues, however only Ser253 and Ser258 have been reported to be phosphorylated (Mody and Carson 1997). It has been reported that Ser253 can be phosphorylated by protein kinase C (PKC) (Dorfleutner and Ruf 2003; Malý *et al* 2007; Butenas 2012) while Ser258 phosphorylation is mediated by p38 α -MAPK (Ettelaie *et al* 2013). It has also been demonstrated that the phosphorylation state of TF acts as a regulator for the release of TF as microvesicles (Collier *et al* 2011), as well as being responsible for the signalling function of TF (Dorfleutner and Ruf 2003; Versteeg *et al* 2004).

1.1.5 The role of TF as a signalling receptor

The first evidence for the signalling ability of TF was reported by Cunningham *et al* (1999) who demonstrated that the binding of FVIIa to TF promoted the activation phospholipase C pathway. Shortly afterwards, a study conducted by Camerer *et al* (2000) also demonstrated that TF requires FVIIa to promote the activation of protease activated receptor (PAR)1 and 2.

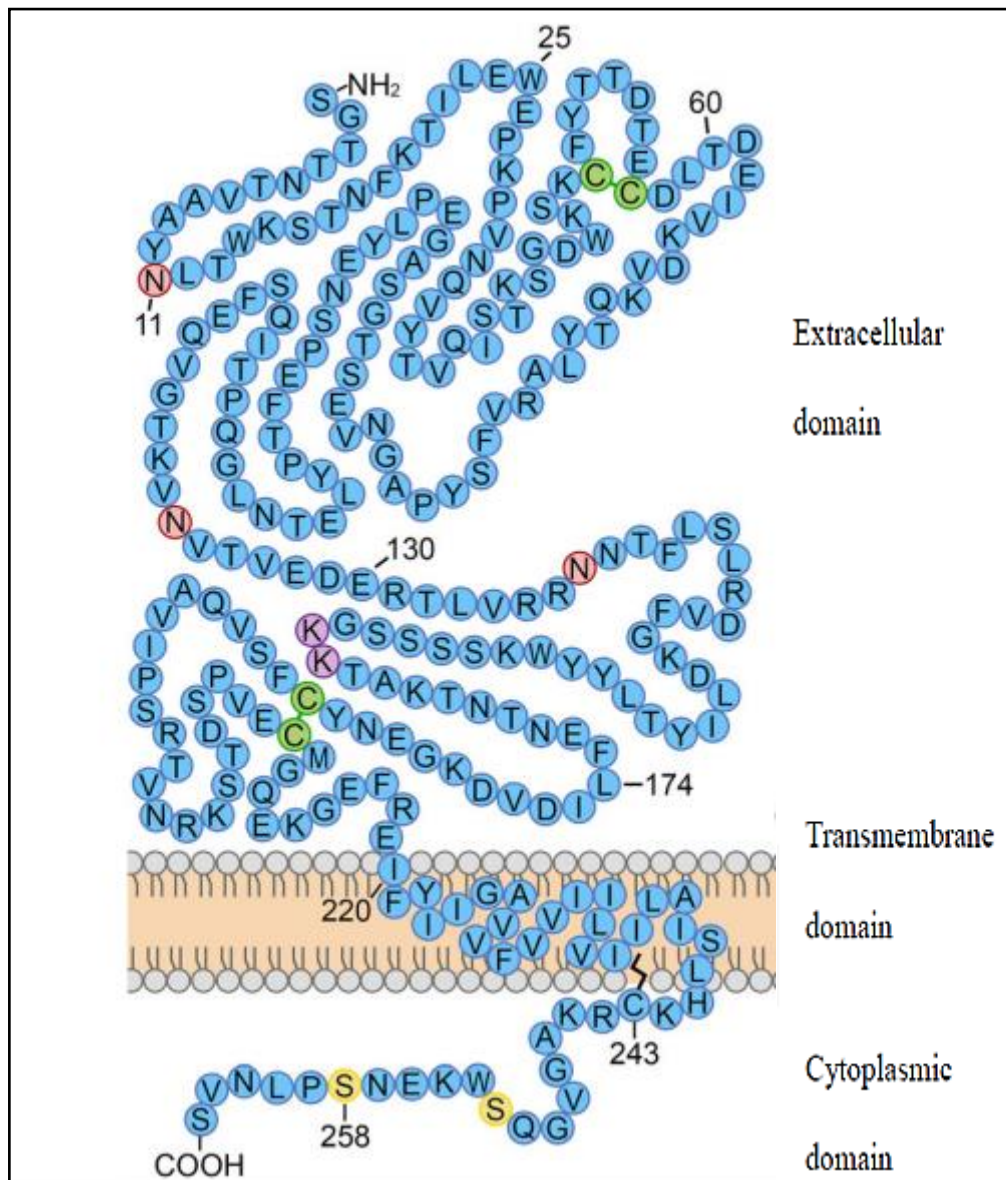


Figure 1. 2 Schematic representation of the structural domains of TF. The structure of human TF is made up of an extracellular domain (residues 1-219) which interacts with FVII. Within the extracellular domain, there are four cysteine residues (shown in blue). The transmembrane domain (residues 220-242) anchors TF to the cell surface. The cytoplasmic C-terminus (residues 243-263) contains three serine residues Ser253, Ser258 and Ser263 but only Ser253 and Ser258 have been reported to become phosphorylated (Adapted from Chu 2011).

However, more recently PAR-independent signalling, arising from the interaction of TF with cell-surface receptors has also been reported (Su *et al* 2007; Kocatürk and Versteeg 2013). In order to discuss the nature and the outcome of the signalling mechanisms arising from the interactions of TF, first the structure and function of PARs are outlined. The mechanisms and outcomes of TF interactions during cancer are then elaborated further.

1.1.6 Protease-activated receptors (PARs)

Protease-activated receptors (PARs) are a sub-family of G-protein-coupled receptors (GPCRs) that include four members PAR1, PAR2, PAR3 and PAR4. These receptors are expressed on the surface of a number of cells including fibroblasts, myocytes, platelets, neutrophils, macrophages, neurons, astrocytes, vascular and endothelial cells (Wojtukiewicz *et al* 2015). The activation of PARs can be initiated by extracellular proteases through digestion of the extracellular N-terminal loop of the receptor. This cleavage results in the exposure of the peptide sequences at the N-terminal domain which serve as tethered ligands that folds back and interact with the second extracellular domain on the receptors, resulting in receptor activation (Holzhausen *et al* 2005; Heuberger and Schuepbach 2019). PARs may also be experimentally activated using agonist peptides, synthesised to correspond to the six amino acids found in the tethered N-terminal ligands (Cimmino and Cirillo 2018). Various proteases have been reported to be responsible for the activation of PARs. The predominant activator of PAR1, PAR3 and PAR4 is thrombin while PAR1 and PAR2 can be activated by trypsin, FVIIa and FXa (Mackman 2004). A recent report suggests that PAR2 can also be activated by thrombin (Mihara *et al* 2016) while other studies discounted this possibility (Coughlin 1999; Camerer *et al* 2000). As mentioned above, the formation of TF-FVIIa or TF-FVIIa-FXa complex at the cell surface is capable of activating PAR2 (Mackman 2004; Hjortoe *et al* 2004; Schaffner *et al* 2010). The activated PAR2 can signal through β -arrestin or alternatively through heterotrimeric G-proteins ($G\alpha$ - or $G\beta\gamma$ -subunits) mediated signalling (Figure 1.3) (Rothmeier and Ruf 2012).

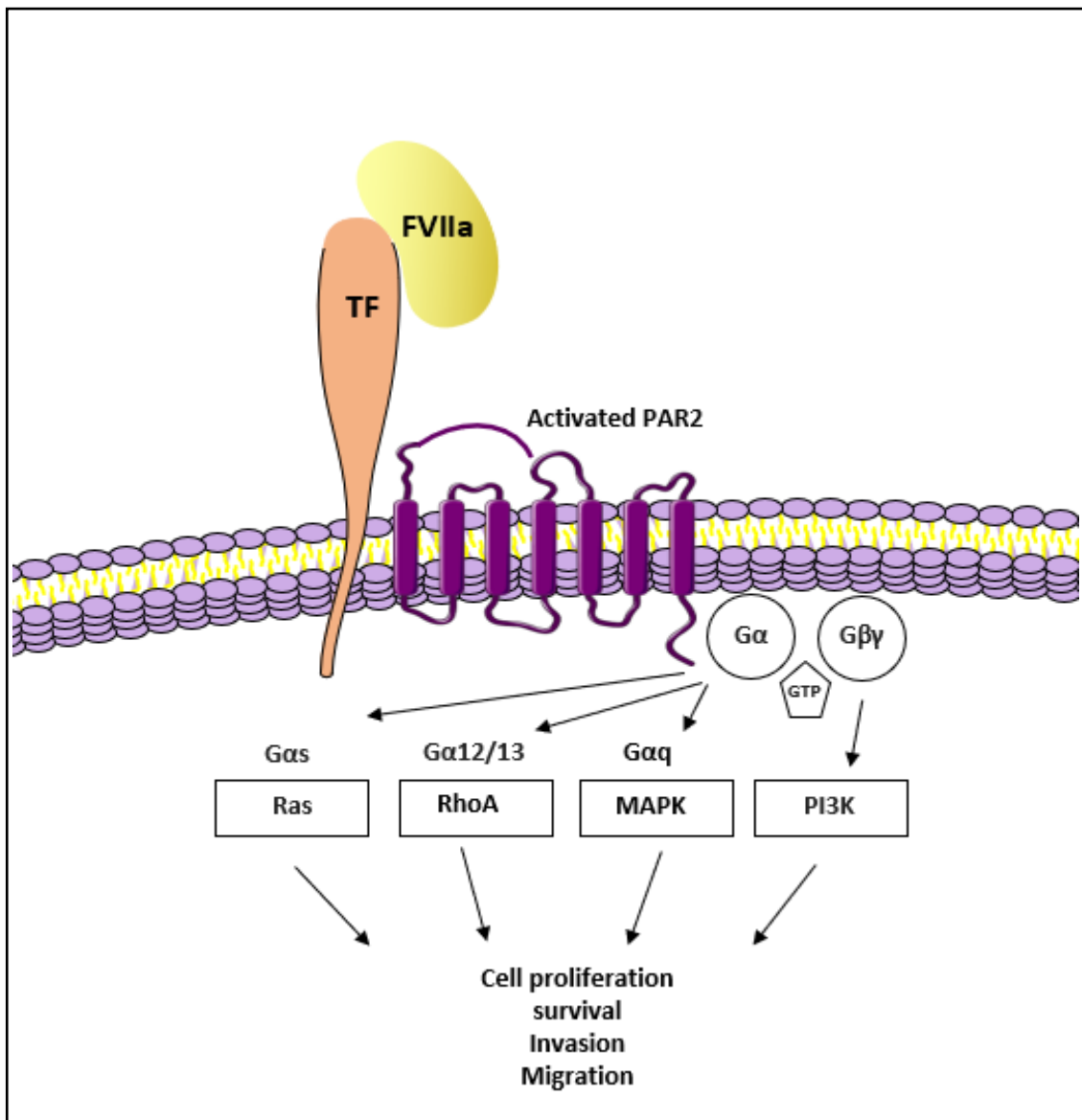


Figure 1. 3 Cellular signalling mechanisms initiated by the TF-FVIIa-PAR2 complex. The inactive GDP-bound heterotrimeric G protein complex are firmly attached to the membrane through the $G\alpha$ -, $G\beta$ - and $G\gamma$ -subunits. Once the receptor is activated, it undergoes conformational change allowing the receptor to function as a guanine nucleotide exchange factor (GEF) that exchanges GDP to GTP. The GTP-bound $G\alpha$ -subunit dissociates from the $G\beta\gamma$ -dimer which activate various signalling pathways triggering a number of cellular functions including cell proliferation, migration and survival.

Upon receptor stimulation, ligand-activated receptors catalyse the exchange of GDP for GTP which disassociate the GTP-bound $G\alpha$ from the $G\beta\gamma$ -dimer (Arora *et al* 2006; Pawar *et al* 2019). The GTP-bound $G\alpha$ -subunit and $G\beta\gamma$ -dimer remain anchored to the plasma membrane where they initiate a number of different signalling mechanisms, but no longer bound to the GPCR (Sidhu *et al* 2014; Zhao *et al* 2015). It has been documented that the activation of $G\alpha_q$ following the digestion of PAR1 by thrombin leads to the activation of the ERK, JNK and p38 MAPK pathway. Also, PAR1-thrombin digestion causes the activation of $G\alpha_{12/13}$ and subsequently the activation of RhoA/Ras signalling. However, induction of PAR2 either by trypsin or FVIIa activates the $G\beta\gamma$ -dimer, resulting in the activation of PI3K pathway (Marinissen and Gutkind 2001; Goldsmith and Dhanasekaran 2007). Importantly, the $G\beta\gamma$ -dimer has been reported to directly bind and recruit the p101/p110 γ -heterodimer protein of PI3K class IB, to the inner cell membrane promoting its activation (Brock *et al* 2003; New *et al* 2007). It has also been documented that the activation of p85/p110 β -heterodimer of PI3K class IA is mediated by direct binding with $G\beta\gamma$ -dimer leading to Akt activation (Kurosu *et al* 1997; Goldsmith and Dhanasekaran 2007). It has been suggested that the activation of the PI3K-Akt pathway can also be triggered directly, or indirectly through several $G\alpha$ -subclasses (New *et al* 2007). For example, by expressing mutationally activated forms of $G\alpha_q$, $G\alpha_{i2}$, $G\alpha_s$, and $G\alpha_{12}$, Murga *et al* (1998) showed that expression of inactive mutants of either $G\alpha_q$ or $G\alpha_i$ in COS-7 kidney cell line resulted in decreased Akt activity. These findings indicate that $G\alpha_q$ or $G\alpha_i$ may directly control Akt activation. In addition, other studies have shown the ability of $G\alpha$ to activate PI3K-Akt pathway indirectly (Bajetto *et al* 2001). For example, it was reported that activation of Ras by $G\alpha_{12/13}$ allows the former to bind and recruit both the p110 α and p110 γ catalytic subunits to the membrane, leading to PI3K activation (Castellano and Downward 2011).

1.1.7 Mechanisms and outcomes of TF signalling in cancer

The association between cancer and thrombosis was established in the early 1860's when Trousseau reported the presence of migratory blood clots in cancer patients (Ruf 2012; Han *et al* 2014). Trousseau's syndrome describes a series of cancer-related coagulopathies which include both venous and arterial thrombosis, as well as precipitation of disseminated intravascular coagulation (Dammacco *et al* 2013; Ikushima *et al* 2016). It was suggested that cancer-associated thrombosis can be driven by the activation of the coagulation pathway as well as the signalling properties of TF mediated by either TF-containing microvesicles and/or abnormal cell-surface expression of TF (Conde *et al* 2007). More recently, the consequences of TF signalling associated with tumour progression and invasiveness have been of interest (Jiang *et al* 2004; Ruf 2011; Sedda *et al* 2014). The activation of PAR2 is a major link between TF-FVIIa complex and alterations in a number of cellular functions including proliferation, invasion, migration and angiogenesis (Morris *et al* 2006; Schaffner and Ruf 2009; Dutra-Oliveira *et al* 2012; Åberg and Siegbahn 2013). It has been documented that PAR2 activation may promote angiogenesis by vascular cells, through enhancing the expression of vascular endothelial growth factor (VEGF) (Fernandez and Rickles 2002.) In support of this finding, a study conducted by Liu and Mueller (2006) reported that the activation of PAR2 induced the expression of VEGF in breast and glioblastoma cancer cells. This upregulation in VEGF expression was suggested to be regulated through the activation of ERK1/2 MAPK which also leads to increased rates of cells proliferation in many types of cancers (Dutra-Oliveira *et al* 2012). Other studies have also implicated signalling by the TF-FVIIa-PAR2 complex in cancer cell survival (Han *et al* 2014). For example, TF-mediated signalling enhanced the cell survival in breast (Sorensen *et al* 2003) and prostate (Åberg and Siegbahn 2013) cancer cells, through the inhibition of caspase-3 mediated and the activation of both PI3K-Akt and p44/42 MAPK pathways (Ruf 2012). Finally, the signalling arising from TF has been documented to promote

cancer cell migration and metastasis (Han *et al* 2014). This link between TF signalling and cancer cell migration was demonstrated by Hjortoe *et al* (2004) who showed that the activation of PAR2 by TF-FVIIa complex resulted in the upregulation of the expression of chemokines including interleukin-8, (IL-8) in MDA-MD-231 breast cancer cells. The increase in IL-8 expression resulted in enhanced cell invasion and migration when analysed by transwell cell migration and Matrigel invasion assays (Jiang *et al* 2004). As stated above, MAPK and the PI3K-Akt pathways are the two major signalling pathways which mediate diverse cellular functions in cells (Lee *et al* 2006). The MAPK pathway can be regulated by various phosphatases (Jiang *et al* 2018). However, the PI3K-Akt pathway is mainly regulated by the lipid phosphatase PTEN (Milella *et al* 2015) and the mechanisms of PTEN function, regulation and signalling are discussed below.

1.2 PTEN

Phosphatase and tensin homolog on chromosome 10 (PTEN) is a protein- and lipid-phosphatase which acts as one of the key regulators of the PI3K-Akt pathway and has been identified as a tumour suppressor (Milella *et al* 2015). PTEN is ubiquitously expressed in normal tissue but its aberrant expression has been associated with a number of cancers (Song *et al* 2012). PTEN is located on chromosome 10q23.3 and encodes a 55 kDa protein. This region of chromosome 10 is known to be highly susceptible to mutations and deletions in advanced tumours leading to mutational inactivation and/or loss of PTEN (Feilotter *et al* 1999; Verhagen *et al* 2006; Lee *et al* 2014).

1.2.1 Structure of PTEN protein

PTEN is a member of the protein tyrosine phosphatase (PTPs) family and is made up of 403-amino acids (Kolmodin and Aqvist 2001). Structurally, PTEN consists of an N-terminal region and a C-terminal region (Figure 1.4) which have both been associated with membrane binding (Molinari and Frattini 2013). The N-terminal region (also known as tyrosine phosphatase

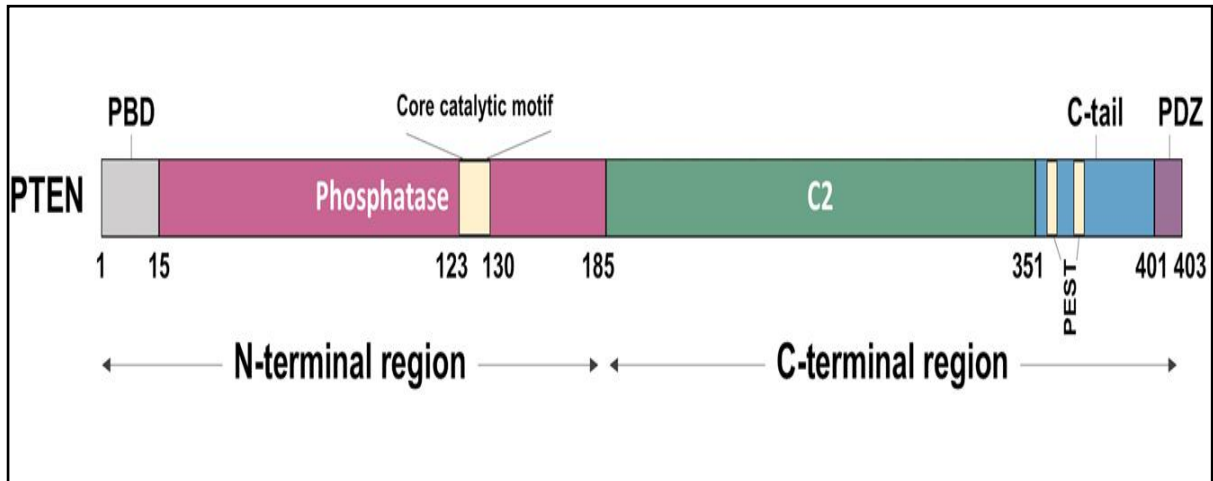


Figure 1. 4 Schematic representation of PTEN protein. The structure of PTEN comprises of the N-terminal region (1–185 aa) which includes PIP2- binding domain (PBD) and the dual protein and lipid-phosphatase domains. The C-terminal region (186–403 aa) contains the C2 domain and the C-tail domain. Within the C-tail there is a PDZ-binding domain, which has been shown to bind other PDZ-containing proteins, and two PEST domains, which are important for PTEN stability (Adapted from Yehia and Eng 2018).

domain) consists of the PIP2/lipid domain binding (PDB) and the dual-specificity phosphatase domain (1-185 aa). The PDB region regulates PTEN membrane localisation by enabling PTEN to anchor to the plasma membrane which is essential for its lipid phosphatase activity (Andrés-Pons *et al* 2007; Gil *et al* 2015). The C-terminal region of PTEN contains the C2 domain (186-351 aa) and the C-terminal tail (354-403 aa). The conservation domain 2 in calcium activated protein kinase C (C2) domain plays an important role in maintaining the function of PTEN by regulating PTEN enzymatic activity (e.g., phosphorylation, ubiquitination and SUMOylation) (Molinari and Frattini 2013; Hopkins *et al* 2014). The C-terminal tail contains a PDZ binding domain that binds PDZ-containing proteins and is important for PTEN stability (Vazquez *et al* 2000; Das *et al* 2003) and membrane localisation (Hopkins *et al* 2014). PTEN also contains two PEST domains sequences rich in proline (P), glutamate (E), serine (S), and threonine (T) residues which have been reported to enhance PTEN protein stability (Tolkacheva *et al* 2001; Trotman *et al* 2007).

1.2.2 Association of PTEN with the phospholipid membrane

In order for PTEN to function as a tumour suppressor, it must bind to the membrane to exert its negative regulatory effects on the PI3K-Akt pathway (see below). This multi-step process is achieved by the activation of several molecules and proteins, leading to the dephosphorylation of phosphatidylinositol PI(3,4,5)P₃ to PI(4,5)P₂ (Maehama and Dixon 1998; Zhang *et al* 2012). Phosphatidylinositols (PtdIns) are a group of phospholipids which are composed of an inositol ring (carbocyclic sugar) and two fatty acid chains connected by a glycerol backbone (Harayama and Riezman 2018). PtdIns are negatively charged and can be phosphorylated by lipid kinases at the OH group positioned on the 3', 4' - and 5' of the inositol ring where it serves as a substrate for producing different phosphoinositides (Auger *et al* 1989; Falkenburger *et al* 2010; Yang *et al* 2018). The phosphoinositides (PIs) can be divided into three groups (Figure 1.5): the monophosphates also known as (PI) which contain PI3P,

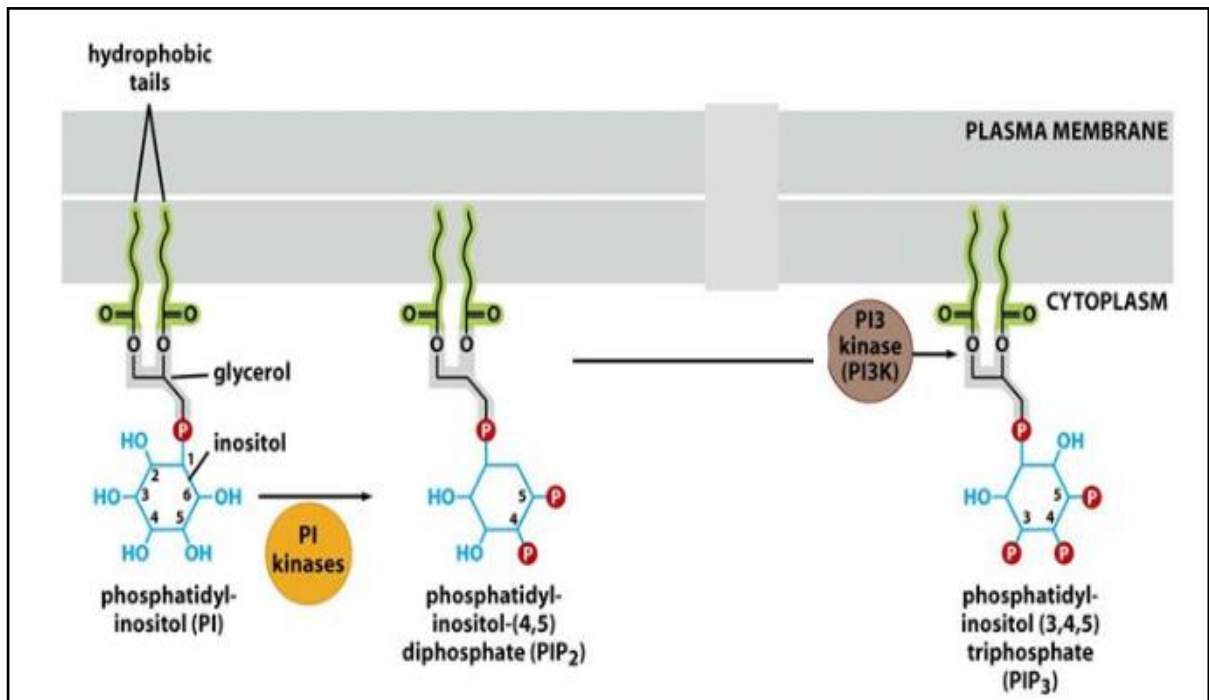


Figure 1. 5 The structure of phosphoinositides. Phosphoinositides consist of an inositol ring and two fatty acid chains connected by a glycerol backbone. Hydroxyl groups located at positions 3, 4 and 5 of the inositol head group which can be phosphorylated by lipid kinases. Two of the most studied PIPs are PIP₂ and PIP₃ which are regulated by PI3K and PTEN (Adapted from McDaniel 2007).

PI4P, and PI5P and has been reported to localised in the Golgi apparatus, the nucleus but mostly at the plasma membrane (Nunès and Guittard 2013). The diphosphates PI(3,4)P₂, PI(3,5)P₂ and PI(4,5)P₂ also known as (PIP₂) and the triphosphates PI(3,4,5)P₃ also known as (PIP₃) are primarily localised at the plasma membrane and regulated by PTEN and PI3K. They can also be localised in the Golgi complex, endoplasmic reticulum and mitochondria (Castellano and Downward 2011; Porta *et al* 2014). The phosphoinositides regulate different cellular events such as cell migration, adhesion and membrane trafficking through direct interaction with membrane proteins such as: (GPCRs), G-protein coupled receptors and (RTKs) receptor tyrosine kinases (Balla 2013; Hammond and Balla 2015).

1.2.3 PTEN activation

It has been well documented that PTEN phosphorylation at Ser380, Thr382, Thr383 and Thr385 alters the stability of PTEN and contribute to the loss of its lipid-phosphatase activity (Vanhaesebroeck *et al* 2010; Milella *et al* 2015; Manning and Toker 2017). In the cytoplasm, phosphorylated PTEN exists in a closed conformation by intramolecular interaction between the C-terminal tail and the C2 domain (Ross and Gericke 2009). The phosphorylation of Ser380, Thr382, Thr383 and Thr385 within the C-terminal tail are required for the intramolecular interaction with Lys260, Lys263, Lys266, Lys267 and Lys269 found in the CBRIII loop within the C2 domain of PTEN (Odrizola *et al* 2007; Rahdar *et al* 2009; Hopkins *et al* 2014; Dempsey and Cole 2018). A recent study by Chen *et al* (2016) reported that PTEN needs to be phosphorylated in at least 3 of the 4 residues to adapt the closed conformation (Figure 1.6). Phosphorylated PTEN remains inactive but stable. PTEN can be mono-ubiquitinated and poly-ubiquitinated by the same ubiquitin ligase NEDD4, an E3 ubiquitin ligase enzyme that targets proteins for ubiquitination. Phosphorylated PTEN can become

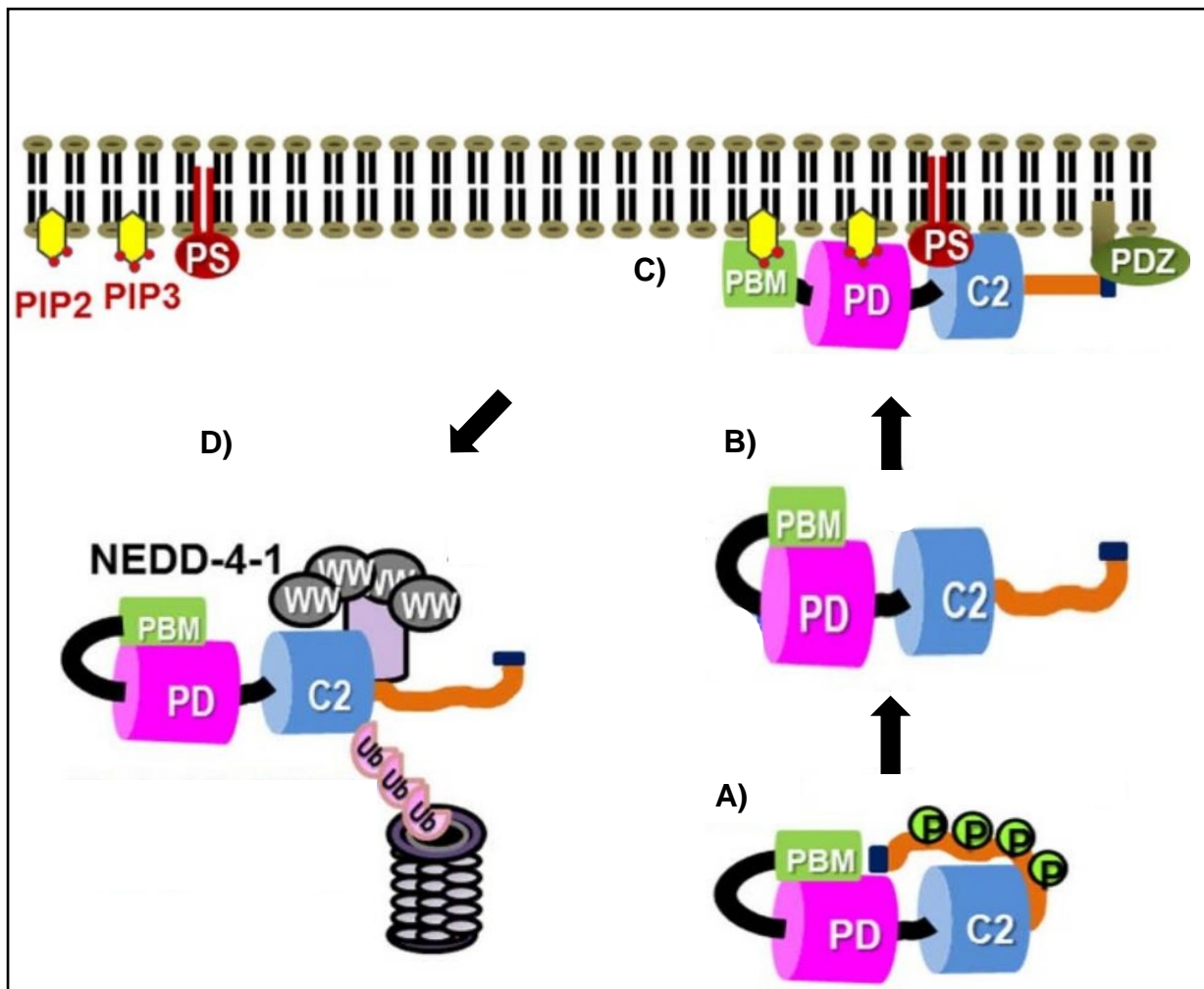


Figure 1. 6 The activation mechanism of PTEN. A) Phosphorylation of PTEN induces conformational change allowing the C-terminal tail to fold onto the C2 domain, restricting its membrane recruitment. PTEN remains stable in the cytoplasm by masking the ubiquitination sites which increases the half-life of PTEN protein within the cell. B) Activation of PI3K and/or accumulation of PIP3 allows PTEN to auto-phosphorylate itself and bind to the membrane. C) Once PTEN binds to the membrane through its C2 and lipid-binding domain/motif, it dephosphorylates PIP3 to PIP2 thus inhibiting the PI3K-Akt signalling pathway. D) PTEN dissociates from the membrane where it can be mono-ubiquitinated by NEDD4 or poly-ubiquitinated and undergo proteasomal degradation (Adapted and modified from Malaney *et al* 2013).

mono-ubiquitinated and transported to the nucleus where the ubiquitin moiety is removed by an unknown deubiquitinase (Trotman *et al* 2007). Alternatively, PTEN can be poly-ubiquitinated and undergo ubiquitin-dependent degradation possibly through the C-terminal PEST domain (Georgescu *et al* 1999; Zhang *et al* 2012). It has been suggested that the accumulation of PIP3 at the inner site of the membrane triggers the auto-de-phosphorylation of PTEN at Thr366 through its protein-phosphatase activity thereby inducing the activation of PTEN (Das *et al* 2003; Zhang *et al* 2012; Tibarewal *et al* 2012; Papa and Pandolfi 2019). Once PTEN is de-phosphorylated, the C-terminal domain of PTEN acts as an electrostatic switch, which controls membrane binding, therefore allowing PTEN to adopt an open conformation (Das *et al* 2003) and bind to the membrane (Platre and Jaillais 2017). Once PTEN is recruited to the membrane, the C2 domain then binds the phosphatidylserines in the inner membrane which permits the lipid-binding domain within the N-terminal to bind to the negatively charged anionic lipids in the inner membrane. This binding induces a conformational change that activates the PTEN phosphatase domain which subsequently results in full PTEN activation and de-phosphorylation of PIP3 to PIP2 (Zhang *et al* 2012; Milella *et al* 2015).

1.2.4 The association of PTEN with the PI3K-Akt pathway

1.2.4.1 The PI3K-Akt pathway

Phosphatidylinositol 3-kinases (PI3Ks) belong to a lipid kinase family characterised by their ability to phosphorylate the inositol ring positioned on the 3rd OH group. There are three classes of PI3K: class-I is the only class which has been documented to phosphorylate PIP2 to PIP3 and mediate the activation of Akt (Figure 1.7). Class II and class III can phosphorylate PtdIns to monophosphates PtdIns3P (PI3P) while class II can only phosphorylate monophosphates (PI4P) to diphosphates (PIP2) (Mazloumi Gavvani *et al* 2018). Class-IA PI3Ks can be subdivided into sub-class IA and sub-class IB. Sub-class IA can be activated by receptor

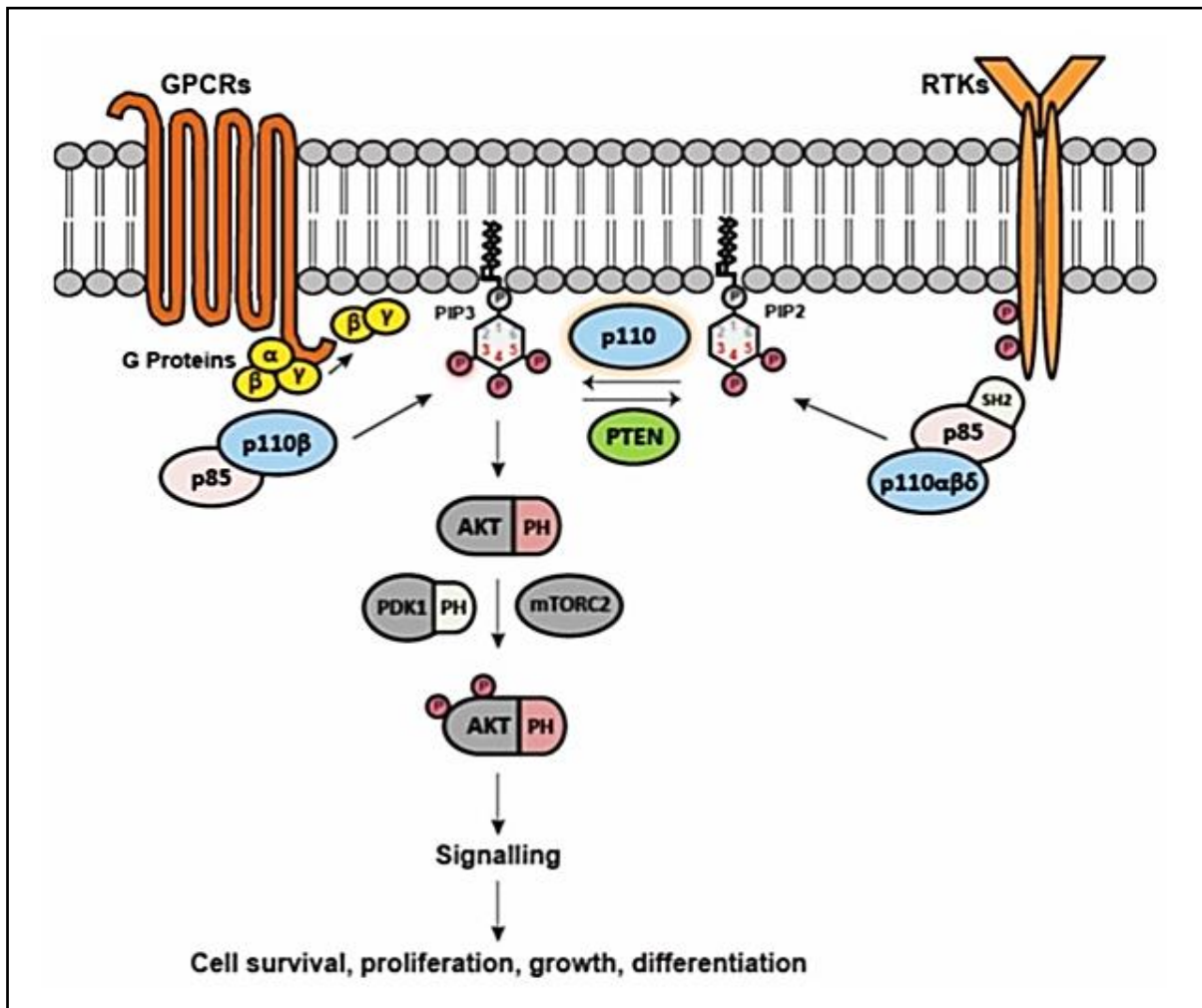


Figure 1. 7 The PI3K-Akt signalling pathway. Class IA PI3K comprises of three different catalytic isoforms (p110 α , β , δ) and associates with p85 regulatory subunit while class IB contains the p110 γ -p101 subunit. The stimulation of GPCRs allow p101 to unmask the G $\beta\gamma$ binding site in the catalytic subunit p110 γ thereby allowing the interactions between G $\beta\gamma$ and p110 γ . The stimulation of RTKs induces the activation of PI3K by recruiting the p110-p85 complex to the membrane. The regulatory p85 subunit loses its inhibitory effects on the catalytic activity of p110, thereby phosphorylating PIP2 to PIP3. PIP3 recruits PH-domain containing proteins (e.g., Akt, PDK1, mTORC) to the membrane. Akt becomes fully active when phosphorylated at Thr308 and Ser473 by PDK1 and mTORC2, respectively. The activation of Akt either induces phosphorylation of pro-survival and anti-apoptotic proteins (e.g., CREB, Bcl-XL) or inhibit phosphorylation of pro-apoptotic proteins (e.g., BAD, caspase-9) (Adapted from Mazloumi Gavani *et al* 2018).

tyrosine kinases (RTKs) and is composed of a catalytic (p110 α,β,δ) and regulatory (p85) subunits (Manning and Toker 2017; Nürnberg and Beer-Hammer 2019). Upon activation of RTKs by growth factor engagement (Figure 1.7), the tyrosine residues within the RTKs are phosphorylated. The Src homology 2 (SH2) domain within the p85 regulatory subunit binds to the phosphorylated tyrosine residues on the activated receptor and triggers the recruitment of the p85-p110 heterodimer to the membrane. The regulatory p85 subunits inhibit the p110 catalytic subunits through the SH2 domains (Bresnick and Backer 2019). These inhibitory interactions are disrupted when tyrosine-phosphorylated proteins bind to the SH2 domain causing the p85 subunit to lose its restricting influence on the catalytic activity of p110, permitting the phosphorylation of PIP2 to PIP3 (Porta *et al* 2014; Mazloumi Gavvani *et al* 2018). The sub-class IB enzymes can be activated by G-protein coupled receptors and contains a catalytic subunit (p110 γ) and a regulatory subunit (p101 or p84/p87) (Thorpe *et al* 2015; Nürnberg and Beer-Hammer 2019). The activation of GPCRs by a ligand (e.g., growth factors or hormones) causes the direct activation of the catalytic subunit (p110 γ) through G-protein $\beta\gamma$ dimers (Liu *et al* 2009; Castellano and Downward 2011). The activation of either p110 or p110 γ /p101 subunits allows the phosphorylation of PIP2 to PIP3 on the inner side of the plasma membrane (Figure 1.7). It has been documented that the pleckstrin homology (PH) domain of Akt has a high affinity for PIP3. Therefore, the phosphorylation of PIP2 to PIP3 promotes a conformational change within the PH domain of Akt, thus exposing its two main phosphorylation sites Thr308 and Ser473 (Vanhaesebroeck *et al* 2010). Akt also known as protein kinase B (PKB), is a serine/threonine kinase which plays an important role in activating multiple signalling mechanisms implicated in cell growth, survival, and apoptosis (Fresno Vara *et al* 2004). Akt is then recruited to the membrane via its PH domain. Phosphoinositide-dependent kinase 1 (PDK1) protein phosphorylates Akt at Thr308 residue and mechanistic target of rapamycin complex 2 (mTORC2) can also activate Akt at Ser473 which is required

for maximal Akt activation. Once Akt is activated, it triggers a diverse downstream signalling cascade which influences cell proliferation, migration and survival (Swat *et al* 2006; Akinleye *et al* 2013).

1.2.5 The regulation of PTEN activity

Many post-translational modifications including ubiquitination, acetylation, phosphorylation and oxidation have been reported to influence the activity of PTEN (Bermúdez Brito *et al* 2015). Moreover, the association of PTEN with the membrane through its interaction with several PDZ-containing proteins has been documented to enhance the stability, membrane localisation and the activity of PTEN (Bononi and Pinton 2015; Yang *et al* 2015). In particular, the role of membrane associated guanylate kinase with the inverted arrangements (MAGI) proteins in regulating the function and stability of PTEN has been highlighted as important (Hopkins *et al* 2014), thus the interaction of PTEN with MAGI proteins is discussed below.

1.3 Membrane-associated guanylate kinase with inverted orientation (MAGI)

MAGI proteins belong to the membrane-associated guanylate kinases (MAGUKs) family, a group of cell junction proteins which have been associated with the regulation of intercellular communication, signalling, cell polarity as well as synapse formation (Zhu *et al* 2011). MAGI proteins differ structurally from other MAGUK proteins (Figure 1.8) by having most of their PDZ domains located after the GK domain while most MAGUK proteins have their PDZ domains located at the N-terminal of the SH3-GK domain (González-Mariscal *et al* 2000). MAGI proteins have been reported to regulate cell adhesion by the assembly of multiprotein complexes at cell-cell contact and tight junctions (Padash Barmchi *et al* 2016; Bhat *et al* 2019). MAGI proteins are widely expressed in different tissues and are comprised of four members: MAGI-1, MAGI-2, MAGI-3, and MAGI-X. MAGI proteins are large adaptor proteins with a structure (Figure 1.8) that is characterised by a guanylate kinase (GUK) domain, two WW domains and six PDZ domains (Hammad *et al* 2016). These domains can form large protein

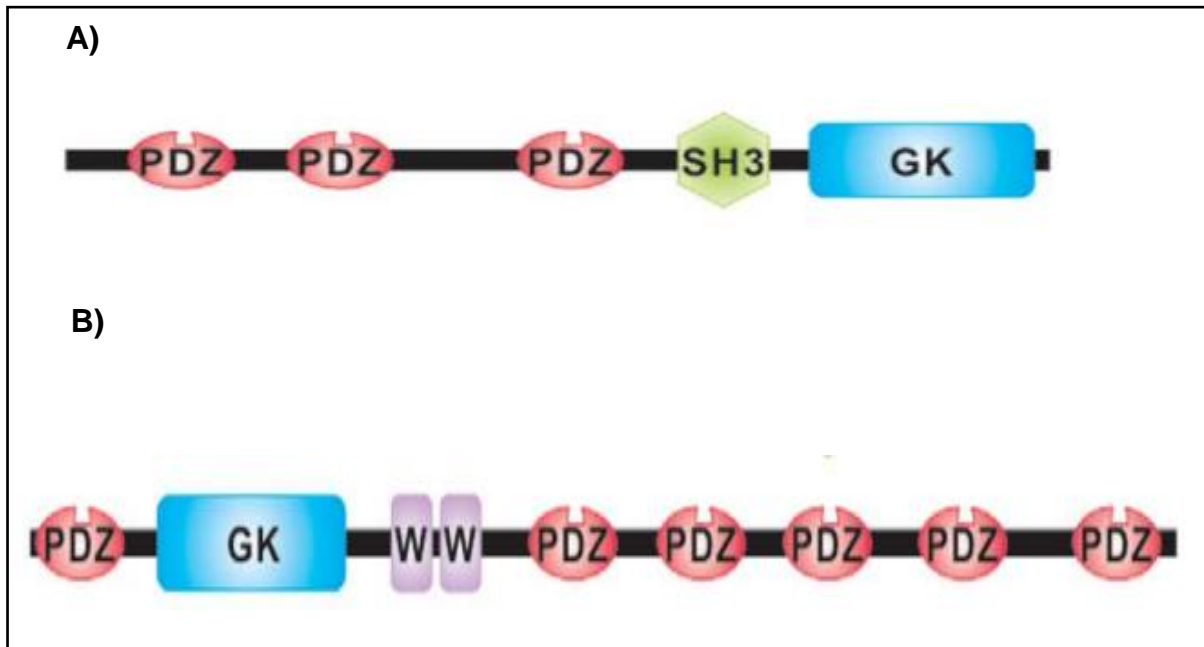


Figure 1. 8 Schematic representation of the structural domains of MAGI proteins. A) All MAGUK classes share the same domain architectures containing PDZ domains, followed by SH3 domain and GK domain. B) All members of the MAGI family share the same building structure with a PDZ domain at its N-terminus followed by guanylate kinase-homology (GK) domain, 2 WW domains (instead of the SH3 domain), followed by 5 PDZ domains (Adapted from Zhu *et al* 2011).

complexes and bind to different proteins simultaneously by interacting and recruiting proteins at cell-cell junctions in endothelial and epithelial cells (Gregorc *et al* 2012; Padash Barmchi *et al* 2016).

1.3.1 The role of MAGIs in the regulation of PTEN

The interaction of the 2nd PDZ domain (PDZ domain number 3 in Figure 1.8) of MAGI proteins with the PDZ domain within the C-terminal of PTEN has been documented previously (Mosessian and Wu 2010; Matsuda and Kitagishi 2013). Moreover, a number of studies have identified MAGI proteins as tumour suppressors due to their role in regulating PTEN activity (Feng *et al* 2014).

1.3.1.1 MAGI-1

MAGI-1, also known as BAP-1 (brain-specific angiogenesis inhibitor associated protein-1) is located on chromosome 3p14.1 and encodes a 164.5 kDa protein. MAGI-1 contains three splice variants, MAGI-1-a, MAGI-1-b, and MAGI-1-c, which are expressed in different tissues (Dobrosotskaya *et al* 1997; Nagashima *et al* 2015). A study by Kotelevets *et al* (2005) showed that MAGI-1 interacts and recruits PTEN and β -catenin, an adhesion protein, to the membrane through its the second and the fifth PDZ domain, respectively. The formation of MAGI-1-PTEN- β -catenin complex at the membrane of kidney cells resulted in enhanced stabilisation of cell-cell junctions which was mediated by β -catenin. The MAGI-1/PTEN/ β -catenin complex was also shown to influence cell invasiveness in kidney MDCKts-Src cells [Src mutated temperature-sensitive cells which adapt an invasive phenotype and lose cell-cell contacts at a specific temperature (Behrens *et al* 1993)]. The reduction in Src-induced invasiveness was mediated by PTEN through downregulation of Akt. This suggests that MAGI-1 may act as a cytoplasmic scaffolding protein by recruiting different proteins through its domains (Kotelevets *et al* 2005). Furthermore, transfection of HepG2 liver cancer cell line with MAGI-

1 cDNA resulted in enhanced reduction in cell migration and invasion through the upregulation of PTEN activity compared to non-transfected HepG2 cells. Therefore, it has been suggested that MAGI-1 interacts and regulates the function and activity of PTEN (Zhang and Wang 2011).

1.3.1.2 MAGI-2

MAGI-2, also known as S-SCAM (synaptic scaffolding molecule) is located on chromosome 7q21 and has two isoforms. MAGI-2 is identified as a neural isoform because it is mainly expressed in the brain and interacts with and assembles different cell adhesion proteins at synaptic junctions (Nagashima *et al* 2015). A study by Wu *et al* (2000) reported the interaction of MAGI-2 with PTEN enhanced PTEN stability and therefore increased its lipid-phosphatase activity. Moreover, it has also been documented that MAGI-2 recruits PTEN to the membrane which enhances the signalling properties of PTEN at the cell membrane (Tolkacheva *et al* 2001). Also, it has been shown that siRNA targeting PTEN resulted in Akt-dependent proliferation and migration of liver cancer cells (Hu *et al* 2007). However, the co-expression of MAGI-2 and PTEN has enhanced PTEN stability as well as inhibition of migration and proliferation of liver tumour cell through the suppression of PI3K-Akt pathway (Hu *et al* 2007).

1.3.1.3 MAGI-3

MAGI-3 is located on chromosome 1p13.2 and is widely expressed in various tissues (Adamsky *et al* 2003). MAGI-3, like MAGI-2, has also been documented to interact with PTEN and enhance the function and stability of PTEN (Wu *et al* 2000). For example, it was shown that MAGI-3 enhances the function of PTEN in glioma cells. This in turn modulates the signalling of PI3K/Akt thereby inhibiting the proliferation of these cells (Ma *et al* 2015). In a separate study, the inhibition of MAGI-3 resulted in a reduction of PTEN stability which promoted intestinal inflammation through the activation of PI3K-Akt pathway (Norén *et al*

2017). Therefore, it has been suggested that the expression of MAGI-3 and the subsequent upregulation of PTEN can modulate the progression of inflammatory bowel disease.

1.4 Aims

The role of TF in tissue haemostasis is well established. There is growing evidence that associates the signalling properties of TF with cellular homeostasis as well as carcinogenesis and cancer progression. The activation of PI3K-Akt pathway by TF-FVIIa-PAR2 complex was shown to influence various cellular functions under both physiological and pathological conditions. Since PTEN is the main regulator of the PI3K-Akt pathway, the first part of the study aimed to examine the mechanisms by which TF may influence the function of PTEN. In addition to its signalling properties, the cytoplasmic domain of TF contains a short sequence motif (ENSPL) which has been shown to interact with other proteins and subsequently regulate TF activity. Therefore, this study has also hypothesised that TF activity might be regulated through interactions with MAGI proteins. This interaction is envisaged to be mediated through the cytoplasmic domain of TF and a PDZ domain within MAGI. To examine these hypotheses, the objectives were planned as follows.

- To investigate the short-term influence of TF as well as the activation of cells by PAR2 across a panel of cancer cell lines, on the phosphorylation state of PTEN and the activities of both PTEN and Akt.
- To examine the influence of prolonged exposure of cells to TF, on PTEN antigen levels, Akt activity and the rate of cell proliferation.
- To examine the influence of PAR2 activation on the association between PTEN and MAGI proteins.
- To examine the cellular localisation and interaction of TF with MAGI proteins.

- To examine the regulation of TF activity by MAGI-1, and identify the interacting domains.
- To examine the influence of PAR2 activation on the interaction between TF and MAGI and the regulation of TF activity.

Chapter 2

Materials and methods

2.1 Materials

Abcam, Cambridge, UK

Human PTEN ELISA Kit

Donkey anti-goat IgG alkaline phosphatase antibody

ATCC, Teddington, UK

MDA-MB-231, MCF-7, T-47D, Caco-2, LoVo, AsPC-1, PANC-1 cell lines

Addgene, Watertown, USA

FLAG-HA-pcDNA3.1- plasmid

pDONR223-MAGI1 plasmid

Bio-Rad, Hemel Hempstead, UK

Mini Trans-Blot cell blotting system

Biomatik, Ontario, Canada

Synthesised biotinylated peptides form of TF cytoplasmic domain

BMG lab Tech, Offenburg, Germany

POLAR star OPTIMA Plate reader

Beckman Coulter, High Wycombe, UK

1.5 ml ultracentrifuge tube

TL-100 Ultracentrifuge

Creative-diagnostics, New York, USA

Mouse anti-MAGI2 monoclonal antibody (7G6)

Dade Behring, Liederbach, Germany

Innovin recombinant human tissue factor reagent (10X)

Echelon Biosciences Inc, Salt Lake City, USA

PTEN Activity ELISA

Enzo Life Sciences Inc, Exeter, UK

PKB (Akt) Kinase Activity ELISA Kit

Eurofin-MWG, Wolverhampton, UK

DNA sequencing

Fisher scientific, Loughborough, UK

Glycine, NaCl, Tris base Phosphate buffered saline (PBS) buffer solution, pH 7.4

Flowgen Bioscience, Nottingham, UK

ProtoFlowGel (acrylamide: bisacrylamide)

ProtoFlowGel resolving buffer

ProtoFlowGel staining buffer

Geneflow, Lichfield, UK

TransIT-2020

Tris-Borate-EDTA Buffer (10 X)

Greiner bio-one, Stonehouse, UK

6-well, 12-well and 24-well culture plates

T25 and T75 tissue culture flasks

<http://imagej.nih.gov/ij/>

ImageJ program

Insight Biotechnology Limited, Wembley, UK

Rabbit polyclonal anti-MAGI2 antibody

InVitro Scientific/Cellvis, Sunnyvale, USA

29 mm-glass based μ -dishes

Lonza, Basel, Switzerland

DMEM medium (4.5 g/L Glucose, with L-Glutamine)

EMEM medium (with L- Glutamine)

RPMI-1640 medium (with L- Glutamine)

Ham's F-12 (F-12K) medium

Merck-Millipore, Watford, UK

Pureproteome protein A-magnetic beads

Miltenyi Biotec, Woking, UK

FITC-conjugated anti-TF monoclonal antibody (HTF1-FITC)

New England Biolabs/ Cell signalling technologies, Hitchin, UK

PTEN polyclonal rabbit antibody

Phospho-PTEN (Ser380/Thr382/383) polyclonal rabbit antibody

Rabbit anti-HA tag antibody (C29F4)

Control rabbit IgG antibody

Control mouse IgG antibody

Monarch® Plasmid Miniprep Kit

Monarch® PCR & DNA Cleanup Kit

Quick dephosphorylation kit

*Bam*HI restriction enzyme

*Hind*III restriction enzyme

*Not*I restriction enzyme

*Eco*RI restriction enzyme

Quick load purple DNA ladder 1kb

Quick load purple DNA ladder 100 bp

Promega Corporation, Southampton, UK

Cell lysis reagent (5X)

Western Blue stabilised substrate for alkaline phosphatase

Midipreps DNA purification kit

R&D Systems/Novus, Abingdon, UK

Rabbit polyclonal anti-MAGI3 antibody

Monoclonal mouse anti-PTEN IgG antibody (217702)

Goat polyclonal anti-human JAM-A antibody

Sigma-Aldrich, Poole, UK

Ammonium persulfate

Antibiotic antimycotic solution (Penicillin – Streptomycin – Neomycin Solution) (100X)

37% Formaldehyde solution

Triton-X-100

Duolink® PLA kit

Mouse monoclonal Anti-FLAG M2 antibody

Bovine serum albumin (BSA), lyophilized powder

Bradford reagent

4',6-Diamidino-2-phenylindole dihydrochloride (DAPI)

Laemmli's lysis-buffer (2X)

N,N,N',N'-tetramethylethylenediamine (TEMED)

PAR2-Agonist Peptide

Trypsin

Tween-20

Crystal violet solution (1%)

Sodium dodecyl sulfate (SDS)

Santa Cruz Biotechnology, Heidelberg, Germany

Rabbit anti-MAGI1 IgG antibody (H-70)

Rabbit anti-human GAPDH polyclonal antibody (V-18)

Rabbit anti-TF polyclonal antibody (FL295)

Mouse anti-MAGI1 antibody (SS-5).

Goat anti-rabbit alkaline phosphatase-conjugated antibody

Goat anti-mouse alkaline phosphatase-conjugated antibody

Goat anti-mouse horseradish peroxidase-conjugated antibody

Goat anti-rabbit horseradish peroxidase-conjugated antibody

Scientific Laboratory Supplies Ltd, Hessle, UK

CO₂ incubator

SPSS Inc. Chicago, USA

Statistical Package for the Social Sciences

Thermo Fisher Scientific, Paisley, UK

Donkey anti-goat IgG-Alexa Fluor 594 antibody

Goat anti-rabbit IgG-Alexa Fluor 594 antibody

Foetal bovine serum (FBS)

Trypan blue solution dye

Thermo Scientific/eBioscience, Warrington, UK

Mouse anti-TF monoclonal antibody (HTF1)

NeutrAvidin-coated 96-well plates

SYBR™ Green I Nucleic Acid Gel Stain

PageRuler™ Plus Prestained Protein Ladder (10-260 kDa)

TCS Cellworks, Claydon, UK

DMSO Freeze medium (2X)

Yorkshire Bioscience, York, UK

DNA loading buffer (5X)

2.2 Methods

2.2.1 Cell culture

The culture of human cancer cell lines was carried out in class II laminar flow biosafety cabinet. Cancer cells from three different tissues were used in the first part of the investigation: breast cancer cell lines (MDA-MB-231, MCF-7 and T-47D), colorectal cancer cell lines (Caco-2 and LoVo) and pancreatic cancer cell lines (PANC-1 and AsPC-1). Prior to cell culture, all media and reagents were warmed in a water bath for approximately 30 min at 37°C. The safety cabinet including pipettes, medium bottles, tubes, flasks were sprayed with 70% (v/v) ethanol to sterilise the cabinet and plasticware. The cells were cultured in T75 flasks as follows: MDA-MB-231, Caco-2 and PANC-1 cells were cultured in DMEM (4.5 g/L Glucose, with L- Glutamine) medium. MCF-7 cells were cultured in EMEM (with L- Glutamine) medium. AsPC-1 and T-47D cells were cultured in RPMI-1640 (with L- Glutamine) medium. In addition, LoVo cells were cultured in Ham's F-12K (with L- Glutamine) medium. All media were supplemented with 10% (v/v) FBS and the cells were cultured in a humidified incubator under 5% CO₂ atmosphere at 37°C. The media were changed every 2-3 days until the cells had reached 85-90% confluency.

2.2.2 Harvesting, subculturing and counting of cells

Once the cells had reached 85-90% confluency, the medium was removed and the cells were washed twice with pre-warmed sterile PBS (5 ml) to remove any traces of FBS. The cells were incubated with 3 ml of pre-warmed trypsin and placed in the incubator for 5 min to allow detachment of the cells. The flask was gently tapped and the appropriate complete medium (5

ml) was added into the detached cells to inactivate the excess trypsin. The cell suspension was then transferred into a fresh 15 ml sterile polypropylene tube and centrifuged at 2,400 g for 5 min. The supernatant was discarded carefully and the pellet was re-suspended in the appropriate fresh medium (2 ml). To count the cells, a haemocytometer was used to determine cell density by loading 10 μ l of cell suspension mixed with 10 μ l of 0.4% (v/v) Trypan blue solution between the haemocytometer and the coverslip. The cell density was determined as follows;

The total cell number = [number of cells counted per square (mm^2) x the dilution volume x 10^4]. Aliquots of the cells were either used for cryopreservation, further cell culture or in experiments.

2.2.3 Cryopreservation and cell recovery

The pelleted cells were re-suspended and thoroughly mixed with 2 ml of pre-warmed dimethyl sulfoxide (DMSO) freezing medium. The cells ($2 \times 10^6/\text{ml}$) were transferred into labelled cryovials and placed in a freezing container filled with 100% (v/v) isopropanol. The container was placed at -70°C overnight to allow the gradual decrease in temperature which, together with DMSO, helps preserve the integrity of the cells. On the following day, the cryovials were transferred into liquid nitrogen, for long-term storage. To start a new batch of frozen cells, cryovials containing the cells were thawed for 1-2 min at 37°C and immediately transferred into a T75 flask containing the appropriate pre-warmed complete medium.

2.2.4 Activation of cells with rec-TF or PAR2-AP

The cells were seeded out in plates (e.g., 6 or 12-well plates) at different volumes depending on the experiment and cultured in the appropriate complete medium overnight. Prior to activation, the medium was removed and the cells were incubated for 60 min with fresh complete medium. The cells were then activated by the addition of rec-TF (0-1300 pg/ml) and

incubated at intervals for up to 120 min. To activate the cells with PAR2, the medium was removed and the cells were washed twice with pre-warmed PBS. The cells were incubated with serum free medium for 60 min and then activated by the addition of PAR2-agonist peptide (PAR2-AP) (SLIGKV-NH; 20 μ M) and incubated for up to 40 min. The medium was removed at intervals and the cells were washed twice with PBS. For western blot analysis, the cells were lysed in 2X Laemmli's buffer (0.125 M Tris-HCl, pH 6.8, 4% (w/v) SDS, 20% (w/v) glycerol, 10% (w/v) 2-mercaptoethanol, 0.004% (w/v) bromophenol blue) diluted 1:1 in dH₂O. The cell lysates were transferred into fresh 1.5 ml polyproptubes and heated for 10 min at 100 °C to denature the proteins. The samples were stored at -20 °C for further analysis.

For ELISA-based procedures, the cells were washed twice with PBS and then lysed in 200 μ l of ice-cold Phospho-Safe extraction buffer on a shaker for 5 min. The cell lysates were transferred into fresh 1.5 ml tubes and centrifuged for 5 min at 14,000 g, at 4 °C. The supernatants (100 μ l) were transferred into fresh pre-cooled 1.5 ml tubes and stored at -20°C for measurement of protein concentrations and activities.

2.3 Molecular biology techniques

2.3.1 SDS-polyacrylamide gel electrophoresis (SDS-PAGE)

A 12% (w/v) separating gel was prepared by mixing 3.3 ml of dH₂O, 100 μ l of 10 % (w/v) ammonium persulphate, 2.6 ml of resolving buffer (1.5 M Tris-HCl pH 8.8, 0.4% (w/v) SDS) and 4 ml of acrylamide solution (30% (w/v) acrylamide, 0.8% (w/v) bis-acrylamide). The solution was gently mixed and 8 μ l of TEMED was added to start the gel polymerisation. The solution was mixed thoroughly and poured between the electrophoresis glass plates in a gel caster and covered with a thin layer of 100% (v/v) butanol to remove any bubbles formed during the process and allowed to set for 60 min at room temperature. Once the gel was set, the butanol was poured off and the 4% (w/v) stacking gel was prepared by mixing 3 ml of dH₂O,

0.65 ml of acrylamide solution, 1.3 ml of stacking buffer (0.5 M Tris-HCl pH 6.8, 0.4 % (w/v) SDS), 10 µl of 10% (w/v) ammonium persulphate and finally 6 µl of TEMED. The solution was mixed thoroughly and poured on top of the resolving gel and the appropriate well-comb was inserted, again the gel was allowed to set for 60 min at room temperature. After the gel had solidified, the cassette was taken out of the gel caster and placed in the electrophoresis tank. The comb was removed and the electrophoresis tank was filled with running buffer (25 mM Tris-HCl pH 8.3, 192 mM glycine, 0.035% (w/v) SDS). A protein ladder (5 µl) (10-260 kDa) was loaded into the first well followed by the protein samples (15 µl). Electrophoresis was carried out at 95 V in a BioRad Tetra Tank until the solvent front had reached the bottom of the gel (Blancher and Jones 2001).

2.3.2 Western blot analysis

Following the electrophoresis, a transfer system was prepared as follows. First, the blotting (filter) papers and nitrocellulose membrane were soaked in transfer buffer (20 mM Tris-HCl, 150 mM glycine, 20 % (v/v) methanol, pH 8.3). The gel sandwich was assembled by placing the gel over the nitrocellulose membrane which was then placed between the blotting papers and sponges on both sides. The gel sandwich was placed into a gel cassette holder and transferred to a tank filled with transfer buffer. The proteins were allowed to transfer to the nitrocellulose membrane at 100 V for 60 min at 4°C. Once the proteins were transferred, the nitrocellulose membrane was blocked with TBST (20 mM Tris, 150 mM NaCl, 0.05 % (v/v) Tween 20, pH 7.4) buffer on a shaker for 60 min at room temperature. The nitrocellulose membrane was then incubated overnight with the appropriate primary antibody diluted (Table 2.1) in 10 ml of TBST at 4°C. On the following day, the membrane was washed three times (5 min each time) with TBST buffer and then incubated with an appropriate alkaline phosphatase conjugated secondary antibody (Table 2.1) in 10 ml of TBST in a shaker for 60 min at room

Table 2. 1 The dilutions of primary and secondary antibodies used in the western blot and co-immunoprecipitation procedures

Primary antibodies	Dilution antibodies: TBST (v/v)	Secondary antibodies	Dilution antibodies: TBST (v/v)
PTEN polyclonal rabbit antibody	1:2000	Goat anti-rabbit alkaline phosphatase-conjugated antibody	1:8000
Phospho-PTEN (Ser380/Thr382/383) polyclonal rabbit antibody	1:2000	Goat anti-rabbit alkaline phosphatase-conjugated antibody	1:8000
Rabbit anti-human GAPDH polyclonal antibody	1:6000	Goat anti-rabbit alkaline phosphatase-conjugated antibody	1:8000
Mouse anti-TF monoclonal antibody	1:4000	Goat anti-mouse alkaline phosphatase-conjugated antibody	1:8000
Rabbit anti-MAGI-1 IgG antibody (H-70)	1:2000	Goat anti-rabbit alkaline phosphatase-conjugated antibody	1:8000
Rabbit anti-HA tag antibody	1:2000	Goat anti-rabbit alkaline phosphatase-conjugated antibody	1:8000

temperature. The membrane was washed three times with TBST and the bands were developed with Western Blue-stabilised substrate for alkaline phosphatase; the pattern of bands was analysed using ImageJ software.

2.3.3 Examination of cell proliferation using the crystal violet assay

The crystal violet assay is a common method used to determine cell viability of adherent cultured cells. The dye binds to adherent cells causes the cell to stain blue while dead cells detached from the cell culture plate and washed away. The dye can then be eluted out using SDS and the amount of dye taken up by the cells is measured at 584 nm using a POLARstar OPTIMA plate reader (Feoktistova *et al* 2016).

To perform the assay, MDA-MB-231, Caco-2 and LoVo cells (2×10^4) were seeded out in 6-well plates and incubated overnight in complete media. On the following day, the media were discarded and the cells were washed three times with PBS. The cells were fixed with 3 % (w/v) glutaraldehyde diluted in PBS for 15 min and then washed three times with dH₂O. The cells were incubated with 0.5% (v/v) crystal violet solution diluted in 10% (v/v) ethanol for 20 min on a shaker. The cells were washed three times with dH₂O and the crystal violet stain was then eluted out with 1% (w/v) SDS in dH₂O, and the plates were incubated on a shaker for 15 min. Aliquots (100 μ l) were added into a 96-well plate and the absorption values were measured at 584 nm using a POLARstar OPTIMA plate reader. A separate stand curve for each cell line was constructed by seeding out cells individually at different volumes at a range of 5-25 $\times 10^4$ cells/well.

2.3.4 Estimation of protein concentration using the Bradford assay

To determine the protein concentration in cell lysates, a standard curve was constructed by preparing a serial dilution of lipid-free BSA (0-200 μ g/ml). The standards and the protein samples (20 μ l) were pipetted into a 96-well plate and 200 μ l of Bradford reagent (Coomassie

G-250 Bradford reagent stock diluted 1:1 (v/v) with dH₂O) was added into each well. The plate was incubated for 15 min in the dark and the absorption values were measured at 584 nm using a plate reader. The absorption readings from the standards were used to calculate a standard curve from which the unknown cell lysate protein concentrations could be calculated (Figure 2.1).

2.3.5 *In situ* examination of protein interaction using the proximity ligation assay (PLA)

The Duolink[®] proximity ligation assay (PLA) is an antibody-based procedure for the analysis of protein-protein interactions *in situ*. The procedure is based on the recognition of two target proteins by specific antibodies raised in two different species (Collier *et al* 2014; Clausson *et al* 2015; Debaize *et al* 2017). The assay employs species-specific secondary antibodies coupled to oligonucleotides (termed as plus and minus probes) directed against the primary antibodies. The connector oligonucleotides attached to the antibody probes hybridise only if the target proteins are within 40 nm of each other and a ligase joins the PLA probes to produce a closed circular DNA template. In the DNA circle, one of the antibody conjugated DNA probes serves as a primer for the rolling circle amplification (RCA). A polymerase is then added to generate repeated complementary sequences using one of the probes as a template. The fluorescently labelled oligonucleotides hybridise to the repeated complementary sequences and generates the signal which can be visualised as red dots by fluorescence microscopy (Figure 2.2). To perform the PLA assay, MDA-MB-231 cells (10^3) were seeded into 35 mm-glass based μ -dishes with 10 mm well size, and grown in complete medium overnight. On the following day, the medium was removed and the cells were washed twice with PBS. The cells were then fixed with 4% (v/v) formaldehyde in PBS for 20 min. The cells were washed twice with PBS and then permeabilised using 0.1% (v/v) Triton X-100 in PBS for 10 min. The cells were washed twice with PBS and then blocked with Duolink[®] blocking solution for 60 min at 37°C. The blocking

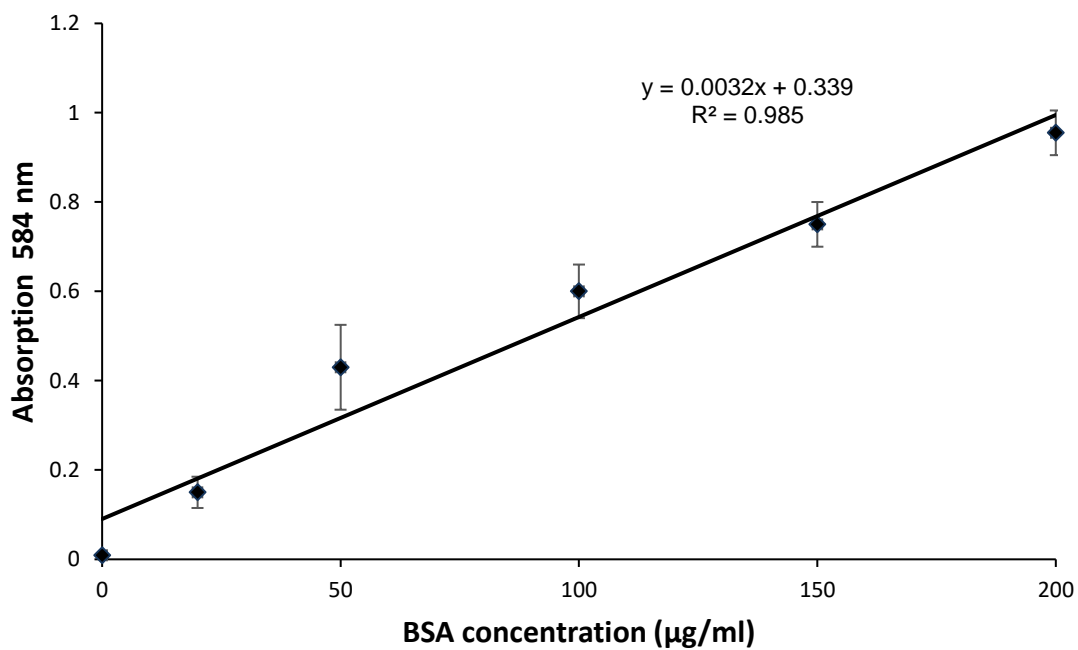


Figure 2. 1 Representative standard curve for Bradford assay. The standard curve was prepared by serially diluting lipid-free BSA (0-200 µg/ml) in dH₂O. The standards (20 µl) were placed in a 96-well plate and mixed with 200 µl of Bradford reagent. The plate was incubated in the dark for 15 min at room temperature and the absorption values were measured at 584 nm using a plate reader.

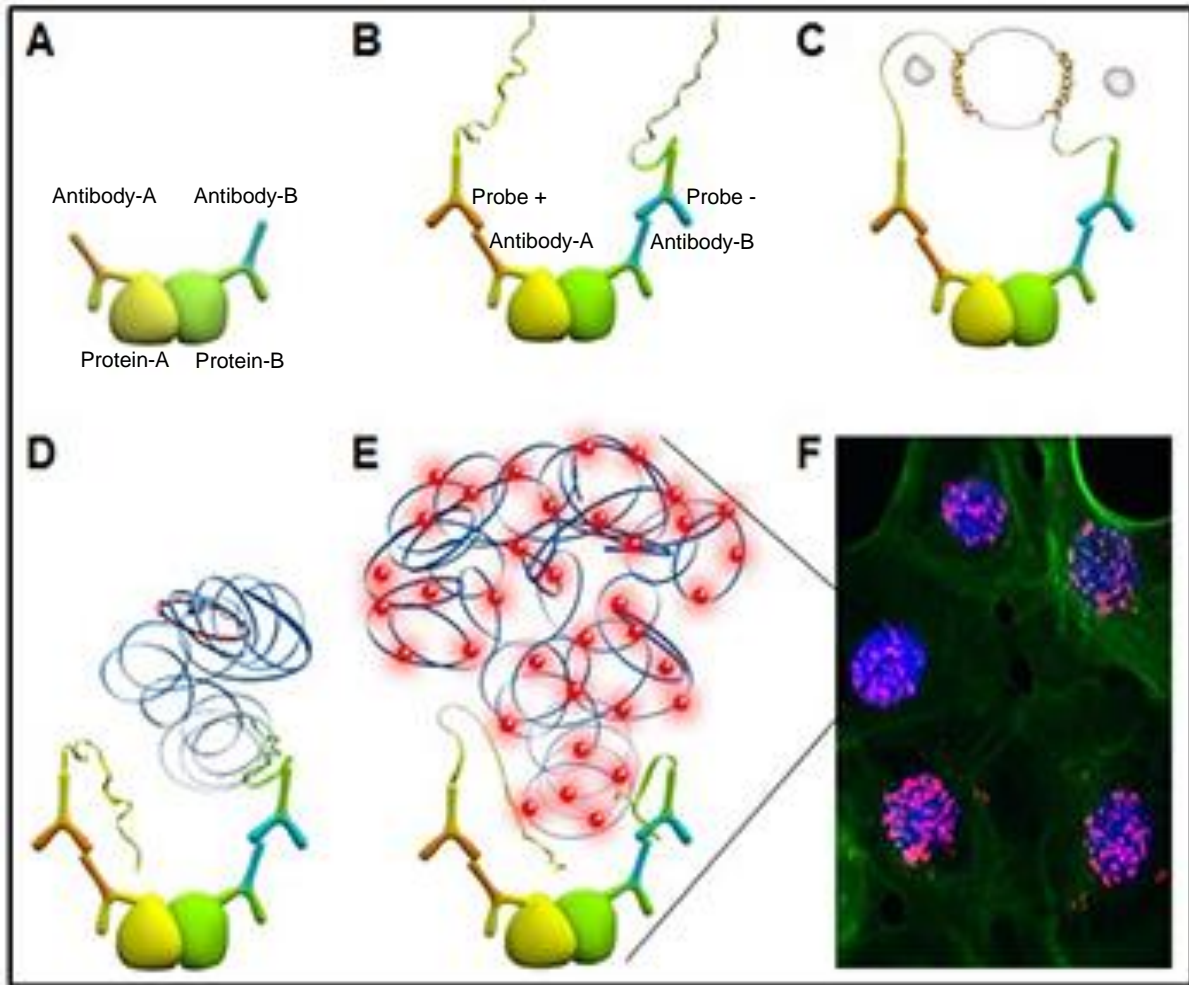


Figure 2. 2 Schematic diagram of a PLA reaction A) Two primary antibodies are used to bind to two target proteins under investigation. B) The secondary antibodies are tagged with small complementary oligonucleotides (plus and minus probes) which specifically recognise the IgG from the species which the primary antibodies were derived from. C) Connector oligonucleotides attach to the probes and a circular DNA is generated when both PLA probes are hybridised by a ligase. D) The closed circular DNA template is amplified by DNA polymerase. E) Fluorescently-labelled complementary oligonucleotide binds to the repeated complementary sequences within the amplified DNA. F) PLA signal is visualised by fluorescence microscopy (Adapted from Merck 2020).

solution was discarded and the cells were incubated overnight at 4°C, with both primary antibodies diluted 1:100 (v/v) in the provided antibody diluent. On the following day, the wells were washed twice for 5 min each, with buffer A (0.01 M Tris, pH 7.4, 0.15 M NaCl and 0.05% (v/v) Tween 20) and then incubated with the plus and minus probes (each probe was diluted 1:5 (v/v) in the antibody diluent) for 60 min at 37°C to allow hybridisation. The wells were washed twice for 5 min each with buffer A and then incubated with the ligation solution (1:40 (v/v) ligase diluted in ligation buffer) for 30 min at 37°C. After the ligation, the wells were washed twice again with buffer A for 2 min each and then incubated in the dark with the DNA amplification solution (1:80 (v/v) DNA polymerase diluted in the amplification buffer containing fluorescently labelled oligonucleotides) for 140 min at 37°C. The wells were washed twice for 10 min each with buffer B (0.2 M Tris, pH 7.5 and 0.1 M NaCl) then twice with 0.01% buffer B. The wells were incubated with DAPI (2 µg/ml) and Alexa Fluor™ 488 Phalloidin (2 µg/ml) in the dark for 10 min and then washed twice with 0.01% buffer B. Images were acquired using a Zeiss Axio Vert.A1 inverted fluorescence microscope with a X40 magnification. The number of red fluorescent events were determined in 10 fields of view from each assay using the ImageJ software.

2.3.6 Examination of protein interaction by co-immunoprecipitation

MDA-MB-231 cells (5×10^5) were seeded into 6-well plates in complete medium overnight. On the following day, the medium was removed and the cells were incubated with serum-free medium for 60 min prior to activation. The cells were then activated with PAR2-AP depending on the experiments as described in each result chapter. After the appropriate stimulation cells were washed twice with ice-cold PBS and then lysed with Phospho-Safe™ extraction buffer (500 µl). The plates were incubated on ice for 10 min on a shaker. The cell lysates (500 µl) were transferred into fresh 1.5 ml Eppendorf polypropylene tubes and incubated with a primary antibody (8 µg) overnight using a rotating mixer at 4°C. On the following day, the antibody in

the cell lysates was captured by the addition of protein A-magnetic beads (100 μ l) diluted in TBST, and was further incubated for 120 min on a rotating mixer at 4°C. The tubes were then placed into the PureProteome magnetic stand, allowing the beads to migrate towards the magnet. The supernatant was discarded and the beads were washed with TBST (1 ml), vortexed and then returned to the magnetic stand to allow the beads to migrate to the magnet gain. TBST was pipetted out and the washing step was repeated five times. To denature the proteins, the beads were lysed in 2X Laemmli's buffer (15 μ l) for 10 min in a heating block at 100°C. The beads were then removed from the tubes using the magnetic stand and discarded. The immunoprecipitated protein samples were separated by SDS-PAGE, transferred to nitrocellulose membranes and blocked as described in section (2.3.2). To avoid any cross reaction, the nitrocellulose membrane was probed overnight at 4°C with a primary antibody raised in a different species (Table 2.1) than the antibody used to capture the target protein. The membrane was washed three times with TBST and then probed with an appropriate alkaline phosphatase conjugated secondary antibody diluted in 10 ml TBST. The bands were developed with Western Blue-stabilised substrate for alkaline phosphatase, photographed and analysed using the ImageJ software.

2.4 Bacterial cell culture and plasmid isolation

2.4.1 Agar selection plates preparation

To prepare agar plates containing Carbenicillin antibiotic (0.1 mg/ml), the Luria Broth agar powder (6.25 g) was dissolved in 250 ml of dH₂O and then autoclaved for 20 minutes at 120 °C. The 1% (w/v) agar medium was cooled down to approximately 55°C and 120 μ l of Carbenicillin antibiotic was added to the media and mixed thoroughly. The LB agar medium (25 ml) was poured into a 75 mm Petri dishes and allowed to solidify in a sterile environment at room temperature. The plates were then sealed and stored at 4°C for further use.

2.4.2 Bacterial cell culture

To prepare the LB broth medium, the LB broth powder (17.5 g) was dispersed in 500 ml of dH₂O, autoclaved and then stored at room temperature. *E. coli* containing pDONR223-MAGI1 or FLAG-HA-pcDNA3.1 DNA plasmids were incubated in sterilised 50 ml tubes containing the LB broth medium (10 ml) in a shaking incubator overnight at 37°C. On the following day, the tubes were centrifuged for 5 min at 12,000 g to pellet the bacteria for DNA isolation or cryopreservation.

2.4.3 Cryopreservation of bacterial cell

In order to prepare stocks of transformed *E. coli*, freezing solution was prepared by mixing 20% (w/v) glycerol with 50 ml of the LB broth media and sterilised by filtering through a 0.22- μ m syringe filter. The isolated bacterial pellets were re-suspended in the sterilised freezing solution and aliquots (300 μ l) were transferred into fresh Eppendorf tubes and stored at -70°C for long term storage.

2.4.4 Isolation of plasmid DNA using the Monarch plasmid Miniprep kit

To extract the DNA from bacteria containing pDONR223-MAGI1/ FLAG-HA-pcDNA3.1 plasmid DNA, pelleted bacteria were re-suspended in the provided resuspension buffer (200 μ l) and vortexed until the cells were completely dispersed. Lysis buffer (200 μ l) was added to each tube, mixed and then incubated for 1 min at room temperature. The lysates were then neutralised by the addition of 400 μ l of the provided neutralisation buffer. The tubes were gently mixed, incubated for 2 min at room temperature and then centrifuged for 5 min at 12,000 g. The supernatants were carefully transferred into the provided spin columns and centrifuged for 1 min at 12,000 g. The flow-through was discarded and the columns were inserted back into the collection tubes. The columns were washed with 200 μ l of the provided wash buffer 1 and centrifuged for 1 min at 12,000 g. The flow-through was discarded and the columns were

washed twice with 400 μ l of the provided wash buffer 2 and centrifuged for 4 min at 12,000 *g* to remove any traces of ethanol. The columns were then transferred into clean 1.5 ml tubes and elution buffer (30 μ l) was added to the centre of each column and incubated for 1 min. To elute the DNA, the columns were centrifuged for 1 min at 12,000 *g* and the DNA samples were stored at -20°C for further use.

2.4.5 Isolation of plasmid DNA using the Wizard plus Midiprep kit

To prepare large quantities of the plasmid DNA, bacterial pellets containing pDONR223-MAGI1/ FLAG-HA-pcDNA3.1 plasmid DNA were re-suspended in 3 ml of the provided re-suspension buffer (50 mM Tris-HCl pH 7.5, 10 mM EDTA, 100 μ g/ml RNase A). The bacteria were lysed in 3 ml of the provided lysis buffer (0.2 M NaOH, 1% (w/v) SDS) and gently mixed and then neutralised by adding 4 ml of the provided neutralising buffer (1.32 M potassium acetate pH 4.8). The tubes were gently mixed and centrifuged at 3,000 *g* for 10 min and the supernatants were transferred into a fresh 15 ml tube and centrifuged again at 3,000 *g* for another 10 min to remove any remaining debris. The supernatants were transferred and mixed with 10 ml of the provided re-suspension resin in the provided midiprep columns and cleared through under vacuum. The columns were washed with 15 ml of the provided wash buffer (8.3 mM Tris-HCl pH 7.5, 80 mM potassium acetate, 40 μ M EDTA, 55% (v/v) ethanol) and cleared through under vacuum. The lower column sections containing the DNA binding-resin were separated from the reservoirs and transferred into 1.5 ml Eppendorf tubes. The tubes were centrifuged at 12,000 *g* for 4 min to remove any residual wash buffer. To elute the DNA, DNase-free water (300 μ l) was added to each column and incubated for 1 min at room temperature. The tubes were then centrifuged at 12,000 *g* for 1 min and the eluted DNA was stored at -70°C for long-term storage.

2.4.6 Examination of the plasmid DNA by agarose gel electrophoresis

Agarose gel electrophoresis was used to examine the isolated plasmid DNA. To prepare a 1% (w/v) agarose gel, 0.5 g agarose was dispersed with 50 ml of TBE buffer (Tris-borate pH 8.3, 89 mM boric acid, 2 mM EDTA) and thoroughly mixed. The mixture was heated in a microwave oven until dissolved, and poured into a gel tray and an appropriate well comb was inserted and the gel was allowed to solidify. The DNA ladder (8 µl) was mixed with 1 µl of 0.1% (v/v) SYBR Green I and loaded into the first well. The DNA samples (10 µl) were also pre-stained with 1 µl of 0.1% (v/v) SYBR Green I and mixed with the loading buffer (10 µl) and loaded into separate wells. Electrophoresis was carried out at 100 V for approximately 90 min and the bands were examined on a UV transilluminator and photographed.

2.4.7 Ethanol precipitation of DNA

The plasmid DNA was precipitated by mixing 200 µl of 5 M sodium acetate (pH 5.2) with 800 µl of 100% (v/v) ethanol. The DNA samples were incubated at -20°C for 60 min and then centrifuged at 12,000 g for 20 min in a microcentrifuge to pellet the DNA. The pelleted DNA was washed with 75 % (v/v) ice-cold ethanol and centrifuged at 12,000 g for a further 10 min. The precipitated DNA was finally re-suspended in 100 µl of nuclease-free water and the concentration of the DNA measured at 260 nm using a spectrophotometer.

2.4.8 Determination of plasmid DNA concentration and purity

The concentration of the eluted plasmid DNA was determined by measuring the absorption of 1:10 dilution (v/v) of the DNA at 260 nm according to the following formula:

DNA concentration (µg/ml) = [Absorption (260 nm) x dilution factor x 50].

The DNA purity in a sample was determined by measuring the ratio of A_{260}/A_{280} . A ratio of (1.8 – 2) was determined as sufficiently pure (Glaseel 1995).

2.4.9 Statistical analysis

The data shown represent the mean value from the number of experiments \pm the standard deviation (SEM). The one-way ANOVA procedure was used to determine significant differences in the variance when data were compared to the control using the Statistical Package for the Social Sciences (SPSS) program.

Chapter 3

**Activation of PAR2 by tissue factor regulates PTEN
and Akt activities by inducing the release of PTEN
from MAGI proteins**

3.1 Introduction

The link between TF and aggressive cancer types is well established (Schaffner and Ruf 2009; Liu *et al* 2011). The intracellular signalling arising from TF is suggested to be induced through the binding to FVIIa which in turn activates PAR2 signalling (Coughlin 2005; Rothmeier and Ruf 2012). The TF-FVIIa-PAR2 complex signals through a number of key signalling pathways associated with tumour progression including the MAPK/ERK and the PI3K-Akt pathways (Åberg and Siegbahn 2013; Hu *et al* 2013) which have been associated with cell survival, proliferation and migration (Rak *et al* 2008; Schaffner *et al* 2009). Furthermore, a number of studies have reported the association of the Akt pathway with TF expression (Jiang *et al* 2006; Åberg *et al* 2013). For example, Rong *et al* (2005) reported that the loss of PTEN in conjunction with hypoxic conditions, increased the expression of TF through the activation of the Akt pathway. Moreover, the inhibition of the PI3K/Akt pathway results in the reduction of TF expression together with a slower growth rate in breast and ovarian tumour cells (Yu *et al* 2005; Hu *et al* 2012). Conversely, the correlation between TF expression and the upregulation of the Akt signalling has also been documented (Åberg *et al* 2013). TF has been reported to mediate angiogenesis through the activation of Akt pathway (Arderiu *et al* 2012). In neuroblastoma cells, the activation of TF signalling was shown to enhance cell survival through the enhancement of Akt pathway (Fang *et al* 2008). Also, TF has been shown to prevent cell apoptosis in serum-starved breast tumour cells through the activation of the Akt pathway (Jiang *et al* 2006). In addition, PAR2 signalling has been shown to enhance or suppress Akt signalling (Arderiu *et al* 2013). For instance, in glioblastoma cells PAR2 activation promoted cell survival through the activation of Akt signalling (Dutra-Oliveira *et al* 2012). Moreover, PAR2 signalling initiated by TF-FVIIa was shown to increase the rate of proliferation in breast cancer cells mediated through the PI3K-Akt pathway (Jiang *et al* 2006) and enhanced migration and invasion of kidney tumour cells (Sun *et al* 2015). Also, in patients diagnosed with head and

neck cancer, PAR2 expression was associated with enhanced cell proliferation and invasion through the activation of the PI3K-AKT pathway (Tang *et al* 2019). In contrast, PAR2 activation has also been reported to inhibit the PI3K-Akt activity mediated through β -arrestin-dependent signalling, leading to a decrease in cell migration in breast cancer cells (Wang and DeFea 2006). Additionally, PAR2 signalling has been reported to increase inflammation in kidney cells by suppressing the PI3K-Akt pathway (Du *et al* 2017). PTEN acts as one of the key regulators of the PI3K-Akt pathway and has been identified as a tumour suppressor (Pendurthi and Rao 2002; Eisenreich *et al* 2016). Therefore, the loss of PTEN has been strongly associated with many types of human cancers (Wu *et al* 2000; Milella *et al* 2015). The activity of PTEN itself, has been suggested to be regulated through its phosphorylation/de-phosphorylation state (Figure 1.6). Moreover, it has also been reported that the recruitment and activation of PTEN to the membrane is mediated through the binding to membrane-associated guanylate kinase with inverted configuration MAGI proteins (Wu *et al* 2000; Li *et al* 2015). To date, four MAGI proteins have been identified MAGI(1-3) and MAGI-X. MAGI(1-3) have been reported to interact with PTEN (Wu *et al* 2000; Li *et al* 2015). However, currently no direct evidence for the interaction between PTEN and MAGI-X exists. The association of PTEN with MAGI proteins has been implicated in the control of cell migration and invasion through enhancing the activity of PTEN and modulating Akt signalling (Wu *et al* 2000; Li *et al* 2015). Also, it has been reported that upon de-phosphorylation, MAGI proteins bind to PTEN to form a complex on the inner cell membrane, and that this interaction is mediated through PDZ-domain interaction (Tolkacheva *et al* 2001; Hu *et al* 2007).

3.1.1 Aims

Acute inflammation as a response to injury, infection or trauma can activate the coagulation as well as the signalling mechanisms by exposing TF at the site of injury. The formation of the TF-FVIIa-PAR2 complex at the cell surface regulates diverse cellular functions through the

activation of multiple signalling pathways including the PI3K-Akt pathway. However, under chronic inflammation the TF-FVIIa-PAR2 complex can signal through the PI3K-Akt pathway leading to carcinogenesis and cancer. Therefore, in this part of the study it was hypothesised that the local concentration of TF may influence the function of PTEN and subsequently Akt activity. To test this hypothesis, seven cancer cells lines were exposed to exogenous TF to investigate the influence of TF concentrations and exposure time on the function of PTEN.

This was carried out by measuring:

- the phosphorylation state of PTEN.
- the lipid-phosphates activity of PTEN.
- the cellular levels of PTEN antigen.
- the kinase activity of Akt.
- the rate of cell proliferation in cells exposed to multiple-dosages of exogenous TF.
- the influence of PAR2 activation on the phosphorylation state of PTEN and the activities of both PTEN and Akt.
- the influence of PAR2 activation on the association of PTEN and MAGI proteins.

3.1 Methods

3.2.1 Activation of cells and preparation of cell lysate

MDA-MB-231, MCF-7, T-47D, LoVo, CaCo-2, PANC-1 and AsPC-1 cells (2×10^5) were seeded out into 6 well plates and propagated to 80% confluency. The media were discarded and the cells were incubated in fresh complete media (1 ml). The cells were incubated with rec-TF (0-1300 pg/ml) for up to 120 min. To study the influence of PAR2 activation on cells, separate sets of cells were incubated with to serum-free medium for 60 min prior to activation. The cells were then activated with PAR2-agonist peptide (PAR2-AP; SLIGKV; 20 μ M) for 30

min. The media were discarded and the cells were washed twice with PBS. The cells were prepared for further experiments as follows:

For western blot analysis, the cells were lysed in Laemmli's buffer as described in section 2.2.4. To denature the proteins, the cell lysates were transferred into fresh (1 ml) tubes and were heated at 100 °C for 10 min. The samples were then stored at -20°C for further analysis by western blot. For measurement of protein levels and activities by ELISA-based methods, the cells were lysed in ice-cold Phospho-Safe extraction buffer as described in section 2.2.4. The cell lysates were transferred into 1.5 ml tubes and centrifuged for 5 min at 14,000 g, at 4 °C. The supernatants were transferred into fresh pre-cooled 1.5 ml tubes and stored at -20°C for further measurements of protein antigen or activity.

3.2.2 Determination of PTEN phosphorylation using western blot analysis

The expression of phosphorylated PTEN in the seven cancer cell lines was examined by western blot as described in section 2.3.2. The protein samples were separated by 12% (w/v) SDS-PAGE, transferred onto nitrocellulose membranes and blocked with TBST (10 mM Tris-HCl pH 7.4, 150 mM NaCl, 0.05% (v/v) Tween-20). The membranes were probed with a rabbit anti-human phosphoSer380/Thr382/Thr383-PTEN antibody, or a rabbit anti-human PTEN antibody diluted 1:2000 (v/v) in TBST or a rabbit anti-human GAPDH polyclonal antibody (V-18) diluted 1:8000 (v/v) in TBST, overnight at 4 °C. The membranes were then washed with TBST and probed with a secondary goat anti-rabbit alkaline phosphatase conjugated antibody diluted 1:8000 (v/v) in TBST, for 60 min. The bands were developed with Western Blue-stabilised substrate for alkaline phosphatase and photographed.

3.2.3 Determination of PTEN lipid-phosphatase activity using an ELISA-based kit

The principle of this Echelon Biosciences ELISA-based assay is to detect PTEN lipid-phosphatase activity in the cell lysate, by measuring the hydrolysis of substrate PIP3 to PIP2

(Guo *et al* 2016). The lysate samples are mixed with the PIP3 substrate to permit PTEN to catalyse the conversion of PIP3 to PIP2. The reactions are then stopped and loaded into the provided PIP2 coated 96-well plate. The PIP2 detector protein is then added to allow competitive binding to both the immobilised and lysate PIP2. The plate is then washed and the binding of the PIP2-binding protein to the plate is then measured using a secondary HRP-conjugated detector and developed by adding TMB substrate. As a result, the signal measured is inversely proportional to the amount of PIP2 produced by PTEN and therefore the lipid-phosphatase activity calculated from a standard curve. To perform the assay, all reagents were equilibrated to room temperature before use and prepared according to the manufacturer's protocol. The lysate samples (6 μ l) were mixed with PTEN reaction buffer (6 μ l) and pipetted into a 96-well plate. The PIP3 substrate (12 μ l) was added to each sample and the plate was incubated at 37 °C for 3 h to allow the conversion of PIP3 to PIP2. The reactions were then terminated by adding the stop solution (60 μ l). To measure the generated PIP2, 60 μ l from each reaction was transferred into the PIP2 coated 96-well plate provided with the kit. The PIP2 detector protein (60 μ l) was added to each sample and the plate was incubated at 37 °C for 60 min on a plate shaker. The solution was then discarded and the wells were washed three times with PBST (200 μ l). 100 μ l of the HRP-conjugated detector diluted 1:60 with PBST was added to each well and the plate was incubated at room temperature for 30 min. The solution was discarded and the wells were washed three times with PBST (200 μ l). TMB substrate (100 μ l) was added to each well and the plate was incubated in the dark for 15 min. The reactions were then terminated by adding 0.16M sulphuric acid stop solution (50 μ l) and the absorption values were measured at 450 nm using a plate reader. A standard curve for PTEN lipid-phosphatase activity was constructed by preparing a serial dilution of PIP2 protein (0-200 pmol). The absorption readings from the standards against protein concentrations were used to determine the equation to calculate the absorption values of the protein samples (Figure 3.1).

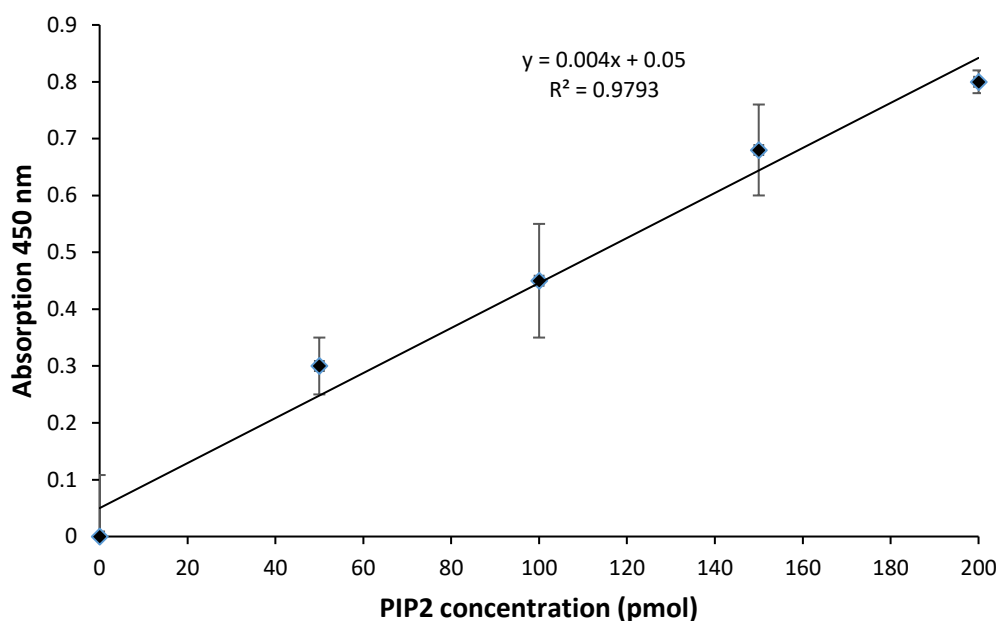


Figure 3. 1 Standard curve for PTEN activity. A serial dilution of PIP2 standard was made to prepare range of concentrations (0-200 pmol). The standard samples (60 μ l) were loaded into the PIP2 coated 96-well plate followed by the PIP2 detector protein (60 μ l). The plate was incubated at 37 $^{\circ}$ C for 60 min and the wells were washed three times with PBST (200 μ l). The HRP-conjugated detector (100 μ l) was added to each well and the plate was incubated at room temperature for 30 min. The wells were washed three times with PBST (200 μ l) and then incubated with TMB substrate (100 μ l) in the dark for 15 min. The reactions were stopped by adding the stop solution (50 μ l) and the absorption values were measured at 450 nm using a plate reader.

3.2.4 Measurement of Akt kinase activity by ELISA

The principle of this Enzo Life Sciences ELISA-based assay is to determine the kinase activity of Akt in lysates using a 96-well plate pre-coated with a substrate peptide, which is readily phosphorylated by Akt (Shervington *et al* 2015). A polyclonal phospho-specific antibody is then added which binds to the phosphorylated form of the substrate peptide in the cell lysates. An HRP-conjugated secondary antibody is then added to each well which binds to the phospho-specific antibody. The assay is developed with TMB substrate and the produced kinase activity of Akt is proportional to the colour produced. To perform the assay, all reagents were equilibrated at room temperature before the assay, except for the Akt recombinant protein which was kept on ice until use. The pre-coated 96 well plate was pre-incubated with the kinase dilution buffer (50 μ l) for 10 min at room temperature. The solution was discarded and the protein samples (30 μ l) were added to each well. The reaction was initiated by adding the (2 mg) ATP solution (10 μ l). The plate was incubated at 30°C for 90 min to permit the phosphorylation of the substrate by Akt. The solution was then discarded and the wells were washed three times with PBST (100 μ l). The phospho-specific antibody (40 μ l) was added to each well. The plate was sealed with adhesive strip and incubated for 60 min to allow the binding to the phosphorylated substrate. The solution was discarded and the wells were washed three times with PBST (100 μ l). The detecting secondary antibody (anti-rabbit IgG: HRP conjugate diluted with 1:1000 (v/v) antibody diluent) was added into each well (40 μ l) and the plate was sealed with adhesive strip and incubated for a further 30 min. The wells were then washed three times with PBST (100 μ l) and incubated with TMB substrate (60 μ l) for 30 min in the dark. The reactions were stopped by adding 10% (v/v) sulphuric acid stop solution (20 μ l) and the absorption values recorded at 450 nm using a plate reader. A standard curve for Akt kinase activity was constructed by preparing a serial dilution of recombinant Akt protein (0-5

μM). The absorption readings from the standards against protein concentrations were used to determine the equation to calculate the absorption values of the protein samples (Figure 3.2).

3.2.5 Analysis of cellular PTEN antigen by ELISA

The principle of this Abcam PTEN antigen ELISA-based assay is that it employs a tag capture antibody against PTEN and a conjugated anti-PTEN detector antibody which are added to the cell lysates. The capture antibody binds to an anti-tag antibody which has been pre-coated within the wells. The capture antibody and the HRP-conjugated detector antibody both bind to the target protein (PTEN). The assay is then developed with TMB substrate and the measured colour is proportional to the amount of PTEN protein present.

To perform the assay, all reagents were equilibrated at room temperature before the assay. The lysate samples (50 μl) were pipetted into the pre-coated 96 well plate provided with the kit. The capture antibody (300 μl) and the detector antibody (300 μl) were both mixed together with the antibody diluent (2.4 ml). The antibody cocktail (50 μl) was then added and the plate was sealed with an adhesive strip and incubated for 60 min on a plate shaker. The solution was discarded and the wells were washed three times with PBST (350 μl). The plate was blotted against paper towel to remove any excess liquid. TMB substrate (100 μl) was added to each well and the plate was incubated for 15 min in the dark. Once the colour had developed, the reactions were terminated by adding 0.16M sulphuric acid stop solution (100 μl). The absorption was recorded at 450 nm using a plate reader. A standard curve for PTEN antigen was constructed by preparing a serial dilution of recombinant PTEN protein (80 ng/ml) was reconstituted. The absorption readings from the standards against protein concentrations were used to determine the equation to calculate the absorption values of the protein samples (Figure 3.3).

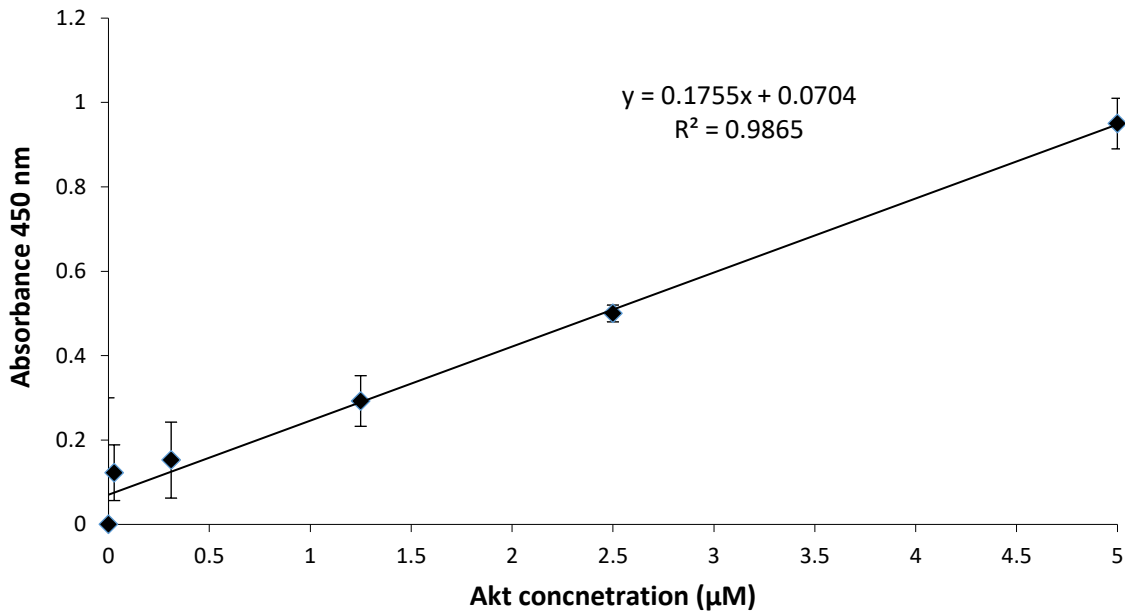


Figure 3. 2 Standard curve for Akt kinase activity. A standard curve was prepared by making serial dilutions (0-5 μM) of recombinant Akt protein diluted in the kinase assay buffer. The standard samples (30 μl) were added into a 96-well plate followed by the ATP solution (10 μl). The plate was incubated for at 30°C for 90 min. The phospho-specific antibody (40 μl) was added to each well and the plate was incubated for 60 min. The wells were then washed with PBST and incubated with 40 μl of the detecting secondary antibody for 30 min. The wells were washed with PBST and then incubated with TMB substrate (60 μl) for 30 min in the dark. The absorption values were recorded at 450 nm using a plate reader.

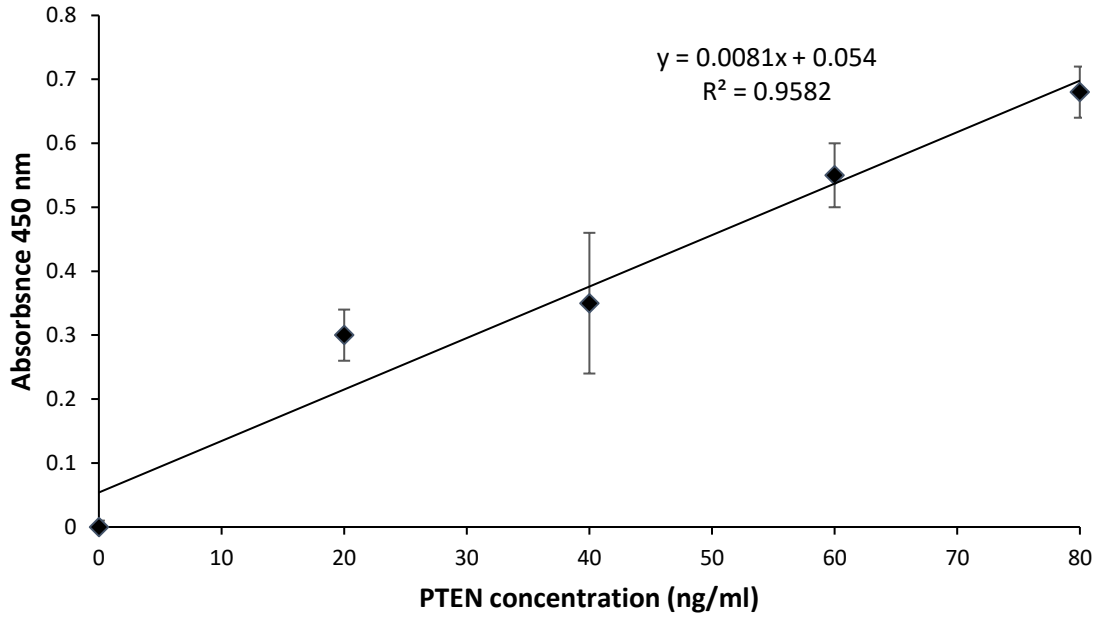


Figure 3. 3 Standard curve for PTEN protein. Recombinant PTEN protein (80 ng/ml) was reconstituted in dH₂O (100 μ l). Serial dilutions of PTEN were prepared covering a range of concentrations (0-80 ng/ml). The samples (50 μ l) were pipetted into the pre-coated 96 well plate and mixed with the antibody mixture. The plate was incubated for 60 min and the wells were washed three times with PBST (350 μ l). The wells were incubated with TMB substrate (100 μ l) for 15 min in the dark. The reactions were stopped by adding the stop solution (100 μ l) and the absorption was recorded at 450 nm using a plate reader.

3.2.6 Examination of the association of PTEN with MAGI proteins using the proximity ligation assay (PLA)

MDA-MB-231 cells (10^3) were seeded into 35 mm-glass based μ -dishes with 10 mm well size, and grown in complete medium overnight. Separate sets of cells were incubated with serum-free medium for 60 min prior to activation. The cells were then activated with PAR2-AP (20 μ M) for up to 30 min. The medium was removed and the cells were washed twice with PBS. The cells were fixed with 4% (v/v) formaldehyde for 20 min and then washed twice with PBS. The cells were permeabilised using 0.1% (v/v) Triton X-100 for 10 min and then washed twice with PBS. The cells were blocked with Duolink® blocking solution at 37°C for 60 min. The blocking solution was then discarded and the cells were incubated with combinations of antibodies overnight at 4°C. Different concentrations of PTEN and MAGI-(1-3) antibodies were used to determine the optimal antibody concentration (Appendix A-2). To examine the potential interactions between PTEN and MAGI-(1-3) proteins, a mouse anti-PTEN antibody (217702) was used together with a rabbit anti-MAGI-1 antibody (H-70), or with a rabbit anti-MAGI-2 antibody (C3) or with a rabbit anti-MAGI-3 antibody diluted 1:100 (v/v) in the provided antibody diluent. As controls, the antibodies were substituted with a rabbit or mouse IgG isotypes, respectively. PLA analysis was performed as described in section 2.3.5. The nuclei were labelled with DAPI (2 μ g/ml) and the cytoskeleton with Phalloidin 488 (2 μ g/ml) for 10 min. Images were acquired using a Zeiss Axio Vert.A1 inverted fluorescence microscope with a X40 magnification. The number of red fluorescent events and the nuclei were determined using ImageJ software, in 10 fields of view from each assay.

3.2.7 Examination of the interaction of PTEN and MAGI-2 using co-immunoprecipitation

MDA-MB-231 cells (5×10^5) were seeded into 6 well plates in complete medium and propagated to 80% confluency. Separate sets of cells were incubated with serum-free medium

for 60 min prior to activation. The cells were then incubated with PAR2-AP (20 μ M) for 20 min. The media were removed and the cells were washed twice with ice-cold PBS. The cells were lysed in PhosphoSafe™ extraction buffer (500 μ l). PTEN protein was immunoprecipitated from cell lysates using a rabbit anti-human PTEN antibody (8 μ g). Also, MAGI-2 protein was immunoprecipitated from cell lysates using a rabbit anti-MAGI-2 antibody (8 μ g; C3). To ensure specificity, a rabbit IgG isotype (8 μ g) was also included as well as an additional control without any antibody. The immunoprecipitated proteins were incubated overnight at 4°C using a rotating mixer. On the following day, the antibody in the cell lysates was captured with protein A-magnetic beads (100 μ) at 4°C for 120 min using a rotating mixer. The supernatants were discarded and the beads were washed five times with PBST (1 ml). The samples were lysed in Laemmli's buffer as described in section 2.3.6. The immunoprecipitated MAGI-2 protein samples were separated by SDS-PAGE, transferred to nitrocellulose membranes and blocked. To assess the presence of PTEN, the membranes were probed with a mouse anti-PTEN primary antibody diluted 1:2000 (v/v) in TBST overnight at 4°C. The membranes were washed with TBST and then probed with a secondary goat anti-mouse alkaline phosphatase-conjugated antibody diluted 1:8000 (v/v) in TBST. Alternatively, to assess the presence of MAGI-2, the membranes were probed with a mouse anti-MAGI-2 antibody diluted 1:2000 (v/v) in TBST overnight at 4°C. The membranes were washed with TBST and then probed with a secondary goat anti-mouse alkaline phosphatase-conjugated antibody diluted 1:8000 (v/v) in TBST. The bands were developed with Western Blue-stabilised substrate for alkaline phosphatase and photographed.

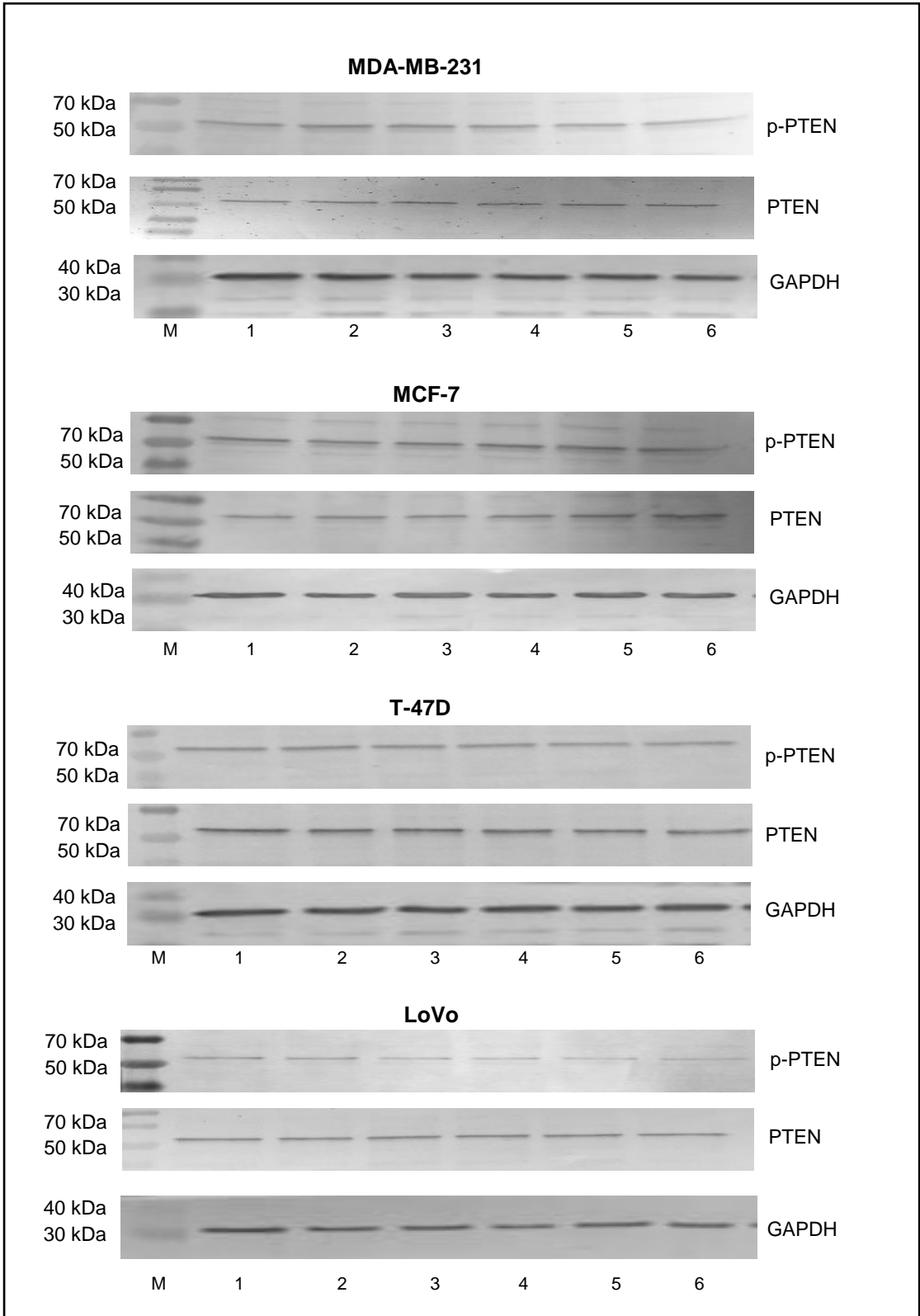
3.2 Results

3.3.1 Assessment of the expression of PTEN in the cell lines

While no PTEN mutations have been reported for MDA-MB-231 (Choi *et al* 2018), MCF-7 (Dunn *et al* 2019), T-47D (Dunn *et al* 2019), LoVo (Ahmed *et al* 2013), CaCo-2 (Ahmed *et al* 2013), AsPC-1 (Li *et al* 2005) and Panc-1 (Ciuffreda *et al* 2017) cell lines used in this study, this possibility can not be ruled out. Western blot analysis of 4 independent repeats using ImageJ software showed differing amounts of expressed PTEN in the cell lines tested with an approximate molecular weight of 54 kDa (Figure 3.4A-C).

3.3.2 The influence of rec-TF on PTEN phosphorylation

The de-phosphorylation of PTEN at Ser380, Thr382 and Thr383 is an essential step in the association of PTEN with the membrane and therefore the activation of PTEN (Tolkacheva *et al* 2001). Seven cancer cells lines expressing high levels of TF (LoVo, ASPC-1 and MDA-MB-231), medium levels of TF (MCF-7 and PANC-1) or low levels of TF (T-47D and Caco-2) (Ettelaie *et al* 2016) were incubated with high (1,300 pg/ml) or low (65 pg/ml) concentrations of rec-TF at intervals up to 120 min. ImageJ analysis of the protein samples (shown in Figure 3.4) indicated that incubation of cells with high levels of rec-TF (1,300 pg/ml) induced the de-phosphorylation of PTEN significantly in LoVo cells by 120 min while the other cell lines showed no significant change in PTEN de-phosphorylation levels (Figure 3.5). Moreover, incubation of cells with low levels of rec-TF (65 pg/ml) induced the de-phosphorylation of PTEN in all cell lines by 60 and 120 min. Specifically, the levels of PTEN de-phosphorylation were significantly higher in MDA-MB-231, MCF-7 and LoVo cells when incubated with rec-TF (65 pg/ml) for 60 min compared with the other cell lines tested (Figure 3.6). Since the concentration of rec-TF (65 pg/ml) produced the greatest level of PTEN de-phosphorylation, further experiments were conducted using this concentration.



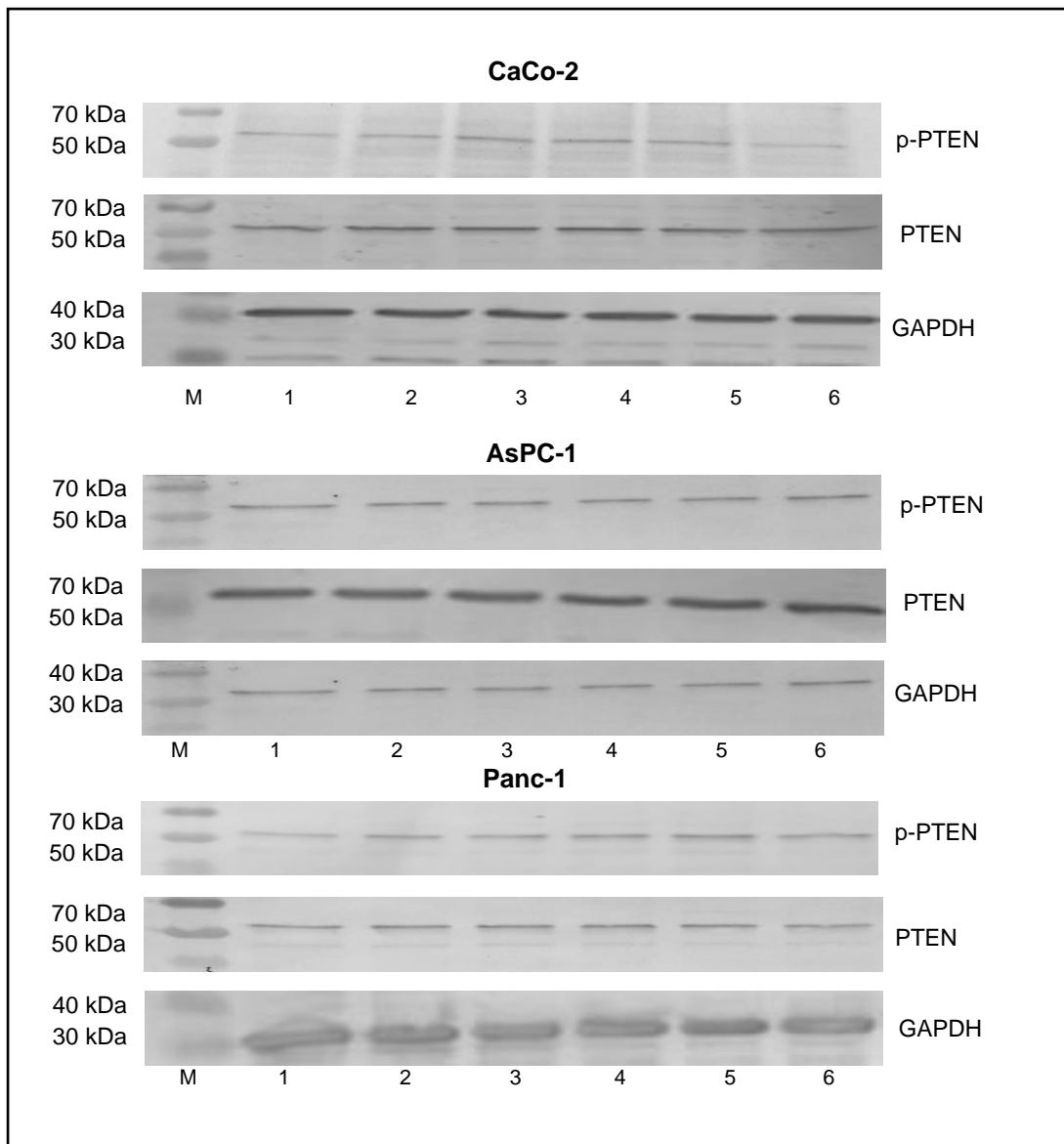


Figure 3. 4 The influence of rec-TF and PAR2 activation on the expression levels of PTEN and P-PTEN in cancer cells. MDA-MB-231, MCF-7, T-47D, LoVo, CaCo-2, AsPC-1 and Panc-1 cells (2×10^5) were seeded out into 6-well plates and cultured in the recommended media. Separate sets of cells were incubated with to serum-free media for 60 min prior to PAR2 activation. Other sets of cells were activated with recombinant TF (0-1300 pg/ml) and incubated for the durations shown: M = Markers, 1 = Untreated, 2 = 1300 pg/ml rec-TF, 60 min, 3 = 1300 pg/ml rec-TF, 120 min, 4 = 65 pg/ml rec-TF, 60 min, 5 = 130 pg/ml rec-TF, 60 min, 6 = PAR2-AP (20 μ M), 30 min. The cells were washed and then lysed in Laemmli's buffer. The protein samples were separated by SDS-PAGE as described in section 3.2.2. The membranes were probed with a rabbit anti-human PTEN antibody or a rabbit anti-human phosphoSer382/Thr382/Thr383-PTEN or a goat anti-human GAPDH antibody overnight at 4°. In order to detect the presence of p-PTEN/total-PTEN, the membranes were washed with TBST and then probed with a secondary goat anti-rabbit alkaline phosphatase conjugated antibody. In order to detect the presence of GAPDH, the membranes were washed with TBST and then probed with a secondary donkey anti-goat alkaline phosphatase conjugated antibody for 60 min. The bands were developed with Western Blue-stabilised substrate for alkaline phosphatase and photographed.

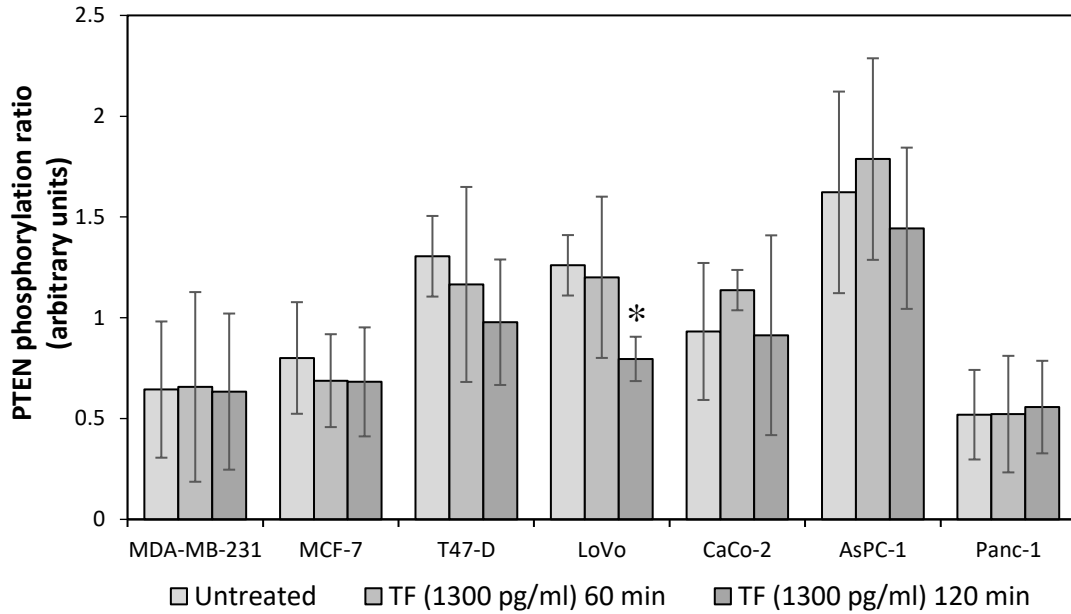


Figure 3. 5 The influence of high concentration rec-TF on PTEN phosphorylation state. MDA-MB-231, MCF-7, T-47D, LoVo, CaCo-2, AsPC-1 and Panc-1 cells (2×10^5) were seeded out into 6-well plates and cultured in the recommended media until reached 80% confluency. The cells were incubated with high concentration of rec-TF (1,300 pg/ml) for 60 or 120 min. The cells were washed three times with PBS and then lysed in Laemmli's buffer. The protein samples were separated by SDS-PAGE, transferred to nitrocellulose membranes and blocked with TBST. The membranes were probed with either a rabbit anti-human PTEN antibody or a rabbit anti-human phosphoSer382/Thr382/Thr383-PTEN or a goat anti-human GAPDH antibody as described in section 3.2.2. The bands were developed with Western Blue-stabilised substrate for alkaline phosphatase and quantified using ImageJ software. The ratio of p-PTEN:total PTEN were determined and normalised against the GAPDH contents ($n = 12$; * = $p < 0.05$ vs. the respective untreated samples).

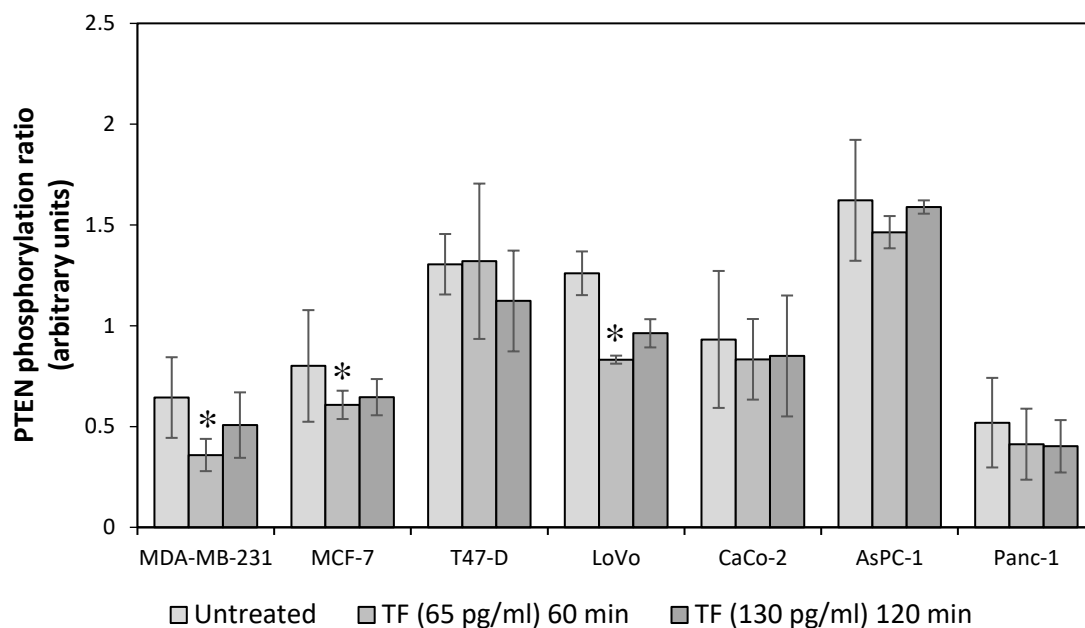


Figure 3. 6 The influence of low concentration rec-TF on PTEN phosphorylation state. MDA-MB-231, MCF-7, T-47D, LoVo, CaCo-2, AsPC-1 and Panc-1 cells (2×10^5) were seeded out into 6-well plates and cultured in the recommended media until reached 80% confluency. The cells were incubated with a low concentration of rec-TF (65 pg/ml) for 60 or 120 min. The cells were washed three times with PBS and then lysed in Laemmli's buffer. The protein samples were separated by SDS-PAGE, transferred to nitrocellulose membranes and blocked with TBST. The membranes were probed with either a rabbit anti-human PTEN antibody or a rabbit anti-human phosphoSer382/Thr382/Thr383-PTEN or a goat anti-human GAPDH antibody as described in section 3.2.2. The bands were developed with Western Blue-stabilised substrate for alkaline phosphatase and quantified using ImageJ software. The ratio of p-PTEN:total PTEN were determined and normalised against the GAPDH contents ($n = 12$; * = $p < 0.05$ vs. the respective untreated samples).

3.3.3 The influence of PAR2 activation on PTEN phosphorylation

To examine the influence of PAR2 activation on the phosphorylation state of PTEN, MDA-MB-231, MCF-7, T-47D, LoVo, CaCo-2, AsPC-1 and Panc-1 cells were activated with PAR2-AP for 30 min. The quantification of protein bands (shown in Figure 3.4) using ImageJ software showed that the activation of cells with PAR2-AP resulted in the de-phosphorylation of PTEN in MDA-MB-231 and LoVo cells. However, no significant change in the level of PTEN de-phosphorylation was detected in MCF-7, CaCo-2, Panc-1, T-47D and AsPC-1 cells compared to untreated samples (Figure 3.7).

3.3.4 Short-term exposure of cells to TF induces the activity of PTEN

The lipid phosphatase activity of PTEN is known to be inversely dependent on the phosphorylation state of PTEN protein (Hopkins *et al* 2014). Therefore, to assess the influence of TF on the lipid-phosphatase activity of PTEN, MDA-MB-231, MCF-7, T-47D, LoVo, CaCo-2, AsPC-1 and Panc-1 cells were incubated with rec-TF (65 pg/ml) for 60 min. Data analysis of 3 independent repeats showed the ability of cells to hydrolyse PIP3 to PIP2 resulted in significantly higher PTEN activity in MDA-MB-231, LoVo, AsPC-1 and CaCo-2 cells. However, incubation of Panc-1, MCF-7, T-47D and cells with rec-TF (65 pg/ml) resulted in no significant change in PTEN activity between treated and untreated samples (Figure 3.8).

3.3.5 PAR2 activation increases the lipid-phosphatase activity of PTEN

To examine the influence of PAR2 activation on the activity of PTEN, the seven cell lines were activated with PAR2-AP for 30 min. Data analysis of 3 independent repeats showed the ability of PAR2 activated cells to hydrolyse PIP3 to PIP2 indicated an increase in the lipid-phosphatase activity of PTEN in MDA-MB-231, MCF-7, LoVo and CaCo-2 cells following PAR2 activation (Figure 3.9). However, there was no change observed in the lipid-phosphatase activity in PAR2-activated and non-activated T-47D, PANC-1 and AsPC-1 cells.

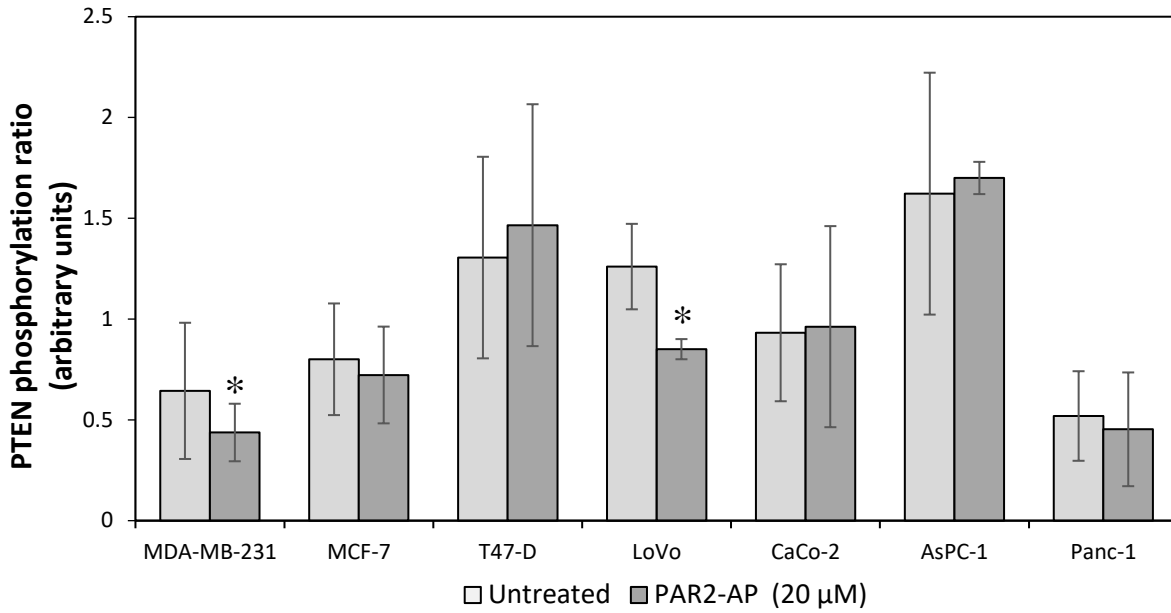


Figure 3. 7 The influence of PAR2 activation on PTEN phosphorylation state. MDA-MB-231, MCF-7, T-47D, LoVo, CaCo-2, AsPC-1 and Panc-1 cells (2×10^5) were seeded out into 6-well plates and cultured in the recommended media until reached 80% confluency. The cells were incubated with to serum-free media for 60 min prior to activation and then activated with PAR2-AP ($20 \mu\text{M}$) for 30 min. The cells were washed three times with PBS and then lysed in Laemmli's buffer. The protein samples were separated by SDS-PAGE, transferred to nitrocellulose membranes and blocked with TBST. The membranes were probed with either a rabbit anti-human PTEN antibody or a rabbit anti-human phosphoSer382/Thr382/Thr383-PTEN or a goat anti-human GAPDH antibody as described in section 3.2.2. The bands were developed with Western Blue-stabilised substrate for alkaline phosphatase and quantified using ImageJ software. The ratio of p-PTEN:total PTEN were determined and normalised against the GAPDH contents ($n = 12$; $* = p < 0.05$ vs. the respective untreated samples).

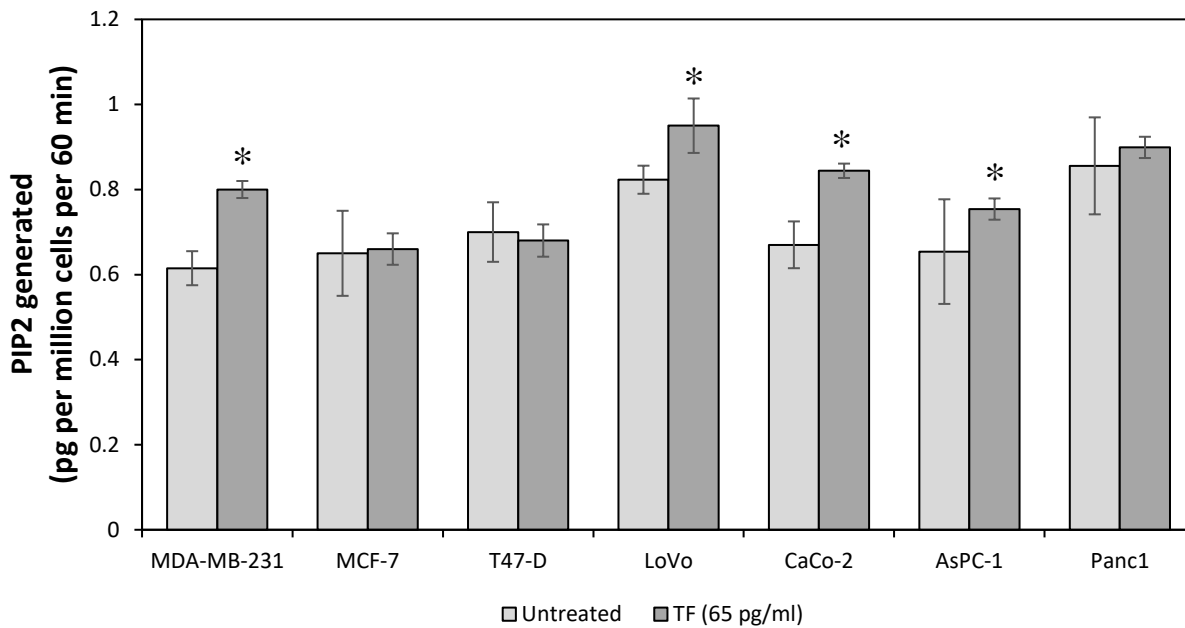


Figure 3. 8 The influence of low rec-TF on the lipid-phosphatase activity of PTEN. MDA-MB-231, MCF-7, T-47D, LoVo, CaCo-2, PANC-1 and AsPC-1 cells (2×10^5) were seeded out into 6-well plates and propagated to 80% confluency. The cells were treated with rec-TF (65 pg/ml) for 60 min and then washed with PBS. The cells were lysed in Phospho-safe extraction buffer (500 μ l). The lysate samples (6 μ l) were mixed with PTEN reaction buffer (6 μ l) and pipetted into a 96-well plate. The PIP3 substrate (12 μ l) was added to each sample and the plate was incubated at 37°C for 3 h. The reactions were then terminated by adding the stop solution (60 μ l). The reactions (60 μ l) were transferred into the PIP2 coated 96-well plate. The PIP2 detector protein (60 μ l) was added to each sample and the plate was incubated at 37°C for 60 min. The solution was then discarded and the wells were washed three times with PBST (200 μ l). HRP-conjugated detector (100 μ l) was added to each well and the plate was incubated at room temperature for 30 min. The solution was discarded and the wells were washed three times with PBST (200 μ l). TMB substrate (100 μ l) was added to each well and the plate was incubated in the dark for 15 min. The reactions were terminated and the absorption values were measured at 450 nm using a plate reader. (n=12; *= p < 0.05 vs. untreated samples). The PTEN activity values were determined and normalised against the total protein concentrations obtained from the Bradford assay.

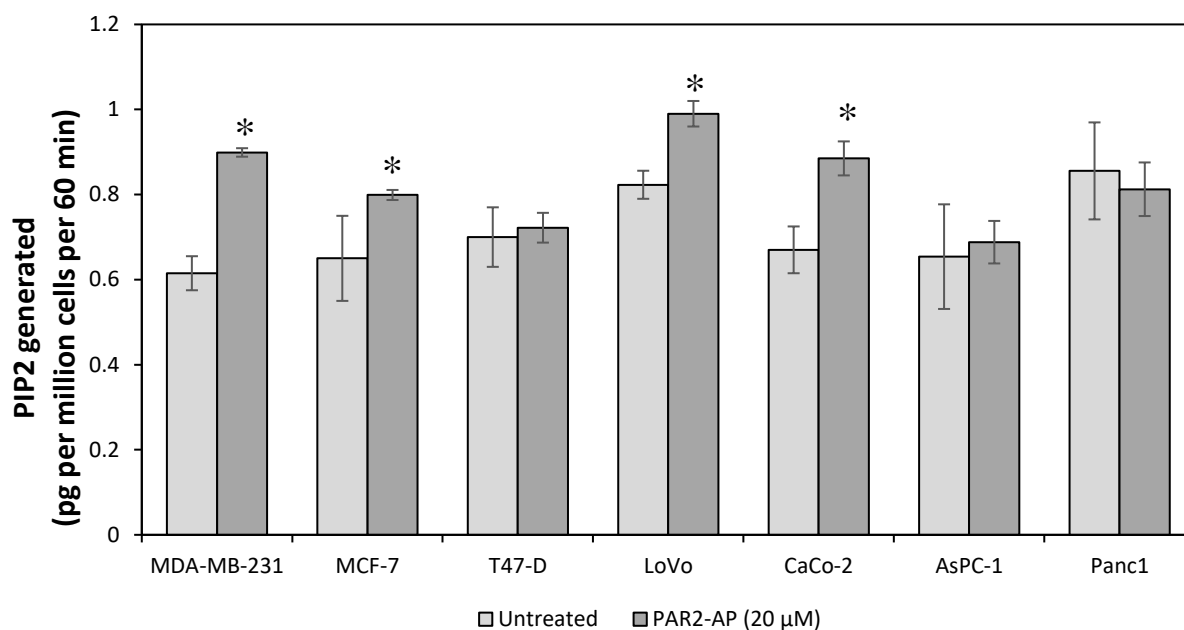


Figure 3. 9 The influence of PAR2-activation on the lipid-phosphatase activity of PTEN. MDA-MB-231, MCF-7, T-47D, LoVo, CaCo-2, PANC-1 and AsPC-1 cells (2×10^5) were seeded out into 6-well plates and propagated to 80% confluency. The cells were incubated with to serum-free medium for 60 min prior to activation. The cells were then activated with PAR2-AP ($20 \mu\text{M}$) for 30 min and then lysed in Phospho-safe extraction buffer ($500 \mu\text{l}$). The lysate samples ($6 \mu\text{l}$) were mixed with PTEN reaction buffer ($6 \mu\text{l}$) and pipetted into a 96-well plate. The PIP3 substrate ($12 \mu\text{l}$) was added to each sample and the plate was incubated at 37°C for 3 h. The reactions were then terminated by adding the stop solution ($60 \mu\text{l}$). The reactions ($60 \mu\text{l}$) were transferred into the PIP2 coated 96-well plate. The PIP2 detector protein ($60 \mu\text{l}$) was added to each sample and the plate was incubated at 37°C for 60 min. The solution was then discarded and the wells were washed three times with PBST ($200 \mu\text{l}$). HRP-conjugated detector ($100 \mu\text{l}$) was added to each well and the plate was incubated at room temperature for 30 min. The solution was discarded and the wells were washed three times with PBST ($200 \mu\text{l}$). TMB substrate ($100 \mu\text{l}$) was added to each well and the plate was incubated in the dark for 15 min. The reactions were terminated and the absorption values were measured at 450 nm using a plate reader. ($n=12$; $*= p < 0.05$ vs. untreated samples). The PTEN activity values were determined and normalised against the total protein concentrations obtained from the Bradford assay.

3.3.6 Short-term exposure of cells to TF reduces the kinase activity of Akt

The tumour suppressing activity of PTEN is associated with its inhibitory effect on Akt activation. Since the concentration of rec-TF (65 pg/ml) was shown to increase lipid-phosphatase activity of PTEN, the cells were incubated with rec-TF (65 pg/ml) for 60 min to assess their ability to phosphorylate Akt. Data analysis of 3 independent repeats indicated that the exposure of cells to rec-TF resulted in significant decrease in Akt kinase activity in MDA-MB-231, LoVo and CaCo-2 cells. However, no change in the kinase activity of Akt was observed in MCF-7, T-47D, PANC-1 and AsPC-1 cells (Figure 3.10).

3.3.7 PAR2 activation reduces the kinase activity of Akt

To examine the influence of PAR2 activation on the kinase activity of Akt, MB-231, MCF-7, T-47D, LoVo, CaCo-2, PANC-1 and AsPC-1 cells were activated with PAR2-AP for 30 min. Data analysis of 3 independent repeats indicated that the activation of cells with PAR2-AP resulted in a reduction in Akt activity in MDA-MB-231 and CaCo-2 cells (Figure 3.11). However, there was no change observed in Akt kinase activity in the other cells tested. Since MDA-MB-231, LoVo and CaCo-2 cell lines were found to be the most responsive to rec-TF (65 pg/ml), these cells were selected for additional studies.

3.3.8 Prolonged exposure of cells to rec-TF increases the rate of cell proliferation

TF is overexpressed during pathological and inflammatory conditions which has been associated with disease progression and high mortality, particularly in cancer (Silva *et al* 2014; Chu 2011). To mimic these conditions and to achieve a sustained exposure of cells to TF, prolonged incubation of cells was carried out by supplementing the cells with rec-TF (65 pg/ml) over a period of five days. Data analysis of 3 independent repeats showed the incubation

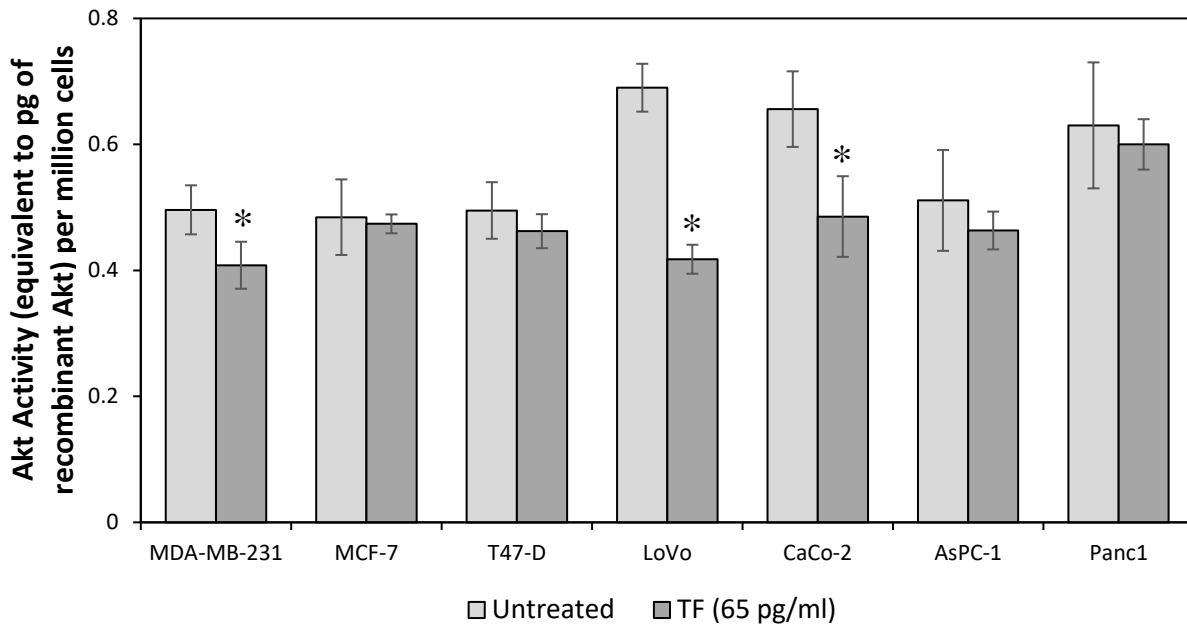


Figure 3. 10 The influence of rec-TF on the cellular activity of Akt. MDA-MB-231, MCF-7, T-47D, LoVo, CaCo-2, PANC-1 and AsPC-1 cells (2×10^5) were seeded out into 6-well plates and propagated to 80% confluency. The cells were treated with rec-TF (65 pg/ml) for 60 min and then washed three times with PBS. The cells were lysed in Phospho-Safe extraction buffer (300 μ l) and the lysate samples (30 μ l) were loaded into the 96-well plate followed by the ATP solution (10 μ l). The plate was incubated at 30°C for 90 min and the reaction was then stopped by inverting the plate on a clean paper towel. The phospho-specific antibody (40 μ l) was added to each well and the plate was incubated for 60 min. The solution was then discarded and the wells were washed three times with PBST. The detecting antibody was added into each well (40 μ l) and incubated for 30 min. The wells were washed three times with PBST and incubated with TMB substrate (60 μ l) for 30 min. The reactions were stopped by adding the stop solution (20 μ l) and the absorption values were recorded at 450 nm using a plate reader. (n=12; *= P < 0.05 vs. untreated samples). The Akt kinase activity values were determined and normalised against the total protein concentrations obtained from the Bradford assay.

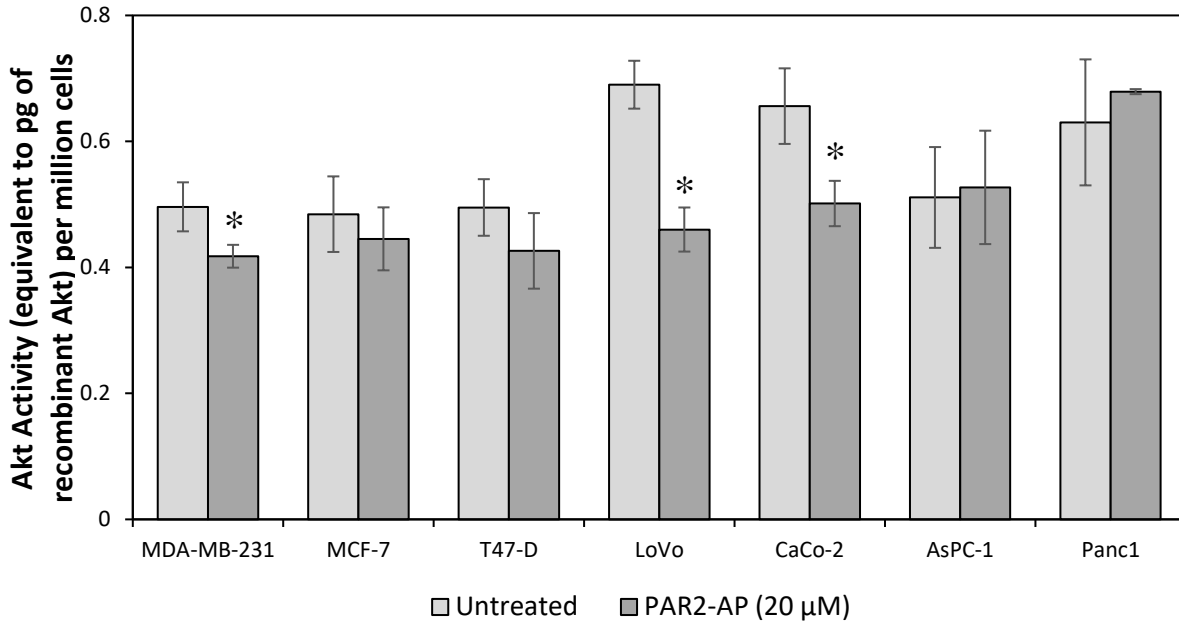


Figure 3. 11 The influence of PAR2 activation on the cellular activity of Akt. MDA-MB-231, MCF-7, T-47D, LoVo, CaCo-2, PANC-1 and AsPC-1 cells (2×10^5) were seeded out into 6-well plates and propagated to 80% confluency. The cells were incubated with to serum-free medium for 60 min prior to activation. The cells were then activated with PAR2-AP ($20 \mu\text{M}$) for 30 min and then lysed in Phospho-Safe extraction buffer ($300 \mu\text{l}$). The lysate samples ($30 \mu\text{l}$) were loaded into the 96-well plate followed by the ATP solution ($10 \mu\text{l}$). The plate was incubated at 30°C for 90 min and the reaction was then stopped by inverting the plate on a clean paper towel. The phospho-specific antibody ($40 \mu\text{l}$) was added to each well and the plate was incubated for 60 min. The solution was then discarded and the wells were washed three times with PBST. The detecting antibody was added into each well ($40 \mu\text{l}$) and incubated for 30 min. The wells were washed three times with PBST and incubated with TMB substrate ($60 \mu\text{l}$) for 30 min. The reactions were stopped by adding the stop solution ($20 \mu\text{l}$) and the absorption values were recorded at 450 nm using a plate reader. ($n=12$; $*$ = $P < 0.05$ vs. untreated samples). The Akt kinase activity values were determined and normalised against the total protein concentrations obtained from the Bradford assay.

of cells with rec-TF resulted in the increased rate of cell proliferation by day 5 in MDA-MB-231 (Figure 3.12 A) and LoVo (Figure 3.12 B) cells compared to the untreated cells. Moreover, the rate of cell proliferation in CaCo-2 cells was increased by day 4 compared to the untreated cells (Figure 3.12 C).

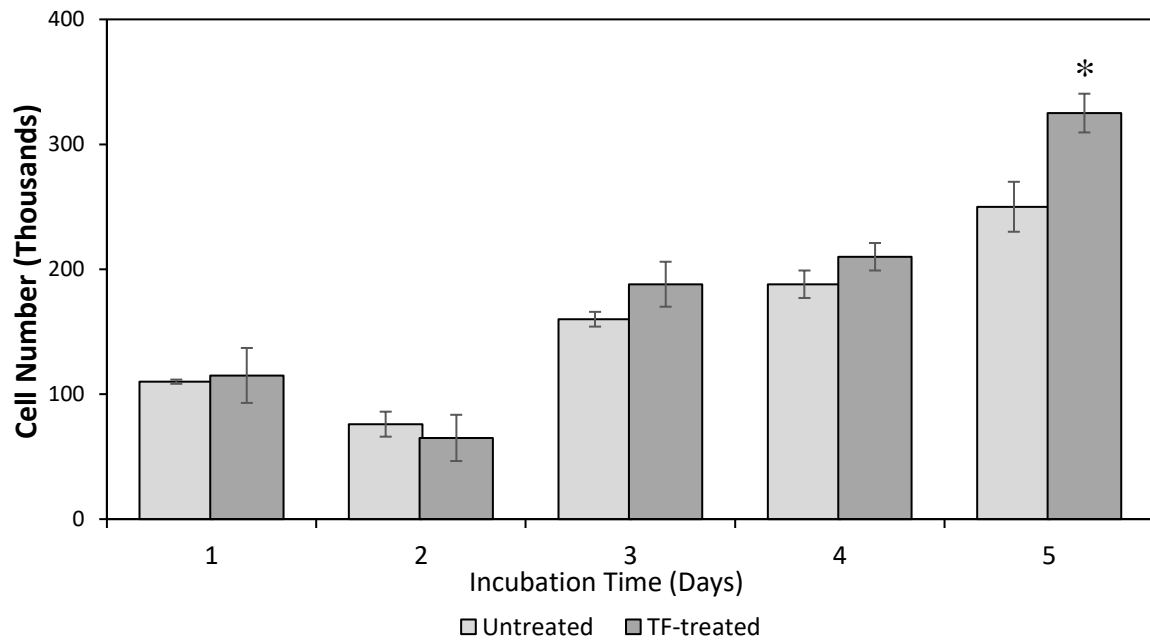
3.3.9 Prolonged exposure of cells to rec-TF reduces total PTEN protein

To investigate the effects of prolonged incubation of cancer cells with rec-TF on the amount of total PTEN, MDA-MB-231, LoVo and CaCo-2 cells were supplemented with multiple doses of rec-TF (65 pg/ml) over 5 days. Measurement of PTEN antigen levels revealed that the prolonged exposure of cells to rec-TF resulted in a decrease in the cellular levels of PTEN antigen in MDA-MB-231, LoVo and CaCo-2 cells by the fifth day, compared to equivalent untreated samples (Figure 3.13).

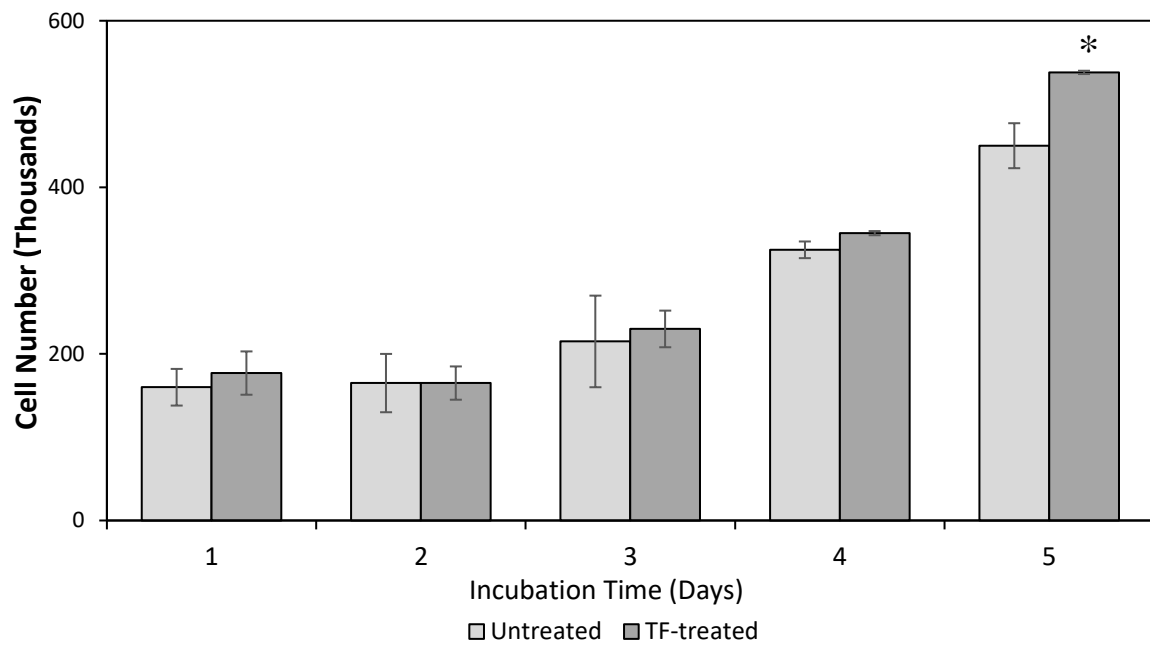
3.3.10 Prolonged exposure of cells to rec-TF increases Akt kinase activity

The role of PTEN as a negative regulator of the PI3K-Akt signalling pathway is well established, and the levels of PTEN inversely correlate with Akt activation (Lee *et al* 2014). since, the prolonged exposure of cells to rec-TF was shown to decrease PTEN protein levels. Therefore, the influence of prolonged incubation of MDA-MB-231, LoVo and CaCo-2 cells to rec-TF on the activity of Akt was examined next. The cells were similarly supplemented with multiple doses of rec-TF (65 pg/ml) over 5 days. The ability of cells to phosphorylate Akt resulted in an increase in the kinase activity of Akt in MDA-MB-231 and LoVo cells, however, no change in Akt activity was observed following the treatment of CaCo-2 cells with rec-TF (Figure 3.14).

A)



B)



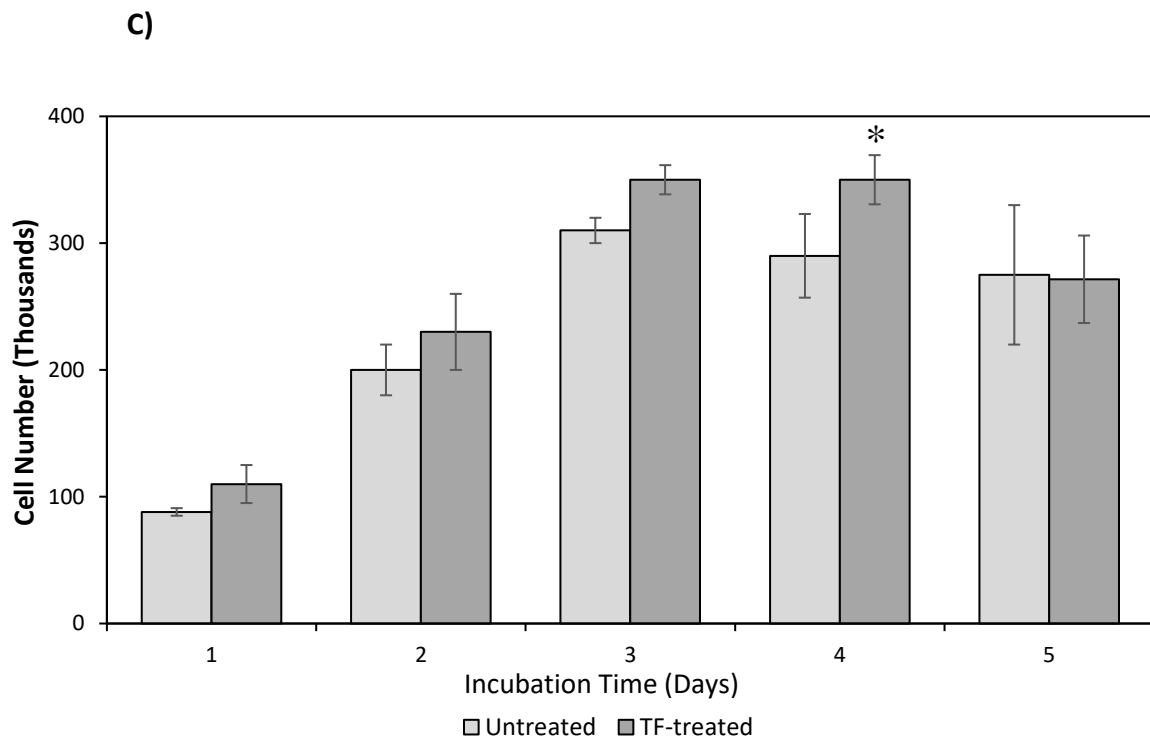


Figure 3. 12 The influence of prolonged exposure of cells to rec-TF on the cell number. A) MDA-MB-231, B) LoVo, C) CaCo2 cells (2×10^4) were seeded out into a T-75 flask and cultured in the recommended medium. The cells were supplemented with rec-TF (65 pg/ml) over a period of five days. On the fifth day, the cells were washed with PBS, fixed with 3% (w/v) glutaraldehyde and the cell numbers were determined using the crystal violet staining assay. Aliquots (100 μ l) were transferred into a 96-well plate and the absorption was measured at 495 nm using a plate reader (n=9; *= P < 0.05 vs. untreated sample).

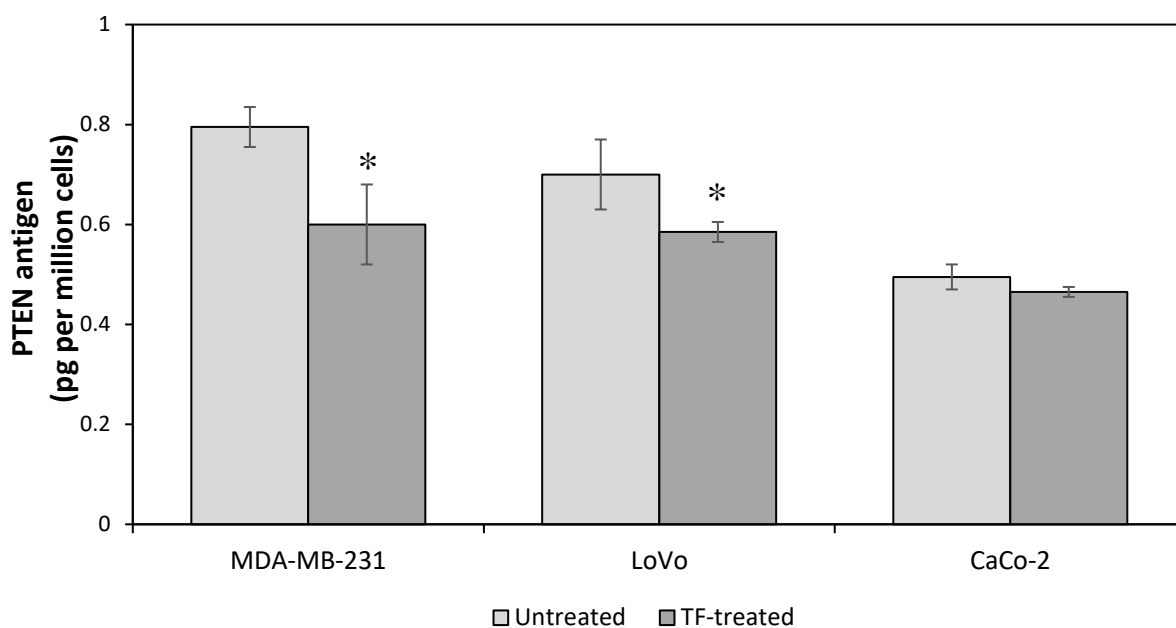


Figure 3. 13 The influence of prolonged exposure of cells to rec-TF on the cellular levels of PTEN antigen. MDA-MB-231, LoVo and CaCo-2 cells (2×10^4) were seeded out into a T-75 flask and cultured in the recommended media. The cells were supplemented with rec-TF (65 pg/ml) over a period of five days. On the fifth day, the cells were washed three times with PBS and then lysed in Phospho-safe extraction buffer (2 ml). The lysate samples (50 μ l) were loaded into the 96 well plate followed by 50 μ l of the antibody mixture (capture antibody (300 μ l) and detector antibody (300 μ l) both diluted in antibody diluent (2.4 ml). The plate was incubated on a plate shaker for 60 min. The solution was discarded and the wells were washed three times with PBST. TMB substrate (100 μ l) was added to each well and the plate was incubated in the dark for 15 min. Once colour had developed, the reaction was terminated by adding stop solution (100 μ l). The absorption was recorded at 450 nm using a plate reader. (n = 16; * = p < 0.05 vs. untreated sample). PTEN antigen values were determined and normalised against the total protein concentrations obtained from the Bradford assay.

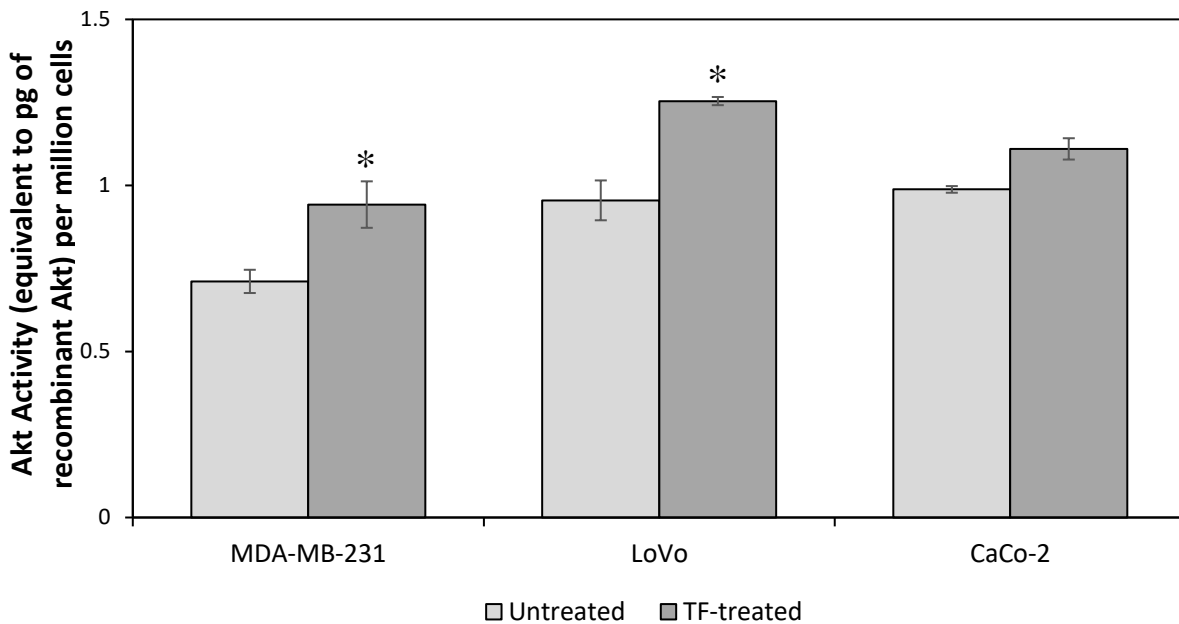
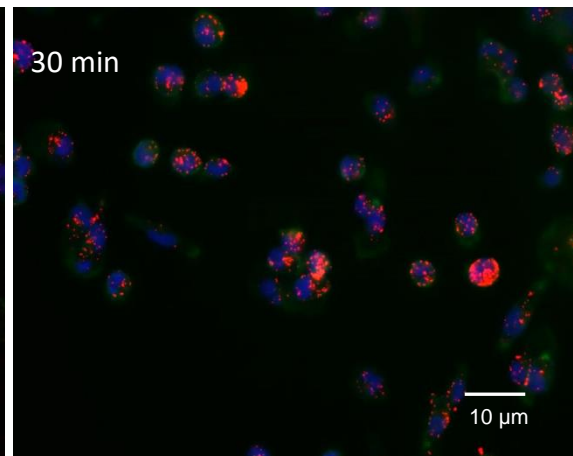
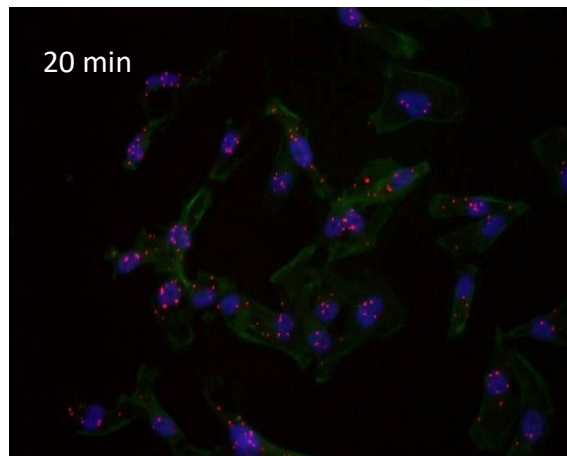
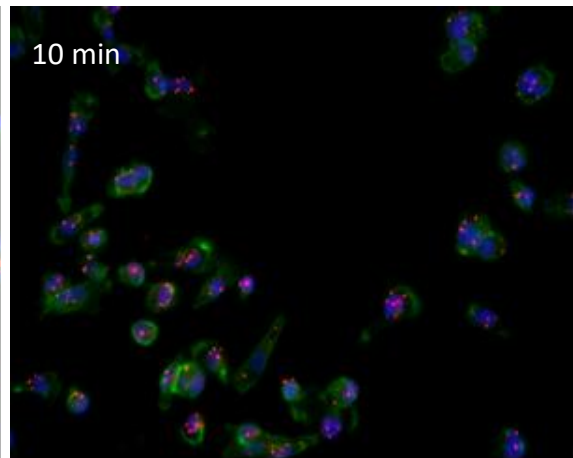
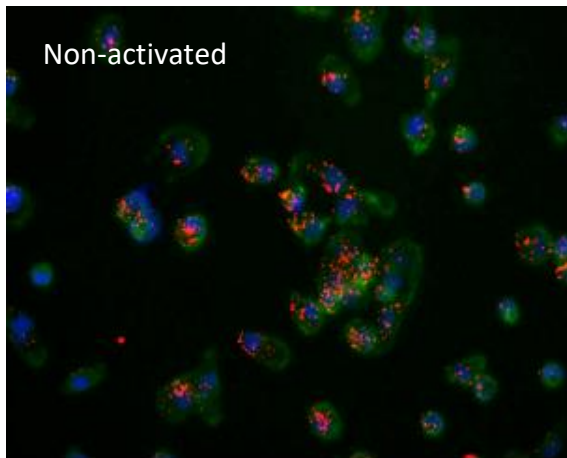
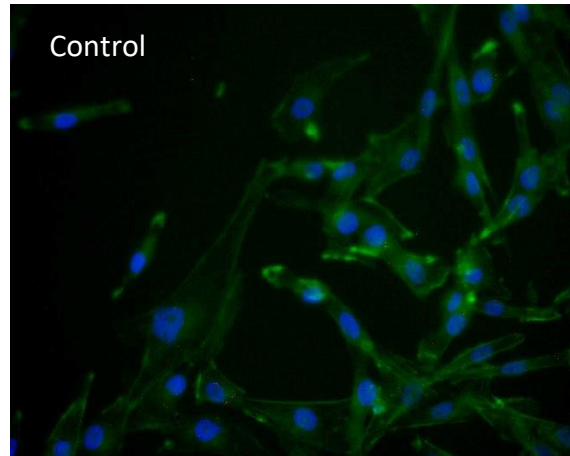


Figure 3. 14 The influence of prolonged exposure of cells to rec-TF on the cellular levels of Akt activity. MDA-MB-231, LoVo and CaCo-2 cells (2×10^4) were seeded out into a T-75 flask and cultured in the recommended media. The cells were supplemented with rec-TF (65 pg/ml) over a period of five days. On the fifth day, the cells were washed three times with PBS and then lysed in Phospho-Safe extraction buffer (300 μ l). The lysate samples (30 μ l) were loaded into the 96-well plate followed by the ATP solution (10 μ l). The plate was incubated at 30°C for 90 min and the reaction was then stopped by inverting the plate on a clean paper towel. The phospho-specific antibody (40 μ l) was added to each well and the plate was incubated for 60 min. The solution was then discarded and the wells were washed three times with PBST. The detecting antibody was added into each well (40 μ l) and incubated for 30 min. The wells were washed three times with PBST and incubated with TMB substrate (60 μ l) for 30 min. The reactions were stopped by adding the stop solution (20 μ l) and the absorption values were recorded at 450 nm using a plate reader. (n=16; *= P < 0.05 vs. untreated samples). The Akt kinase activity values were determined and normalised against the total protein concentrations obtained from the Bradford assay.

3.3.11 Activation of PAR2 releases PTEN from MAGI complexes

The interaction between PTEN and MAGI proteins has been well documented, particularly the recruitment and stabilisation of PTEN to the membrane via MAGI proteins (Wu *et al* 2000; Adey *et al* 2000; Tolkacheva *et al* 2001). In addition, PAR2 activation has been reported to suppress (Badeanlou *et al* 2011; Du *et al* 2017) or enhance PI3K/Akt activation (Jiang *et al* 2006; Roy *et al* 2017). Therefore, the PLA technique was employed to examine the association of PTEN with MAGI proteins in resting and PAR2-activated MDA-MB-231 cells. Since both PTEN and MAGI are cytoplasmic proteins, different permeabilising reagents were optimised and used to ensure sufficient antibody delivery inside the cell (Figure A-1). Examination of the non-activated cells by PLA indicated that PTEN was associated with all MAGI proteins. However, the association between PTEN and MAGI-1 (Figure 3.15A) or PTEN and MAGI-2 (Figure 3.16A) was significantly higher compared to MAGI-3 (Figure 3.17A). To examine the influence of PAR2 activation on the association between PTEN and MAGI proteins, MDA-MB-231 cells were activated with PAR2-AP for up to 30 min. Examination of PAR2 activated cells by PLA showed a reduction in the association of PTEN with MAGI-1 at 10 min and 20 min post-activation (Figure 3.15B). Moreover, the cells also showed a reduction in the association of PTEN with MAGI-2 at 10 min and 20 min post-activation (Figure 3.16B). Since the association between PTEN and MAGI3 was not significant compared to MAGI-1 or MAGI-2, MDA-MB-231 cells were only activated for only 20 min and measured at one time point. Activation of cell with PAR2-AP resulted in no significant change in the association of PTEN from MAGI-3 compared (Figure 3.17B).

A)



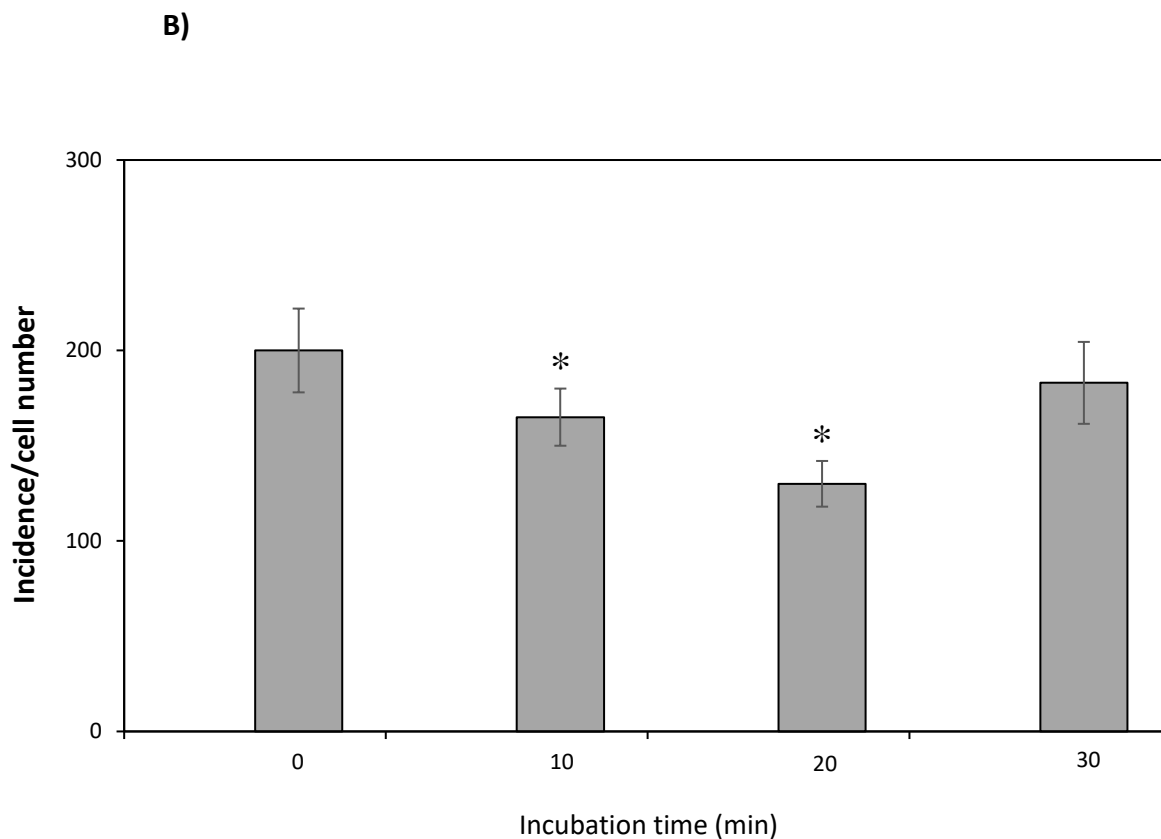
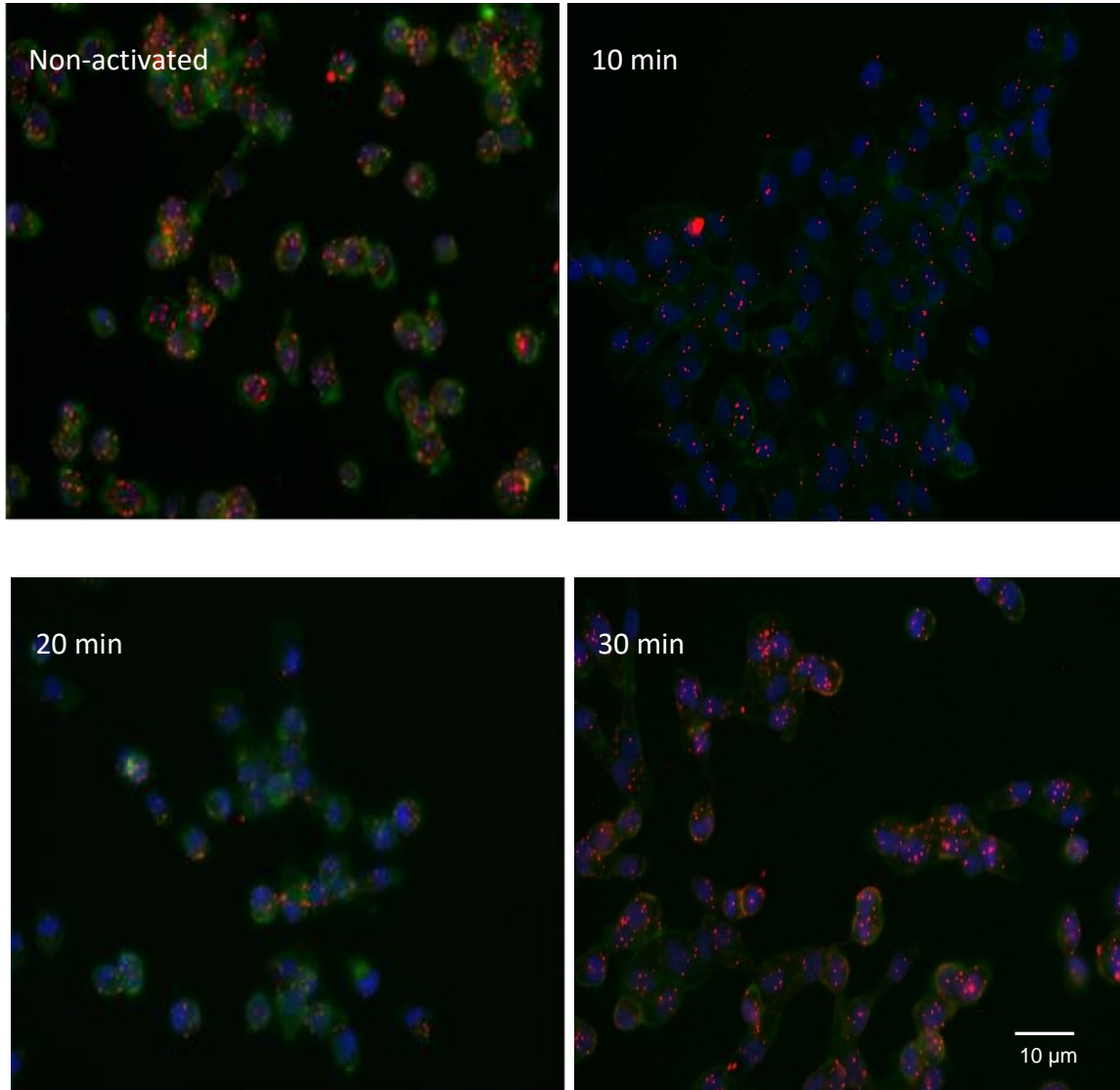


Figure 3. 15 Analysis of the influence of PAR2 activation on the association of PTEN with MAGI-1 by PLA. MDA-MB-231 cells (10^3) were seeded into 35 mm-glass based μ -dishes with 10 mm well size, and grown in complete medium overnight. Separate sets of cells were incubated with to serum-free medium for 60 min prior to activation. The cells were then activated with PAR2 (20 μ M) for 20 min. The cells were fixed with 4% (v/v) formaldehyde for 20 min and then washed twice with PBS. The cells were permeabilised using 0.1% (v/v) Triton X-100 for 10 min and then washed twice with PBS. The cells were blocked with Duolink® blocking solution at 37°C for 60 min. A) The proximity between PTEN and MAGI-1 was examined using a mouse anti-human PTEN antibody mixed together with a rabbit anti-MAGI-1 antibody. As controls, the antibodies were substituted with rabbit or mouse IgG isotypes. The PLA analysis was performed as described in section 2.3.5. Images were acquired using a Zeiss Axio Vert.A1 inverted fluorescence microscope with a X40 magnification. The micrographs are representative of 10 fields of view from 4 independent experiments. (RED= PLA incidences; GREEN = Phalloidin; BLUE = DAPI). B) The interaction of PTEN and MAGI-1 was determined based on the quantified number of red fluorescent events around each nuclei using ImageJ software. (n = 12; * = $p < 0.05$ vs. the respective non-activated samples).

A)



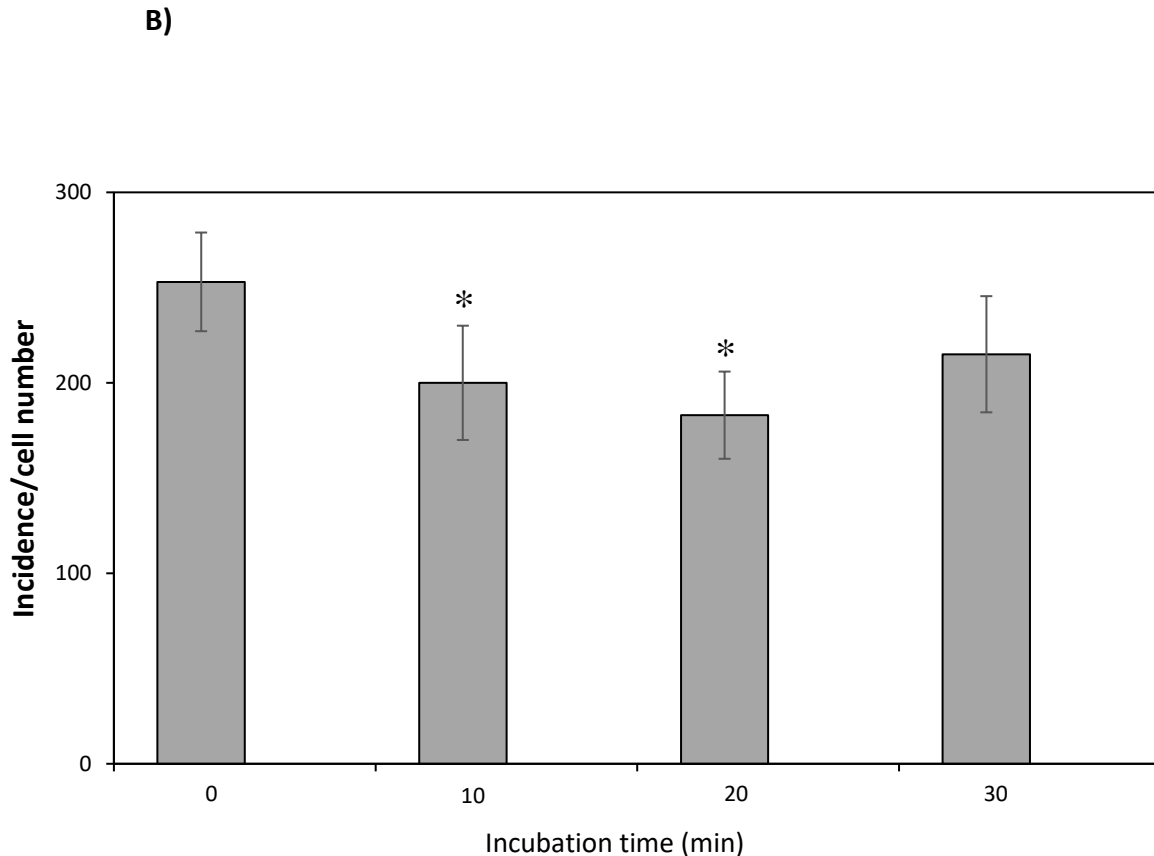
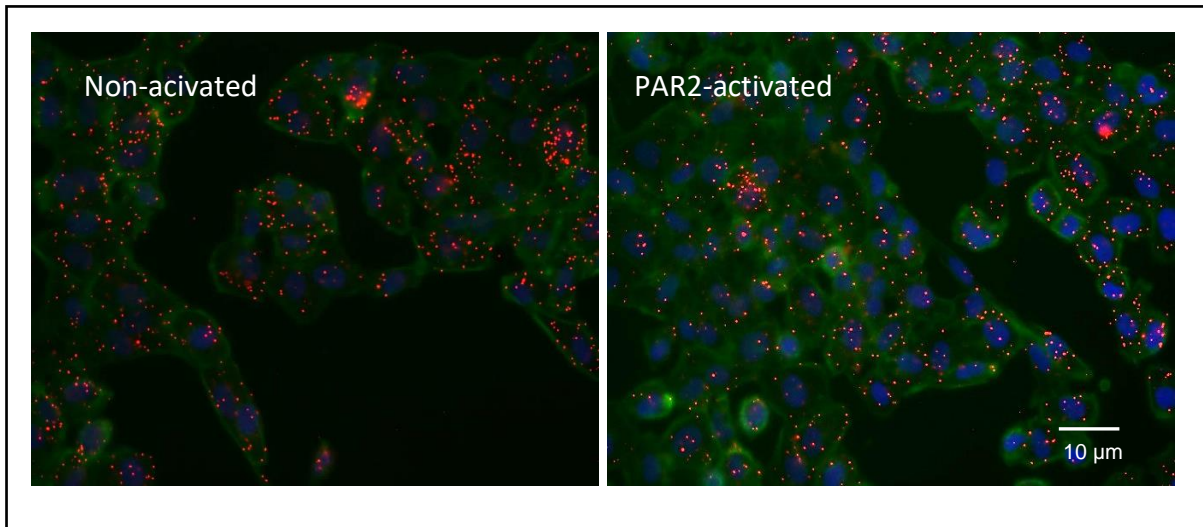


Figure 3. 16 Analysis of the influence of PAR2 activation on the association of PTEN with MAGI-2 by PLA. MDA-MB-231 cells (10^3) were seeded into 35 mm-glass based μ -dishes with 10 mm well size, and grown in complete medium overnight. Separate sets of cells were incubated with to serum-free medium for 60 min prior to activation. The cells were then activated with PAR2 (20 μ M) for 20 min. The cells were fixed with 4% (v/v) formaldehyde for 20 min and then washed twice with PBS. The cells were permeabilised using 0.1% (v/v) Triton X-100 for 10 min and then washed twice with PBS. The cells were blocked with Duolink® blocking solution at 37°C for 60 min. A) The proximity between PTEN and MAGI-2 was examined using a mouse anti-human PTEN antibody mixed together with a rabbit anti-MAGI-2 antibody. The PLA analysis was performed as described in section 2.3.5. Images were acquired using a Zeiss Axio Vert.A1 inverted fluorescence microscope with a X40 magnification. The micrographs are representative of 10 fields of view from 4 independent experiments. (RED= PLA incidences; GREEN = Phalloidin; BLUE = DAPI). B) The interaction of PTEN and MAGI-2 was determined based on the quantified number of red fluorescent events around each nuclei using ImageJ software. (n = 4; * = p< 0.05 vs. the respective non-activated samples).

A)



B)

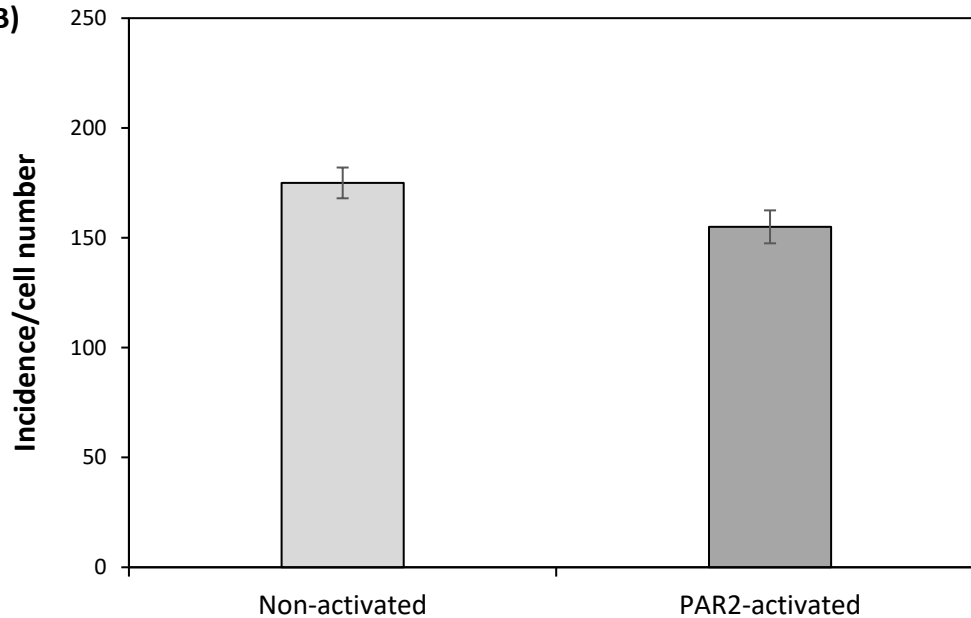


Figure 3. 17 Analysis of the influence of PAR2 activation on the association of PTEN with MAGI-3 by PLA. MDA-MB-231 cells (10^3) were seeded into 35 mm-glass based μ -dishes with 10 mm well size, and grown in complete medium overnight. The cells were activated with PAR2 and then fixed, permeabilised and blocked as described in Figure 3.16. A) The proximity between PTEN and MAGI-3 was examined using a mouse anti-human PTEN antibody mixed with a rabbit anti-MAGI-3 antibody. The PLA analysis was performed as described in section 2.3.5. Images were acquired using a Zeiss Axio Vert.A1 inverted fluorescence microscope with a X40 magnification. B) The interaction of PTEN and MAGI-3 was determined based on the quantified number of red fluorescent events around each nuclei using ImageJ software. (n = 4; * = $p < 0.05$ vs. the respective non-activated samples).

3.3.12 Confirmation of the interaction between MAGI-2 and PTEN by co-immunoprecipitation

The data obtained from PLA showed PTEN to associate with MAGI-2. Therefore, to further confirm the association between PTEN and MAGI-2, MAGI-2 protein was immunoprecipitated from cell lysates using a rabbit anti-MAGI-2 antibody. Western blot analysis of immunoprecipitated MAGI-2 exhibited that MAGI-2 associates with PTEN. Moreover, to confirm the influence of PAR2 activation on the association between PTEN and MAGI-2, MDA-MB-231 cells were activated with PAR2-AP for 20 min. Western blot assessment of PAR2-activated cells showed a reduction in the interaction between MAGI-2 and PTEN (Figure 3.18).

3.3.13 Confirmation of the interaction between PTEN and MAGI-2 by co-immunoprecipitation

To further confirm the interaction between PTEN and MAGI-2, PTEN protein was immunoprecipitated from cell lysates using a mouse anti-PTEN antibody. Western blot analysis of 3 independent immunoprecipitated PTEN repeats confirmed the interaction between PTEN and MAGI-2. Furthermore, to confirm the influence of PAR2 activation on the interaction of PTEN with MAGI-2, MDA-MB-231 cells were activated with PAR2-AP for 20 min. PAR2 activation of cells resulted in a reduction in the interaction between PTEN and MAGI-2 (Figure 3.19).

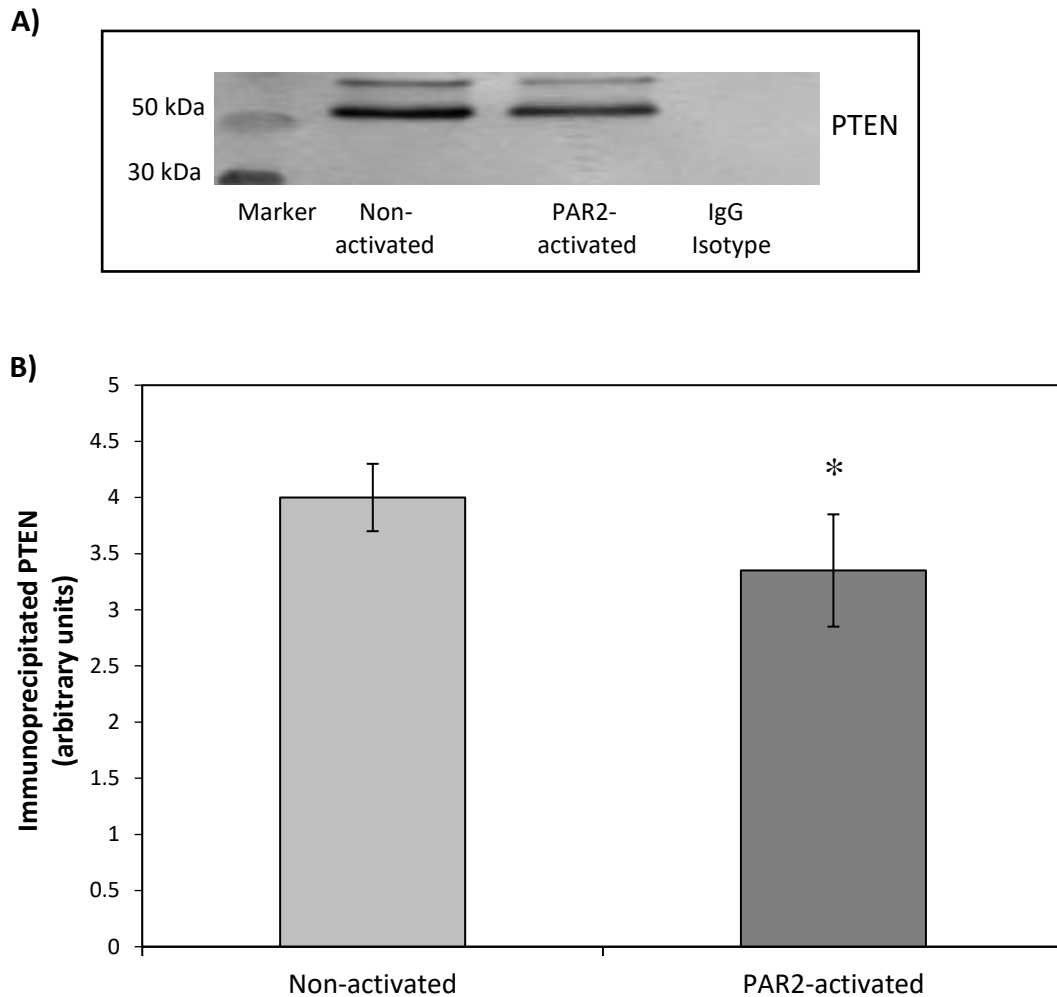


Figure 3. 18 Analysis of the interaction between PTEN and MAGI-2 using co-immunoprecipitation. MDA-MB-231 (5×10^5) were seeded out into 6-well plates in complete medium and propagated to 80% confluency. Separate sets of cells were incubated with serum-free medium for 60 min prior to activation. The cells were then activated with PAR2-AP (20 μ M) for 20 min. MAGI-2 protein was immunoprecipitated from cell lysates using a rabbit anti-MAGI-2 antibody and captured with protein A-magnetic beads. The immunoprecipitated protein samples were separated by SDS-PAGE, transferred to nitrocellulose membranes and blocked. In order to detect the presence of PTEN, the membranes were probed with a mouse anti-PTEN primary antibody overnight at 4°C. As a control, the antibodies were substituted with a mouse IgG isotype. The membranes were probed with a secondary goat anti-mouse alkaline phosphatase conjugated antibody. The bands were developed with Western Blue-stabilised substrate for alkaline phosphatase and photographed. B) The band densities were quantified to determine the interaction of PTEN and MAGI-2 between activated and non-activated samples. (n = 3; * = p < 0.05 vs. the non-activated sample).

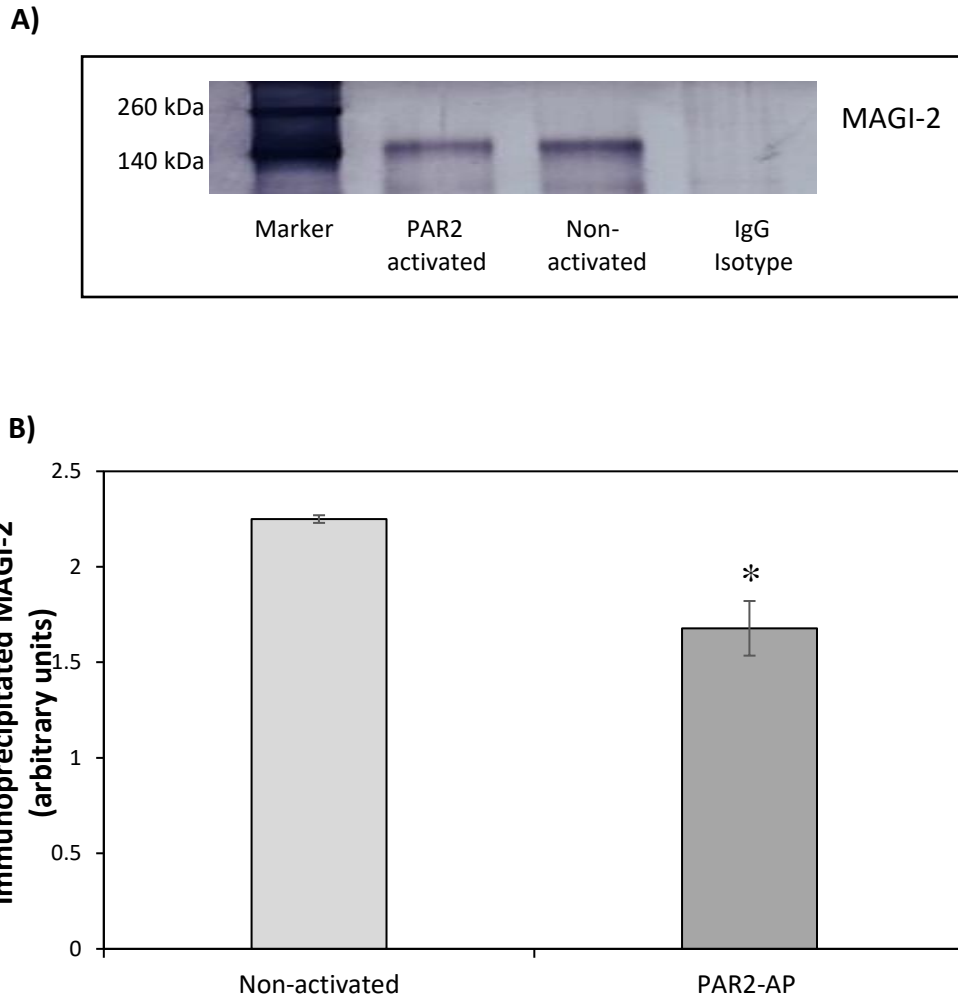


Figure 3. 19 Analysis of the interaction between MAGI-2 and PTEN using co-immunoprecipitation MDA-MB-231 (5×10^5) were seeded out into 6-well plates in complete medium and propagated to 80% confluency. Separate sets of cells were incubated with to serum-free medium for 60 min prior to activation. The cells were then activated with PAR2-AP ($20 \mu\text{M}$) for 20 min. PTEN protein was immunoprecipitated from cell lysate using a mouse anti-PTEN antibody captured with protein A-magnetic beads. The immunoprecipitated protein samples were separated by SDS-PAGE, transferred to nitrocellulose membranes and blocked. In order to detect the presence of MAGI-2, the membranes were probed with a rabbit anti-MAGI-2 primary antibody overnight at 4°C . As a control, the antibodies were substituted with a rabbit IgG isotype. The membranes were probed with a secondary goat anti-rabbit alkaline phosphatase-conjugated antibody. The bands were developed with Western Blue-stabilised substrate for alkaline phosphatase and photographed. B) The band densities were quantified to determine the interaction of MAGI-2 with PTEN between activated and non-activated samples ($n = 3$; $* = p < 0.05$ vs. the non-activated sample).

3.3 Discussion

The signalling arising from TF has been associated with normal physiological processes (Pradier and Ettelaie 2007) as well as cancer cell proliferation, migration and metastasis (Ruf 2012). Under pathological conditions, the signalling process is mediated by constitutive activation of several signalling pathways one of which is the PI3K-Akt pathway. The downregulation of PTEN together with the activation of Akt results in the induction of downstream signalling that is essential for the promotion of proliferation and survival in cancer cells (Zhang *et al* 2012). In addition, there is already an established association between PTEN mutation/deregulation and increased TF expression in tumour cells (Rong *et al* 2005; Fang *et al* 2006). In this section of the study, it was hypothesised that PTEN activity may also vary depending on the level and type of inflammation. It was proposed that the response of cells to acute levels of TF such as those found in injury and trauma may differ from the adaptive behaviour of the cells as observed in longer-term chronic diseases. For this reason, the phosphorylation state of PTEN as well as the activities of PTEN and Akt in seven cancer cell lines were monitored in the short-term following a single treatment with rec-TF, or following PAR2 activation. In addition, the rate of cell proliferation on exposure of cells to repeated doses of TF was also monitored over five days. The auto-de-phosphorylation of PTEN is reported to be the first step in the activation process of PTEN (Vazquez *et al* 2000). The cellular exposure to TF (Figure 3.5) or activation with PAR2-AP (Figure 3.7), induced some level of PTEN de-phosphorylation in all cell lines examined. However, the levels of PTEN de-phosphorylation were particularly highest in MDA-MB-231, CaCo-2 and LoVo cells (Figure 3.6). The de-phosphorylation of PTEN was concurrent with the enhanced lipid-phosphatase activity (Figure 3.8 and 3.9) which was also reflected in the reduced kinase activity of Akt (Figure 3.10 and 3.11). Following injury or trauma, cells may become exposed to large quantities of TF together with the activation PAR2 by coagulation proteases. Therefore, as a possible explanation, the

activation of PTEN may prevent the survival of severely damaged cells by lowering the cellular activity of Akt.

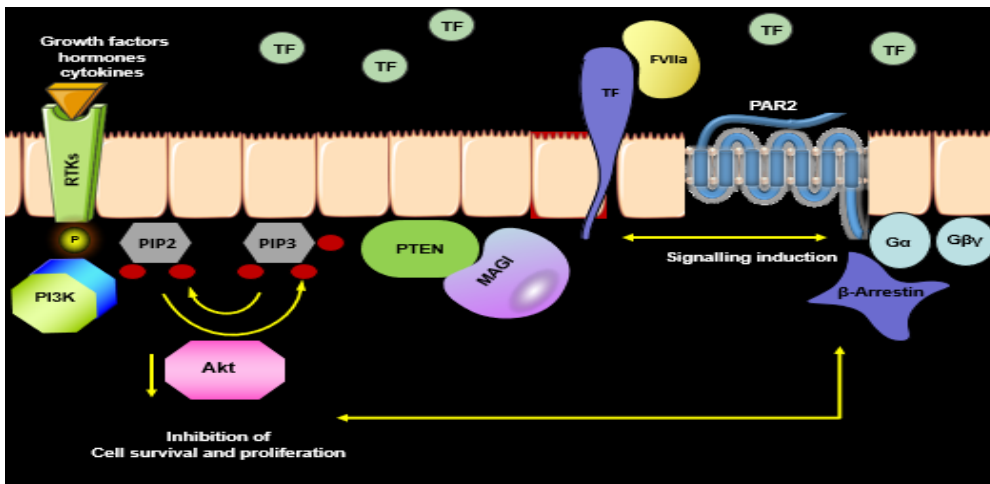
The interaction of MAGI proteins with PTEN plays an important role in the recruitment of PTEN to the inner membrane and the regulation of PTEN function as a tumour suppressor (Georgescu *et al* 2000; Leslie *et al* 2000). Moreover, the interaction of MAGI with PTEN at the cell membrane has been reported to protect PTEN from degradation (Subauste *et al* 2005). However, the release of PTEN from MAGI proteins has been reported to destabilise PTEN and promote its degradation (Hu *et al* 2007). PAR2 activation of MDA-MB-231 cells resulted in a reduction in the association of PTEN with MAGI-1 and MAGI-2 (Figure 3.15 and 3.16) which was further confirmed by co-immunoprecipitation (Figure 3.18 and 3.19). Several studies have reported that caspases can cleave MAGI proteins (Torres *et al* 2003; Ivanova *et al* 2007). Moreover, it has been reported that caspase-1 is needed for the release of procoagulant TF-bearing microvesicles (Rothmeier *et al* 2015) and PAR2 activation is known to induce the release of procoagulant TF-bearing microvesicles (Collier and Ettelaie 2011; Ettelaie *et al* 2016). In addition, it also been reported that caspase-3 can also be activated by PAR2 (Iablokov *et al* 2014). Therefore, the activation of PAR2 may trigger the induction of caspases which result in the degradation of MAGI proteins which suggests a mechanism for the dissociation of PTEN from MAGI proteins. Upon injury, PAR2 activation causes the release of PTEN from MAGI proteins which in the short-term may increase the PTEN activity. This in turn, suppresses the Akt kinase activity to prevent aberrant cell survival and proliferation.

The activation of the coagulation mechanism is a common feature associated with cancer. As a result, PAR2 activation mediated by the TF-FVIIa complex promotes various signalling pathways which have been linked to tumour growth (Ruf *et al* 2010; Grover and Mackman 2018). To mimic the continuous activation of the coagulation mechanism observed in long-term chronic diseases, the cells were exposed to multiple doses of TF over five days. The

prolong incubation of cells with rec-TF resulted in the reduction of cellular PTEN antigen levels (Figure 3.13). It is possible that the activation of PAR2 due to the constant exposure of cells to TF could progressively reduce cellular PTEN levels which subsequently degrade PTEN. In fact as mentioned above, it has been reported that caspase-3 is capable of digesting PTEN (Torres *et al* 2003). Therefore, it is possible that the continuous activation of PAR2 induces caspase activation which subsequently and progressively reduces the amount of PTEN through degradation. As a result, the regulation of cell survival and proliferation becomes compromised through increased Akt activity (Figure 3.14) and manifests in the increased rate of cell proliferation (Figure 3.12A-C).

The perturbation of cells often occurs as a consequence of injury which can also result in the exposure of TF and the activation of coagulation (Figure 3.20). Under such conditions, it is imperative to make a distinction between the severely injured cells and those which may be revived. Since TF is one of the first proteins which appears at the site of injury, it may possess the ability to subsequently initiate differing signals in order to direct the cells towards apoptosis or proliferation respectively. This study has demonstrated the ability of TF to induce PTEN activation in the short term, while prolonged exposure to TF appears to reduce the total cellular PTEN protein. This may in turn result in aberrant cell survival and proliferation during chronic conditions.

A)



B)

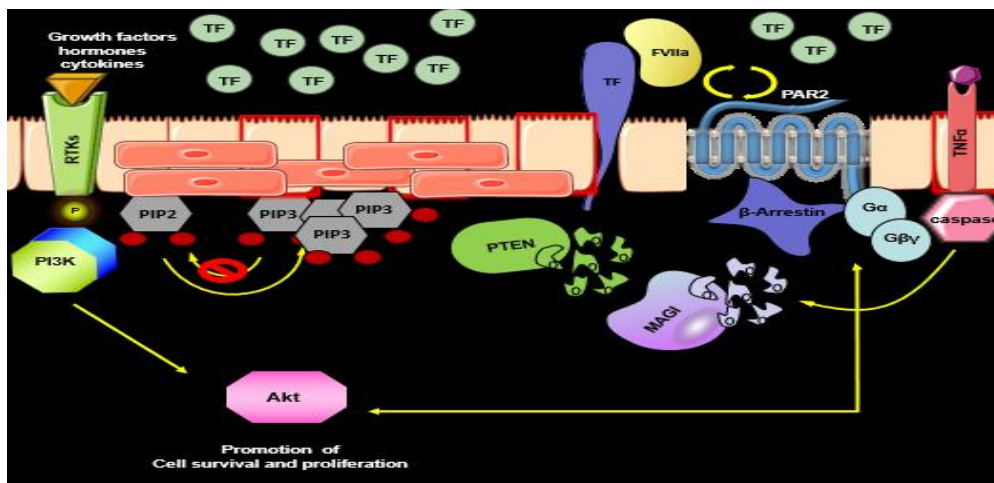


Figure 3. 20 The proposed role of TF on the regulation of PTEN. A) Under normal physiological conditions, TF together with the activation of PAR2 promotes PTEN activation leading to an increase in the lipid-phosphatase activity of PTEN. B) Under chronic conditions, the signalling arising from TF-FVIIa-PAR2 decreases cellular PTEN antigen levels resulting in enhanced Akt activity and aberrant cell formation.

Chapter 4

Investigation of the regulation of TF localisation by

interaction with MAGI proteins

4.1 Introduction

The cellular expression of TF is tightly controlled to balance the procoagulant activity and to prevent the formation of thrombosis (Kothari *et al* 2013). Moreover, the expression of TF at the apical side of endothelial cells and the basolateral regions of epithelial cell lines has been reported (Camerer *et al* 1996). In addition, it has been documented that TF is localised at the tight junctions in confluent MDCK cell lines (Camerer *et al* 1996). The cellular localisation of TF at cell-cell junctions of myocytes was also reported (Luther *et al* 2000; Ruf and Riewald 2000). In cancer cell lines, TF was reported to localise at the intercellular boundaries of MCF-7 breast cancer cell line (Müller *et al* 1993) and at the cell-cell junction of skin and colorectal cancer cells (Garnier *et al* 2012). However, this property was absent from J82 bladder carcinoma cells which were incapable of forming tight junctions (Narahara *et al* 1994). In addition, it has been documented that the cytoplasmic domain of TF interacts with filamin-A, a cytoskeletal protein that regulates the trafficking of TF (Collier *et al* 2017). Furthermore, the regulation of TF-containing microvesicles release has also been shown to be modified by peptidyl-prolyl trans/cis isomerase 1 (Pin-1). Pin-1 regulates the function of proteins through conformational changes, by isomerisation of phosphorylated Serine/Threonine-Proline (pSer/Thr-Pro) motifs (Ettelaie *et al* 2018; Kurakula *et al* 2018). This interaction is mediated through a well-conserved Ser258-Pro259 amino acid motif, which is present in the cytoplasmic domain of TF in many species. Therefore, in this part of the investigation it was hypothesised that TF might be restrained at the cell junctions through binding to MAGI proteins. This interaction may be mediated by a putative PDZ-binding sequence found within the cytoplasmic domain of TF. Using the PDZ domain-peptide interaction website (POW) program (Hui *et al* 2013) which predicts PDZ domain-peptide interactions based on sequence and structural predictors. It suggested that TF may interact with a few PDZ-containing proteins including MAGI proteins. Since the data produced in the previous chapter showed that TF may regulate

the function of PTEN, which influences the interaction of the latter protein with MAGI proteins. Therefore, the next series of experiments were designed to explore the possibility that any of the MAGI proteins may interact with TF and to examine the possibility that such an interaction may control the localisation of TF at the cell junction.

4.1.1 MAGI proteins

Endothelial and epithelial cells maintain homeostasis, provide protective barriers to organs from the surrounding environments and regulate movement of solutes across the epithelium. These protective barriers are formed, in part, of an intercellular adhesion complex which consists of desmosomes, adherens and tight junctions. The junctional adhesion molecule (JAM), claudin and occludin are integral tight junction proteins, whereas proteins such as zonula occludens (ZO1-3) and MAGI(1-3) belong to the membrane-associated tight junction proteins (Padash Barmchi *et al* 2016; Bhat *et al* 2019). It has been reported that the interaction between integral membrane proteins and membrane-associated proteins is crucial for the correct organisation of tight junctions (Hirabayashi *et al* 2003). It has been documented that tight and adherens junctions are tightly associated and often reside at the polarised apical end of epithelial cells, however in endothelia, tight and adherens junctions are often intermixed (Padash Barmchi *et al* 2016). There is a growing body of evidence implicating these junctional proteins in cell signalling, migration, a range of inherited human diseases and cancer progression (Zihni *et al* 2016). In recent years, the MAGI family has emerged as an example of the vast number of tight junction proteins which function to recruit and stabilise several membrane proteins at the cell-cell junctions (Hammad *et al* 2016). Several studies have reported that MAGI proteins are localised at the tight junctions and regulate the function of a number of different proteins mediated through the WW and PDZ domains in the MAGI proteins (Feng *et al* 2014; Padash Barmchi *et al* 2016). For example, in kidney and small intestine cells, MAGI-1 was shown to interact with junctional adhesion molecule JAM-4, a

homolog of JAM-A, through PDZ1 and PDZ4 (Hirabayashi *et al* 2003). This interaction gives rise to enhanced JAM-4 mediated cell adhesion and strengthening of the tight junctions. MAGI-1 has also been reported to recruit E-cadherin and β -catenin at the junctional sites of colorectal cells again resulting in enhanced stability of the resulting tight junctions (Zaric *et al* 2012; Zaessinger *et al* 2015). Moreover, a study by Wegmann *et al* (2004) reported that endothelial cell-selective adhesion molecule (ESAM), immunoglobulin-like transmembrane cell surface protein associated with endothelial tight junctions, interacts with the third PDZ domain of MAGI-1. This interaction anchors MAGI-1 at endothelial tight junctions, resulting in an enhanced stability of endothelia cell-cell contacts. In *C. elegans*, MAGI-1 was shown to localise and interact with apical junction molecule-1 (AJM-1), a homolog of the vertebrate transmembrane tight junction protein, JAM-1, thereby increasing junctional stability and cell adhesion (Stetak and Hajnal 2011). Furthermore, MAGI-3 has been shown to localise with ZO-1 at the tight junctions of epithelial cells, and with E-cadherin at cell junctions of neuronal cells (Adamsky *et al* 2003). The localisation of these proteins at the tight junctions enhanced the adhesion and stability of these cells. Finally, MAGI-2 has been reported to interact with a number of cell adhesion molecules and cytoskeleton-associated proteins, resulting in the stabilisation of these proteins thereby, supporting the architecture of cellular junctions (Nagashima *et al* 2015).

4.1.2 Aim

Under normal conditions, TF was reported to localise at the tight junctions of several cell types. However, this characteristic is lost in cells lacking tight junctions. Since MAGI are a multi-domain tight junctional protein. This study hypothesised that TF might be restrained at the tight junctions through MAGI-dependent interaction (Figure 4.1). However, upon vascular injury or loss of cell-cell contacts this interaction is disrupted resulting in the dissociation of TF from

MAGI proteins. To examine this hypothesis, PLA and co-immunoprecipitation techniques were employed to investigate:

- The interaction between TF and each of the three MAGI proteins separately in endothelial and MDA-MB-231 cells.
- The ability of PAR2 activation to alter any putative interaction between TF and MAGI proteins.
- The association of TF with tight junction proteins, MAGI-1 and JAM-A by fluorescence microscopy.

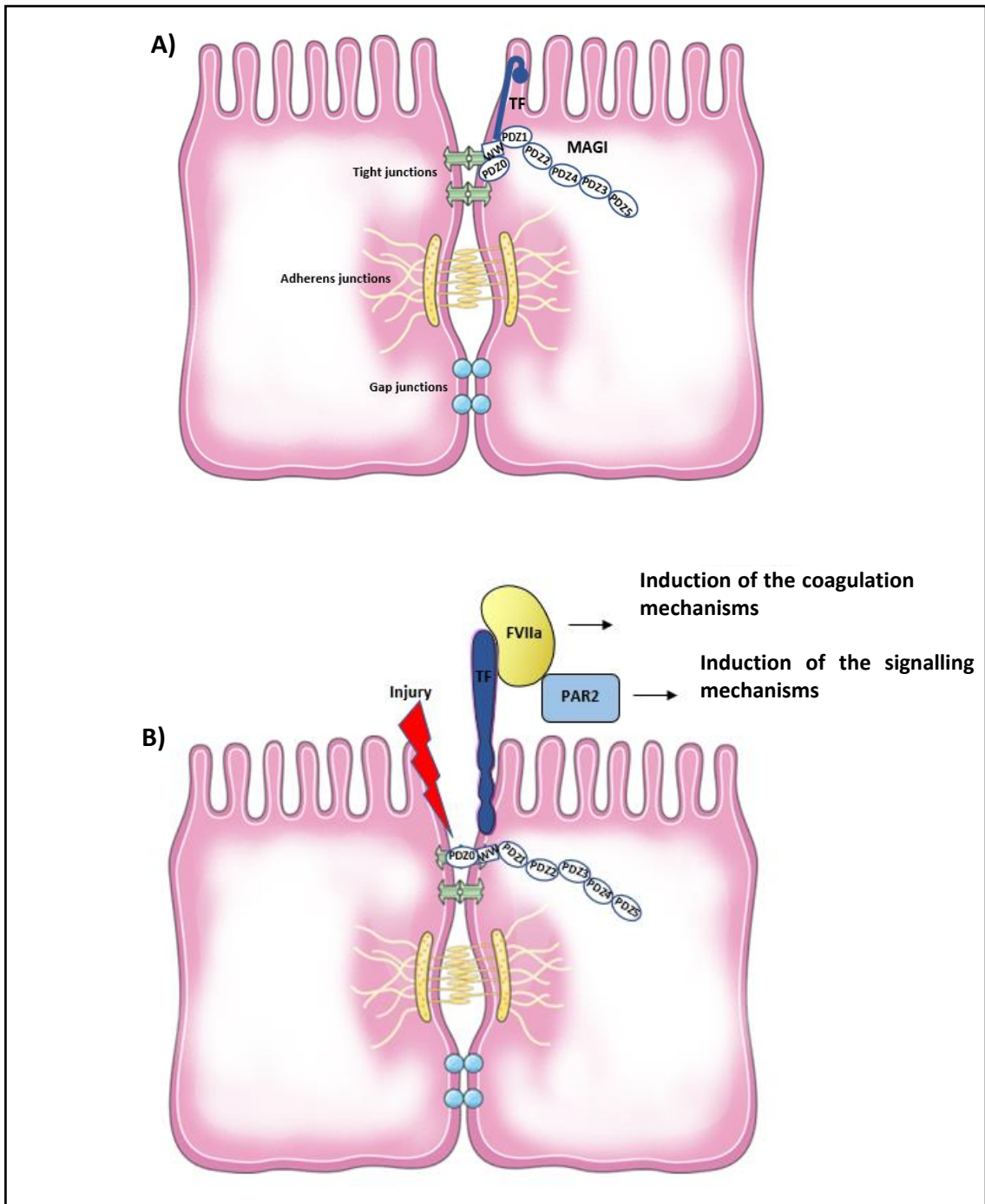


Figure 4. 1 The proposed study by which MAGI proteins may restrain TF at the cellular junctions. A) Under normal conditions, MAGI may prevent the exposure of TF to the cell surface by restraining the latter protein at the tight junctions. B) Disruption of cell membrane integrity due to injury or loss of cell-cell contacts exposes TF to the cell surface where it interacts with FVIIa and activates the coagulation as well as the signalling mechanisms.

4.2 Methods

4.2.1 Examination of the association of TF with MAGI proteins using the PLA

MDA-MB-231 cells (10^3) were seeded into 35 mm-glass based μ -dishes with a 10 mm diameter glass well, and propagated overnight in complete medium. Separate sets of cells were incubated with serum-free medium for 60 min prior to activation. The cells were then activated with PAR2-AP (20 μ M) for up to 40 min. The cells were washed three times with PBS and fixed with 4% (v/v) formaldehyde in PBS for 20 min, washed three times again and then permeabilised using 0.1% (v/v) Triton X-100 in PBS for 10 min. The dishes were washed three times with PBS and then blocked with Duolink® blocking solution at 37°C for 60 min. The blocking solution was discarded and the cells were incubated with primary antibodies diluted 1:100 (v/v) in the provided antibody diluent. Different concentrations of TF and MAGI(1-3) antibodies were used to determine the optimal antibody concentration required for the visualisation of these proteins through fluorescence microscopy (Appendix A-2). To examine the potential association between TF and MAGI proteins, the cells were incubated with a mouse anti-TF antibody (HTF1) together with a rabbit anti-MAGI-1 antibody (H-70) or with a polyclonal rabbit anti-MAGI-2 antibody (C3) or with a polyclonal rabbit anti-MAGI-3 antibody overnight at 4°C. As controls, the antibodies were substituted with a rabbit or mouse IgG isotype controls, respectively. PLA analysis was performed as described in section 2.3.5. The nuclei were labelled with DAPI (2 μ g/ml) and the cytoskeleton with Phalloidin 488 (2 μ g/ml) for 10 min. Images were acquired using a Zeiss Axio Vert.A1 inverted fluorescence microscope with a X40 magnification. The number of red fluorescent events and the nuclei were determined using ImageJ software, in 10 fields of view from each assay.

4.2.2 Examination of the interaction between TF and MAGI-1 by co-immunoprecipitation

MDA-MB-231 cells (5×10^5) were seeded out into a 6-well plate and propagated to 80% confluency. The cells were washed three times with PBS and then lysed with Phospho-Safe™ extraction buffer (500 µl). TF was immunoprecipitated from cell lysates with a mouse anti-TF antibody (8 µg; HTF1). In a reverse of the procedure, MAGI-1 protein was immunoprecipitated from cell lysates with a rabbit anti-MAGI-1 antibody (8 µg; H-70). To ensure specificity, a mouse or rabbit IgG isotype control (8 µg) was also included as well as an additional control without any antibody. The immunoprecipitated proteins were incubated overnight at 4°C using a rotating mixer. On the following day, the antibody in the cell lysates was captured with protein A-magnetic beads (100 µl) for 120 min using a rotating mixer, at 4°C. The supernatants were discarded and the beads were washed five times with TBST. The samples were lysed in Laemmli's buffer and the immunoprecipitated proteins were separated by SDS-PAGE, transferred to nitrocellulose membranes and blocked. In order to detect the presence of TF, the membranes were probed with a mouse anti-TF primary antibody (HTF1) diluted 1:2000 (v/v) in TBST overnight at 4°C. The membranes were probed with an alkaline phosphatase-conjugated goat anti-mouse IgG antibody diluted 1:8000 (v/v) in TBST. In order to detect the presence of MAGI-1, the membranes were probed with a rabbit anti-MAGI-1 antibody diluted 1:2000 (v/v) in TBST overnight at 4°C. The membranes were then probed with an alkaline phosphatase-conjugated goat anti-rabbit IgG antibody diluted 1:8000 (v/v) in TBST. In both cases bands were developed with Western Blue-stabilised substrate for alkaline phosphatase and photographed.

4.2.3 Examination of the association of TF with tight junction proteins JAM-A and MAGI-1

MDA-MB-231 cells (10^3) were seeded out into 35 mm-glass based μ -dishes with 10 mm diameter glass well in complete medium and propagated to confluency. The cells were fixed with 4% (v/v) formaldehyde for 20 min and then washed with PBS. The cells were permeabilised using 0.1% (v/v) Triton X-100 for 10 min, washed with PBS and blocked with 3% (w/v) BSA diluted in PBS, for 60 min. In order to demonstrate the co-localisation of TF with MAGI-1 within the cell boundaries, the cells were probed for TF using a FITC-conjugated anti-TF antibody (HTF1-FITC), and MAGI-1 using a rabbit anti-MAGI-1 antibody (H-70) diluted 1:100 (v/v) 3% BSA in PBS, and incubated overnight at 4°C. In order to visualise MAGI-1 protein, the cells were washed three times with PBS and then probed with a goat anti-rabbit IgG-Alexa Fluor 594 antibody diluted 1:100 (v/v) in 3% BSA in PBS for 60 min. Furthermore, to demonstrate the co-localisation of TF with JAM-A within the cell boundaries, another set of cells were probed with TF using a conjugated anti-TF antibody (HTF1-FITC) and JAM-A protein using a goat anti-JAM-A antibody both diluted 1:100 (v/v) 3% BSA in PBS, and incubated overnight at 4°C. The cells were washed three times with PBS and then probed with a donkey anti-goat IgG-Alexa Fluor 594 antibody diluted 1:100 (v/v) in blocking buffer to detect JAM-A protein. The nuclei were stained with DAPI (2 μ g/ml) for 10 min. Images were acquired using a Zeiss Axio Vert.A1 inverted fluorescence microscope with a X40 magnification.

4.2.4 Examination of the influence of PAR2 activation on the localisation of TF within the cell junction

To examine the influence of PAR2 activation on the localisation of TF within the cell boundaries, MDA-MB-231 cells (10^3) were seeded out into 35 mm-glass based μ -dishes with 10 mm well size in complete medium and propagated to confluency. Separate sets of cells were

incubated with serum-free medium for 60 min prior to activation. The cells were then activated with PAR2-AP (20 μ M) for 20 min. The cells were fixed with 4% (v/v) formaldehyde for 20 min, washed twice with PBS and then permeabilised using 0.1% (v/v) Triton X-100 for 10 min. After further washes, the cells were blocked with 3% (w/v) BSA diluted in PBS for 60 min and then probed for TF using a conjugated anti-TF antibody (HTF1-FITC) diluted 1:100 (v/v) in blocking buffer for another 60 min. The cells were washed with PBS and the nuclei were stained with DAPI (2 μ g/ml) for 10 min. Images were acquired using a Zeiss Axio Vert.A1 inverted fluorescence microscope with a X40 magnification.

4.3 Results

4.3.1 Prediction of the interacting motifs between TF and MAGI proteins using the POW software

The activity of TF has been suggested to be regulated through the ENSPL sequence motif located within its cytoplasmic domain (Ettelaie *et al* 2018; Kurakula *et al* 2018). In addition, MAGI proteins are characterised by their structure consisting of six PDZ domain, guanylate kinase domain as well as two WW domains (Padash Barmchi *et al* 2016). Therefore, the POW software (Hui *et al* 2013) was used to predict the capability of the cytoplasmic domain of TF to interact with any PDZ-containing proteins. This produced high scores for PDZ domains in MAGI-1, MAGI-3, MAGI-X proteins and also for rhophilin. In addition, the amino acid sequence ENSPL (256-260 aa) within the cytoplasmic domain of TF was identified as the most likely PDZ binding sequence in TF (Table 4.1). The interaction of TF with rhophilin and MAGI-X was ruled out in a separate study in the laboratory, therefore MAGI(1-3) proteins were selected for further analyses.

Table 4. 1 Sequences and scores for the predicted PDZ domains capable of interacting with TF peptides

PDZ Domain Name	Sequence of Domain Binding Site	Peptide Sequence	SVM Decision Score
ARHGAP23-1	GFGFTLNGKNKGYSIS	ENSPL	0.03
GRIP2-5	ELGITISSDKSMEVC	SPLNV	0.056
LIN7B-1	GLGFNIMGSRIGHEVA	KENSP	0.184
LIN7C-1	GLGFNIMGSRIGHEVA	KENSP	0.184
MAGI1-6	GFGFSLRGLRAGHSIG	ENSPL	0.429
MAGI3-6	GFGFSLRGLRAGHTIG	ENSPL	0.438
MAGIX-1	GFGLTLGGRGLGHA VG	ENSPL	0.48
MPP4-1	FKGATIKRARIGPEIS	KENSP	0.057
PDLIM1-1	GWGFRLVGSRTSHLQC	ENSPL	0.035
PDLIM5-1	PWGFRLQGSSKGHLQC	ENSPL	0.073
RHPN1-1	GFGLTLRGAAISHAVG	ENSPL	0.603

The POW software sequence predication parameter showing the protein name, the Support Vector Machines (SVM) decision scores which measure the predicted interaction score and the possible interacting sequences between the target protein and the PDZ-containing protein with values ≥ 1 are considered relevant (Hui and Bader 2010).

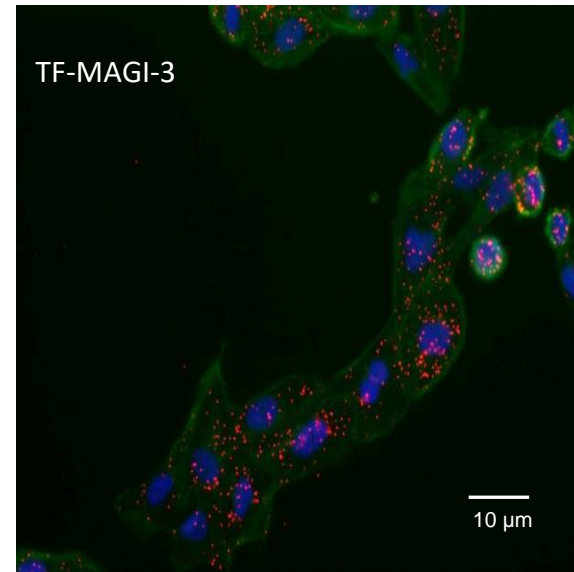
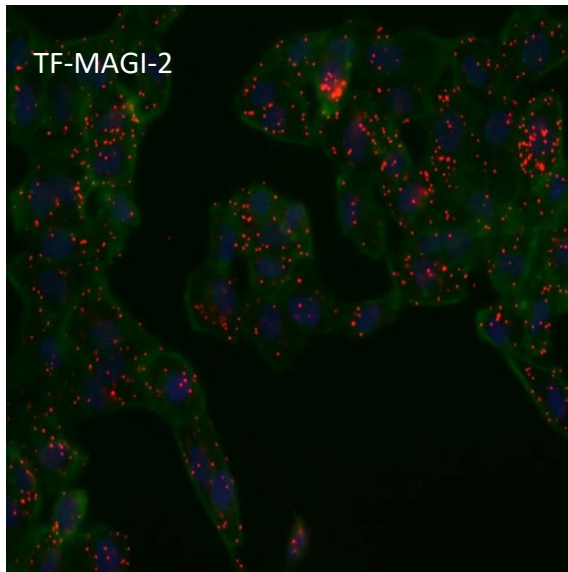
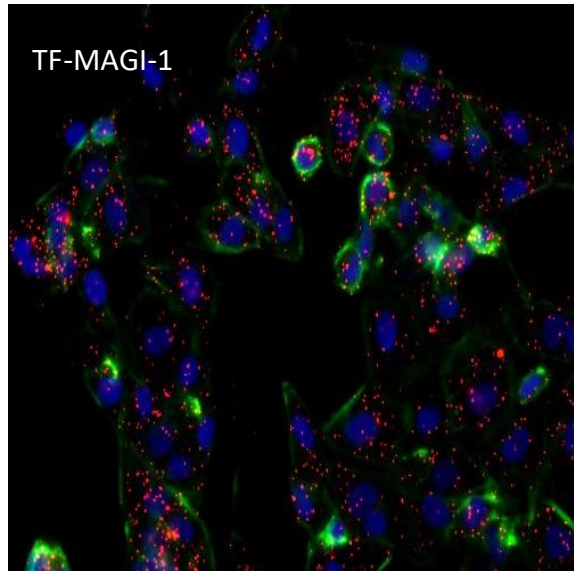
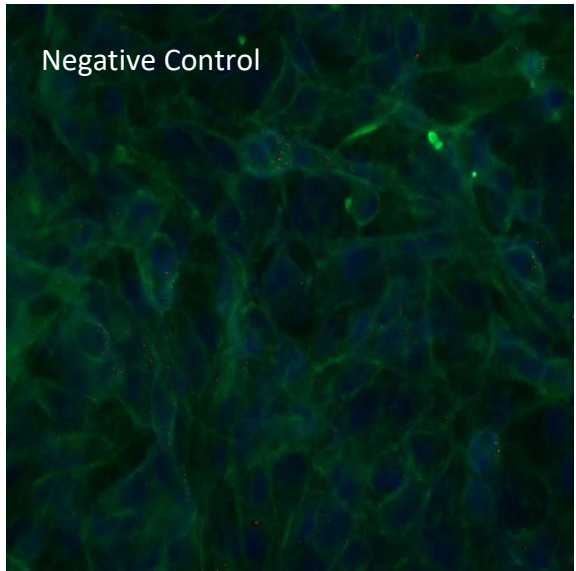
4.3.2 Examination of the association of TF with MAGI-(1-3) proteins using the PLA

Firstly, to ensure the interaction between TF and MAGI proteins are not influenced by non-specific binding, PLA was performed between TF and each of the MAGI-(1-3) protein using a mouse anti-TF antibody together with a rabbit IgG isotype control. Other PLA sets were also performed, using rabbit anti-MAGI-(1-3) antibodies together with a mouse IgG isotype control (Figure 4.2). Next, PLA was employed to investigate the possible association of TF with each of the proteins using a mouse anti-TF antibody together with a rabbit anti-MAGI-1 antibody, a rabbit anti-MAGI-2 or a rabbit anti-MAGI-3 antibody. Analysis of 4 independent PLA repeats indicated that TF associates with all three members of the MAGI family. However, the association between TF and MAGI-1 was higher than those observed with either MAGI-2 or MAGI-3 (Figure 4.2).

4.3.3 Activation of PAR2 reduces the association between TF and MAGI-1

To examine the influence of PAR2 activation on the association between TF and MAGI proteins, MDA-MB-231 cells were propagated overnight and then activated with PAR2-AP over a period of 40 min, on the following day. PLA was then carried out and the data obtained from 4 independent PLA repeats showed a transient reduction in the association between TF and MAGI-1 at around 20 min post activation (Figure 4.3) which then normalised by 30 min. Since the association between TF and MAGI-2 or MAGI-3 was not significant, the time course was not carried out and the association was only measured at 20 min. PLA analysis of cells did not show a significant change in the association of TF with either MAGI-2 (Figure 4.4) or MAGI-3 (Figure 4.5) following PAR2 activation.

A)



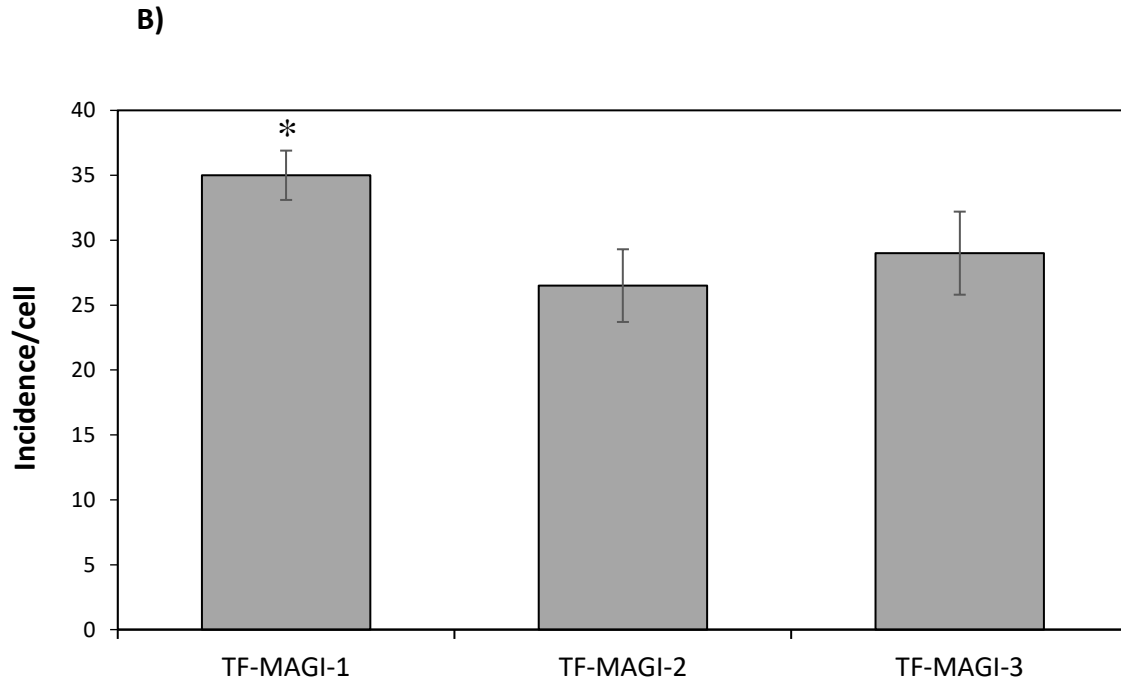
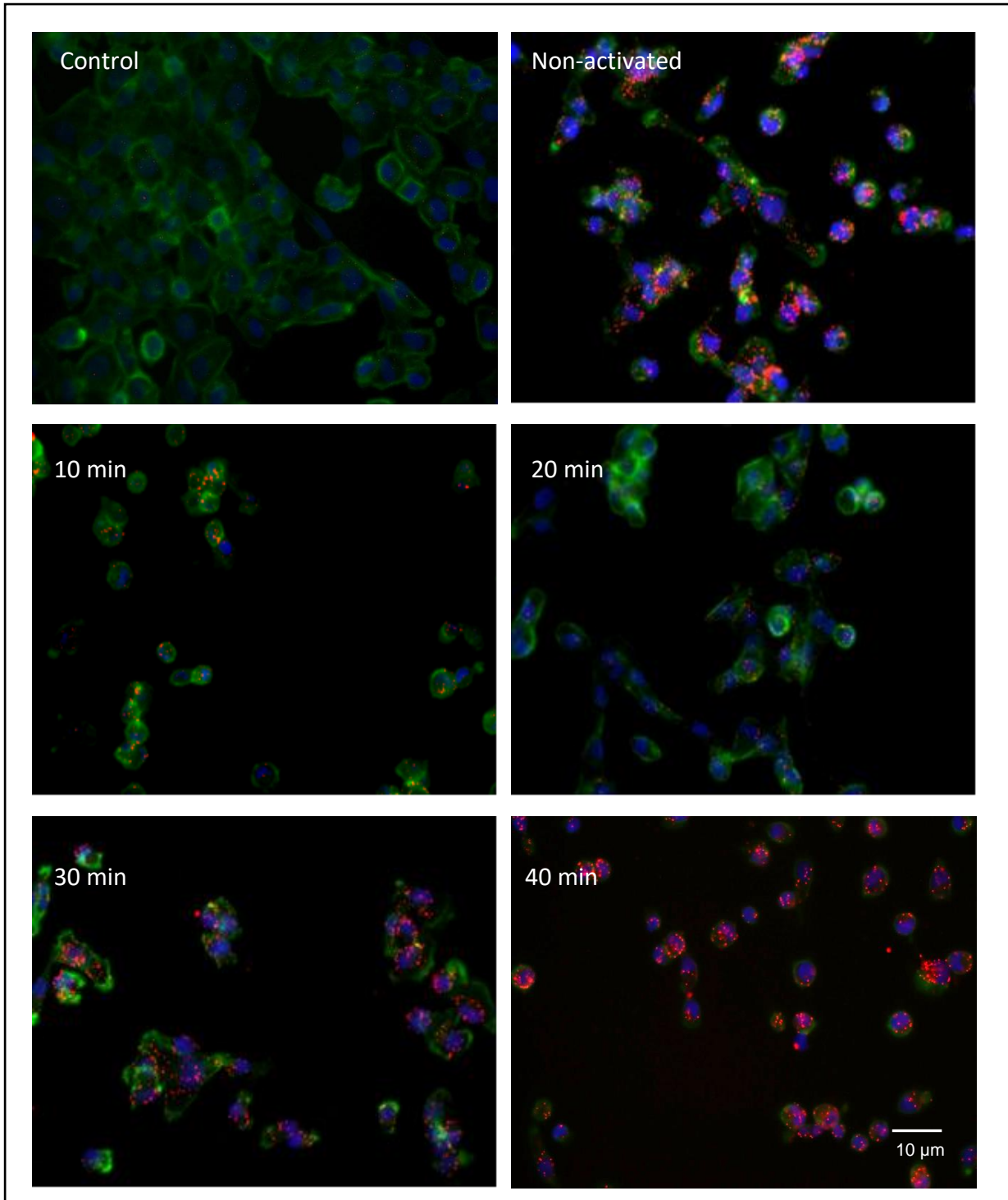


Figure 4. 2 Examination of the association between TF and MAGI (1-3) proteins using PLA. A) MDA-MB-231 cells (10^3) were seeded into 35 mm-glass based μ -dishes and grown in complete medium overnight. The cells were fixed with 4% (v/v) formaldehyde for 20 min, washed twice with PBS and then permeabilised using 0.1% (v/v) Triton X-100 for 10 min. After further two washes with PBS, the cells were blocked with Duolink® blocking solution at 37°C for 60 min. The proximity between TF and MAGI-(1-3) was examined using a mouse anti-human TF antibody mixed together with a rabbit anti-MAGI-1 antibody or with rabbit anti-MAGI-2 antibody or with rabbit anti-MAGI-3 antibody diluted 1:100 (v/v) in the provided antibody diluent. As controls, the antibodies were substituted with rabbit or mouse IgG isotypes. The PLA analysis was performed as described in section 2.3.5. The nuclei were then labelled with DAPI and the cytoskeleton with Phalloidin 488 for 10 min and images were acquired using a Zeiss Axio Vert.A1 inverted fluorescence microscope with a X40 magnification. The micrographs are representative of 10 fields of view from 4 independent experiments. (RED= PLA incidences; GREEN = Phalloidin; BLUE = DAPI). B) The interaction of TF and MAGI(1-3) were determined based on the quantified number of red fluorescent events around the nuclei using ImageJ software. (n = 4; * = p< 0.05 vs. MAGI-2 and/or MAGI-3 samples).

A)



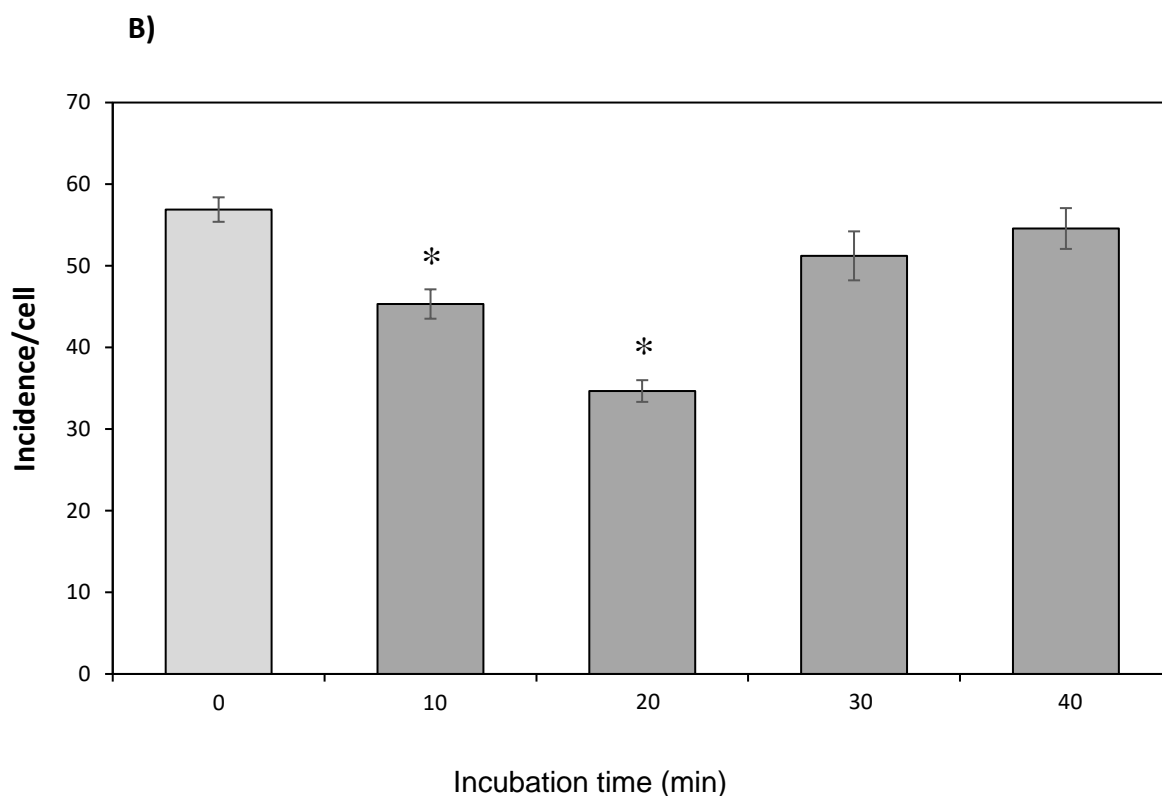


Figure 4. 3 Examination the influence of PAR2 activation on the association of TF with MAGI-1 by PLA assay. A) MDA-MB-231 cells (10^3) were seeded out into 10 mm-glass based μ -dishes in complete medium overnight. Separate sets of cells were incubated with serum-free medium for 60 min prior to activation. The cells were then activated with PAR2-AP ($20 \mu\text{M}$) over a period of up to 40 min. The cells were fixed, permeabilised and blocked. The proximity between TF and MAGI-1 was examined using a mouse anti-TF antibody together with a rabbit anti-MAGI-1 antibody as described in Figure 4.1. PLA analysis was performed as described in section 2.3.5. Images were acquired using a Zeiss Axio Vert.A1 inverted fluorescence microscope with a X40 magnification. The micrographs represent 10 fields of view from 4 independent experiments. RED= PLA incidences; GREEN = Phalloidin; BLUE = DAPI. B) The interaction of TF and MAGI-1 at intervals up to 40 min were determined based on the quantified number of red fluorescent events around the nuclei using ImageJ software ($n = 4$; * = $p < 0.05$ vs. the respective non-activated samples).

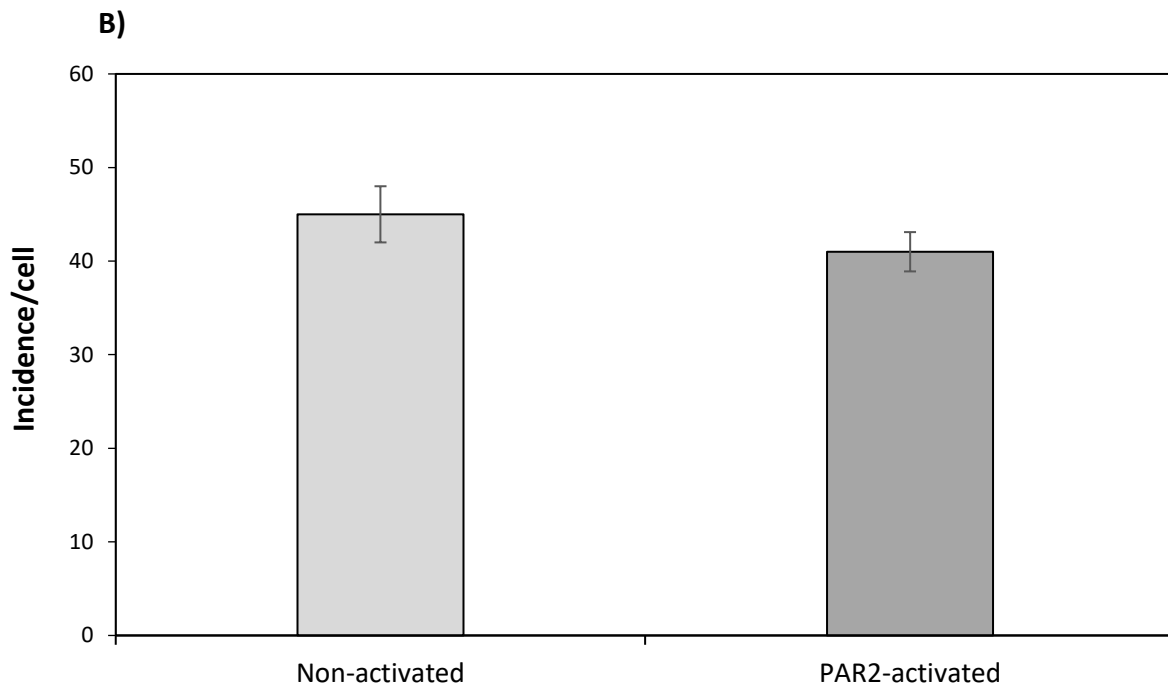
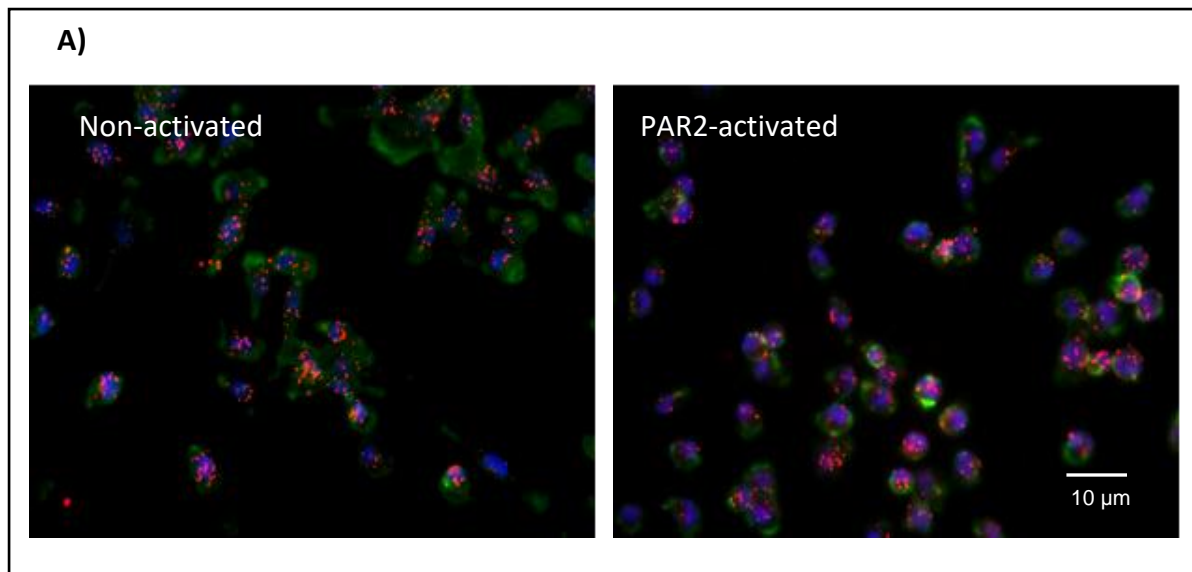


Figure 4. 4 Examination the influence of PAR2 activation on the association of TF with MAGI-2 by PLA. A) MDA-MB-231 cells (10^3) were seeded out into 10 mm-glass based μ -dishes in complete medium overnight. Separate sets of cells were incubated with serum-free medium for 60 min prior to activation. The cells were then activated with PAR2-AP (20 μ M) for 20 min. The cells were fixed, permeabilised and blocked as described in section 4.2.1. The proximity between TF and MAGI-2 was examined using a mouse anti-TF antibody together with a rabbit anti-MAGI-2 antibody. PLA analysis was performed as described in section 2.3.5. Images were acquired using a Zeiss Axio Vert.A1 inverted fluorescence microscope with a X40 magnification. The micrographs represent 10 fields of view from 4 independent experiments. B) The interaction of TF and MAGI-2 at intervals up to 40 min were determined based on the quantified number of red fluorescent events around the nuclei using ImageJ software ($n = 4$).

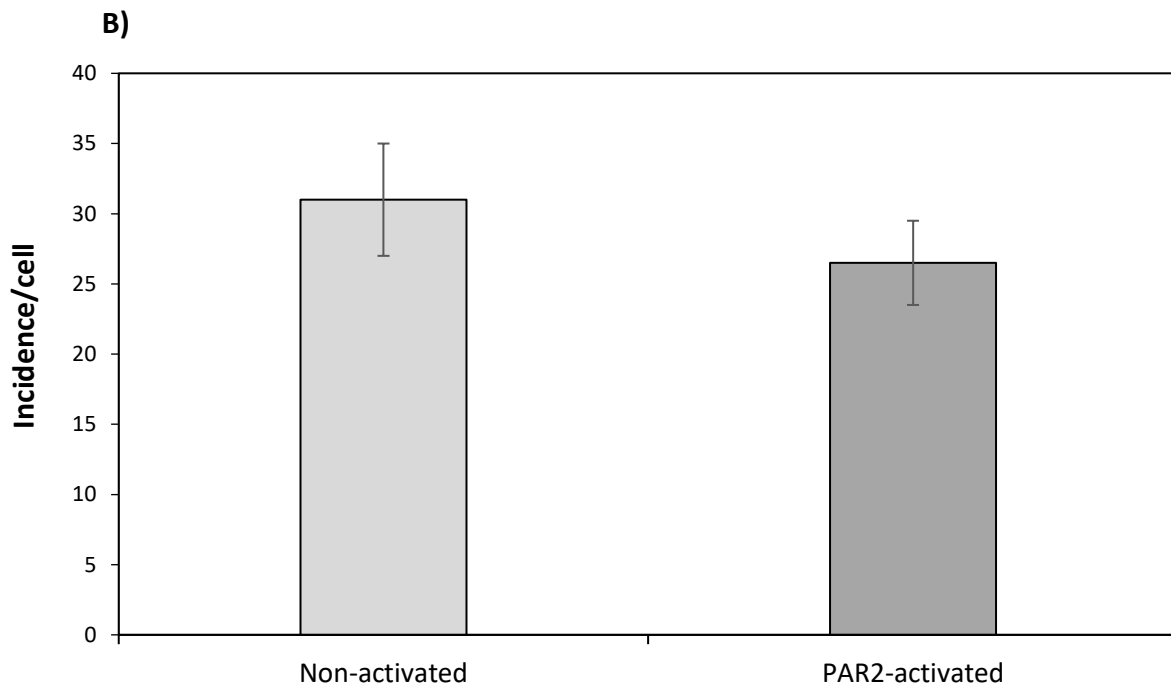
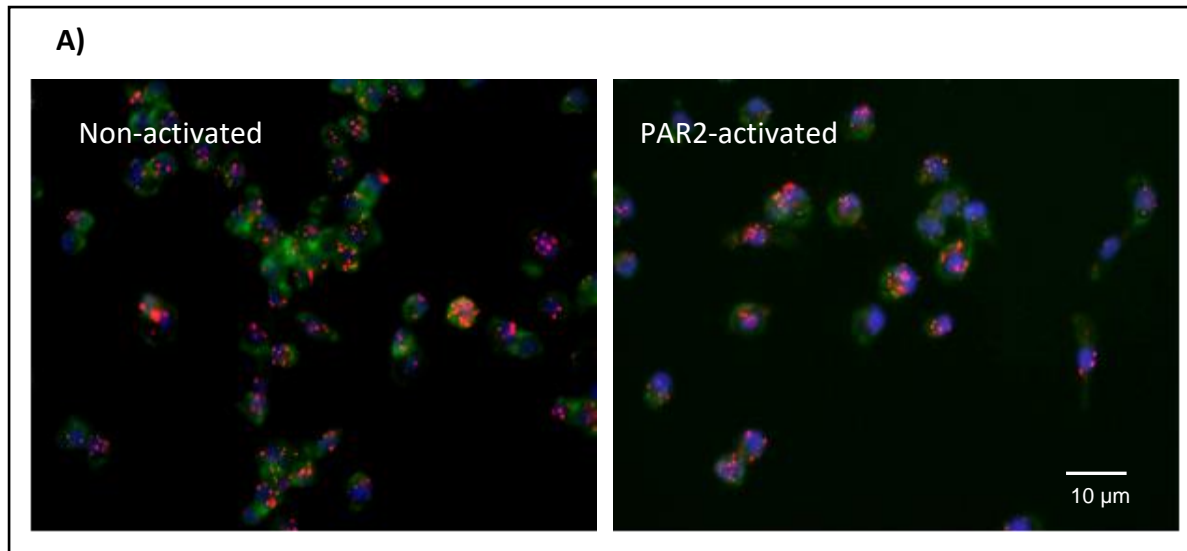


Figure 4. 5 Examination the influence of PAR2 activation on the association of TF with MAGI-3 by PLA assay. MDA-MB-231 cells (10^3) were seeded out into 10 mm-glass based μ -dishes in complete medium overnight. The cells were activated with PAR2-AP for 20 min and then fixed, permeabilised and blocked as described in section 4.2.1. A) The proximity between TF and MAGI-3 was examined using a mouse anti-TF antibody together with a rabbit anti-MAGI-3 antibody. PLA analysis was performed as described in section 2.3.5. B) The interaction of TF and MAGI-3 at 20 min were determined based on the quantified number of red fluorescent events around the nuclei using ImageJ software (n=4).

4.3.4 Examination the influence of PAR2 activation on the interaction between TF and MAGI-1 by co-immunoprecipitation

Since the association of TF with MAGI-1 was shown to be significant, the subsequent co-immunoprecipitation experiments were designed to further investigate the interaction of TF with MAGI-1. Therefore, to confirm the interaction between TF and MAGI-1, TF protein was immunoprecipitated from cell lysates using a mouse anti-TF antibody. Representative examples of western blot analysis from 3 independent immunoprecipitated TF samples confirmed the interaction of TF with MAGI-1 (Figure 4.6). Furthermore, to examine the influence of PAR2 activation on the interaction of TF with MAGI-1, MDA-MB-231 cells were activated with PAR2-AP for 20 min. The cells were lysed and TF antigen was immunoprecipitated using a mouse anti-TF antibody. Western blot analysis of 3 independent repeats from the immunoprecipitated TF samples resulted in a reduction in the interaction between TF and MAGI-1 (Figure 4.6). Alternatively, MAGI-1 protein was immunoprecipitated from cell lysates using a rabbit anti-MAGI-1 antibody. Western blot analysis of 3 independent repeats from the immunoprecipitated MAGI-1 samples also confirmed the interaction between MAGI-1 and TF (Figure 4.7) Similarly, to the results for TF, the interaction of MAGI-1 with TF was reduced in PAR2 activated MDA-MB-231 cells (Figure 4.7).

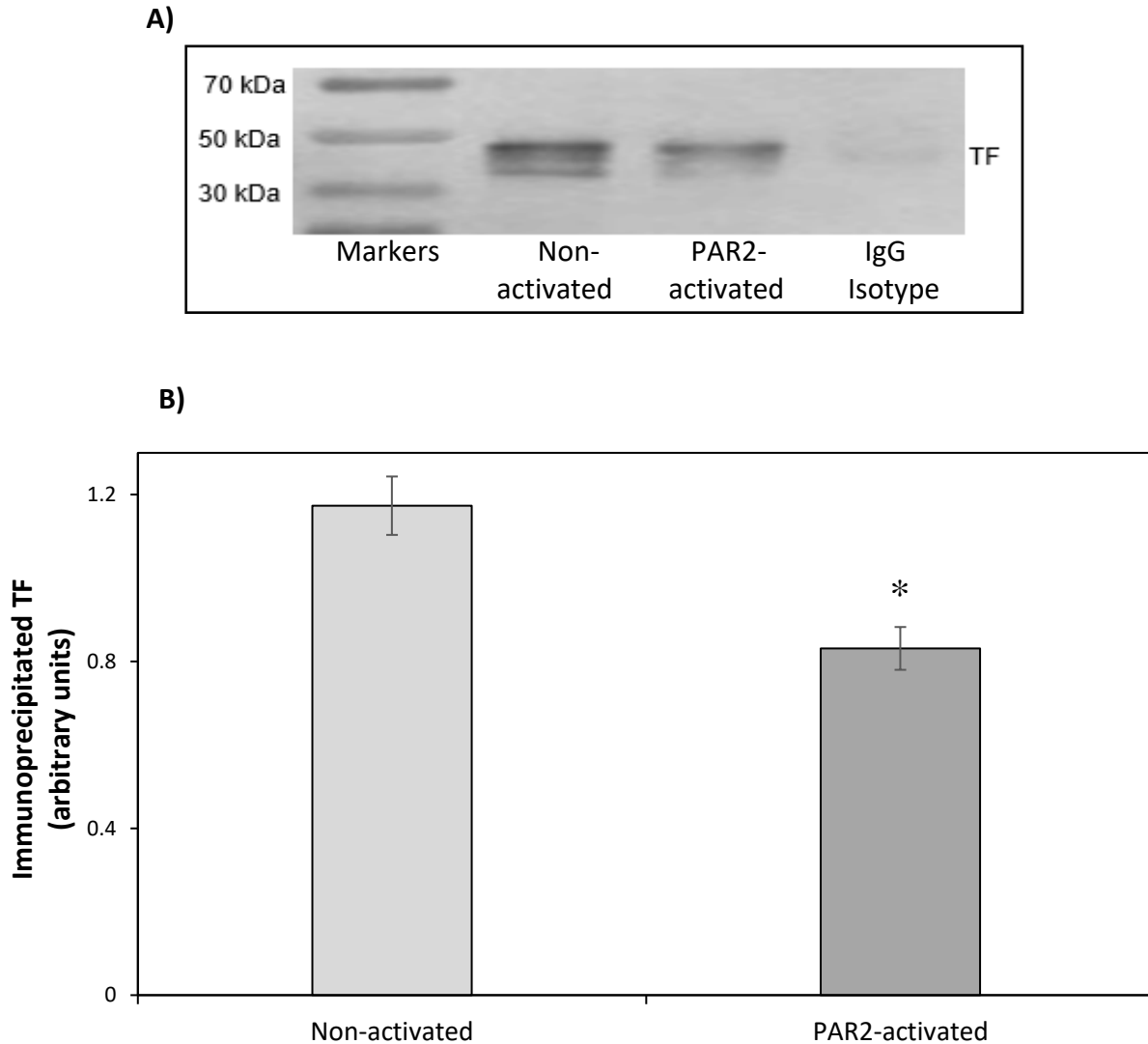


Figure 4. 6 Analysis of PAR2 activation on the interaction of TF with MAGI-1 by co-immunoprecipitation. MDA-MB-231 cells (5×10^5) were seeded out into 6-well plates in complete medium and propagated to 80% confluency. Sets of cells were incubated with serum-free medium for 60 min prior to activation. The cells were then activated with PAR2-AP (20 μ M) for 20 min. MAGI-1 was immunoprecipitated from cell lysates with a rabbit anti-MAGI-1 antibody using protein A-magnetic beads. The immunoprecipitated MAGI-1 protein samples were separated by SDS-PAGE, transferred to a nitrocellulose membrane and blocked. The membranes were probed with a mouse anti-TF primary antibody overnight at 4°C. In order to detect the presence of TF, the membrane was probed with a goat anti-mouse alkaline phosphatase-conjugated antibody. B) The band densities were quantified to determine the interaction of TF and MAGI-1 between activated and non-activated samples ($n = 3$; * = $p < 0.05$ vs. the respective non-activated samples).

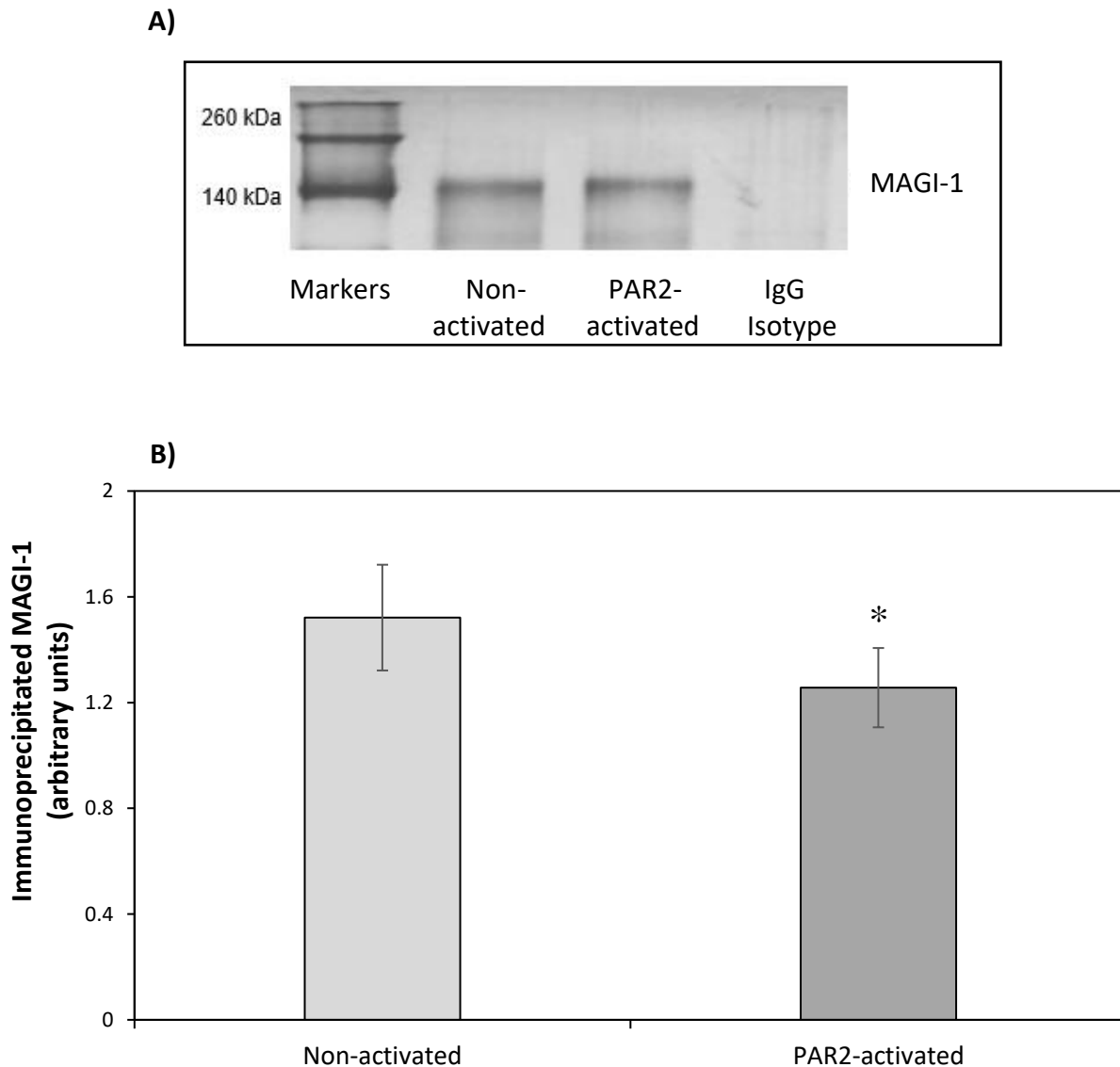


Figure 4. 7 Examination the influence of PAR2 activation on the interaction of MAGI-1 with TF by co-immunoprecipitation. MDA-MB-231 cells (5×10^5) were seeded out into 6-well plates in complete medium and propagated to 80% confluency. Sets of cells were incubated with serum-free medium for 60 min prior to activation. The cells were then activated with PAR2-AP ($20 \mu\text{M}$) for 20 min. TF protein was immunoprecipitated from cell lysates using a mouse anti-TF antibody and captured with protein A-magnetic beads. The immunoprecipitated TF proteins were separated by SDS-PAGE, transferred to a nitrocellulose membrane and blocked. The membranes were probed with a rabbit anti-MAGI-1 primary antibody overnight at 4°C . In order to detect the presence of MAGI-1, the membranes were probed with an alkaline phosphatase-conjugated goat anti-mouse IgG antibody. B) The band densities were quantified to determine the interaction of TF and MAGI-1 between activated and non-activated samples. ($n = 3$; * = $p < 0.05$ vs. the respective non-activated samples).

4.3.5 The association of TF with tight junction MAGI-1 and JAM-A proteins

To explore the localisation of TF at the cellular tight junctions, sets of confluent MDA-MB-231 cells were fixed and probed for TF using a FITC-conjugated anti-TF antibody together with a rabbit anti-MAGI-1 antibody. Another set of confluent MDA-MB-231 cells were probed using a FITC-conjugated anti-TF antibody together with a goat anti-JAM-A antibody. ImageJ analysis of MDA-MB-231 cells indicated that TF localises with JAM-A (Figure 4.8) and with MAGI-1 (Figure 4.9) with overlap coefficient value of (0.512) and (0.523), respectively.

4.3.6 The localisation of TF within intercellular regions is disrupted following PAR2 activation

To investigate the influence of PAR2 activation on the localisation of TF within the tight junctions of cells, confluent MDA-MB-231 cells were activated with PAR2-AP for 20 min. ImageJ analysis of PAR2-activated cells showed a disruption in the pattern of localised TF within the cell junctions when compared to non-activated cells (Figure 4.10).

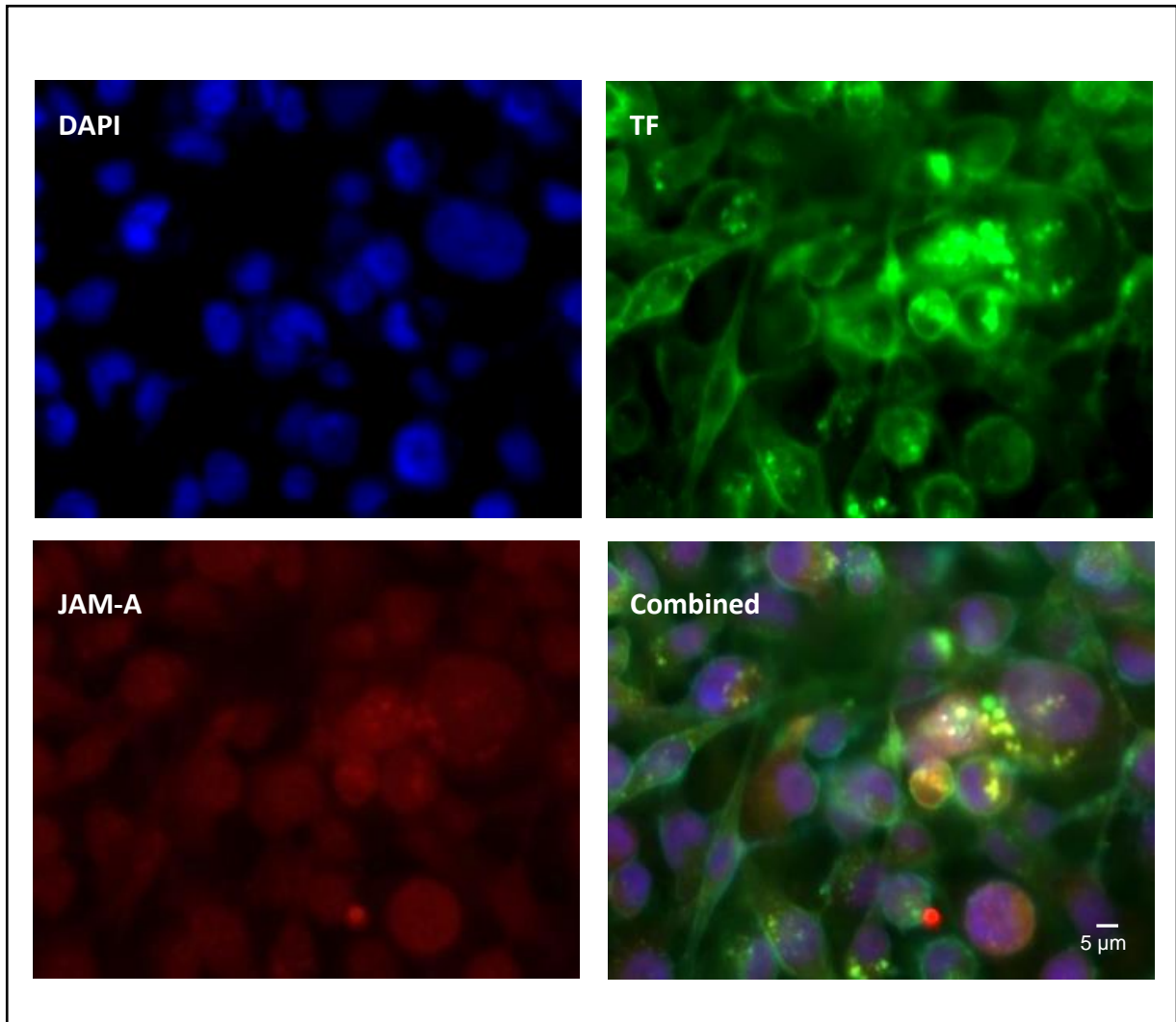


Figure 4. 8 Co-localisation patterns of TF with JAM-A protein. MDA-MB-231 cells (10^4) were seeded out into 10 mm-glass based μ -dishes and permitted to reach confluence. The cells were fixed with 4% (v/v) formaldehyde for 20 min and then washed with PBS. The cells were probed for TF and MAGI-1 using a FITC-conjugated anti-TF antibody together with a goat anti-JAM-A antibody and incubated overnight at 4°C. The cells were washed with PBS and then probed with a donkey anti-goat IgG-Alexa Fluor 594 antibody to detect JAM-A protein. The nuclei were stained with DAPI for 10 min. Images were acquired using a Zeiss Axio Vert.A1 inverted fluorescence microscope with a X40 magnification and the co-localisation overlap values were determined using ImageJ program. (n = 3; BLUE = DAPI; GREEN= TF; RED=JAM-A).

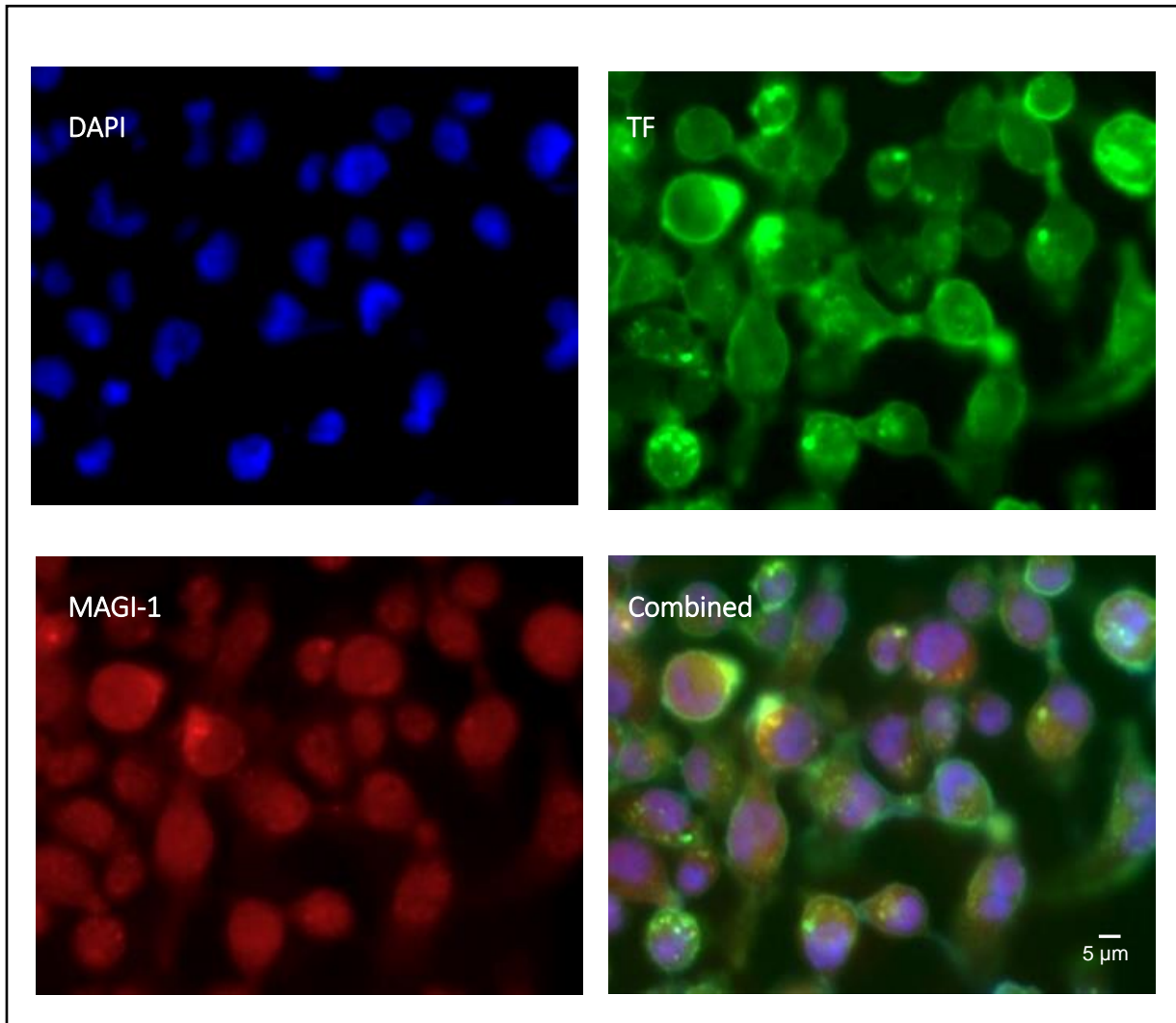


Figure 4. 9 Co-localisation patterns of TF with MAGI-1 protein. MDA-MB-231 cells (10^4) were seeded out into 10 mm-glass based μ -dishes and permitted to reach confluence. The cells were fixed with 4% (v/v) formaldehyde for 20 min and then washed with PBS. The cells were probed for TF and MAGI-1 using a FITC-conjugated anti-TF antibody together with a rabbit anti-MAGI-1 antibody and incubated overnight at 4°C. The cells were washed with PBS and then probed with a goat anti-rabbit IgG-Alexa Fluor 594 antibody to detect MAGI-1 protein. The cell nuclei were stained with DAPI for 10 min. Images were acquired using a Zeiss Axio Vert.A1 inverted fluorescence microscope with a X40 magnification and the co-localisation overlap values were determined using ImageJ program (n = 3; BLUE = DAPI; GREEN= TF; RED=MAGI-1).

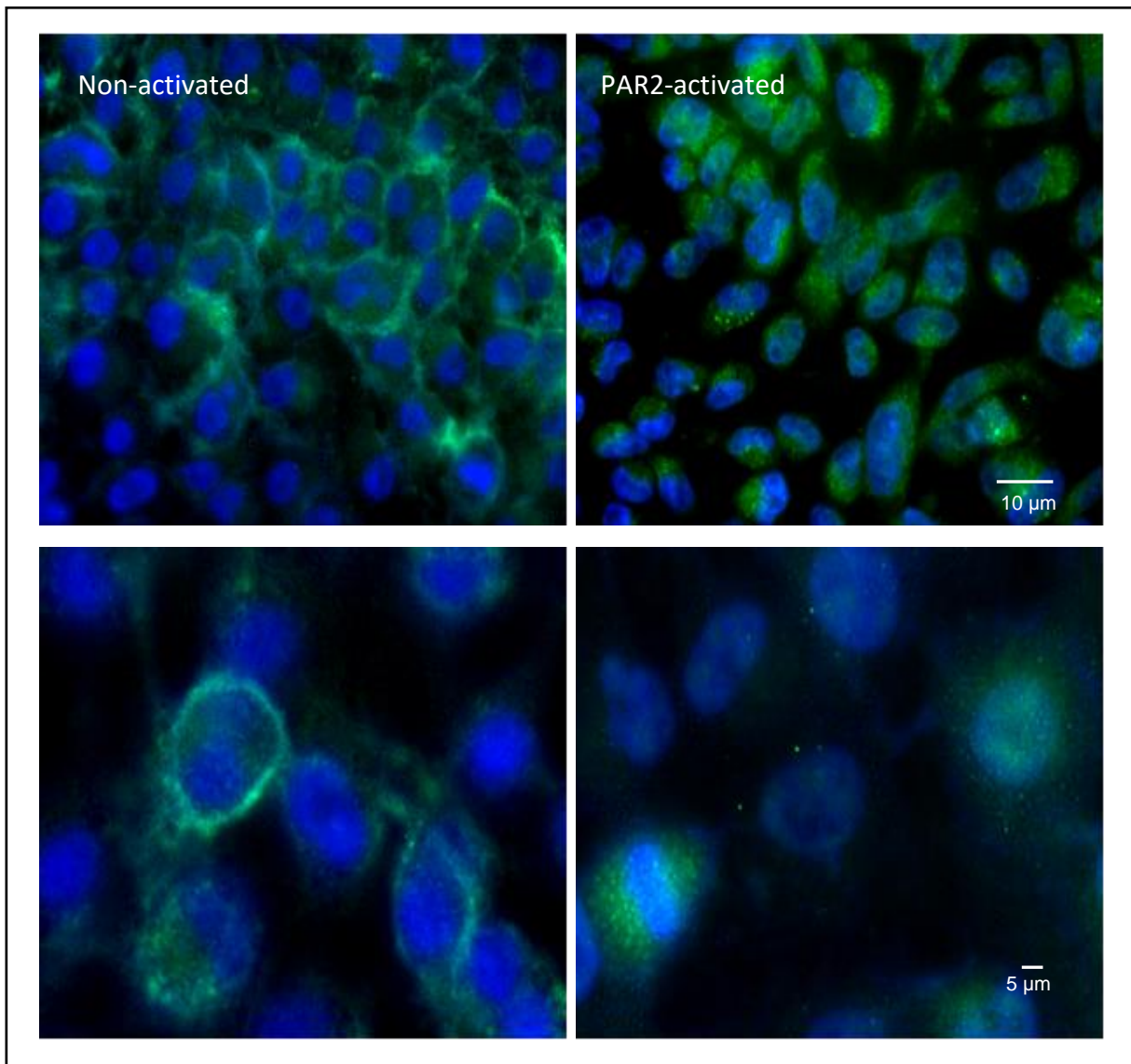


Figure 4. 10 Localisation of TF in PAR2 activated confluent MDA-MB-231 cells. MDA-MB-231 cells (10^4) were seeded out into 10 mm-glass based μ -dishes and permitted to reach confluence. A set of cells were incubated with serum-free medium for 60 min prior to activation. The cells were then activated with PAR2-AP (20 μ M) for 20 min and then washed twice with PBS. The cells were fixed with 4% (v/v) formaldehyde for 20 min and then washed twice with PBS. The cells were probed for TF using an FITC-conjugated anti-TF antibody for 60 min then the nuclei were stained with DAPI for further 10 min. Images were acquired using a Zeiss Axio Vert.A1 inverted fluorescence microscope with a X40 magnification (n = 4; GREEN= TF; BLUE = DAPI).

4.4 Discussion

It has been documented that under normal conditions, TF expression is suppressed on the cell-surface of endothelial cells (Butenas 2012; Palta *et al* 2014). However, the strict regulation of TF expression is lost during pathological conditions such as those observed in cancer (Bluff *et al* 2008). In addition, the localisation of MAGI proteins at the tight junctions plays an essential role in the stabilisation of cellular adhesion (Ide *et al* 1999; Wu *et al* 2000; Vazquez *et al* 2001; Tolkacheva *et al* 2001; Laura *et al* 2002). However, the downregulation of MAGI as well as other cell junction proteins has been associated with cancer progression (Bhat *et al* 2019; Alday-Parejo *et al* 2020). Therefore, the initial strategy for this investigation was to examine the localisation of TF at the cell junctions between cells which characterised by their formation of cell junction (e.g., endothelial cells or MCF-7) (Cunliffe *et al* 2012), and also in MDA-MB-231 cell line which do not form distinct cell junctions. However, due to time restriction, only the investigation using MDA-MB-231 cells was carried out.

Analysis of the amino acid sequence coding for the cytoplasmic domain of TF by the POW software suggested the possibility of an interaction between a putative PDZ-binding domain (ENSPL) within TF and the PDZ domains of MAGI proteins (Table 4.1). PLA analysis of MDA-MB-231 cells indicated that TF associates with MAGI-(1-3) proteins (Figure 4.2). However, the association between TF and MAGI-1 was the highest and therefore only this interaction was examined further. To confirm the association of TF with MAGI-1, immunoprecipitation of each of these proteins was carried out separately. Western blot analysis of immunoprecipitated proteins was then used to demonstrate the presence of TF and MAGI-1 in turn, confirming the interaction of TF and MAGI-1 (Figure 4.6 and 4.7). In principle, the underlying reason for the significantly stronger interaction of TF with MAGI-1 compared to MAGI-2 or MAGI-3 is not clear, since there are considerable amino acid sequence similarities between the three MAGI proteins. However, small amino acid

variations may cause functional differences in these proteins as previously suggested by (Laura *et al* 2002).

It has been documented that PAR2 induces the phosphorylation of TF (Ahamed and Ruf 2004; Rydén *et al* 2010; Collier *et al* 2017; Ettelaie *et al* 2018). Therefore, in this study, pull-down assays were used to examine the influence of PAR2 activation on the association of TF with MAGI-1. Time-course analysis of the capture of MAGI-1 from cell lysates, using an unphosphorylated TF peptide as the “bait”, showed a drop in the amount of captured MAGI-1 following 20 min incubation of the cells with the PAR2-agonist peptide. Moreover, to examine whether the phosphorylation of TF at different serine residues could modulate the binding of MAGI-1, pull-down assays were carried out using the cytoplasmic domain of TF peptide, in different phosphorylation states (Ettelaie *et al* 2020, unpublished data). MAGI-1 was shown to preferentially interact with the non-phosphorylated TF, but the presence of the phosphate group associated with Ser253 hindered the interaction of TF with MAGI-1 because the phosphorylation of amino acid side chains inhibits the ability of PDZ domains to form hydrogen bonds with target proteins (Chung *et al* 2004). In addition, MAGI-1 was shown to interact with Ser258-phosphorylated TF. However, this interaction may arise from the two WW domains within MAGI protein as TF was documented to interact with other proteins through their WW domain and the phosphoserine-proline motif (termed an MPM-2 motif) within the cytoplasmic domain of TF (Ettelaie *et al* 2018; Kurakula *et al* 2018).

The data obtained in the previous chapter indicated that PAR2 activation resulted in a reduced interaction between PTEN and MAGI proteins. Therefore, to demonstrate the outcome of PAR2 activation on the association between TF and MAGI-1 *in situ*, MDA-MB-231 cells were activated with PAR2-AP over a period of 40 min and the proximity of TF and MAGI-1 was examined by PLA. In agreement with the above data, the activation of PAR2 on MDA-MB-231 cells resulted in reduced proximity between TF and MAGI-1 which reached a

minimum level at 20 min post-activation (Figure 4.3). Similarly, the interaction between TF and MAGI-1 was reduced after 20 min incubation with PAR2-AP, demonstrated by co-immunoprecipitation of TF with anti-MAGI-1 antibody (Figure 4.6), and by co-immunoprecipitation of MAGI-1 with anti-TF antibody (Figure 4.7). However, no significant difference between PAR2-activated and non-activated cells was observed when the interaction of TF and MAGI-2 (Figure 4.4) or TF and MAGI-3 (Figure 4.5) were examined. It has been reported that PAR2 activation is capable of inducing the activation of caspase-3 (Chin *et al* 2003; Iablokov *et al* 2014) and caspase-7 (Zhou *et al* 2011) and that caspase-3 and -7 can cleave MAGI-1 at the intersection between PDZ1-PDZ2 and PDZ2-PDZ3 (Gregorc *et al* 2007). This digestion subsequently triggers the total degradation of MAGI-1 (Gregorc *et al* 2007; Ivanova *et al* 2012). Therefore, the activation PAR2 may cause the cleavage of MAGI-1 which in turn would disrupt the ability of MAGI-1 to bind other proteins. As a result, TF dissociates from MAGI-1 which could explain the reduced association between TF and MAGI-1. This also could explain the observed release of the localised TF (Figure 4.10) from the cell junctions. To further examine the localisation of TF at the cell junctions, MDA-MB-231 cells were probed with MAGI-1 and JAM-A proteins together with TF. Analysis of MDA-MB-231 cells using fluorescence microscopy indicated that TF might localise with JAM-A (Figure 4.8) and MAGI-1 (Figure 4.9). However, the localisation patterns were not well defined, due to the possibility that MDA-MB-231 cells may not form apparent tight junctions.

Cellular tight junctions are one of the most characteristic features that distinguish between normal and cancer cells. The deregulation of these tight junction proteins may impact tumour progression by altering cellular processes that regulate polarity, differentiation and migration (Brennan *et al* 2010). For example, several studies demonstrated that low expression levels of MAGI-1 in glioma (Li *et al* 2019), colorectal (Zaric *et al* 2012) and liver cancer cells (Zhang

and Wang 2011) positively correlated with tumour proliferation, migration and invasion through the PI3K-Akt pathway. Similarly, loss of MAGI-2 and MAGI-3 have also resulted in a reduction in cell permeability and disassembly of cell-cell contacts leading to prostate (Goldstein *et al* 2016) and breast carcinogenesis (Ni *et al* 2016), respectively. In addition, it has been well documented that TF can be expressed in different cancer types including pancreatic, breast, prostate, ovarian, colorectal and liver cancers (Kasthuri *et al* 2009). Moreover, the level of expression can vary among different types of cancers and, in general, the expression of TF increases with advanced cancer stage resulting in high procoagulant and signalling activities (Kakkar *et al* 1995; Ruf 2012). Also, several studies have reported that invasive and metastatic cancer cells such as MDA-MB-231 cell line display mesenchymal-like phenotype (Martin *et al* 2010; Holliday and Speirs 2011; Salvador *et al* 2016) and express relatively low levels of several cell junction proteins such as MAGI-1 (Alday-Parejo *et al* 2020), JAM-A (Naik *et al* 2008), occludins (Martin *et al* 2010), E- and P-cadherin (Sarrió *et al* 2009), ZO-1 (Martin and Jiang 2009) and connexins (Kazan *et al* 2019). Therefore, in such cells, it is possible that the interaction between TF and MAGI-1 becomes weaker, subsequently TF is released from MAGI-1. The resultant exposure of TF on the cell surface interacts with FVIIa which activates the coagulation pathway (Figure 4.11). This also could explain the increased risk of thrombosis (Steffel *et al* 2006; Rickles 2006; Han *et al* 2014) as well as the increased rate of tumour cell growth and proliferation associated with cancer (Liu and Mueller 2006; Khorana *et al* 2007).

In conclusion, this study has shown that TF interacts with MAGI-1 and this interaction is reduced in PAR2 activated cells. As previously described, MAGI-1 contains multiple PDZ binding domains. Therefore, in the next chapter, experiments were designed to identify the PDZ domain within MAGI-1 that has the ability to bind to TF

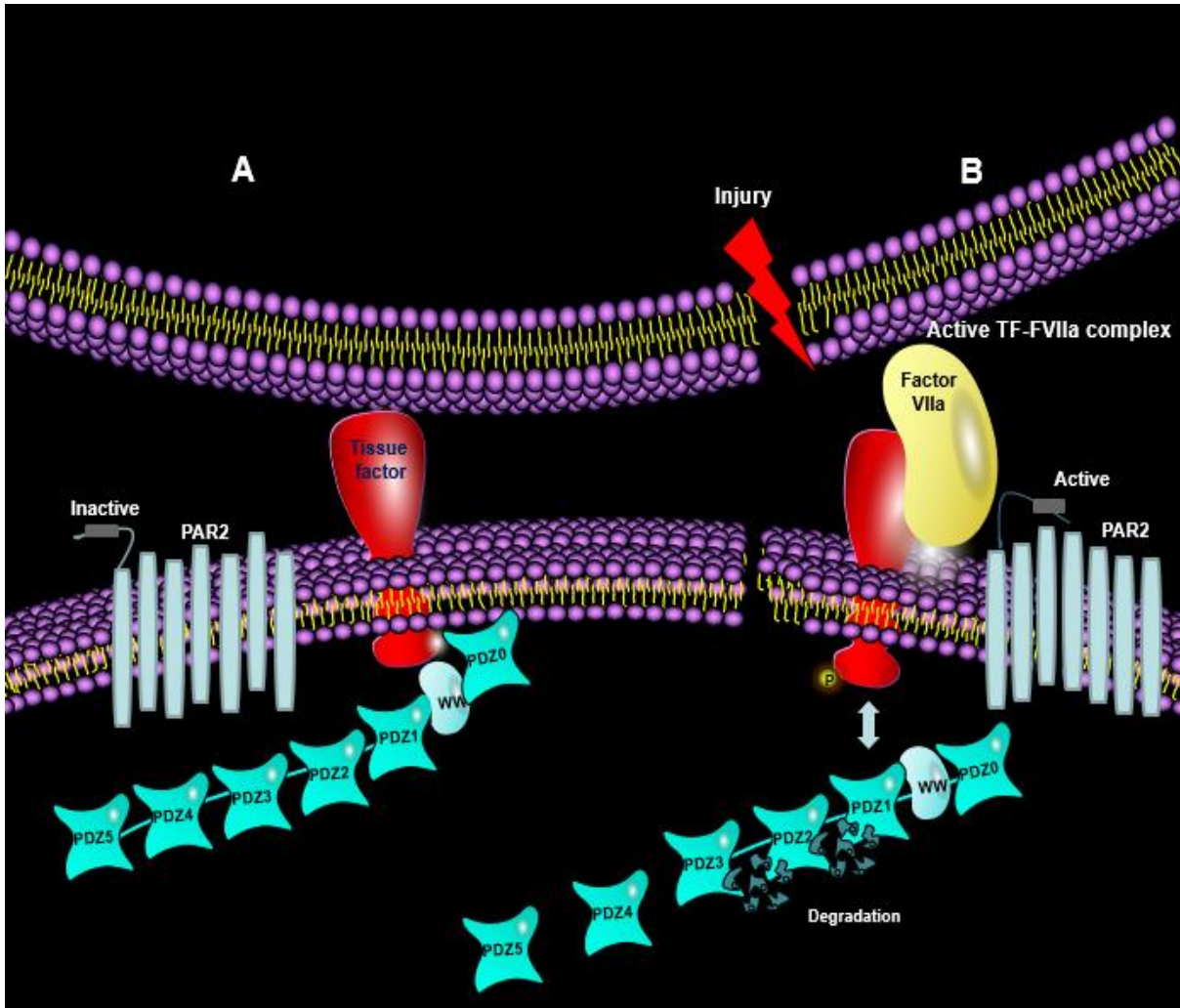


Figure 4. 11 The Proposed mechanism for the interaction of TF with MAGI-1 and the release of TF following PAR2 activation. A) The encrypted inactive form of TF is restrained at the tight junctions by MAGI-1. B) The perturbation of cells as a consequence of injury or loss of cellular junctional complex can result in the dissociation of TF from MAGI-1 leading to the exposure of TF to the cell surface. The exposed TF binds FVIIa and activates the coagulation pathway and also forms a signalling complex with PAR2.

Chapter 5

Characterisation of the interaction between TF and PDZ domains of MAGI-1

5.1 Introduction

The procoagulant activity of TF is tightly regulated to ensure correct haemostasis and to limit blood loss without causing thrombosis following an injury (Østerud 2010). This regulation of the procoagulant TF activity is primarily mediated by retaining TF in an encrypted, inactive, form which is only activated following injury and trauma to initiate the coagulation cascade. Currently, the exact mechanism for the encryption of TF is not clear although several mechanisms for the regulation of TF activity have been proposed. One of the main mechanisms includes the exposure of phosphatidylserine on the surface of cells following cellular perturbation (Ansari *et al* 2019). The role of phospholipid-dependent TF encryption is well established (Chen and Hogg 2013). It has been proposed that in resting cells TF is kept in the encrypted state in the inner surface of the plasma membrane by association with neutrally charged phosphatidylcholine and sphingomyelin. However, cellular damage disrupts the asymmetry of the plasma membrane leading to the exposure of negatively charged phosphatidylserine on the outer surface, thus increasing the procoagulant activity of TF (Neuenschwander *et al* 1995). However, on its own, this mechanism is not sufficient for the rigorous control required for TF activity.

The second proposed mechanism involves the formation of a disulphide bridge between the thiol groups within the extracellular domain of TF through a protein disulphide isomerase (Schmidt *et al* 2006). It has been proposed that encrypted TF remains in the reduced inactive free-thiol form at the Cys186 and Cys209 residues (Chen *et al* 2006). Upon disulphide bond formation, TF undergoes conformational change in this region, enhancing its interaction with phosphatidylserine (Chen *et al* 2006; Reinhardt *et al* 2008). However, the lack of evidence for the presence of free thiol groups within the extracellular domain of TF, in resting cells casts doubt on the involvement of this mechanism as a means of TF de-encryption.

Another mechanism for the decryption of TF was suggested by Mulder *et al* (1996) based on the hypothesis that the association of TF with caveolae may restrain TF activity, but can be activated rapidly following injury. This mechanism was supported by a later study which demonstrated the increase in TF activity following the disruption of caveolar structure through depleting membrane cholesterol using methyl β -cyclodextrin (Dietzen *et al* 2004). However, TF is usually associated with caveolae after cellular activation, thus this mechanism is likely to be a means of regulating TF activity post-activation.

A fourth proposed model for TF decryption assumes that TF exists as dimers on the surface of resting cells and suggests that the dissociation of dimers into procoagulant TF monomers, resulting in the exposure of the FX binding site on TF (Bach 2006; Rao and Pendurthi 2014). However again, the lack of detectable TF dimers on resting cells cast doubt on the validity of this mechanism.

It is envisaged that in order to achieve such strict regulation of the procoagulant and signalling activities of TF, more robust mechanisms must be present. Recently, it has become apparent that the procoagulant and signalling functions of TF, as well as its cellular localisation on the cell membrane may also be regulated through the post-translational modification of its cytoplasmic domain. Several post-translational modification processes including the phosphorylation and palmitoylation of the cytoplasmic domain of TF have been reported to regulate the activity of TF (Collier and Ettelaie 2011; Butenas *et al* 2012; Collier *et al* 2013; Collier *et al* 2017). In the previous chapter, the ENSPL sequence motif within the cytoplasmic domain of TF was identified as a possible target for the interaction between TF and MAGI-1. Therefore, the aim of this part of the investigation was to identify the PDZ domain within MAGI-1 that is responsible for the interaction with TF and examine the outcome on TF activity

5.1.1 PDZ domains

There is an increasing body of evidence highlighting the importance of MAGI-1 as a multi-domain binding protein (Feng *et al* 2014). A number of studies have documented the involvement of MAGI-1 in protein-protein interactions through the WW and PDZ domains of this protein (Patrie *et al* 2002; Simonson *et al* 2005; Duning *et al* 2008). MAGI-1 contains a guanylate kinase domain, two WW domains and six PDZ domains (Figure 1.8). The PDZ domain (Figure 5.1) derives its name from the first three proteins reported to contain this domain which are the **P**ost-synaptic density protein 95 (PSD-95), the **D**rosophila tumour suppressor Discs large (DlgA), and the mammalian tight junction protein **Z**ona-occludins-1 (ZO-1). PDZ domains have also been previously referred to as DHR (Discs large homology repeat) domains or GFGF (glycine-phenylalanine-glycine-phenylalanine) repeat due to the highly conserved four-residue GFGF sequence found in each PDZ domain within the same protein (Cho *et al* 1992). PDZ-containing proteins have been found in many bacteria, plants and vertebrate genomes (Duning *et al* 2008). Additionally, PDZ domains have been reported to occur in multiple copies within the same protein and can function independently, or in conjunction with other protein-binding domains such as the WW domains (Patrie *et al* 2002; Simonson *et al* 2005). PDZ domains are often associated with scaffolding proteins involved in protein-protein interactions, cell adhesion, cell polarity, cell junction stabilisation and synaptic scaffold formation (Hui *et al* 2013; Manjunath *et al* 2018). Typically, PDZ domains (Figure 5.1) consist of 80–90 amino acids and are formed by two α -helices (α A and α B) and six β -strands (β A– β F). Between β A and β B sheets, the carboxylate-binding loop also known as glycine-phenylalanine-glycine-phenylalanine “GFGF” loop which is constituted by several hydrophobic amino acids that adopt a conformational change to allow the C-terminal domain of the target protein to interact with the PDZ domain (Sotelo *et al* 2015; Zhu *et al* 2016). While

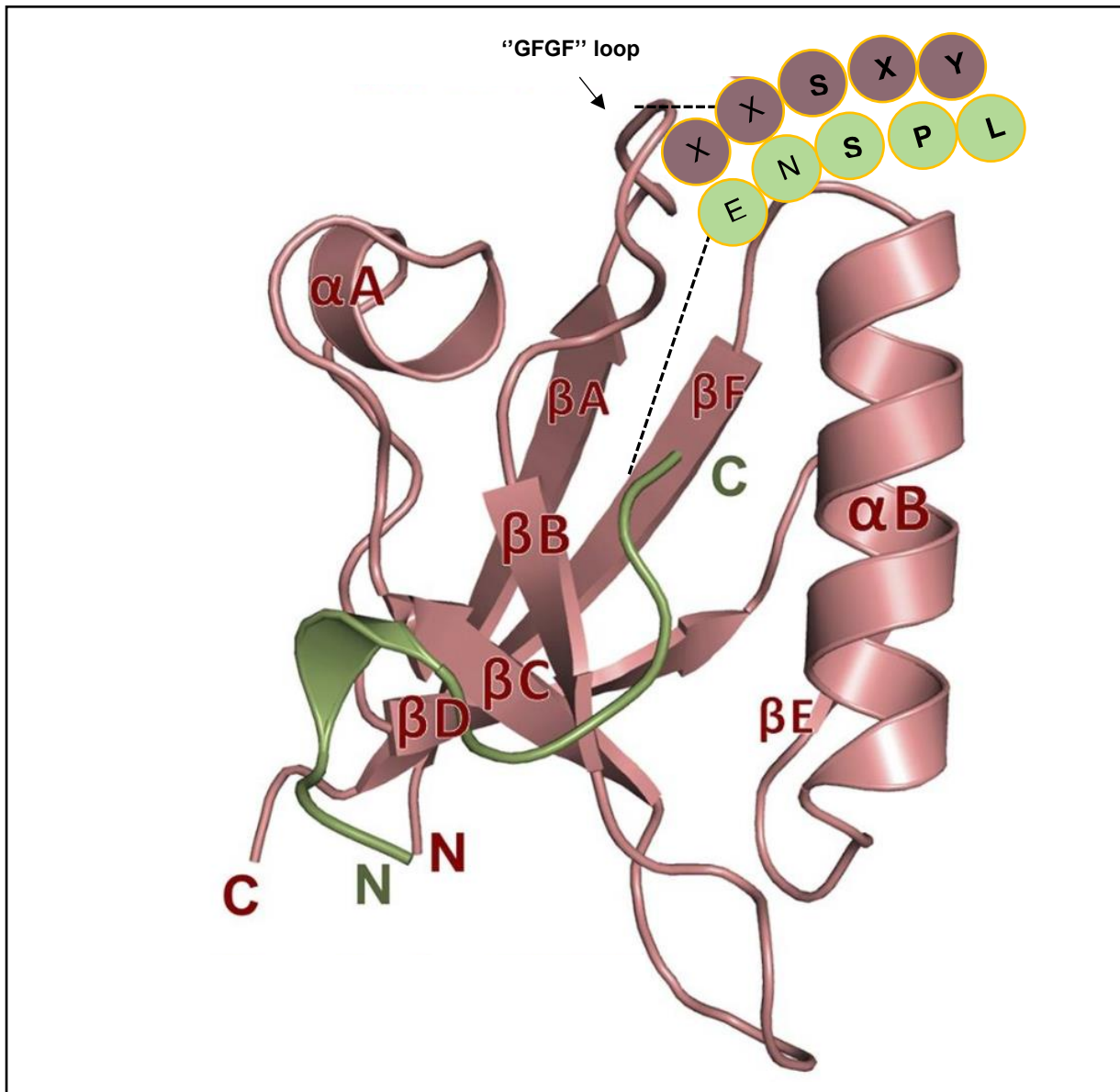


Figure 5. 1 The PDZ domain structure. The protein structure of a typical PDZ domain showing the six β -strands and the two α -helices. Typically, protein-protein interaction is mediated via the "GFGF" loop located between β A and β B where the target protein (green) binds to the PDZ-binding motif [X=any amino acid; Y= hydrophobic amino acid; the diagram was adapted from (Weng *et al* 2018)].

there is some debate over how many distinct PDZ-binding motifs exist, the PDZ binding motifs are commonly categorised into three classes. Class-I PDZ-binding motif recognises the Thr/Ser-X-Y motif (where X is any amino acid and Y is a hydrophobic amino acid) with leucine, valine and isoleucine being the most common hydrophobic amino acids occupying the X position. Class-II PDZ-binding motif recognises the Ser/Thr/Pro-Y-X-Y motif and class-III PDZ-binding motif which recognises the Glu/Asp -X-Y residue motif (Sotelo *et al* 2015; Manjunath *et al* 2018; Genera *et al* 2019).

5.1.2 Aims

The presence of the unphosphorylated Ser-Pro motif in the cytoplasmic domain of encrypted TF suggest that this may be a target for the Class-I PDZ domain. However, the phosphorylated Ser-Pro motif may also be a target for the two WW domains present in MAGI-1. Therefore, in this section of the study two strategies were used to explore the possibility that one or more of the PDZ domains within MAGI-1 are capable of interacting with the cytoplasmic domain of TF. The first strategy was based on cloning the entire MAGI-1 cDNA into the FLAG-HA-pcDNA3.1 expression vector and using site directed mutagenesis to individually delete each PDZ domain in turn. Each tagged mutant-PDZ domain within MAGI-1 cDNA would then be expressed in MDA-MB-231 cells and the interaction between TF and each of the tagged mutant-PDZ domain would be examined by PLA and by co-immunoprecipitation techniques. Any protein incapable of binding to TF would then be identified as devoid of the TF-binding PDZ domain.

The second strategy was based on sub-cloning each PDZ domain individually from the cDNA of MAGI-1 into the FLAG-HA-pcDNA3.1 expression vector and expressing the constructs as FLAG-HA-tagged hybrid proteins in MDA-MB-231 cells. The interaction between TF and each expressed PDZ domain would then be examined using PLA and co-immunoprecipitation

techniques. In this case, any domain capable of binding TF would then be identified directly, as the TF-binding PDZ domains. As a consequence of the initial experiments, the second strategy was used to express the N-terminal of MAGI-1 to include or exclude PDZ1, and the ability to bind TF was also examined. The data from both strategies were used to determine if the interaction of TF with MAGI-1 was mediated through a PDZ domain alone, or was supported by other domains such as the WW domains, within the N-terminal of the latter protein. Finally, following the characterisation of the interaction of TF with MAGI-1, the outcome of the expression of the PDZ domain in cells on TF activity was investigated.

5.2 Methods

5.2.1 Design of primers and PCR amplification of MAGI-1 cDNA, the individual PDZ domains and the N-terminal regions including or excluding the PDZ1 domain

FLAG-HA-pcDNA3.1 and pDONR223-MAGI-1 plasmids were purchased from Addgene. The sequence of pDONR223-MAGI-1 was compared to the sequence of MAGI-1 as published by Dobrosotskaya *et al* (1997). To ensure the insertion of the amplified DNA in the correct orientation into the expression vector, the primers were designed to contain different restriction sites, which were also present in the multi-cloning site within the FLAG-HA-pcDNA3.1 vector (Figure 5.2). The forward primer was designed to include a 19 bp of MAGI-1 cDNA coding sequence. This was preceded by a *Bam*HI restriction site and an additional 4 bp to ensure efficient restriction enzyme digestion (these additional 4 bases were included in all primers). Additionally, the reverse primer was designed to include a stop codon, 19 bp of MAGI-1 cDNA coding sequence and *Hind*III restriction site (Table 5.1)

The forward primers for each of the PDZ domains, or the N-terminal region including or excluding the PDZ1 domain were designed to include a *Bam*HI restriction site followed by the complementary sequence for each PDZ domain from the cDNA of MAGI-1. Similarly, the

Table 5. 1 The sequences of forward and reverse primers used for PCR

MAGI-1	
Forward primer	5'-GGCG GGATCC GTTCCAAAGTGATCCAGAAGA- 3'
Reverse primer	5' -GGACA AAGCTTAAT GCGTCACTTCCGGAACACCTTGTG- 3'
MAGI-1 N-terminal domain– Excluding PDZ1	
Forward primer	5' -CCCG GGATCC TCCAAAGTGATCCAGAAGAAGAACCA- 3'
Reverse primer	5' -GAGCA AAGCTTAAT GAACTTGCCTTTCAACTCAGAAGG- 3'
MAGI-1 N-terminal domain– Including PDZ1	
Forward primer	5' -CCC AGGATCC TCCAAAGTGATCCAGAAGAA- 3'
Reverse primer	5' -GATGA AAGCTTAAT GCAGAGTTCAAGGTCCACGC- 3'
PDZ1	
Forward primer	5' -CAAG GGATCC CACACAAAGCTGCGGAAAAG- 3'
Reverse primer	5' -GATCA AAGCTTAAT GCAGAGTTCAAGGTCCACGCT- 3'
PDZ2	
Forward primer	5' -AGCG GGATCC ACTGTTTCATATTGTCAAAGG- 3'
Reverse primer	5' -GCGGA AAGCTTAAT TTGCACCAACAATGTGACCTC- 3'
PDZ3	
Forward primer	5' -CGCC GGATCC GACATCTTCCTCTGGAGAAA- 3'
Reverse primer	5' -CCGG AAGCTTAAT CCGCACCGTGAGATTGACGT- 3'
PDZ4	
Forward primer	5' -TACC GGATCC GACGTGGAGATCCGGCGCG- 3'
Reverse primer	5' -CTGCA AAGCTTAAT ATCTTGCTCCTGTGCTGCTTG- 3'
PDZ5	
Forward primer	5' -ATGC GGATCC ACTGTGGAAGTGGAAAGAG- 3'
Revers primer	5' -CTCG AAGCTTAAT CAGAAACAGACGAACTCTG- 3'

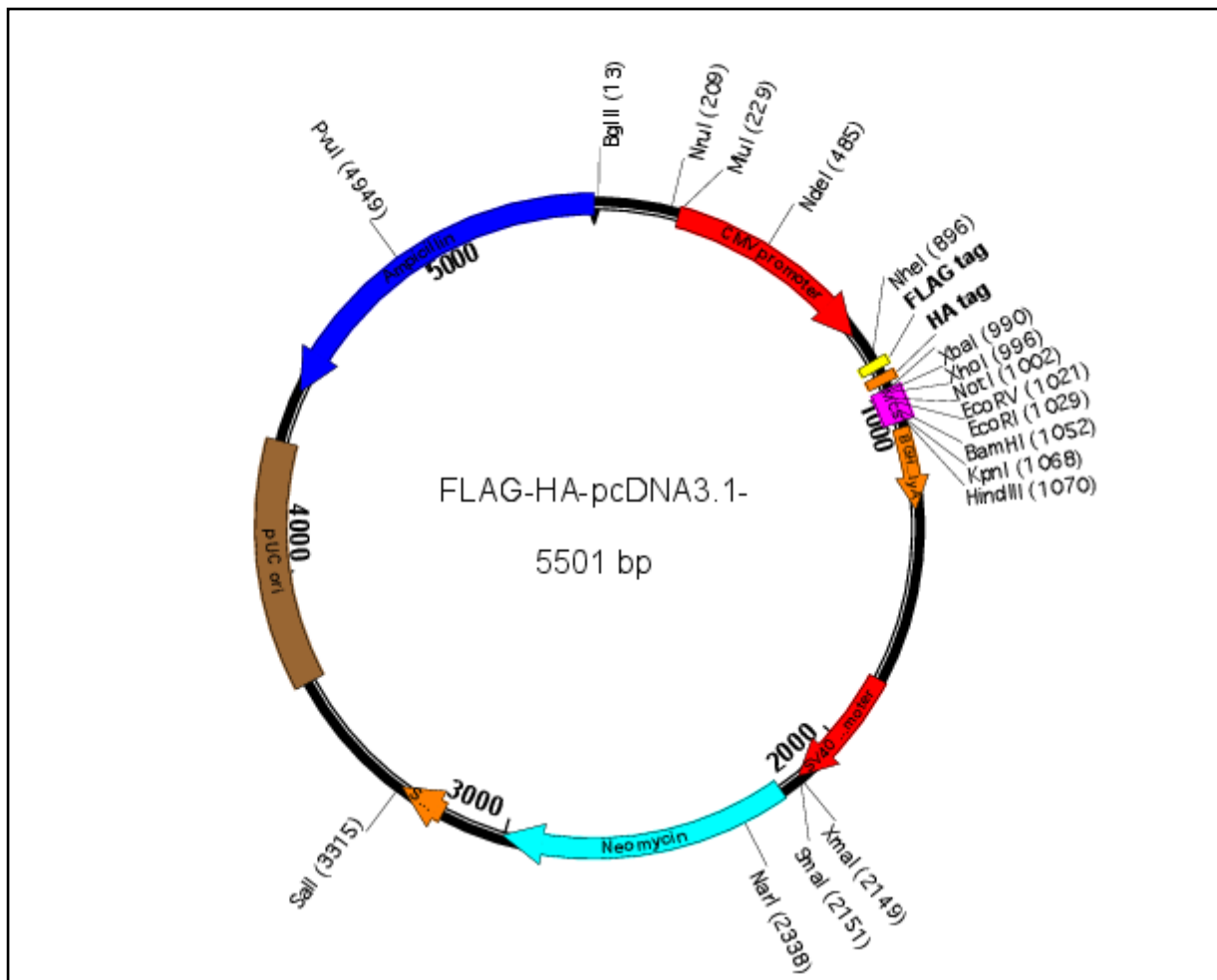


Figure 5. 2 Vector map of FLAG-HA-pcDNA3.1 expression plasmid. The forward and reverse primers were designed to include two restriction sites found within the multi-cloning site (MCS). This vector contains a cytomegalovirus (CMV) promoter to drive expression and the target protein is expressed in tandem with a FLAG/HA tag (Adapted from Addgene.com)

reverse primer was also designed to include coding sequence for each PDZ domain from the cDNA of MAGI-1, followed by a *HindIII* restriction site (Table 5.1).

5.2.2 Amplification of MAGI-1 cDNA, PDZ sequences and the N-terminal sequences of MAGI-1

Each of the amplification reactions were prepared by assembling 10x PCR buffer (5 µl), 50 mM MgCl₂ (1.5 µl), 10 mM dNTP (1 µl), 10 µM forward primer (2.5 µl), 10 µM reverse primer (2.5 µl), DNA template (3 µg), 5 units of Taq DNA polymerase (0.2 µl) and were made up to 50 µl with nuclease-free water. The tubes were briefly centrifuged and the DNA amplification was carried out as outlined in (Table 5.2). In order to ensure efficient DNA amplification, the PCR conditions were adjusted depending on the size (bp) of each DNA being amplified according to Thermo Scientific guidelines (Table 5.2). PCR was performed using a thermal cycler and the PCR products were separated by 1 % (w/v) agarose gel electrophoresis and viewed on a UV transilluminator as described in section (2.4.6).

5.2.3 Restriction digestion of the DNA inserts and the FLAG-HA-pcDNA3.1 vector

The multi-cloning site (MCS) of the FLAG-HA-pcDNA3.1 expression vector includes the unique restriction sites incorporated into the primers which allows the cleavage of DNA and formation of 5' overhangs sticky ends. The amplified MAGI-1 DNA was digested with *BamHI* and *HindIII* restriction enzymes. In a separate reaction, the FLAG-HA-pcDNA3.1 expression vector was also digested with the same two restriction enzymes. Similar reactions were also prepared to digest the amplified DNA coding for each PDZ domain and the FLAG-HA-pcDNA3.1 vector with *BamHI* and *HindIII* restriction enzymes. Finally, another set of

Table 5. 2 PCR conditions for DNA amplification

cDNA amplification of MAGI-1				
Step		Temperature (°C)		Time
Initial Denaturation		95		2 min
30 PCR cycles	Denature	95		1.5 min
	Anneal	68		2 min
	Extend	72		4 min
Final Extension		72		10 min
cDNA amplification of PDZ domains				
Initial Denaturation		95		1.5 min
30 PCR cycles	Denature	95		25 sec
	Anneal	PDZ 2, 3 & 5	PDZ 1 & 4	30 sec
		64	68	
	Extend	72		30 sec
Final Extension		72		10 min
cDNA amplification of N-terminal regions of MAGI-1 including and excluding PDZ1				
Initial Denaturation		95		2 min
30 PCR cycles	Denature	95		Exclude- PDZ1
				60 sec
	Anneal	Exclude- PDZ1	Include- PDZ1	75 sec
		61	66	
Extend	72		75 sec	
Final Extension		72		10 min

reactions were prepared to digest the amplified DNA coding for the N-terminal region including PDZ1 or the amplified DNA of the N-terminal region excluding PDZ1, and also the FLAG-HA-pcDNA3.1 vector, using *Bam*HI and *Hin*DIII enzymes. Each digestion reaction contained DNA template (2 ng), restriction enzymes (20 U/ng DNA) and the reaction was made up to (50 µl) with 10x CutSmart® buffer (50 mM potassium acetate, 20 mM Tris-acetate pH 7.9, 10 mM magnesium acetate, 100 µg/ml BSA). The samples were incubated at 37°C for 35 min and the digested DNA was then purified using the Monarch DNA Clean-up kit as described in section 5.2.4.

5.2.4 Purification of the digested DNA using the Monarch DNA Clean-up kit

The digested DNA samples (50 µl) were diluted in DNA clean-up binding buffer (250 µl) and mixed by pipetting. The provided collection columns were inserted into the collection tubes and the DNA samples were loaded onto the inserted columns. The DNA samples were centrifuged for 1 min at 12,000 g and the flow-through was discarded. The columns were inserted back into collection tube and washed with the provided DNA wash buffer (200 µl). The columns were centrifuged for 4 min at 12,000 g to remove any traces of ethanol and then transferred into fresh 1.5 ml tubes. DNA elution buffer (10 µl) was added to the centre of each column, incubated for 1 min and then centrifuged for 1 min at 12,000 g to elute the DNA. The DNA samples were stored at -20°C for further use.

5.2.5 Ligation of the digested MAGI-1 DNA and the PDZ DNA fragments into the FLAG-HA-pcDNA3.1 expression vector

A set of reaction mixtures were prepared to ligate the digested MAGI-1 DNA into the FLAG-HA-pcDNA3.1 expression vector. Similar reactions were also prepared to separately ligate the digested DNA coding for each of the PDZ domains into the FLAG-HA-pcDNA3.1 expression vector. Finally, separate reactions were also prepared to ligate the digested DNA of the N-

terminal region including or excluding the PDZ1 domain into the FLAG-HA-pcDNA3 vector. The ligation reactions were set up in total volumes of 10 μ l. Each ligation reaction was performed at molar ratios of 1:3, 1:5 and 1:10 (vector:insert) and contained 50 ng of total amount DNA and 5 μ l of 2x T4 DNA Ligase instant sticky-end ligase master solution. The reactions were mixed by pipetting and incubated on ice for 10 min. The vector:insert molar ratios were calculated using the University of Texas website

(http://2011.igem.org/Team:UT_Dallas/ligation).

5.2.6 Bacterial transformation

Competent 5-alpha *E. coli* cells were thawed on ice. The products from each ligation reaction (3 μ l) were transferred into 0.5 ml micro-centrifuge tubes and mixed with *E. coli* cells (15 μ l) by gently flicking the tube. The tubes were incubated on ice for 30 min and the cells were then heat shocked at 42°C for 30 seconds. The cells were immediately cooled-down on ice for 5 min and then mixed with pre-warmed SOC medium (150 μ l). Each transformation reaction was transferred into a micro-centrifuge tubes and incubated at 37°C for 60 min in a shaking incubator. The transformed cells (70 μ l) were plated out on agar plates prepared and incubated overnight at 37°C to allow colonies to grow. On the following day, single colonies were picked out and propagated overnight in LB broth (10 ml) at 37°C in a shaking incubator.

5.2.7 Confirmation of sub-cloning by restriction digestion

The plasmid DNA was isolated from transformed bacteria using the Monarch plasmid miniprep kit as described in section (2.4.4). Separate digestion reactions were prepared which contained DNA template (2 ng), *Bam*HI and *Hind*III restriction enzymes (20 U/ng DNA) and the reaction was made up to 50 μ l with 10x CutSmart® buffer. The samples were incubated at 37°C for 35

min and the digested DNA was then purified using the Monarch DNA Clean-up kit as described in 5.2.4.

5.2.8 Confirmation of sub-cloning by DNA sequencing

The isolated DNA (100 ng) from transformed bacteria were diluted in dH₂O to a volume of 15 µl. The DNA samples were submitted to MWG Eurofins Genomics for sequencing using a pre-designed primer. The DNA sequences were then examined using the BLAST software (<https://blast.ncbi.nlm.nih.gov/Blast.cgi>) and compared to the published sequences of MAGI-1 cDNA (Dobrosotskaya *et al* 1997). Bacterial colonies containing the confirmed DNA constructs were then propagated and stored at -70°C as described above.

5.2.9 Determination of the optimal incubation time for the expression of FLAG-HA tagged PDZ proteins in MDA-MB-231 cells

In order to express the constructs PDZ domains as hybrid proteins in mammalian cells, transfection reactions were prepared in a total volume of 1 ml (Madkhali *et al* 2019). Separate reactions were prepared by mixing Opti-MEM reduced-serum medium (90 µl), the DNA constructs expressing each of the PDZ1-5 domains/or the N-terminal regions of MAGI-1 (DNA: 1 µg) and TransIT®-2020 reagent (3 µl). The mixture was centrifuged and incubated at room temperature for 25 min. DMEM base medium (900 µl) was added into each tube and mixed by pipetting. MDA-MB-231 cells were cultured and suspended in 1 ml of fresh medium. The transfection mixture was then aliquoted (200 µl) into a 24-well plate and MDA-MB-231 cells (105) were pipetted (15 µl) into the wells. To determine the incubation time for the optimal expression of the proteins, MDA-MB-231 cells were incubated for 24, 36 or 45 h at 37°C. The protein expression was determined using dot blot as described in (5.2.10) and the fluorescence intensity was also determined using the PLA as described in (5.2.11).

5.2.10 Confirmation of protein expression using dot blot

To ensure the expression of the desired HA-tagged proteins, MDA-MB-231 cells (10^5) were seeded into a 12-well plates and transfected as described above. The cells were washed twice with PBS and then lysed in Laemmli's buffer (100 μ l). The cell lysates (2.5 μ l) were pipetted onto a nitrocellulose membrane and left to dry for 10 min. The membrane was then blocked with TBST for 60 min and probed with a rabbit anti-HA primary antibody diluted 1:2000 (v/v) in TBST and incubated overnight at 4°C. The membrane was washed twice with TBST for 10 min and probed with an alkaline phosphatase-conjugated goat anti-rabbit IgG antibody diluted 1:8000 (v/v) in TBST for 60 min. The membrane was washed twice with TBST and the bands were developed with Western Blue-stabilized substrate for alkaline phosphatase and photographed.

5.2.11 Examination of the association of TF with FLAG-HA-dual tagged PDZ proteins using the PLA

MDA-MB-231 cells (10^3) were seeded into 35 mm-glass based μ -dishes with a 10 mm diameter glass well, and grown in complete medium, overnight. The cells were washed three times with PBS and then fixed with 4% (v/v) formaldehyde for 20 min. The cells were washed with PBS and permeabilised using 0.1% (v/v) Triton X-100 for 10 min, washed again with PBS and then blocked with Duolink® blocking solution at 37°C for 60 min. To examine the potential association between TF and each FLAG-HA-tagged PDZ constructs, the cells were incubated with a mouse anti-TF antibody (HTF1) and with a rabbit anti-HA tag primary antibody (C2954) diluted 1:100 (v/v) in the provided antibody diluent overnight at 4°C. As control, the mouse anti-TF antibody was substituted with an irrelevant mouse IgG isotype, diluted accordingly. PLA analysis was performed as described in (section 2.3.5). The nuclei were labelled with DAPI (2 μ g/ml) and the cytoskeleton labelled with Alexa Fluor® 488 Phalloidin (2 μ g/ml) for

10 min. Images were acquired using a Zeiss Axio Vert.A1 inverted fluorescence microscope with a X40 magnification. The number of red fluorescent events and nuclei were determined using ImageJ in 10 fields of view from each assay.

5.2.12 Examination of the interaction between TF and Flag-HA-dual tagged PDZ proteins using co-immunoprecipitation

MDA-MB-231 cells (5×10^5) transfected with FLAG-HA-dual tagged constructs were permitted to express the PDZ constructs as proteins for 45 h in 6 well plates. The wells were washed with PBS and then lysed in Phospho-Safe™ extraction buffer (500 μ l). The PDZ1 or PDZ2 domain hybrid proteins were separately immunoprecipitated from cell lysates with a rabbit anti-HA tag primary antibody (8 μ g; C2954) by overnight incubation at 4°C on a rotating mixer. On the following day, protein A-magnetic beads (100 μ l) were added into each immunoprecipitated sample and incubated for 120 min on a rotating mixer to allow antibody capture. To ensure specificity of the interactions, samples of the lysates were also incubated with a rabbit IgG isotype control (8 μ g), as well as an additional control without any antibody. The supernatants were discarded and the protein-A coated magnetic beads with immunoprecipitated samples were washed five times with PBST and then solubilised in Laemmli's buffer. The immunoprecipitated samples were separated by SDS-PAGE, transferred to a nitrocellulose membrane and blocked. In order to detect the presence of TF, the membranes were probed with a mouse anti-TF primary antibody diluted 1:2000 (v/v) in TBST overnight at 4°C. The membranes were washed twice with TBST and then probed with an alkaline phosphatase conjugated goat anti-mouse IgG antibody diluted in 1:8000 (v/v) in TBST. The bands were developed with Western Blue-stabilised substrate for alkaline phosphatase and photographed as described in section (2.3.6).

5.2.13 Measurement of cell surface TF activity using the thrombin generation assay

This assay measures the activity of TF in the presence of an excess of coagulation proteins which are provided by the addition of the barium sulphate adsorbable proteins, as well as calcium ions. Furthermore, the assay buffers TBS containing 1% (w/v) BSA, is compatible with live cells but due to the short duration of the assay no other additives are necessary. The generated thrombin is then measured using a chromogenic substrate and is directly proportional to the amount of active TF (Petrovan *et al* 1999).

To perform the assay, MDA-MB-231 cells (5×10^4) were separately transfected with FLAG-HA-tagged constructs expressing PDZ1, PDZ2, or the N-terminal region of MAGI-1 including or excluding the PDZ1 domain. The cells were allowed to express the FLAG-HA-tagged PDZ constructs as hybrid proteins for 45 h. To measure the activity of TF on the cell surface, MDA-MB-231 cells were washed three times with TBS containing 1% (w/v) BSA and were incubated with barium sulphate adsorbable proteins (2 mg/ml final concentration) and 5 mM CaCl₂ (final concentration) diluted in TBS buffer (150 µl) at 37°C for 30 min. Precise aliquots of the reaction (100 µl) were transferred into a 96-well plate containing 100 µl of thrombin substrate (0.2 mM H-D-Phe-Pip-Arg-pNA) diluted in TBS buffer and incubated at 37°C for 60 min. Once the colour had developed, the reactions were stopped by adding 2 M sulphuric acid (50 µl) and the absorptions were measured at 410 nm using a plate reader. A standard curve for TF activity was constructed by preparing a serial dilution of recombinant TF protein (0-10 units/ml). The absorption readings from the standards were used to determine an equation and calculate the cell-surface TF concentration from the cell samples (Figure 5.3).

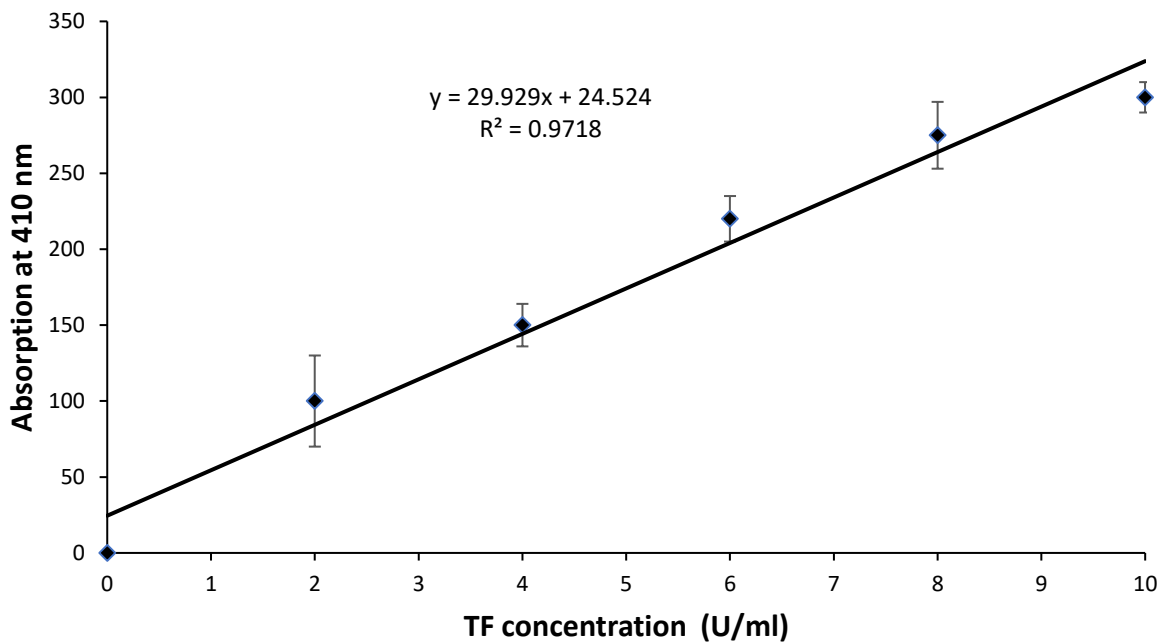


Figure 5. 3 The standard curve for TF activity. A standard curve for TF activity was made by preparing serial dilutions of recombinant human TF diluted in dH₂O (0-10 U/ml). The wells were incubated with barium sulphate absorbable proteins (2 mg/ml) mixed with 5 mM CaCl₂ for 30 min at 37°C. Aliquots (100 µl) were transferred to a 96-well plate containing (100 µl) thrombin substrate diluted in TBS buffer. The plate was incubated for 60 min at 37°C and the reactions were stopped by adding 2 M sulphuric acid (50 µl). The absorption values were measured at 410 nm using a plate reader (n=3).

5.3 Results

5.3.1 Optimisation of digestion of MAGI-1 cDNA with *BamHI* and *HindIII* restriction enzymes

The digestion procedure of the FLAG-HA-pcDNA3.1 plasmid has been optimised in our laboratory. Therefore, different reagents and conditions were optimised to facilitate the cloning of MAGI-1 cDNA into the vector. In separate reactions, the plasmid was incubated with *BamHI* and *HindIII* restriction enzymes provided from either Promega or New England Biolabs for up to 3 h at 37°C. The examined samples by agarose gel electrophoresis showed that digestion of the plasmid with restriction enzymes from Promega resulted in no change in DNA mobility compared to samples digested with restriction enzymes from New England Biolabs (Figure 5.4). Therefore, the restriction enzymes from New England Biolabs were used for the digestion of the DNA inserts.

5.3.2 PCR amplification of MAGI-1 cDNA and the PDZ domains

For the purpose of sub-cloning, the pDONR223-MAGI-1 plasmid was isolated using the Monarch plasmid miniprep kit as described in section 2.4.4. The MAGI-1 cDNA and the individual PDZ domains were then separately amplified by PCR using the designed primers specified in section 5.2.1. Agarose gel electrophoresis of the PCR products showed one band with an approximate size corresponding to that expected for MAGI-1 (4389 bp) (Figure 5.5A). In addition, bands were detected corresponding to each of the PDZ domains, PDZ1 (246 bp), PDZ2 (234 bp), PDZ3 (246 bp), PDZ4 (252 bp) and PDZ5 (237 bp) (Figure 5.5B). Finally, bands corresponding to the expected size of the N-terminal region with and without the PDZ1 domain (1660 and 1400 bp respectively) were detected (Figure 5.5C).

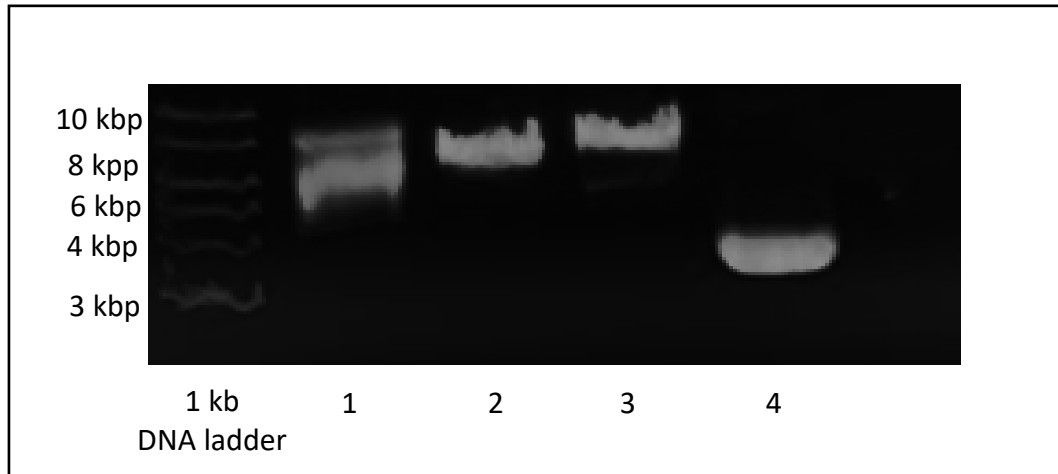


Figure 5. 4 Optimisation of the digestion of MAGI-1 cDNA with *BamHI* and *HindIII* restriction enzymes. The plasmid containing MAGI-1 cDNA was digested using *BamHI* and *HindIII* restriction enzymes for up to 3 h at 37°C. The digested DNA samples were examined by 1% (w/v) agarose gel electrophoresis. Lane 1) the Bands correspond to the undigested MAGI-1, lane 2) digested MAGI-1 with Promega for 1 h, lane 3) digested MAGI-1 with Promega for 3 h and lane 4) digested MAGI-1 with New England biolabs for 35 min.

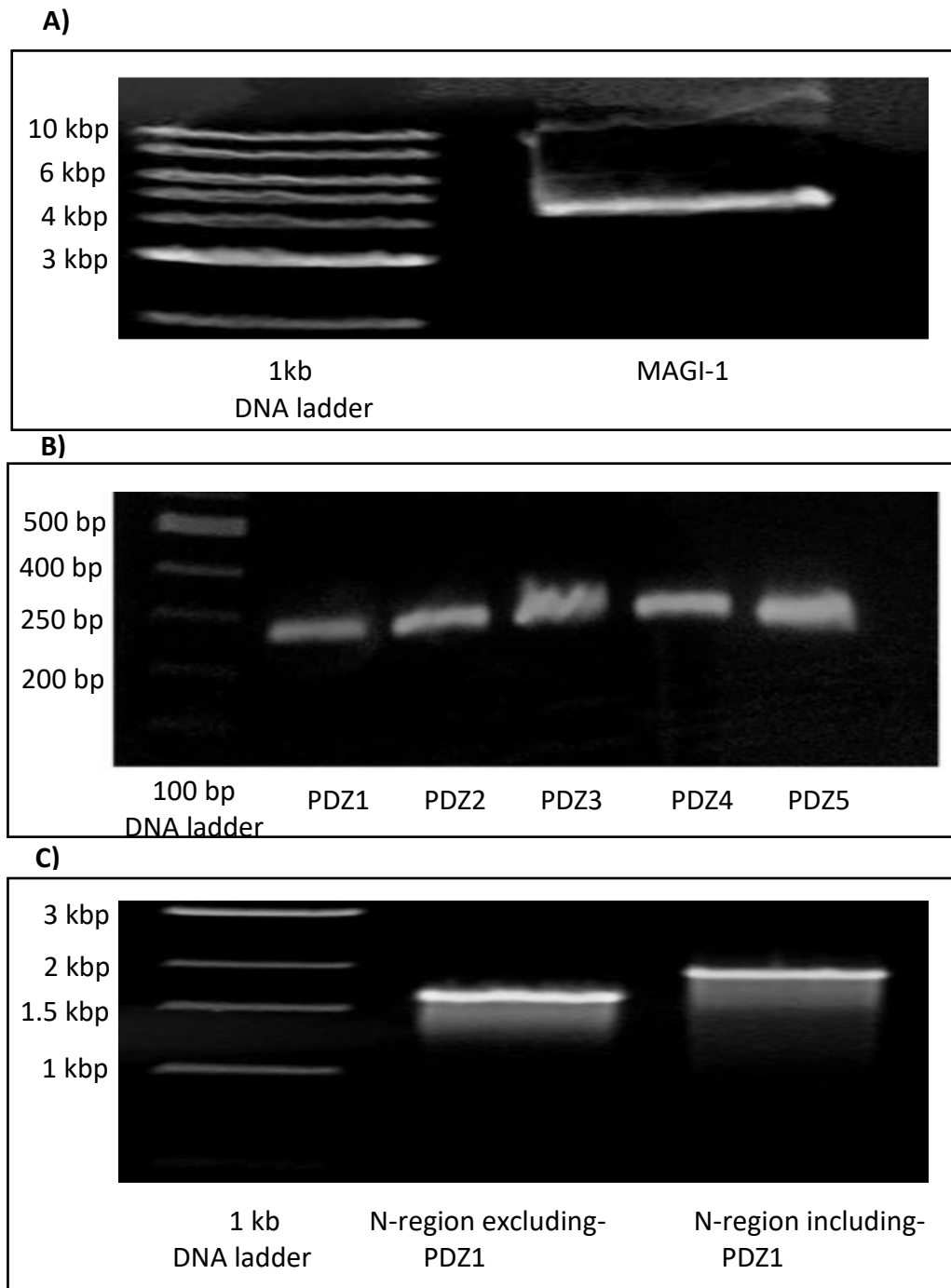


Figure 5. 5 Agarose gel electrophoresis of the amplified DNA. The DNA for A) MAGI-1, B) individual PDZ domains and C) the N-terminal region including or excluding PDZ1 domain were amplified by PCR using primers specified in section 5.2.2 and examined by agarose gel electrophoresis. Bands corresponding to the expected size of A) MAGI-1 (4389 bp), B) PDZ1 (246 bp), PDZ2 (234 bp), PDZ3 (246 bp), PDZ4 (252 bp) and PDZ5 (237 bp) or C) the N-terminal regions excluding or including PDZ1 domain (1400 bp and 1660 bp respectively) were detected.

5.3.3 Verification of MAGI-1 DNA sub-cloning using restriction digestion

Following transformation of the competent bacteria, plasmid DNA was isolated from the selected colonies and digested as described in section 5.2.3. Representatives of the experiments are shown in (Figure 5.6) but many repeated attempts using a range of insert:vector ratios to sub-clone the MAGI-1 cDNA into the FLAG-HA-pcDNA3.1 expression vector were unsuccessful. Although bands corresponding to the approximate size of the expression vector + insert were observed and sent for sequence analysis, correct inserts were not obtained.

5.3.4 Verification of sub-cloning of PDZ domains using restriction digestion

Agarose gel electrophoresis of the digested DNA samples showed bands corresponding to each of the PDZ domains: PDZ1 (246 bp), PDZ2 (234 bp), PDZ3 (246 bp), PDZ4 (252 bp) and PDZ5 (237 bp). Representative examples of multiple repeated experiments are shown in (Figure 5.7A). Also, agarose gel electrophoresis of the digested plasmid containing the N-terminal regions showed separate bands corresponding to the N-terminal region including or excluding PDZ1 domain (1660 and 1400 bp respectively) (Figure 5.7B) together with a heavier band corresponding to the expected size of the expression vector FLAG-HA-pcDNA3.1 (5501 bp) without the insert.

5.3.5 Verification of DNA sub-cloning by sequencing

BLAST alignment software was used to further confirm the successful sub-cloning of the DNA. The sequencing results obtained from Eurofins Genomics (Appendix A-3) were aligned against the full-length sequence of the published MAGI-1 cDNA (Dobrosotskaya *et al* 1997) and any positive clones identified.

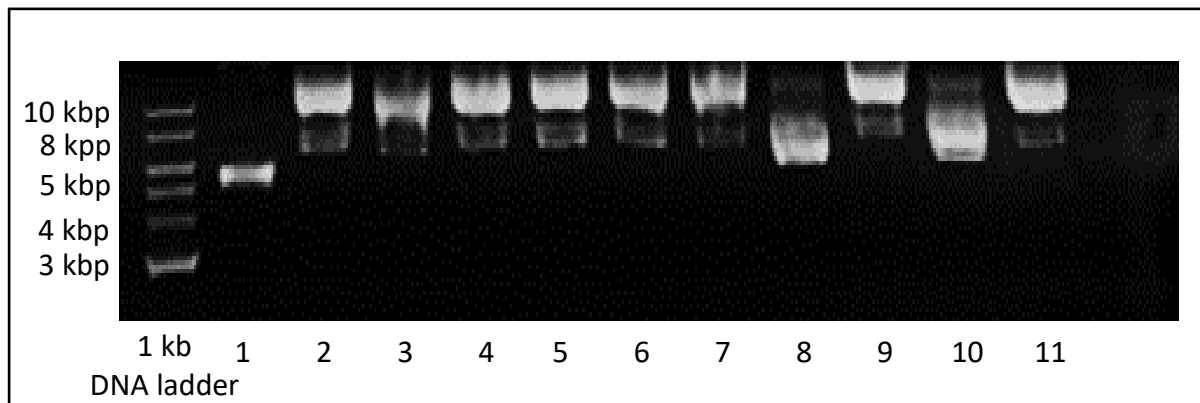


Figure 5. 6 Agarose gel electrophoresis of purified MAGI-1- FLAG-HA-pcDNA3.1 construct DNA. MAGI-1 DNA was digested, ligated into FLAG-HA-pcDNA3.1 expression plasmid and transformed into competent 5-alpha *E. coli*. The DNA samples were purified and examined by agarose gel electrophoresis. 1) vector control (5501 bp), 2-5) 3:1 insert:vector ratio, 6-8) 2:1 insert:vector ratio and 9-11) 1:1 insert:vector ratio (approximately 10 kbp)

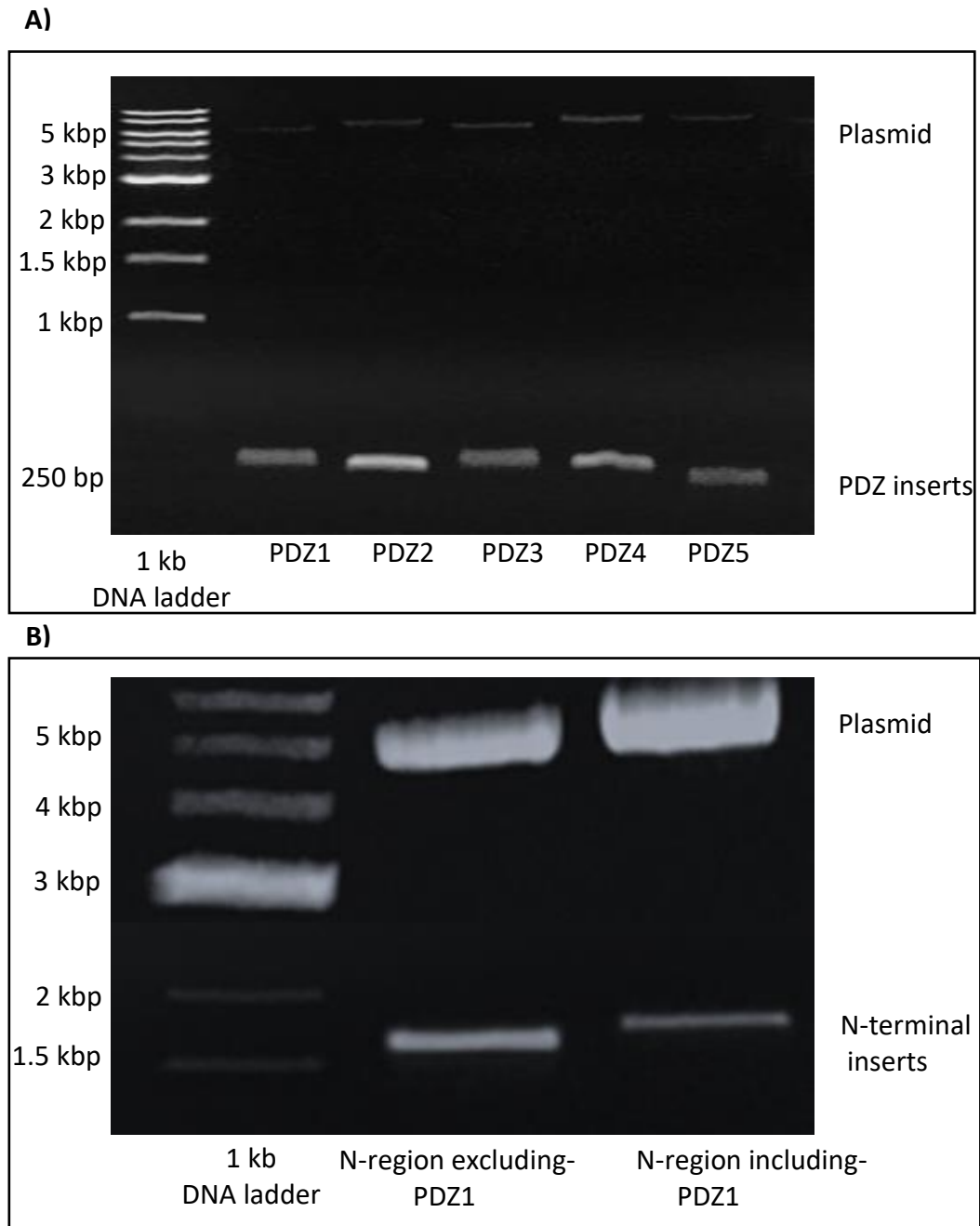


Figure 5. 7 Analysis of the sub-cloning of the amplified DNA by restriction digestion. The recombinant plasmids containing the sub-cloned DNA were digested using *Bam*HI and *Hind*III restriction enzymes. The digested DNA samples were examined by 1 % (w/v) agarose gel electrophoresis. Bands corresponding to A) each PDZ domain: PDZ1 (246 bp), PDZ2 (234 bp), PDZ3 (246 bp), PDZ4 (252 bp), PDZ5 (237 bp) or B) the N-terminal regions including and excluding PDZ1 domain (1660 and 1400 bp respectively) were detected as well as a heavier band corresponding the parent plasmid (5501 bp).

5.3.6 Determination of the optimal duration for protein expression

In order to determine the optimal duration for the expression of the hybrid protein, MDA-MB-231 cells were separately transfected with FLAG-HA-dual tagged constructs expressing the PDZ1-5 domains using TransIT®-2020 transfection reagent as described in (section 5.2.9). The cells were permitted to express the FLAG-HA-tagged PDZ domains as hybrid proteins for 24, 36 or 45 h. The cells were lysed and analysed by dot-blot as described in section 5.2.10. ImageJ analysis of the membrane indicated higher levels of protein expression in cells transfected for 45 h compared to the cells transfected for 36 or 24 h. A representative example of data from 2 independent experiments is shown in (Figure 5.8).

5.3.7 Analysis of the interaction of the PDZ domains with TF by PLA, using the FLAG-tag antibody

In order to examine the possible interaction of TF with any of the PDZ domains, MDA-MB-231 cells were transfected with FLAG-HA-constructs to express the PDZ domains as tagged hybrid proteins according to the published transfection protocol optimised in this laboratory (Madkhali *et al* 2019). To assess the binding ability of each PDZ domain to TF, PLA analysis was carried out using a mouse anti-FLAG-tagged antibody together with a rabbit anti-TF antibody. Analysis of 3 independent repeats using ImageJ software showed high levels of background, possibly due to non-specific binding of the antibody. Consequently, the analysis using the anti-FLAG antibody was not pursued further (Figure 5.9).

5.3.8 Analysis of the interaction of the PDZ domains with TF by PLA, using the HA-tag antibody

Due to the non-specific binding of the FLAG-tagged antibody, the HA-tag was then used to investigate the possible association of TF with the expressed PDZ domains using PLA. The cloned DNA regions coding for each of the PDZ domains were expressed in MDA-MB-231

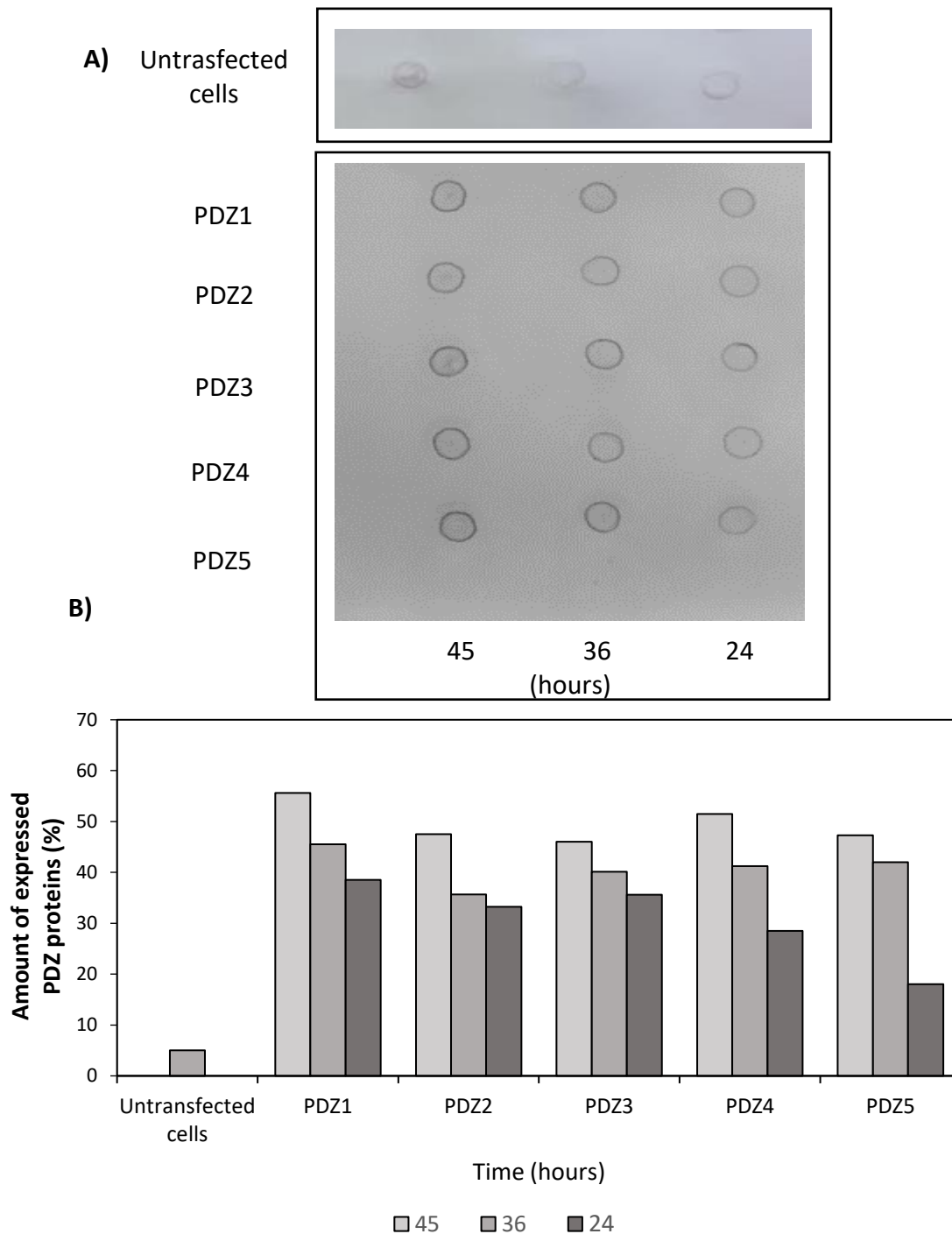
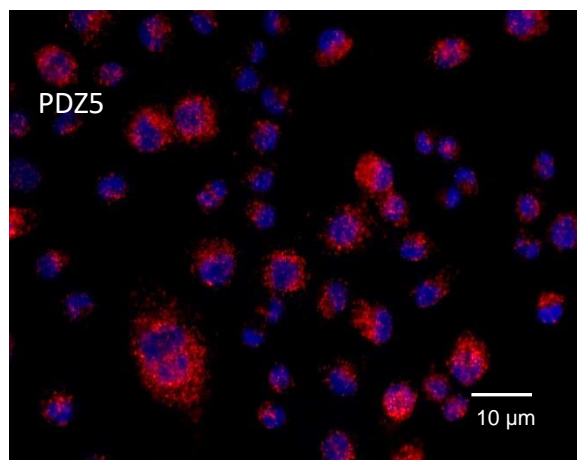
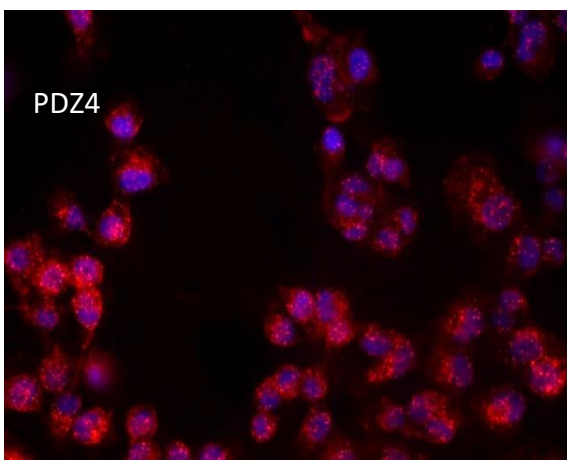
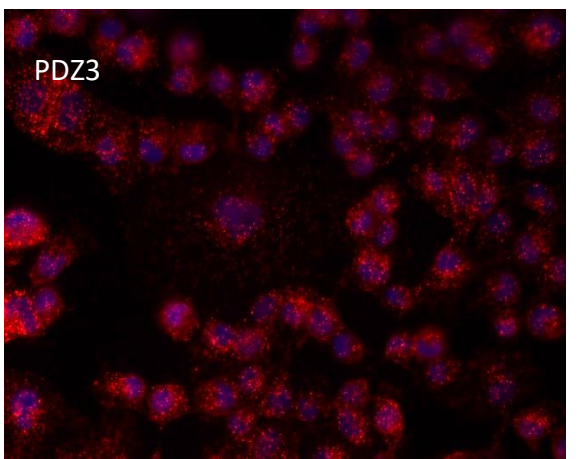
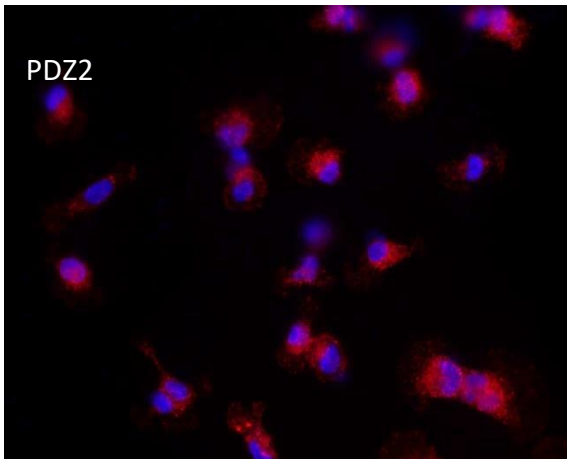
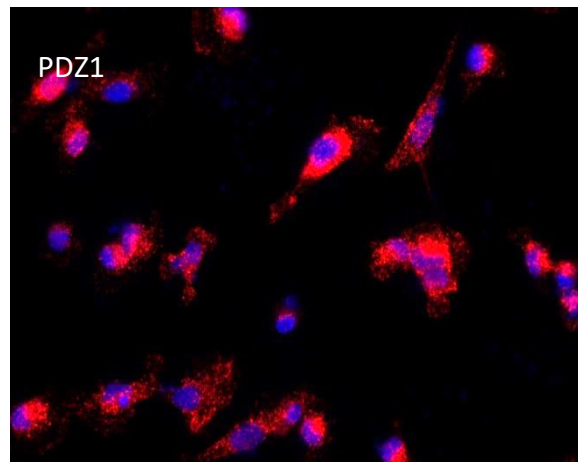
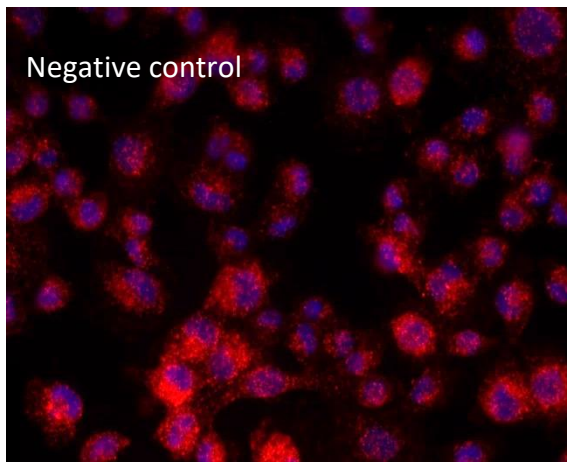


Figure 5. 8 Confirmation of the expression of FLAG-HA-tagged PDZ proteins in MDA-MB-231 cells by dot-blot. MDA-MB-231 cells (10^5) were transfected with FLAG-HA-constructs to express the PDZ domains as tagged hybrid proteins. The cells were permitted to express the proteins for up to 45 h, washed with PBS and then lysed in (200 μ l) Laemmli's buffer. A) the lysates (5 μ l) were pipetted onto a nitrocellulose membrane and allowed to dry for 10 min. The membranes were then blocked and probed with a rabbit anti-HA tag primary antibody overnight at 4°C. The membranes were washed with TBST, probed with an alkaline phosphatase conjugated goat anti-rabbit IgG antibody and developed with Western Blue-stabilised substrate for alkaline phosphatase. B) the quantified dots were analysed using the ImageJ software and calculated as percentage (n=2).

A)



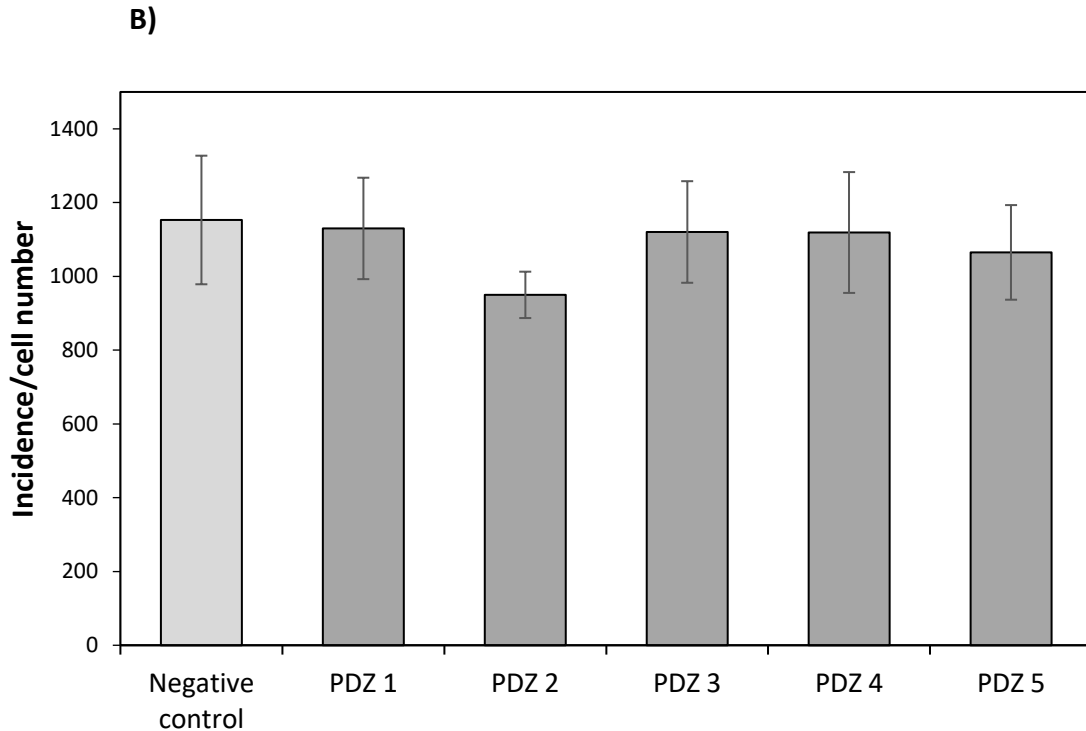


Figure 5. 9 Analysis of the association of TF with MAGI-1-PDZ domains by PLA using the FLAG-tag antibody. A) MDA-MB-231 cells (10^3) were seeded out into 10 mm-glass based μ -dishes and separately transfected with FLAG-HA-tagged constructs to express PDZ 1-5 domains as hybrid proteins. The cells were permitted to express the proteins for 45 h and then fixed with 4% (v/v) paraformaldehyde, washed three times with PBS and then permeabilised with 0.1% (v/v) Triton X-100. The samples were then washed with PBS and blocked with Duolink blocking buffer for 60 min. To assess the association between TF and each expressed PDZ proteins, the cells were incubated with a mouse anti-FLAG antibody together with a rabbit anti-TF antibody overnight at 4°C. As a control, the antibodies were substituted with a rabbit IgG isotype. PLA analysis was performed as described in section 2.3.5. Images were acquired using a Zeiss Axio Vert.A1 inverted fluorescence microscope with a X40 magnification. RED= PLA incidences; BLUE = DAPI. The micrographs represent 10 fields of view from 3 independent experiments. B) The association of TF with each of the expressed PDZ hybrid proteins was determined based on the quantified number of red fluorescent events around each nuclei using the ImageJ software.

cells as FLAG-HA-tagged hybrid proteins PLA was then carried out using a mouse anti-TF antibody together with a rabbit anti-HA antibody. Data were obtained from 6 independent PLA repeats and indicated that the highest level of association of TF occurred with PDZ1 while the lowest level was detected with PDZ2. TF was also shown to associate with PDZ4 and PDZ5 although the association was lower than that observed with PDZ1 (Figure 5.10).

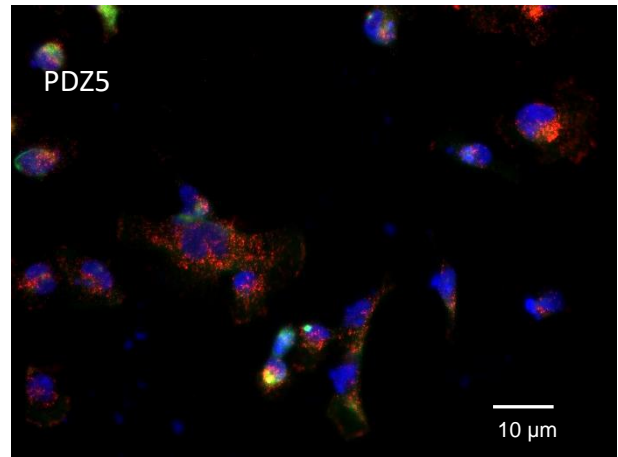
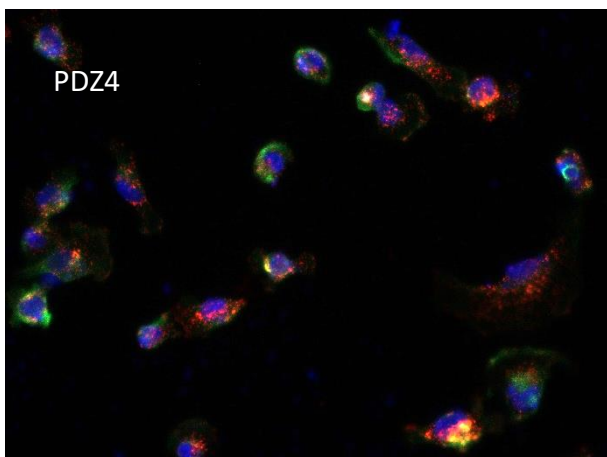
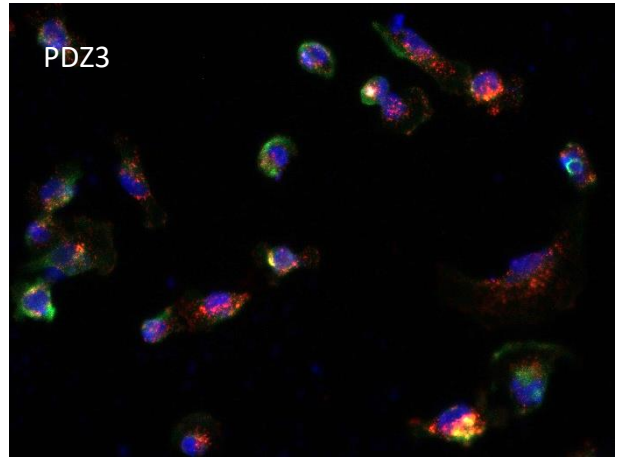
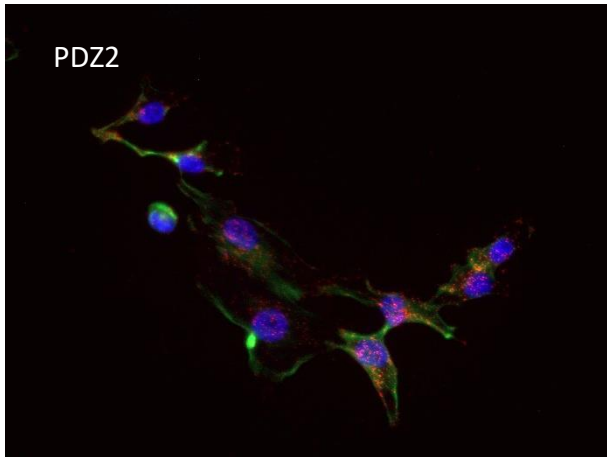
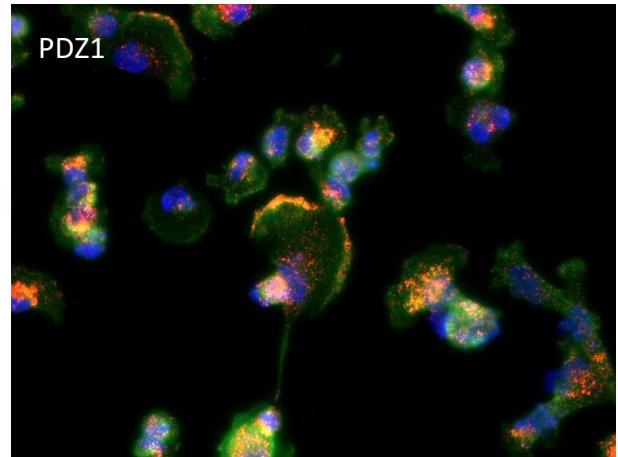
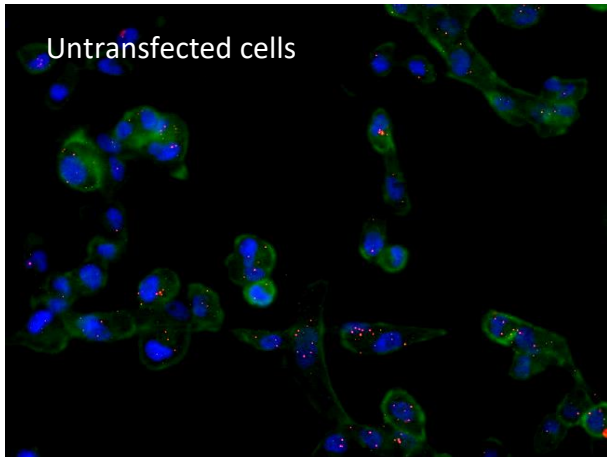
5.3.9 Examination of the association of TF with the N-terminal regions of MAGI-1

To further examine the role of PDZ1 domain in the interaction of MAGI-1 with TF, two modified MAGI-1 constructs were produced: i) the N-terminal domain of MAGI-1 including and excluding PDZ1 were expressed in MDA-MB-231 cells as FLAG-HA-tagged proteins. Data obtained from 4 independent PLA repeats showed a significant association between TF and the N-terminal region of PDZ1 but was significantly weaker on the expression of the N-terminal region without the PDZ1 domain (Figure 5.11).

5.3.10 Analysis of the interaction between TF and the N-terminal regions of MAGI-1 by co-immunoprecipitation

To further confirm the interaction between TF and PDZ1, the two constructs were separately expressed. Transfected MDA-MB-231 cells were permitted to express the N-terminal regions of MAGI-1 as hybrid proteins. The cells were lysed and the hybrid proteins were then immunoprecipitated using a rabbit anti-HA antibody. Using the ImageJ programme, the amount of the co-immunoprecipitated TF was quantified and determined as a ratio. Representative examples of the western blot analysis from 3 independent repeats indicated a strong interaction with TF in the presence of the PDZ1 of MAGI-1. However, the interaction between TF and the N-terminal domain of MAGI-1 devoid of PDZ1 domain was significantly lower (Figure 5.12).

A)



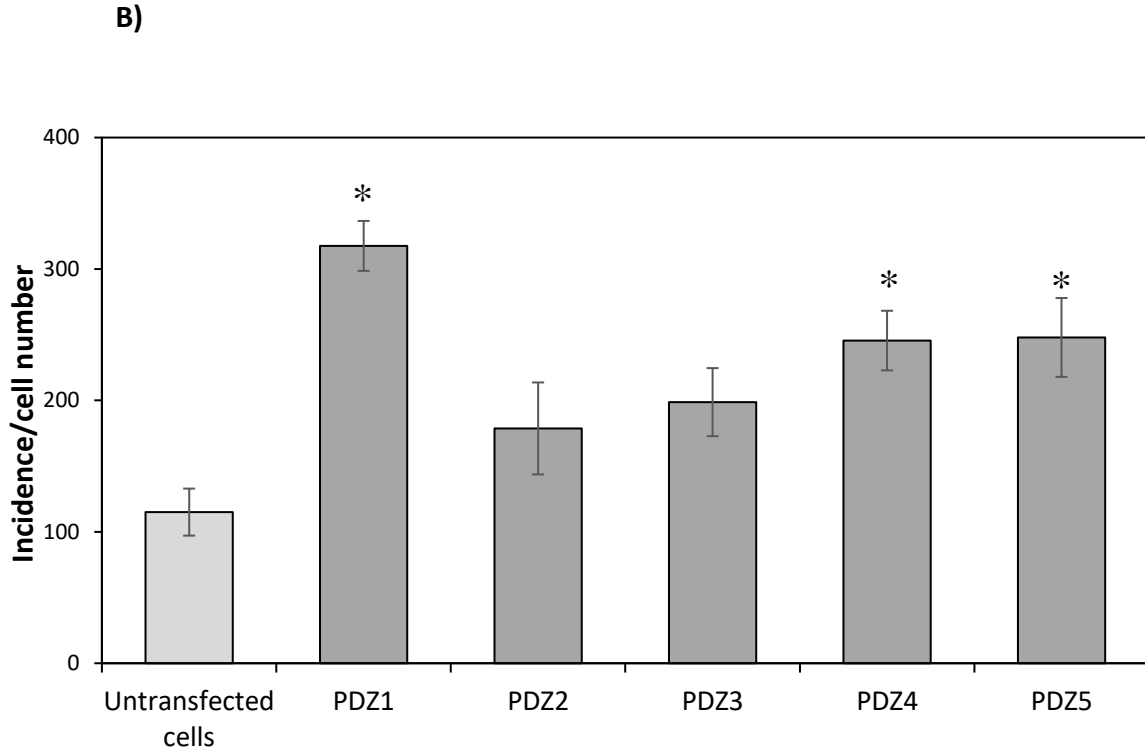
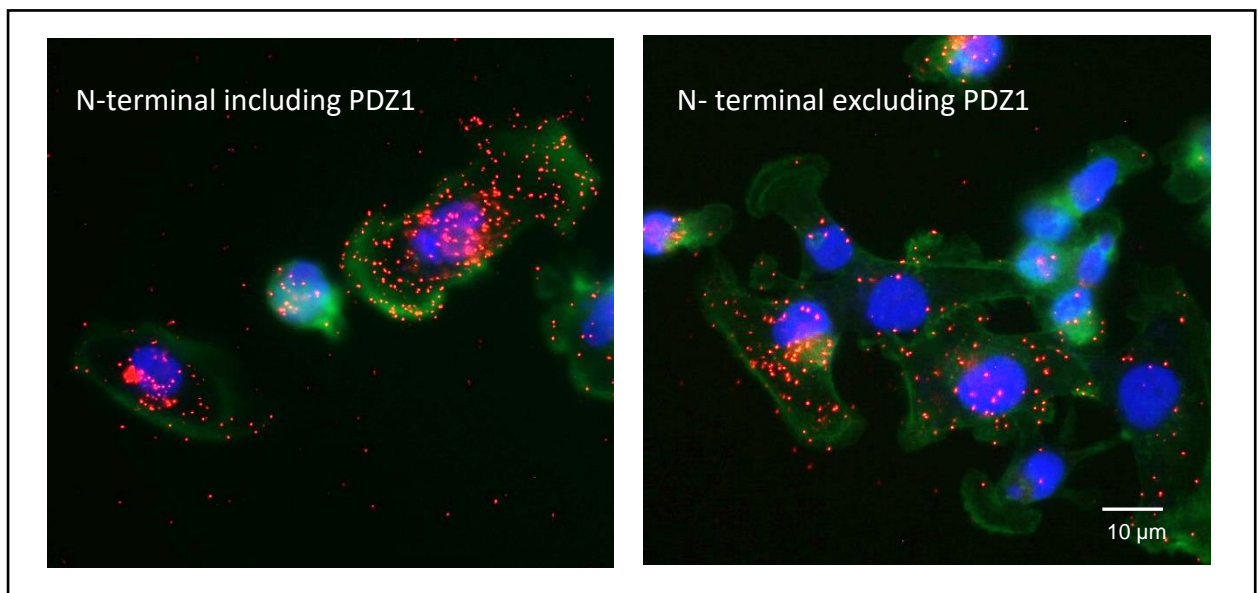
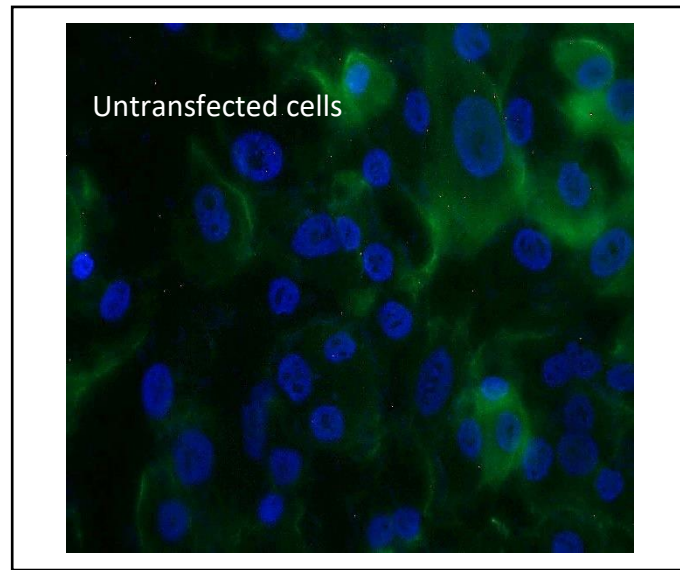


Figure 5. 10 Analysis of the association of TF with MAGI-1-PDZ domains by PLA using the HA-tag antibody. A) MDA-MB-231 cells (10^3) were seeded out into 10 mm-glass based μ -dishes and separately transfected with FLAG-HA-tagged constructs to express PDZ 1-5 domains as hybrid proteins. The cells were permitted to express the proteins for 45 h and then fixed with 4% (v/v) paraformaldehyde, washed three times with PBS and then permeabilised with 0.1% (v/v) Triton X-100. The samples were then washed with PBS and blocked with Duolink blocking buffer for 60. To assess the association between TF and each expressed PDZ proteins, the cells were incubated with a rabbit anti-HA antibody together with a mouse anti-TF antibody overnight at 4°C. PLA analysis was performed as described in section 2.3.5. Images were acquired using a Zeiss Axio Vert.A1 inverted fluorescence microscope with a X40 magnification. RED= PLA incidences; BLUE = DAPI. The micrographs represent 10 fields of view from 6 independent experiments. B) The association of TF with each of the expressed PDZ hybrid proteins was determined based on the quantified number of red fluorescent events around each nuclei using the ImageJ software. (n = 6; * = $p < 0.05$ vs. the untransfected cells).

A)



B)

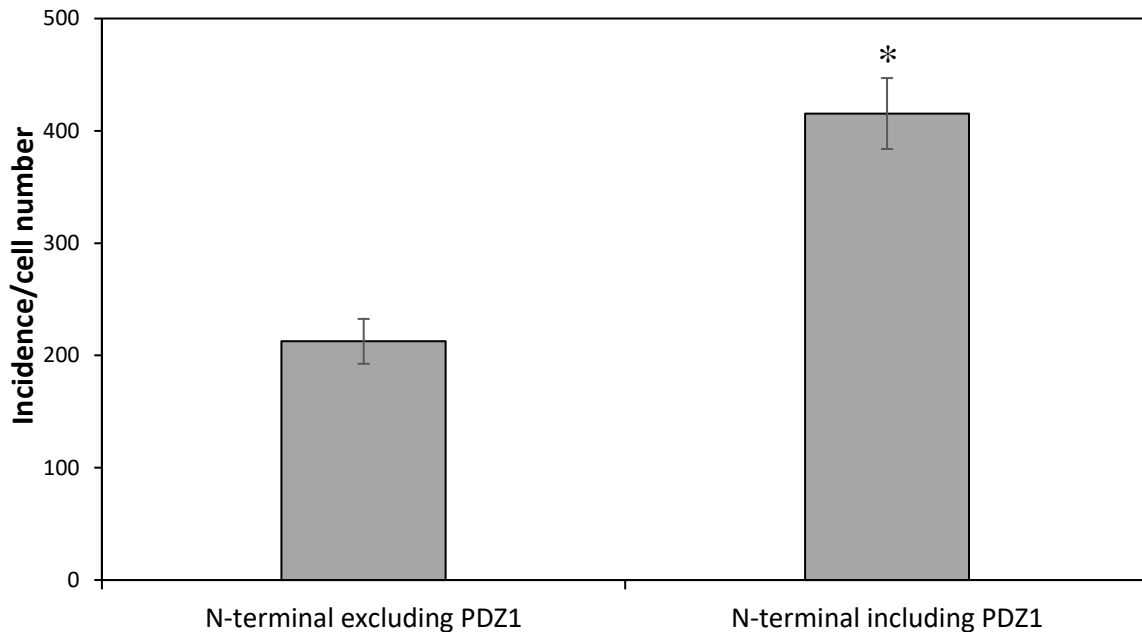


Figure 5. 11 Analysis of the association between TF and the N-terminal regions of MAGI-1 using PLA. A) MDA-MB-231 cells (10^3) were seeded out into 10 mm-glass based μ -dishes and separately transfected with constructs to express the N-terminal region of MAGI-1 including, or excluding the PDZ1 domain. The cells were permitted to express the proteins for 45 h and then fixed with 4% (v/v) paraformaldehyde, washed three times with PBS and then permeabilised with 0.1% (v/v) Triton X-100. The cells were then washed with PBS and blocked with Duolink blocking buffer for 60 min. To assess the association between TF and the N-terminal region of MAGI-1, the cells were incubated with a rabbit anti-HA antibody together with a mouse anti-TF antibody overnight at 4°C. PLA analysis was performed as described in section 2.3.5. Images were acquired using a Zeiss Axio Vert.A1 inverted fluorescence microscope with a X40 magnification. RED= PLA incidences; BLUE = DAPI. The micrographs represent 10 fields of view from 4 independent experiments. B) The association of TF with the expressed N-terminal regions of MAGI-1 was determined by analysing the number of red fluorescent events around each nuclei using the ImageJ software (n =12; * = p< 0.05 vs. samples excluding PDZ1 domain).

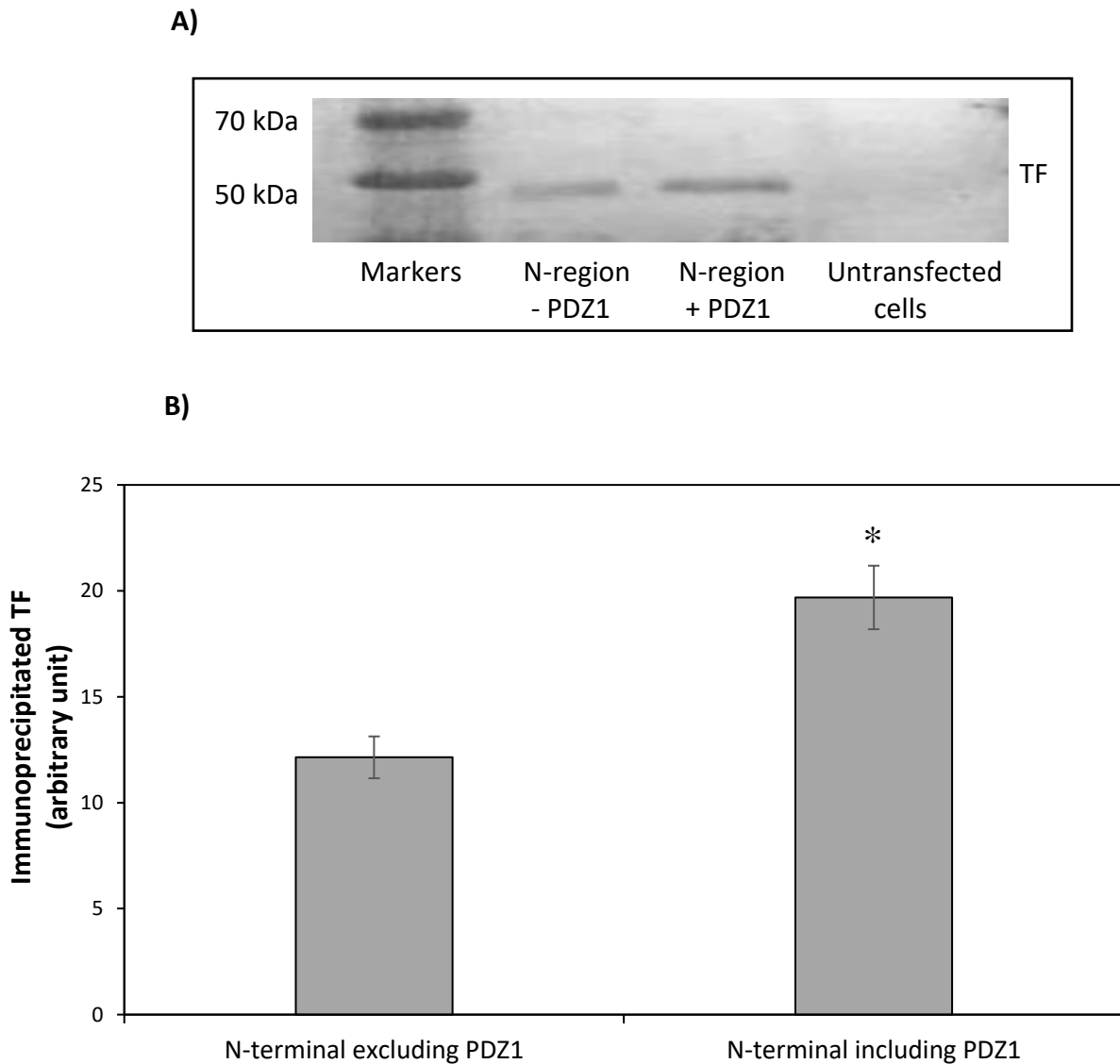


Figure 5. 12 Analysis of the interaction of TF with the N-terminal region of MAGI-1 using co-immunoprecipitation. MDA-MB-231 cells (10^5) were seeded out into 6-well plates and transfected with constructs to express the hybrid proteins of the N-terminal domain of MAGI-1 including or excluding the PDZ1 domain. The expressed FLAG-HA-tagged proteins were immunoprecipitated from cell lysates expressing the two hybrid proteins using a rabbit anti-HA antibody and captured with protein-A magnetic beads. A) The immunoprecipitated TF proteins were separated by 12% (w/v) SDS-PAGE, transferred onto nitrocellulose membranes and blocked. The membranes were probed with a mouse anti-TF antibody overnight at 4°C. The membranes were probed with an alkaline phosphatase-conjugated goat anti-mouse IgG antibody. The bands were developed with Western Blue-stabilised substrate for alkaline phosphatase and photographed. B) The band densities were quantified to determine the interaction of TF with the expressed proteins of the N-terminal regions of MAGI-1. (n = 3; * = p < 0.05 vs. samples excluding PDZ1 domain).

5.3.11 Measurement of the activity of TF on the cell surface

MDA-MB-231 cells (10^5) were separately transfected with FLAG-HA-dual tagged constructs expressing either the PDZ1 or the PDZ2 domain as hybrid proteins. The activity of TF was then measured in confluent live cells expressing either construct. Data analysis of 3 independent experiments showed significantly higher TF activity in cells expressing the PDZ1 domain compared to cells expressing the PDZ2 domain, or the empty vector (Figure 5.13). Another set of cells were separately transfected with FLAG-HA-dual tagged constructs expressing the N-terminal region of MAGI-1 with or without the PDZ1 domain. The activity of TF in MDA-MB-231 cells expressing the N-terminal region including the PDZ1 domain, was shown to be higher compared to that in cells expressing the protein devoid of PDZ1 domain, or cells expressing the empty vector (Figure 5.14).

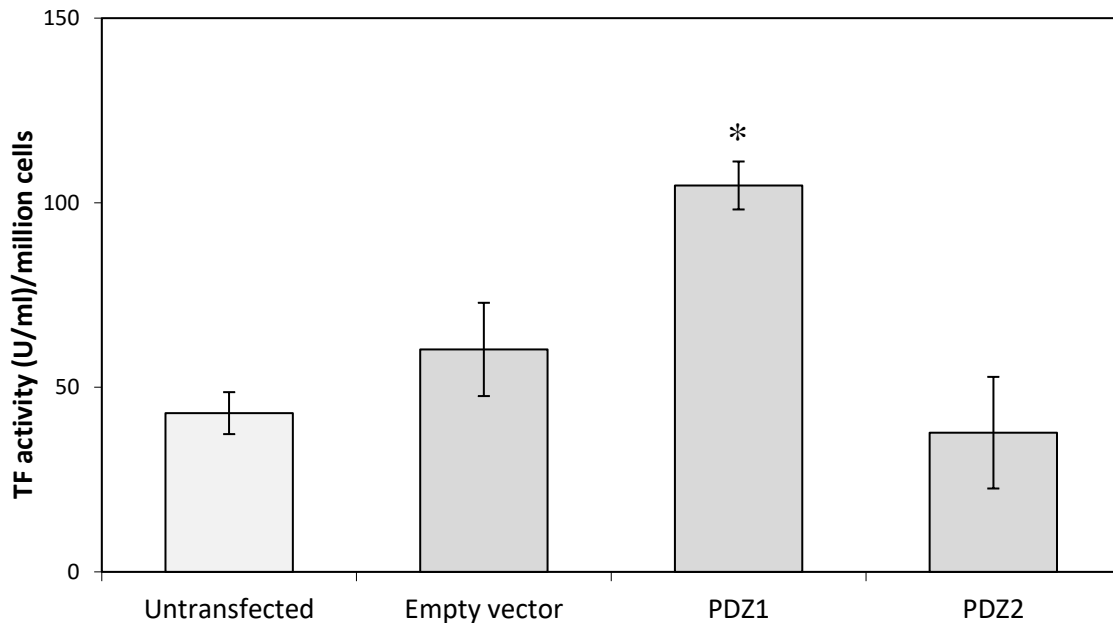


Figure 5. 13 Examination the influence of expressing the PDZ1 and PDZ2 domains on TF activity by a modified thrombin generation assay. MDA-MB-231 cells (5×10^4) were transfected with FLAG-HA-tagged constructs to express PDZ1 or PDZ2 domains as hybrid proteins in a 96-well plate. The cells were allowed to express the proteins for 45 h and then washed three times with TBS containing 1% (w/v) BSA and then incubated with barium sulphate absorbable proteins (2 mg/ml) mixed with CaCl_2 (5 mM). The plate was incubated at 37°C for 30 min and aliquots of the reactions (100 μl) were then transferred to a 96-well plate containing (100 μl) thrombin substrate (0.2 μM) diluted in the TBS buffer. The plate was incubated for 60 min at 37°C and once the colour had developed, the reactions were stopped by adding sulphuric acid (50 μl). The absorptions were measured at 410 nm using a plate reader (n = 4; * = $p < 0.05$ vs. untransfected samples).

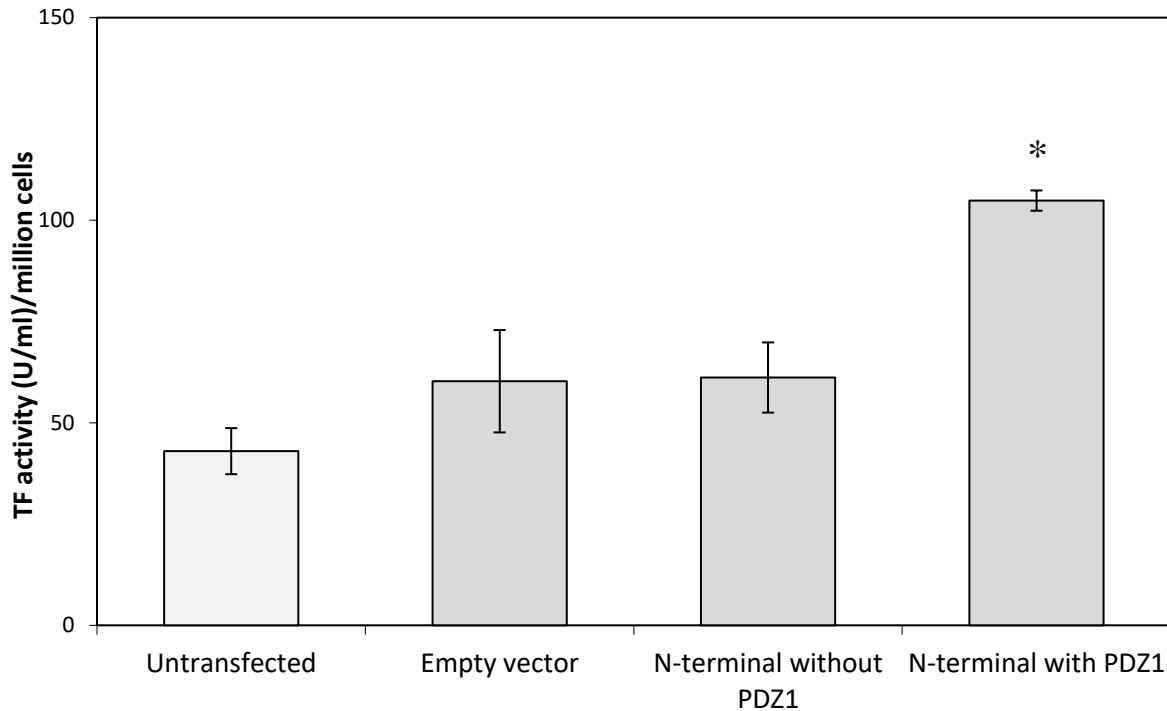


Figure 5. 14 Examination the influence of the expression of the N-terminal regions of MAGI-1 on TF activity by thrombin generation assay. MDA-MB-231 cells (5×10^4) were transfected with FLAG-HA-tagged constructs to express the N-terminal region of MAGI-1 including or excluding the PDZ1 domain as hybrid proteins in a 96-well plate. The cells were allowed to express the proteins for 45 h and then washed three times with TBS containing 1% (w/v) BSA and then incubated with barium sulphate absorbable proteins (2 mg/ml) mixed with CaCl_2 (5 mM). The plate was incubated at 37°C for 30 min and aliquots of the reactions (100 μl) were then transferred to a 96-well plate containing (100 μl) thrombin substrate (0.2 μM) diluted in the TBS buffer. The plate was incubated for 60 min at 37°C and once the colour had developed, the reactions were stopped by adding sulphuric acid (50 μl). The absorptions were measured at 410 nm using a plate reader ($n = 4$; * = $p < 0.05$ vs. untransfected samples).

5.4 Discussion

The regulation of TF activity is dependent on its decryption at the cell surface. It has been well documented that the cytoplasmic domain of TF does not directly influence the procoagulant activity of TF. However, post-translational modifications such as phosphorylation, palmitoylation and ubiquitination have all been reported to alter the cell surface activity of TF (Dorfleutner and Ruf 2003; Ettelaie *et al* 2016). It has been documented that the activity of TF can be modulated through the interaction between the cytoplasmic domain of TF and Pin1 (Collier *et al* 2013; Collier *et al* 2017) which is mediated by a phosphorylation site X-Ser*/Thr*-Pro-X within the cytoplasmic domain of TF (Zioncheck *et al* 1992). Therefore, in this part of the study a mechanism for the regulation of TF is proposed based on the ENSPL sequence located within the phosphorylation site of the cytoplasmic domain of TF. It was hypothesised that this sequence may be a target for PDZ domain-dependent interactions.

The results produced in the previous (chapter 4) indicated that TF interacts with MAGI-1. Therefore, the aim of this section of the study was to identify the PDZ domain within MAGI-1 that has the potential to interact with TF. The first part of the study aimed to sub-clone the entire MAGI-1 DNA into the FLAG-HA-pcDNA3.1 expression vector and to produce a series of constructs by deleting each PDZ domain in turn using site directed mutagenesis. A number of attempts were made to sub-clone the MAGI-1 cDNA into the expression vector; however, these attempts failed. Initially, it was thought that the vector was self-ligating, therefore, several modifications of the procedure were carried out including de-phosphorylation of the expression vector DNA using calf intestinal alkaline phosphatase (CIP), as well as DNA precipitation and DNA isolation after agarose gel separation. However, neither of these approaches were successful and it was concluded that the vector was not designed to accept such a long sequence of DNA. Consequently, the second strategy

was used to individually sub-clone each PDZ domain and to examine the potential of each of these proteins as binding partners for TF. This strategy was successful in sub-cloning and expression of each of the five PDZ domains, as well as the two N-terminal domains of MAGI-1.

MDA-MB-231 cells were transfected with constructs to express each PDZ domain as proteins and were examined for their interaction with cellular TF. Higher association between TF and the constructs expressing either the PDZ1 domain or the N-terminal region of MAGI-1 with PDZ1 domain was observed when examined by the PLA (Figure 5.10 and 5.11) and the interactions were then confirmed using co-immunoprecipitation (Figure 5.12). Therefore, these data have identified PDZ1 as a putative site for interaction with TF. Moreover, it is likely that this interaction may be mediated by class-I type PDZ binding, where the **ENSP**L sequence within TF provides the classic **X-X-Ser-X-Y** motif that is recognised by Class-I PDZ. Since MAGI proteins localise to the cell junctions, it was also hypothesised that this interaction may restrict TF to cell junctions. The restriction of TF, mediated through a PDZ-domain may in turn hinder the accessibility of TF to FVIIa and regulate the procoagulant activity of TF on the cell surface. It is therefore proposed that the restriction of TF within the cell junctions, mediated through the interaction with MAGI-1, may act as an encryption mechanism for TF. Since it was not possible to sub-clone the entire MAGI-1 cDNA, an attempt to measure TF following over-expression of MAGI-1 was not possible. Therefore, as an alternative, the activity of TF was measured in cells expressing the PDZ1 (which binds TF) and PDZ2 (which did not bind TF) domains of MAGI-1, as well as the two N-terminal regions of the PDZ1 domain. The procoagulant activity of TF was shown to be higher in MDA-MB-231 cells expressing either the PDZ1 domain (Figure 5.13) or the N-terminal region that included the PDZ1 domain (Figure 5.14) compared to those devoid of PDZ1. It is proposed that the over-expressed PDZ1 domain can interact with TF, competing out the

cellular MAGI-1 and therefore releasing TF from the intercellular regions which in turn would lead to the observed increase in the apparent TF activity on the cell surface (Figure 5.13 and 5.14). It has been documented that cancer cells exhibit reduced intercellular adhesion due to loss of cell junction protein expression (Leech *et al* 2015). Therefore, it is also possible that MDA-MB-231 which do not form distinct cell junctions, would not have foci of MAGI-1 to bind TF which leads to increased TF activity. Additional experiments measuring the activity of TF in MDA-MB-231 cells expressing MAGI-1 as a whole protein could further confirm the role of MAGI-1 as a possible regulatory partner for TF activity. Also, further studies examining the localisation of TF and MAGI-1 at the tight junctions of endothelial or epithelial cells could further validate the role of MAGI-1 in the encryption of TF.

In conclusion, MAGI-1 appears to interact with the PDZ1 domain of MAGI-1. However, this interaction could be disrupted upon cell injury thereby compromising the integrity of cell-cell contacts and concurrently, activating the coagulation mechanism.

Chapter 6

Discussion

6.1 General discussion

In addition to its procoagulant activity, the exposure of TF at the site of injury induces multiple cellular signalling pathways (Bluff *et al* 2008; Lee *et al* 2011; Åberg and Siegbahn 2013). The ability of TF to confer improved survival, proliferation and migration in cancer cells has been attributed to the activation of Akt pathway following the activation of TF (Sorensen *et al* 2003; Jiang *et al* 2005; Arderiu *et al* 2012; D'Asti *et al* 2017;). It has been postulated that cellular proliferation and apoptosis are two contrasting cellular processes which are determined by the local concentration of TF at the site of injury (Pradier and Ettelaie 2007; ElKeeb *et al* 2015; Ethaeb *et al* 2020). Therefore, the first part of this study aimed to examine the hypothesis that the response of cells to acute levels of TF, such as those encountered during injury and trauma, may differ from the adaptive behaviour of the cells, as observed in longer-term chronic conditions such as cancer.

Initially, the outcomes of the exposure of cells to TF and/or the activation of PAR2 were examined in seven cancer cell lines. As part of the normal physiological responses to injury, the coagulation cascade is activated once TF is exposed to the bloodstream. The binding of TF to FVIIa activates PAR2 which subsequently leads to the induction of multiple signalling pathways. The short-term exposure of cells to rec-TF at 65 pg/ml, or the activation of PAR2, induced the dephosphorylation of PTEN in most cell lines tested. Interestingly, at high concentrations (rec-TF 1300 pg/ml), the de-phosphorylation of PTEN was relatively lower. The mechanism by which TF promotes the de-phosphorylation of PTEN is not currently known.

However, the interaction of TF with cell-surface proteins such as β 1-integrin has been reported to facilitate TF-PAR2 dependent signalling (Versteeg *et al* 2008; Kocatürk and Versteeg 2013). In addition, the activation of PI3K is thought to be mediated by β 1-integrin and has been implicated in cancer cell migration, proliferation and survival (Su *et al* 2007; Matsuoka *et al*

2012; Zeller 2012; Guidetti *et al* 2015). Therefore, it is possible that low concentrations of TF may initiate multiple signals that promote the activation of PTEN. The mechanism and the outcome of such interactions were not investigated in this study, but future studies are essential to further elucidate the complex mechanism involved in the regulation of cell homeostasis. Furthermore, it has been documented that activated PAR2 couples with either $G\alpha$ or $G\beta\gamma$ -subunits of the trimeric G-protein and signal through a variety of downstream signalling pathways (Sidhu *et al* 2014; Zhao *et al* 2015; Heuberger and Schuepbach 2019). Specifically, the $G\beta\gamma$ -subunit can bind and recruit PI3K to the membrane, catalysing the phosphorylation of PIP2 to PIP3. PIP3 in turn binds Akt through its PH-domain and recruits it to the inner membrane surface which results in Akt phosphorylation and activation (New *et al* 2007; Goel *et al* 2009; Lima-Fernandes *et al* 2011; Nitulescu *et al* 2018; Jean-Charles *et al* 2018). Therefore, the signalling mediated by the G-protein subunits as well as those initiated through β 1-integrin activation may trigger the activation of PI3K. Generation of PIP3 at the inner membrane has been shown to promote the auto-dephosphorylation of PTEN at Thr366 through its protein-phosphatase activity, thereby inducing the activation of PTEN which acts a negative feedback to regulate the PIP3 (Tibarewal *et al* 2012; Papa and Pandolfi 2019). In addition, de-phosphorylation of PTEN results in its membrane recruitment and stabilisation through interaction with MAGI proteins thereby enhancing its lipid-phosphatase activity (Georgescu *et al* 2000; Leslie *et al* 2000; Valiente *et al* 2005;). The increase in PTEN activity was also reflected in the increased lipid-phosphatase activity generated, which was measured in this study. The de-phosphorylation and hence, the reduction in the amount of PIP3 reduces the recruitment of Akt to the membrane and restrains its activation which would explain the reduced kinase activity of Akt, observed.

It has been suggested that normal tissue maintenance and homeostasis is controlled by the balance between the function of PTEN and Akt (Gao *et al* 2016). A recent study of western

blot and immunofluorescence analyses, using rat corneal epithelium, showed the downregulation of PTEN activity within 30 min of skin incisions. Simultaneously, the elevated levels of phospho-Akt resulted in an increase in cell migration, accelerating the healing process (Cao *et al* 2011). The activation of the Akt in response to tissue repair after damage has also been documented (Castilho *et al* 2013). For instance, immunohistochemistry and western blot analyses of skin samples from mice following wounding showed elevated levels of phospho-Akt. Also, in the same study RT-PCR measurements showed the upregulation in Akt mRNA expression during the proliferative and remodelling phases (Gao *et al* 2016) compared to uninjured skin (Squarize *et al* 2010). As a consequence of PI3K-Akt signalling a number of genes downstream of this pathway are upregulated, and have been associated with cell proliferation, migration and collagen synthesis all of which are essential in accelerating the process of wound healing. For example, endothelial nitric oxide synthase (eNOS) is a downstream target of Akt signalling; this enzyme produces nitric oxide which is essential for vasodilation and remodelling and has been associated with angiogenesis and collagen deposition required for the healing process (Luo and Chen 2005; Zhang *et al* 2019; Yu *et al* 2020). Akt has also been reported to upregulate neovascularisation through the upregulation of VEGF and EGF expression (Peng *et al* 2003; Zhang *et al* 2016; Di and Chen 2018). In contrast, the inhibition of PI3K-Akt using LY294002 leads to significant reduction in skin regeneration and wound contraction delaying the healing process (Li *et al* 2016). In summary, immediately after injury, the surrounding cells undergo several interrelated phases which include haemostasis, inflammation, proliferation and remodelling to initiate repair to restore the integrity of tissue (Jere *et al* 2019). Both PTEN and Akt appear to have important physiological roles in the maintenance of normal tissue architecture and correct homeostasis. Therefore, this study adds to the current understanding of the link between haemostasis, inflammation and

repair by suggesting that exposure of cells to TF at the site of injury, modulates the activity of PTEN which can determine the fate of the injured cells.

In addition to its function in tissue repair, the signalling properties arising from TF have also been implicated in chronic inflammation leading to tumourigenesis as well as cancer progression (Dutra-Oliveira *et al* 2012; Han *et al* 2014; Hisada and Mackman 2019). One main cellular property associated with tumourigenesis is the uncontrolled proliferation of cells which in some circumstances, has been attributed to the deregulation of PTEN function (Chin *et al* 2014). The loss of PTEN function or impairment in its activity through mutational inactivation or deletions has been strongly associated with aberrant tissue formation and progression of many cancers (Milella *et al* 2015). Furthermore, mutational loss of the PTEN gene not only elevates the probability of tumourigenesis, but also has been associated with many disorders like Cowden's syndrome and Bannayan-Riley-Ruvalcaba which are characterised by growth of non-cancerous tumours (Pilarski and Eng 2004; Yang and Karin 2014; Luongo *et al* 2019). Moreover, the reductions in the levels of cellular PTEN or the deregulation of PTEN function have been reported to promote tumourigenesis in breast (Petrocelli and Slingerland 2001), renal (Brenner *et al* 2002), prostate (Schmitz *et al* 2007), head and neck (Squarize *et al* 2012) and lung cancers (Yanagawa *et al* 2012). Therefore, the mechanisms by which TF may influence PTEN were examined next.

To produce an *in vitro* model where cells may become exposed to increased levels of TF over prolonged periods, MDA-MB-231, LoVo and CaCo-2 cells were repeatedly supplemented with rec-TF (65 pg/ml) over a period of 5 days. Measurement of PTEN antigen levels in these cells, resulted in a reduction in the amount of PTEN antigen levels. As described above, the dephosphorylation of PTEN can be influenced by crosstalk between PI3K and other signalling pathways. Therefore, it is possible that excessive amounts of TF may initiate multiple signalling pathways which may exhaust the ability of cells to perceive and correctly respond

to the initiated signals (Cully *et al* 2006). As a result, the cells become unable to regulate the function of PTEN. The de-phosphorylation of PTEN, especially when not protected by MAGI, may destabilise PTEN leading to further modification and proteasomal degradation of the protein. This reduction of PTEN over time may be a determining factor in the alterations which lead to cell proliferation as well as aberrant cell survival and are mediated through deregulation of the Akt pathway. Specifically, the activation of Akt pathway has been shown to influence the progressions of cancers by a number of separate mechanisms. For example, Akt has been implicated in carcinogenesis through downregulation of E-cadherin expression, leading to destabilisation of cell junctions. This in turn increases the rate of epithelial-mesenchymal transition (EMT) and therefore cellular invasiveness (Larue and Bellacosa 2005; Barber *et al* 2015). Akt also regulates cell survival through the inhibition of several pro-apoptotic proteins (Los *et al* 2009). It was reported that Akt inactivates Bax protein by preventing translocation to the mitochondria, and therefore inhibiting the Bax-dependent mitochondrial permeabilisation and the subsequent release of cytochrome *c* (Uren *et al* 2016; Simonyan *et al* 2016). Akt can also regulate cell proliferation and survival in part by direct inhibition of the forkhead box class O (FoxO) proteins (Zhang *et al* 2011). Activated Akt is capable of phosphorylating the FoxO transcription factor which in turn localises the latter proteins to the cytoplasm; FoxO is a multifunction protein which induces the expression and stabilisation of the inhibitors of cell cycle checkpoints such as p27 and p21 (Liu *et al* 2008). In addition, FoxO acts directly as an inhibitor of cyclin D preventing entry into the cell cycle (Ho *et al* 2008). Therefore, the phosphorylation of FoxO by Akt restricts the former protein outside the nucleus permitting the progression of cell division (Ho *et al* 2008). However, while the increases in Akt activity observed in this study were significant reaching up to 29% in LoVo cells, such outcomes are only likely to become dominant over longer periods of time (e.g., months or years) as observed during chronic inflammatory diseases.

Moreover, it has been reported that subtle reductions in PTEN protein levels increase the susceptibility of cells to tumourigenesis through the activation of the PI3K-Akt pathway (Milella *et al* 2015). The decrease in PTEN levels have already been implicated in non-malignant tumourigenesis (Pilarski *et al* 2004), carcinogenesis (Lee *et al* 2018) as well as the progression of cancers (Carracedo *et al* 2011). It would be of interest to determine if the levels of PTEN antigen and those of Akt activity within tumour tissue correlate with the formation and progression of tumours, during inflammatory diseases in which the local levels of TF are elevated. In summary, the current study suggests that the prolonged exposure of cells to TF together with the activation of PAR2 may contribute to tumourigenesis through the degradation of PTEN. Furthermore, the study may further explain the complex cellular connections between the exposure of TF during inflammatory conditions and the regulation of PTEN and Akt activity.

As stated above, augmentations in the levels of Akt activity are also associated with the loss of cell junction. The destabilisation of the cell junctions invariably involves functional changes in MAGI proteins. The loss of these interfaces is likely to expose latent forms of TF which in turn exacerbate the process by positive feedback through the aforementioned PAR2 signalling mechanism. To examine the hypothesis that MAGI proteins are capable of localising and therefore regulating TF activity, the next part of the study focused on examining the ability of TF to interact with MAGI proteins. Additionally, the study endeavoured to identify and confirm whether the PDZ domain within MAGI-1 was responsible for interaction with the cytoplasmic domain of TF. Finally, the possibility of dissociation of TF from MAGI, following PAR2 activation was examined.

TF exhibits a wide tissue distribution ranging from vascularised organs and epithelial cells to smooth muscle cells and fibroblasts (Østerud and Bjørklid 2006). TF is also reported to localise at the tight junctions of cells such as shown in confluent kidney epithelial cells (Camerer *et al*

1996), myocytes (Luther *et al* 2000) as well as other cell lines (Müller *et al* 1993; Garnier *et al* 2012). Although TF is widely expressed in the vasculature, its expression is suppressed on the cell-surface of endothelial cells. The exact mechanism involved in the suppression of TF activity is unclear. However, several mechanisms have been suggested to mediate the regulation of TF activity through a process termed TF encryption (Dietzen *et al* 2004; Schmidt *et al* 2006; Bach 2006; Shaw *et al* 2007; Rao and Pendurthi 2012). The regulation of TF activity has also been reported to be mediated through interaction with other cellular proteins and is thought to involve the sequence ENSPL within the cytoplasmic domain of the TF (Collier and Ettelaie 2011; Collier *et al* 2017; Ettelaie *et al* 2018). Analysis of this motif using the POW software indicated that TF may interact with selective PDZ domain-containing proteins, such as the MAGI proteins. Since MAGI proteins are predominantly localised to the tight junction of epithelial and endothelial cells of many tissues (Laura *et al* 2002), it was hypothesised that the encrypted form of TF may be localised at the cell junctions through MAGI-dependent interactions. PLA and co-immunoprecipitation analysis of MDA-MB-231 cells indicated that TF mainly interacts with MAGI-1. Previously it has been documented that TF can be targeted at specific subcellular compartments within endothelial cells which may influence its activity (Ruf 2012). For example, TF was reported to localise at the apical regions of endothelial cell monolayer (Camerer *et al* 1996) whereas basolateral expression of TF may indicate that TF is present in a cryptic pool in the subendothelial which become active upon vascular injury (Weiss *et al* 1989; Ryan *et al* 1992; Lopes-Bezerra and Filler 2003). Therefore, it is suggested that under normal conditions, MAGI-1 may restrain TF at the tight junctions and thereby prevents TF exposure to the cell surface. Additional experiments examining the localisation of both TF and MAGI-1 at the tight junctions of endothelial cells and other cancer cell lines (e.g., McF-7) which form distinct tight junctions may elucidate a mechanism for TF encryption. It has been documented that the encrypted form of TF is localised at the lipid rafts of several cell types

(Dietzen *et al* 2004; Mandal *et al* 2005; del Conde *et al* 2005). Moreover, several studies have suggested the compartmentalization of TF in lipid rafts/caveolae either alone or in complex with FVIIa (Mulder *et al* 1996; Mandal *et al* 2006) and possibly with PAR2 (Awasthi *et al* 2007). However, the disruption of lipid rafts/caveolae induced both the procoagulant and the signalling activities of TF (Pendurthi and Rao 2008). MAGI-1 was also suggested to be localised at the lipid rafts of kidney epithelial cells (Patrie *et al* 2002). Therefore, it would be of interest to explore the localisation of TF with MAGI-1 at the lipid rafts which may further provide an insight into the complex regulatory mechanism of TF.

The capacity of MAGI proteins in maintaining the functional barrier between cells arises from regulating tight junction proteins through interactions with both the WW and PDZ domains (Hirabayashi *et al* 2003; Zaric *et al* 2012; Zaessinger *et al* 2015). In order to identify the specific PDZ domain responsible for interaction with TF, two strategies were implemented. The first strategy aimed to sub-clone the entire MAGI-1 DNA into the FLAG-HA-pcDNA3.1 expression vector. Each PDZ domain could then be deleted using site directed mutagenesis and expressed as tagged mutant-PDZ proteins in cells and the interaction between TF and each tagged mutant-PDZ examined. However, several attempts to sub-clone the cDNA of MAGI-1 resulted in the failure of this strategy because the vector was not designed to accommodate such a large DNA insert. Subsequently, a second strategy was implanted where each of the PDZ1-5 domains of MAGI-1 were sub-cloned and expressed separately, as hybrid proteins. PLA and co-immunoprecipitation analysis of MDA-MB-231 cells expressing each of the PDZ domains indicated that the association between TF and MAGI-1 is mediated through the PDZ1 domain of the latter protein. This interaction was also confirmed by expressing the N-terminal region of MAGI-1 including or excluding the PDZ1 domain. It was hypothesised that TF is restrained at the cellular junctions through a PDZ-domain interaction which might hinder the

accessibility of TF to FVIIa. Therefore, the influence of MAGI-1 interaction on the regulation of TF procoagulant activity on the cell surface was examined next.

Measurement of activated FXa generated by TF using FXa generation assay revealed high TF procoagulant activity levels following cells expressing the PDZ1 domain compared to cells devoid of the latter domain. The increase in TF activity might suggest that the cytoplasmic domain of TF is being occupied by the expressed PDZ1, therefore competing out the cellular MAGI-1, thus preventing MAGI-1 from binding to TF. Recently, the cell-surface expression levels of MAGI-1 were shown to be low in MDA-MB-231 cells (Alday-Parejo *et al* 2020) which might explain the loss of cell-cell contacts associated with the morphological characteristics associated with these cells (Martin and Jiang 2009). Since MDA-MB-231 cells do not form distinct tight junctions, it is also possible that TF is not restrained at the tight junctions by MAGI-1, consequently TF becomes exposed to the cell surface resulting in the increase of TF activity. To further elucidate how PDZ domains might influence the interactions between MAGI-1 and TF, future studies will be conducted using site directed mutagenesis to generate mutated PDZ domains. The PDZ domains will contain a mutated “GFGF” binding motif which is required for the interaction between the target protein and the PDZ domain. The expression of these mutated PDZ domains will determine the ability of each PDZ domain to bind efficiently to TF and the influence of these interactions on its procoagulant activity. Furthermore, structural analysis using protein-ligand softwares such as, SwissDock would also provide information regarding the molecular interactions between the cytoplasmic domain of TF and the PDZ1 domain of MAGI-1. It has been reported that MAGI-1 can interact with single and/or multiple proteins through several of its domains simultaneously (Dobrosotskaya and James 2000; Patrie *et al* 2002). For example, a study by Hirabayashi *et al* (2003) reported that both PDZ1 and PDZ4 domains of MAGI-1 are required for the efficient binding and stability of junctional adhesion molecule (JAM4) at the tight junction of kidney cells leading to

enhanced cell adhesion. Another study reported that MAGI-1 binds through its WW domain with synaptopodin and through its PDZ5 domain with α -actinin-4 (Patrie *et al* 2002). The recruitment of these actin binding proteins by MAGI-1 results in actin cytoskeleton organisation at the cell-cell junctions, thereby enhancing cellular adhesion (Lampugnani 2010). Since MAGI-1 contains two WW domains, and the cytoplasmic domain of TF was also reported to interact with the WW domain of Pin1 (Ettelaie *et al* 2018; Kurakula *et al* 2018). Therefore, it is possible that MAGI-1 may also interact with TF through its WW domains. Future experiments examining the interaction between TF and the WW domain of MAGI-1 may be required to elucidate the regulation of TF activity by MAGI-1.

The association between TF decryption and TF-mediated-dependent signalling is well established. The aberrant expression of TF by cancer cells has been associated with increased procoagulant and signalling activities which are linked with the risk of thrombosis as well as tumour growth and chemo-resistance (Khorana *et al* 2007; Manly *et al* 2010; Dutra-Oliveira *et al* 2012; Unruh and Horbinski 2020). Additionally, signalling arising from PAR2 activation promotes the induction of multiple signalling pathways associated with tumourigenesis and cancer progression (Su *et al* 2007; Kocatürk and Versteeg 2013). One hallmark of cancer progression is the deregulation of tight junctions in tumour cells, leading to the loss of cell-cell contacts and increased cell migration and invasiveness. Such alterations encourage cancer cells to invade across the basement membrane and establish secondary metastasis (Martin and Jiang 2009; Knights *et al* 2012; Leech *et al* 2015; Alday-Parejo *et al* 2020). Several studies have linked the activation of PAR2 with the downregulation of E-cadherin, VE-cadherin and zonula occludens (ZO-1) protein expression leading to longer-term disruption of cell junctions and consequently increased cellular permeability (Chin *et al* 2003; Winter *et al* 2006; Peerapen and Thongboonkerd 2013; Enjoji *et al* 2014). Examination of PAR2-activated MDA-MB-231 cells using PLA, co-immunoprecipitation techniques showed a reduced association between TF and

MAGI-1, reaching minimum levels at 20 min post-activation. The reduced association between TF and MAGI-1 could be attributed to the previously explained mechanism involving the possible induction of caspase-3 arising from PAR2 activation. Therefore, the persistent activation of PAR2 by TF-FVIIa observed during pathological conditions such as chronic inflammation and cancer may lead to the constitutive activation of caspase-3 resulting in the degradation of MAGI-1. This in turn might result in the destabilisation of cellular junctions leading to the dissociation of TF from MAGI-1. Therefore, it is suggested that once TF dissociates from MAGI-1, it becomes exposed to the cell surface leading to its decryption and activation (Figure 6.1). The constitutive activation of TF thereby amplifies a feedback mechanism which further promotes thrombin generation and the activation of PAR2 signalling leading to the deregulation of tissue homeostasis. This deregulation results in the imbalance between cell proliferation and apoptosis and consequently the initiation of tumourigenesis, cancer and ultimately cancer progression and metastasis.

TF is a central protein that is capable of regulating both blood haemostasis and tissue homeostasis (Mackman 2010). TF regulates haemostasis through the binding of FVIIa promoting the activation of the coagulation mechanism. Concurrently, TF regulates tissue homeostasis through the activation of PAR2 signalling mediated by forming TF-FVIIa and TF-FVIIa-FX complexes (Chu 2011; Palta *et al* 2014; Sidhu *et al* 2014). The work in this thesis has demonstrated that the signalling arising from PAR2, together with the local concentration of TF may influence the function of PTEN. Under physiological conditions, TF appears to induce the dephosphorylation of PTEN. As a result, TF may control normal tissue maintenance and homeostasis through the upregulation of PTEN lipid-phosphatase activity. However, under pathological conditions TF together with the activation of PAR2 can contribute to tumourigenesis through the degradation of PTEN. These activities also may promote the deregulation of cells causing pathological conditions by initiating carcinogenesis. Importantly,

this study has elucidated a novel mechanism for the regulation of TF activity itself, through interaction with the PDZ1 domain of MAGI-1. This interaction appears to be disrupted following the activation of PAR2, resulting in further increases in TF activity on the surface of the cells. Therefore, this study has identified a new possible mechanism for the encryption of TF through interaction with MAGI-1 and the rapid upregulation of TF activity following injury to the cellular layer, or cell activation.

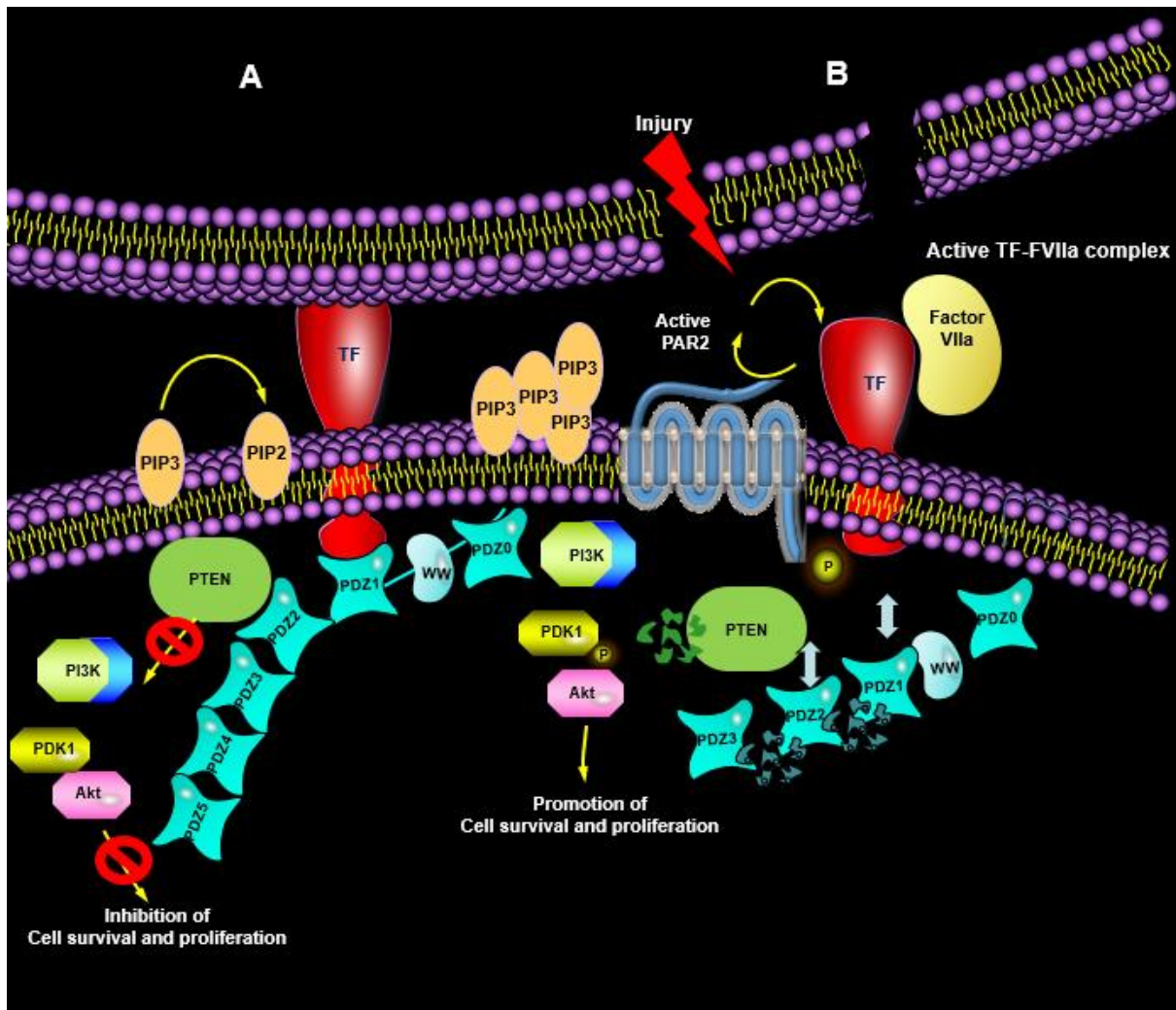
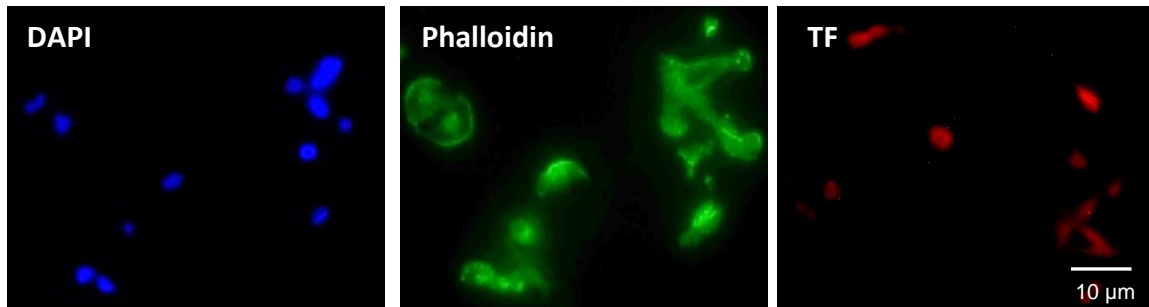


Figure 6. 1 The proposed mechanism for TF signalling and the regulation of its TF procoagulant activity. A) Under normal conditions, TF remain encrypted through interaction with the PDZ1 domain of MAGI-1. PTEN is also stabilised by MAGI-1 through PDZ domain-dependent interactions. B) Under chronic inflammation as well as loss of cell-cell contacts, TF dissociates from MAGI-1 resulting in its decryption. The exposed TF binds FVIIa and initiates the coagulation mechanism. TF-FVIIa activates PAR2 resulting in the activation of several signalling pathways leading to cancer cell proliferation and survival. The signalling arising from PAR2 also triggers the dissociation of PTEN from MAGI-1, resulting in the degradation of both PTEN and MAGI-1.

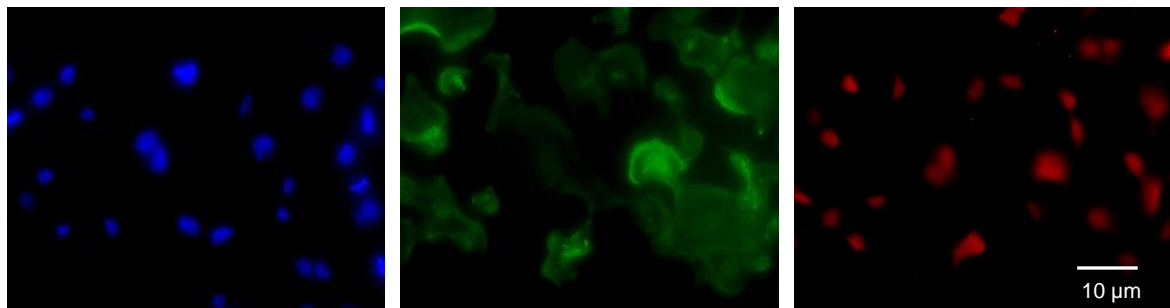
Appendix

A) TF

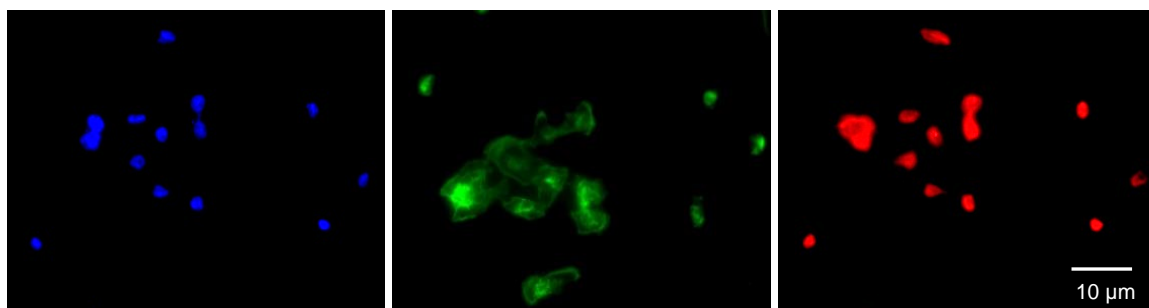
i) Non-permeabilised



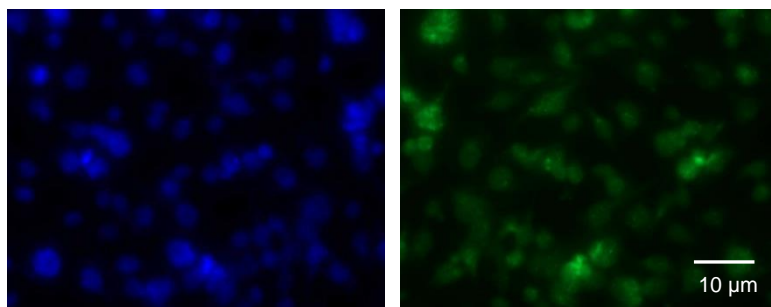
ii) Permeabilised with 0.2% (v/v) saponin



iii) permeabilised with 0.1% (v/v) Triton X-100

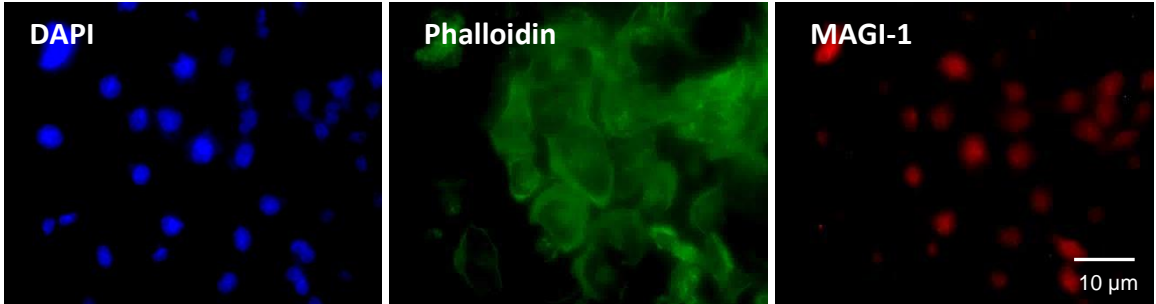


iv) permeabilised with 100% (v/v) methanol

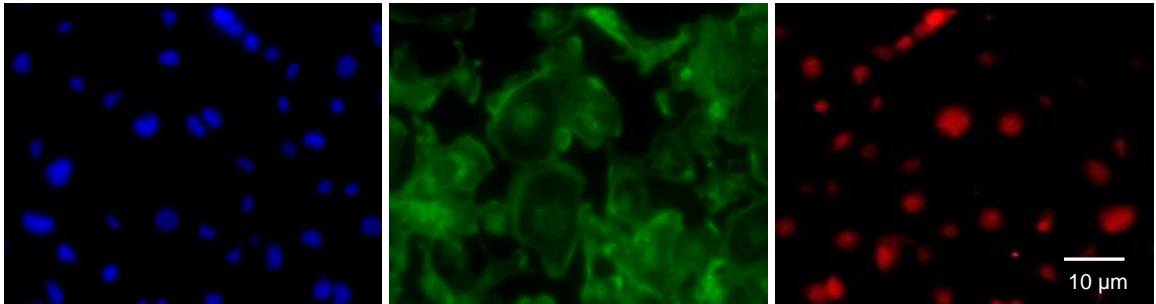


B) MAGI-1

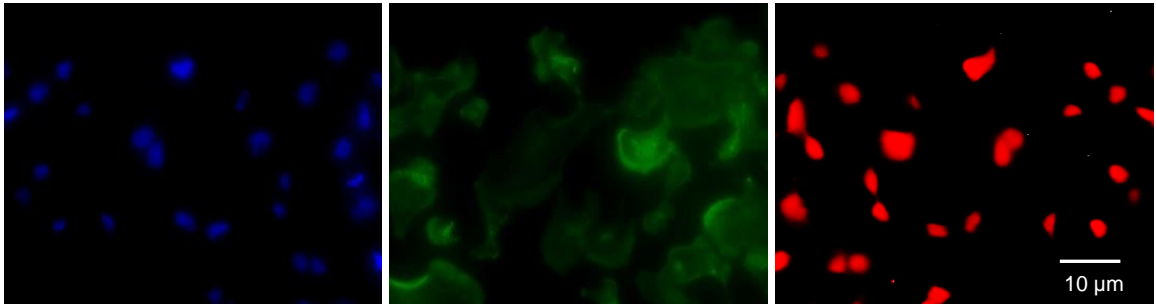
i) Non-permeabilised



ii) Permeabilised with 0.2% (v/v) saponin



iii) permeabilised with 0.1% (v/v) Triton X-100



iv) permeabilised with 100% (v/v)

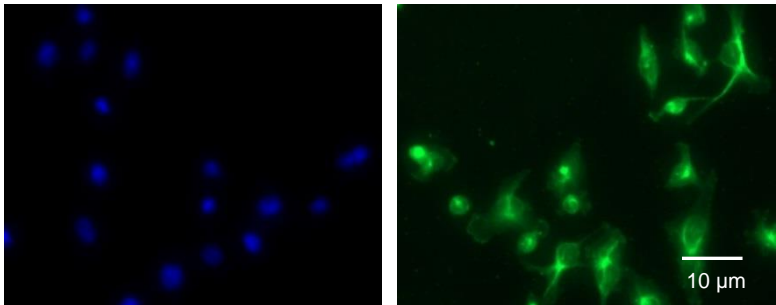
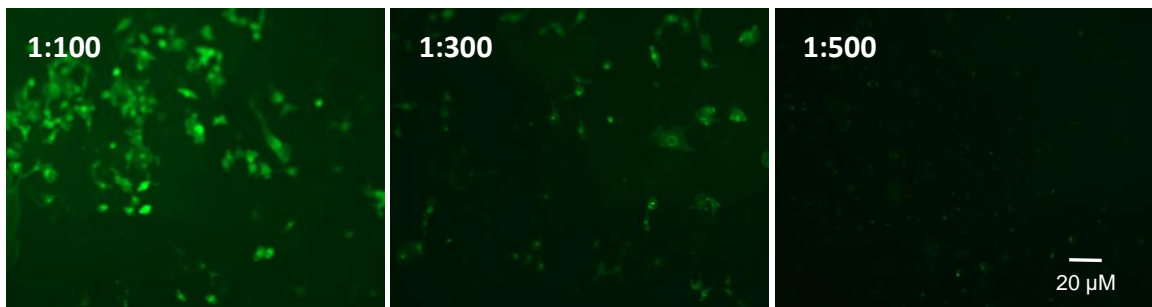
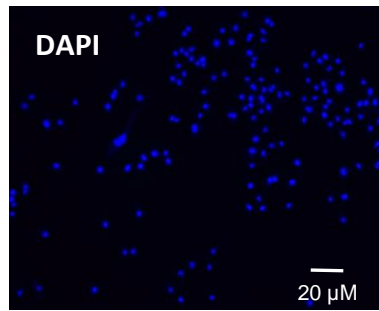
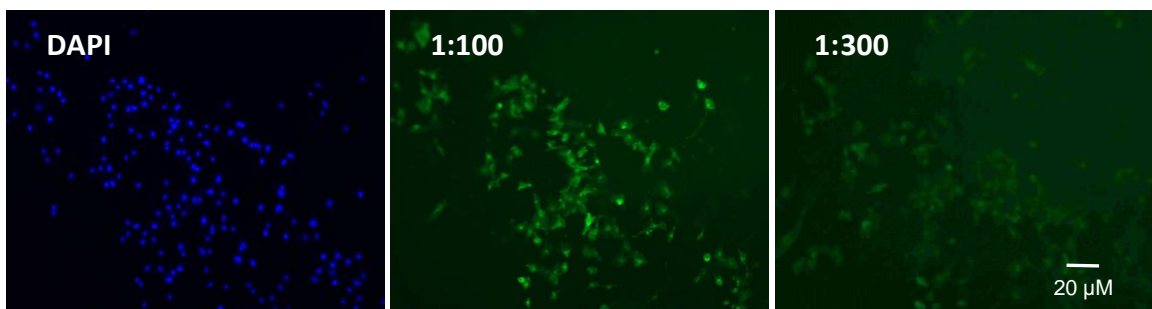


Figure A- 1 Optimisation of cell permeabilising reagents. MDA-MB-231 (3×10^5) cells were seeded out into 6 well plate and propagated to 80% confluency. The cells were washed with PBS and then fixed with 4% (v/v) formaldehyde for 20 min. The cells were prepared as; i) non-permeabilised, ii) permeabilised with 0.2% (v/v) saponin, iii) permeabilised with 0.1% (v/v) Triton X-100 or iv) other set of cells were permeabilised and fixed with 100% (v/v) methanol for 10 min. The cells were washed with PBS and then blocked with 3% (w/v) BSA for 60 min. The cells were incubated with either A) a mouse anti-TF antibody (HTF1) or B) a rabbit anti-MAGI-1 antibody (H-70) overnight at 4°C. The cells were washed with PBS and then probed with a goat anti-mouse secondary antibody (sc-2008) to detect TF. In order to detect the presence of MAGI-1, the cells were incubated with a goat anti-rabbit secondary antibody (sc-2004) for 60 min. The nuclei were incubated in DAPI (2 $\mu\text{g}/\text{ml}$) and the cytoskeleton with Phalloidin 488 (1:1000) for 10 min. (BLUE = DAPI; GREEN = Phalloidin; RED= Protein). Images were acquired using a Ziess Axio Vert.A1 inverted fluorescence microscope with a X40 magnification.

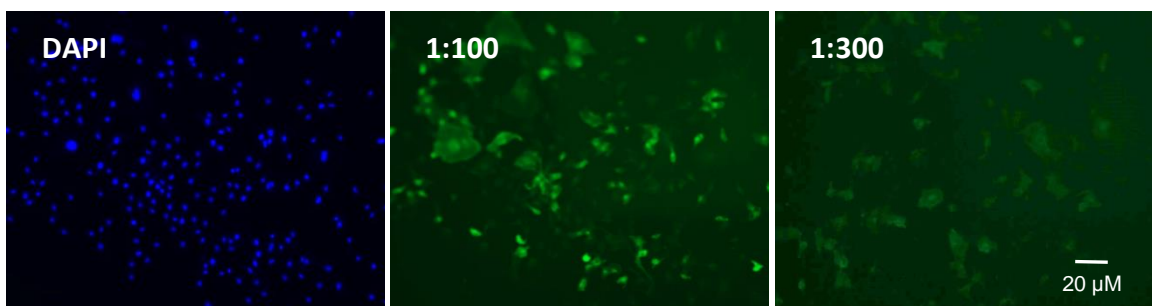
A) TF



B) PTEN



C) MAGI-1



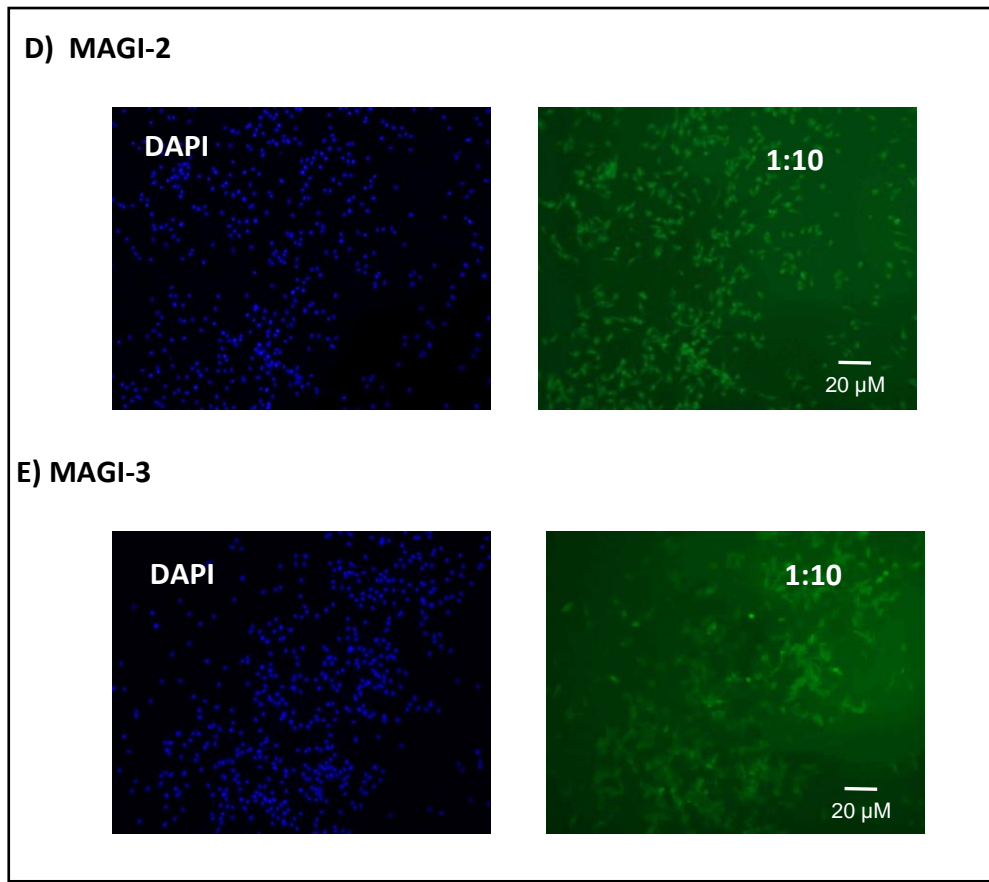


Figure A- 2 Optimisation of the concentration of primary antibodies. MDA-MB-231 (3×10^5) cells were seeded out into 6 well plates and propagated to 80% confluency. The cells were fixed with 4% (v/v) paraformaldehyde for 20 min. The cells were washed with PBS and then permeabilised with 0.1% (v/v) Triton X-100 in PBS, for 10 min. The cells were incubated with different concentrations (1:100- 1:500) of primary antibodies. A) a mouse anti-TF antibody (HTF1), B) a mouse anti-PTEN antibody (217702), C) a rabbit anti-MAGI-1 antibody (H-70), D) a rabbit anti-MAGI-2 antibody (C3) and E) a rabbit anti-MAGI-3 (sc136471) antibody overnight at 4°C. The cells were washed with PBS and then probed with a goat anti-mouse secondary antibody (sc-2008) to detect the presence of TF or PTEN. Another set of cells were incubated with a goat anti-rabbit secondary antibody (sc-2004) to detect the presence of MAGI (1-3) proteins. The nuclei were stained with DAPI (2 μg/ml). (BLUE= DAPI; Green= protein). Images were acquired using a Zeiss Axio Vert.A1 inverted fluorescence microscope with a X10 magnification.

W/O-PDZ1 MAGI-1	-----ATGTCCAAAGTGATCCAGAAGAAGAACC CAGAATTCCACCACACTGGACTAGTGGATCCGATGTCCAAAGTGATCCAGAAGAAGAACC *****	28 180
W/O-PDZ1 MAGI-1	ACTGGACTAGCAGGGTTCACGAATGCACCGTGAAGCGGGACCCCAGGGCGAGCTGGGGG ACTGGACTAGCAGGGTTCACGAATGCACCGTGAAGCGGGACCCCAGGGCGAGCTGGGGG *****	88 240
W/O-PDZ1 MAGI-1	TGACGGTGCTGGGAGGCGCGGAGCACGGGGAGTTCCGTACGTTCGGAGCGGTGGCGGCGG TGACGGTGCTGGGAGGCGCGGAGCACGGGGAGTTCCGTACGTTCGGAGCGGTGGCGGCGG *****	148 300
W/O-PDZ1 MAGI-1	TCGAGGCAGCGGGCTTCCCGCGCGCGGAGGGCCCGAGGCTGGGCGAAGGGGAGCTGC TCGAGGCAGCGGGCTTCCCGCGCGCGGAGGGCCCGAGGCTGGGCGAAGGGGAGCTGC *****	208 360
W/O-PDZ1 MAGI-1	TTCTGGAGGTGCAGGGGTCCGGGTGTCCGGCTTGCCCCGTATGACGTGCTGGGGGTCA TTCTGGAGGTGCAGGGGTCCGGGTGTCCGGCTTGCCCCGTATGACGTGCTGGGGGTCA *****	268 420
W/O-PDZ1 MAGI-1	TCGACAGCTGCAAGGAGGCCGTACCTTCAAGGCCGTAGACAAGGAGGAAGGCTGAACA TCGACAGCTGCAAGGAGGCCGTACCTTCAAGGCCGTAGACAAGGAGGAAGGCTGAACA *****	328 480
W/O-PDZ1 MAGI-1	AGGACCTGCGACATTTTCTCAATCAGCGATTCCAGAAGGGGTCTCCTGATCATGAGCTCC AGGACCTGCGACATTTTCTCAATCAGCGATTCCAGAAGGGGTCTCCTGATCATGAGCTCC *****	388 540
W/O-PDZ1 MAGI-1	AGCAGACCATAAGGGATAACCTTTACCGCCATGCTGTGCCTTGCACAACCCGATCTCCCA AGCAGACCATAAGGGATAACCTTTACCGCCATGCTGTGCCTTGCACAACCCGATCTCCCA *****	448 600
W/O-PDZ1 MAGI-1	GAGAAGGAGAAGTGCCTGGCGTGGACTATAACTTTCTGACTGTGAAGGAGTTCTTGACC GAGAAGGAGAAGTGCCTGGCGTGGACTATAACTTTCTGACTGTGAAGGAGTTCTTGACC *****	508 660
W/O-PDZ1 MAGI-1	TCGAGCAGAGTGGGACTCTTCTGGAAGTCGGCACCTATGAAGGAACTATTATGGGACAC TCGAGCAGAGTGGGACTCTTCTGGAAGTCGGCACCTATGAAGGAACTATTATGGGACAC *****	568 720
W/O-PDZ1 MAGI-1	CCAAGCCTCCTAGCCAGCCAGTCAGTGGGAAAGTGATCACGACGGATGCCTTGCACAGCC CCAAGCCTCCTAGCCAGCCAGTCAGTGGGAAAGTGATCACGACGGATGCCTTGCACAGCC *****	628 780
W/O-PDZ1 MAGI-1	TTCAGTCTGGCTCTAAGCAGTCGACCCGAAGCGAACCAAGTCCTACAATGATATGCAAA TTCAGTCTGGCTCTAAGCAGTCGACCCGAAGCGAACCAAGTCCTACAATGATATGCAAA *****	688 840

W-PDZ1	ATGCTGGCATAGTCCACGGGAGAATGAGGAG	720
MAGI-1	ATGCTGGCATAGTCCACGGGAGAATGAGGAG	720

W-PDZ1	GAGGATGACGTTCTGAAATGAACAGCAGCTTTACAGCCGATTCTGGTGAACAAGAGGAG	780
MAGI-1	GAGGATGACGTTCTGAAATGAACAGCAGCTTTACAGCCGATTCTGGTGAACAAGAGGAG	780

W-PDZ1	CACACTCTCCAAGAAACAGCATTACCACCTGTGAATAGTAGCATCATCGCTGCTCCCATC	840
MAGI-1	CACACTCTCCAAGAAACAGCATTACCACCTGTGAATAGTAGCATCATCGCTGCTCCCATC	840

W-PDZ1	ACGGACCCCTTCTCAGAAGTTCCCTCAATACCTACCTCTTTCTGCAGAGGATAATTTAGGT	900
MAGI-1	ACGGACCCCTTCTCAGAAGTTCCCTCAATACCTACCTCTTTCTGCAGAGGATAATTTAGGT	900

W-PDZ1	CCTCTACCTGAAAACCTGGGAGATGGCCTATACTGAAAATGGAGAAGTCTATTTTATAGAC	960
MAGI-1	CCTCTACCTGAAAACCTGGGAGATGGCCTATACTGAAAATGGAGAAGTCTATTTTATAGAC	960

W-PDZ1	CATAACACGAAAACAACATCTTGGTTAGACCCTCGGTGCCTAAACAAGCAGCAGAAGCCA	1020
MAGI-1	CATAACACGAAAACAACATCTTGGTTAGACCCTCGGTGCCTAAACAAGCAGCAGAAGCCA	1020

W-PDZ1	CTGGAAGAGTGTGAAGATGATGAAGGGGTACACACCGAGGAGCTGGACAGTGAAGTAGAA	1080
MAGI-1	CTGGAAGAGTGTGAAGATGATGAAGGGGTACACACCGAGGAGCTGGACAGTGAAGTAGAA	1080

W-PDZ1	CTGCCTGCTGGTTGGGAAAAGATTGAAGACCCTGTCTATGGTATCTACTATGTAGACCAC	1140
MAGI-1	CTGCCTGCTGGTTGGGAAAAGATTGAAGACCCTGTCTATGGTATCTACTATGTAGACCAC	1140

W-PDZ1	ATCAACAGGAAGACACAATATGAGAACCCGGTTCTAGAAGCCAAACGGAAGAAGCAGCTT	1200
MAGI-1	ATCAACAGGAAGACACAATATGAGAACCCGGTTCTAGAAGCCAAACGGAAGAAGCAGCTT	1200

W-PDZ1	GAGCAGCAGCAGCAGCAGCAACAGCAGCAGCAACAGCAGCAGCAGCAGCAGCAGCAGCAG	1260
MAGI-1	GAGCAGCAGCAGCAGCAGCAGCAACAGCAGCAGCAACAGCAGCAGCAGCAGCAGCAGCAGCAG	1260

W-PDZ1	CAGACAGAAGAATGGACAGAAGATCACTCAGCCCTTGTGCCTCCTGTTATTCCAACCAC	1320
MAGI-1	CAGACAGAAGAATGGACAGAAGATCACTCAGCCCTTGTGCCTCCTGTTATTCCAACCAC	1320

W-PDZ1	CCTCCAAGCAATCCAGAGCCAGCCAGAGAAGTTCCACTTCAGGGCAAACCCTTTTTTACA	1380
MAGI-1	CCTCCAAGCAATCCAGAGCCAGCCAGAGAAGTTCCACTTCAGGGCAAACCCTTTTTTACA	1380

W-PDZ1	CGAAACCCTTCTGAGTTGAAAGGCAAGTTCATTACACAAAAGCTGCGGAAAAGCAGTCGT	1440
MAGI-1	CGAAACCCTTCTGAGTTGAAAGGCAAGTTCATTACACAAAAGCTGCGGAAAAGCAGTCGT	1440

Chapter 7

References

References

- Åberg, M. Johnell, M. Wickström, M. and Siegbahn, A. (2011) Tissue Factor/ FVIIa prevents the extrinsic pathway of apoptosis by regulation of the tumor suppressor Death-Associated Protein Kinase 1 (DAPK1). *Thrombosis Research* 127 (2), 141-8.
- Åberg, M. and Siegbahn, A. (2013) Tissue factor non-coagulant signaling - molecular mechanisms and biological consequences with a focus on cell migration and apoptosis. *Journal of Thrombosis and Haemostasis* 11 (5), 817-25.
- Adamsky, K, Arnold, K. Sabanay, H. and Peles, E. (2003) Junctional protein MAGI-3 interacts with receptor tyrosine phosphatase beta (RPTP beta) and tyrosine-phosphorylated proteins. *Journal of Cell Science* 116(7), 1279-89.
- Adey, N.B. Huang, L. Ormonde, P.A. Baumgard, M.L. Pero, R. Byreddy, D.V. Tavigian, S.V. and Bartel, P.L. (2000) Threonine phosphorylation of the MMAC1/PTEN PDZ binding domain both inhibits and stimulates PDZ binding. *Cancer Research* 60(1), 35-37.
- Ahamed, J. and Ruf W. (2004) Protease-activated receptor 2-dependent phosphorylation of the tissue factor cytoplasmic domain. *Journal of Biological Chemistry* 279 (22), 23038-23044.
- Ahmed, D. Eide, P. W. Eilertsen, I. A. Danielsen, S. A. Eknæs, M. Hektoen, M. Lind, G. E. and Lothe, R. A (2013). Epigenetic and genetic features of 24 colon cancer cell lines. *Oncogenesis* 2(9), e71.
- Akinleye, A. Avvaru, P. Furqan, M. Song, Y. and Liu, D. (2013) Phosphatidylinositol 3-kinase (PI3K) inhibitors as cancer therapeutics. *Journal of Hematology and Oncology* 6: 88.
- Albrektsen, T. Sørensen, B.B. Hjortø, G.M. Fleckner, J. Rao, L.V. and Petersen, L.C. (2007) Transcriptional program induced by factor VIIa-tissue factor, PAR1 and PAR2 in MDA-MB-231 cells. *Journal of Thrombosis and Haemostasis* 5(8), 1588-97.
- Alday-Parejo, B. Richard, F. Wörthmüller, J. Rau, T. Galván, J. A. Desmedt, C. Santamaria-Martinez, A. and Rüegg, C. (2020). MAGI1, a New Potential Tumor Suppressor Gene in Estrogen Receptor Positive Breast Cancer. *Cancers* 12(1), 223.
- Alfieri, R. Giovannetti, E. Bonelli, M. and Cavazzoni, A. (2017) New Treatment Opportunities in Phosphatase and Tensin Homolog (PTEN)-Deficient Tumors: Focus on PTEN/Focal Adhesion Kinase Pathway. *Frontiers in Oncology* 7:170.
- Andres-Pons, A. Rodriguez-Escudero, I. Gil, A. Blanco, A. Vega, A. Molina, M. Pulido, R. and Cid, V.J. (2007) In vivo functional analysis of the counterbalance of hyperactive phosphatidylinositol 3-kinase p110 catalytic oncoproteins by the tumor suppressor PTEN. *Cancer Research* 67, 9731-9739.

- Ansari, S.A. Pendurthi, U.R. and Rao, L.V.M. (2019) Role of Cell Surface Lipids and Thiol-Disulphide Exchange Pathways in Regulating the Encryption and Decryption of Tissue Factor. *Thrombosis and Haemostasis* 119(6), 860-870.
- Arderiu, G. Peña, E. Aledo, R. and Badimon, L. (2012) Tissue factor-Akt signaling triggers microvessel formation. *Journal of Thrombosis and Haemostasis* 10 (9), 1895-905.
- Arora, P. Ricks, T.K. and Trejo, J. (2007) Protease-activated receptor signalling, endocytic sorting and dysregulation in cancer. *Journal of Cell Science* 120, 921-928.
- Auger, K.R. Serunian, L.A. Soltoff, S.P. Libby, P. and Cantley, L.C. (1989) PDGF-dependent tyrosine phosphorylation stimulates production of novel polyphosphoinositides in intact cells. *Cell* 57, 167-175.
- Awasthi, V. Mandal, S. Papanna, V. Rao, L. and Pendurthi, U. (2007) Modulation of Tissue Factor-Factor VIIa Signaling by Lipid Rafts and Caveolae. *Blood* 108(11), 1744-1744.
- Bach, R.R. (2006) Tissue factor encryption. *Arteriosclerosis, Thrombosis, and Vascular Biology* 26(3), 456-61.
- Bajetto, A. Barbero, S. Bonavia, R. Piccioli, P. Pirani, P. Florio, T. and Schettini, G. (2001) Stromal cell-derived factor-1 α induces astrocyte proliferation through the activation of extracellular signal-regulated kinases 1/2 pathway. *Journal of Neurochemistry* 77, 1226-1236.
- Balla, T. (2013) Phosphoinositides: tiny lipids with giant impact on cell regulation. *Physiological Reviews* 93 (3), 1019-137.
- Barber, A. G. Castillo-Martin, M. Bonal, D. M. Jia, A. J. Rybicki, B. A. Christiano, A. M. and Cordon-Cardo, C. (2015) PI3K/AKT pathway regulates E-cadherin and Desmoglein 2 in aggressive prostate cancer. *Cancer medicine* 4(8), 1258-1271.
- Baumgartner, M. Radziwill, G. Lorger, M. Weiss, A. and Moelling, K. (2008) c-Src-mediated epithelial cell migration and invasion regulated by PDZ binding site. *Molecular Cell Biology* 28, 642-655.
- Behrens, J. Vakaet, L. Friis, R. Winterhager, E. Van Roy, F. Mareel, M. M. and Birchmeier, W. (1993) Loss of epithelial differentiation and gain of invasiveness correlates with tyrosine phosphorylation of the E-cadherin/beta-catenin complex in cells transformed with a temperature-sensitive v-SRC gene. *The Journal of cell biology* 120 (3), 757-66.
- Bendapudi, P. Deceunynck, K. Koseoglu, S. Bekendam, R. Mason, S. Kenniston, J. and Flaumenhaft R. (2016) Stimulated platelets but not endothelium generate thrombin via a factor XIIa-dependent mechanism requiring phosphatidylserine exposure. *Blood* 128, 258.
- Bermúdez Brito, M. Goulielmaki, E. and Papakonstanti, E. A. (2015) Focus on PTEN Regulation. *Frontiers in oncology* 5, 166.
- Bhat, A.A. Uppada, S. Achkar, I.W. Hashem, S. Yadav, S.K. Shanmugakonar, M. Al-Naemi, H.A. Haris, M. and Uddin, S (2019). Tight Junction Proteins and Signaling Pathways in Cancer and Inflammation: A Functional Crosstalk. *Frontiers in Physiology* 23,9-1942.

- Blackadar, C. B. (2016) Historical review of the causes of cancer. *World Journal of Clinical Oncology* 7 (1), 54-86.
- Blancher, C. and Jones, A. (2001) SDS -PAGE and Western Blotting Techniques. *Methods in Molecular Medicine* 57,145-62.
- Bluff, J. E. Brown, N. J. Reed, M. W. and Staton, C. A. (2008) Tissue factor, angiogenesis and tumour progression. *Breast Cancer Research* :10(2), 204.
- Bogdanov, V. Y. and Versteeg, H. H. (2015) "Soluble Tissue Factor" in the 21st Century: Definitions, Biochemistry, and Pathophysiological Role in Thrombus Formation. *Seminars in thrombosis and hemostasis* 41(7), 700-707.
- Bononi, A. and Pinton, P. (2015) Study of PTEN subcellular localization. *Methods* 77-78:92-103.
- Breitenstein, A. Camici, G.G. and Tanner, F.C. (2009) Tissue factor: beyond coagulation in the cardiovascular system. *Clinical Science* 118 (3), 159-72.
- Brennan, K. Offiah, G. McSherry, E. A. and Hopkins, A. M. (2010) Tight junctions: a barrier to the initiation and progression of breast cancer?. *Journal of biomedicine & biotechnology* 2010, 460607.
- Brenner, W. Färber, G. Herget, T. Lehr, H.A. Hengstler, J.G. and Thüroff, J.W. (2002) Loss of tumor suppressor protein PTEN during renal carcinogenesis. *International Journal of Cancer* 99(1), 53-57.
- Bresnick, A.R. and Backer, J.M. (2019) PI3K β -A Versatile Transducer for GPCR, RTK, and Small GTPase Signaling. *Endocrinology* 160(3), 536-555.
- Brock, C. Schaefer, M. Reusch, H.P. Czupalla, C. Michalke, M. Spicher, K. Schultz, G. and Nürnberg, B. (2003) Roles of G beta gamma in membrane recruitment and activation of p110 gamma/p101 phosphoinositide 3-kinase gamma. *Journal of Cell Biology* 160(1), 89-99.
- Bromberg, M. E., Konigsberg, W. H., Madison, J. F., Pawashe, A. and Garen, A. (1995) Tissue factor promotes melanoma metastasis by a pathway independent of blood coagulation. *Proceedings of the National Academy of Sciences of the United States of America*, 92(18), 8205-8209.
- Butenas, S. (2012) Tissue Factor Structure and Function. *Scientifica* 964862.
- Butenas, S. Amblo-Krudysz, J. and Mann, K. G. (2012) Posttranslational modifications of tissue factor. *Frontiers in bioscience (Elite edition)* 4, 381-391.
- Butenas, S. Bouchard, B.A. Brummel-Ziedins, K.E. Parhami-Seren, B. and Mann, K.G. (2005) Tissue factor activity in whole blood. *Blood* 105(7), 2764-70.
- Butenas, S. Orfeo, T. and Mann, K. G. (2009) Tissue factor in coagulation: Which? Where? When?. *Arteriosclerosis, thrombosis, and vascular biology* 29(12), 1989-1996.
- Byun, D. S. Ahmed, N. Nasser, S. Shin, J. Al-Obaidi, S. Goel, S. Corner, G. A. Wilson, A. J. Flanagan, D. J. Williams, D. S. Augenlicht, L. H. Vincan, E. and Mariadason, J. M. (2011)

Intestinal epithelial-specific PTEN inactivation results in tumor formation. *American journal of physiology Gastrointestinal and liver physiology* 301(5), G856-G864.

Camerer, E. Huang, W. and Coughlin, S.R. (2000) Tissue factor- and factor X-dependent activation of protease-activated receptor 2 by factor VIIa. *Proceedings of the National Academy of Sciences of the United States of America* 97(10), 5255-60.

Camerer, E. Pringle, S. Skartlien, A.H. Wiiger, M. Prydz, K. Kolstø, A.B. and Prydz, H. (1996) Opposite sorting of tissue factor in human umbilical vein endothelial cells and Madin-Darby canine kidney epithelial cells. *Blood* 88(4), 1339-49.

Cao, L. Graue-Hernandez, E. O. Tran, V. Reid, B. Pu, J. Mannis, M. J. and Zhao, M. (2011) Downregulation of PTEN at corneal wound sites accelerates wound healing through increased cell migration. *Investigative ophthalmology & visual science* 52(5), 2272-2278.

Carmeliet, P., Mackman, N., Moons, L., Luther, T., Gressens, P., Van Vlaenderen, L., Demunck, H., Kasper, M., Breier, G., Evrard, P., Müller, M. Risau, W. Edgington, T. and Collen, D. (1996) Role of tissue factor in embryonic blood vessel development. *Nature* 383(6595), 73-5.

Carracedo, A. Alimonti, A. and Pandolfi, P.P. (2011) PTEN level in tumor suppression: how much is too little? *Cancer Research* 71(3), 629-33.

Castellano, E. and Downward, J. (2011) RAS Interaction with PI3K: More Than Just Another Effector Pathway. *Genes & Cancer* 2(3), 261-274.

Castilho, R. M. Squarize, C. H. and Gutkind, J. S. (2013) Exploiting PI3K/mTOR signaling to accelerate epithelial wound healing. *Oral diseases* 19(6), 551-558.

Chalhoub, N. and Baker, S. J. (2009) PTEN and the PI3-Kinase Pathway in Cancer. *Annual Review of Pathology*, 4, 127-150.

Chen, V.M. Ahamed, J. Versteeg, H.H. Berndt, M.C. Ruf, W. and Hogg, P.J.(2006) Evidence for activation of tissue factor by an allosteric disulfide bond. *Biochemistry* 45(39), 12020-8.

Chen, V.M. and Hogg, P.J. (2013) Encryption and decryption of tissue factor. *Journal of Thrombosis and Haemostasis* 11(1), 277-84.

Chen, Z. Dempsey, D. R. Thomas, S. N. Hayward, D. Bolduc, D. M. and Cole, P. A. (2016) Molecular Features of Phosphatase and Tensin Homolog (PTEN) Regulation by C-terminal Phosphorylation. *The Journal of biological chemistry* 291(27), 14160-14169.

Chin, A. C. Vergnolle, N. MacNaughton, W. K. Wallace, J. L. Hollenberg, M. D. and Buret, A. G. (2003) Proteinase-activated receptor 1 activation induces epithelial apoptosis and increases intestinal permeability. *Proceedings of the National Academy of Sciences of the United States of America* 100(19), 11104-11109.

Chin, Y. R. Yuan, X. Balk, S. P. and Toker, A. (2014) PTEN-deficient tumors depend on AKT2 for maintenance and survival. *Cancer discovery* 4(8), 942-955.

- Cho, K.O. Hunt, C.A. and Kennedy M.B. (1992) "The rat brain postsynaptic density fraction contains a homolog of the Drosophila discs-large tumor suppressor protein". *Neuron*. 9 (5), 929-42.
- Choi, A. H. O'Leary, M. P. Lu, J. Kim, S. I. Fong, Y and Chen, N. G. (2018) Endogenous Akt Activity Promotes Virus Entry and Predicts Efficacy of Novel Chimeric Orthopoxvirus in Triple-Negative Breast Cancer. *Molecular therapy oncolytics* 9, 22-29.
- Christensen, N. R. Čalyševa, J. Fernandes, E. F. Lüchow, S. Clemmensen, L. S. Haugaard-Kedström, L. M. and Strømgaard, K. (2019) PDZ Domains as Drug Targets. *Advanced Therapeutics* 2(7), 1800143.
- Chu, A.J. (2011) Tissue Factor, Blood Coagulation, and Beyond: An Overview. *International Journal of Inflammation* 367284.
- Chung, H.J. Huang, Y.H, Lau, L.F, Haganir, R.L. (2004) Regulation of the NMDA receptor complex and trafficking by activity-dependent phosphorylation of the NR2B subunit PDZ ligand". *The Journal of Neuroscience* 24 (45), 10248-10259.
- Cimmino, G. and Cirillo, P (2018). Tissue factor: newer concepts in thrombosis and its role beyond thrombosis and hemostasis. *Cardiovascular Diagnosis and Therapy* (5), 581-593.
- Ciuffreda, L. Del Curatolo, A. Falcone, I. Conciatori, F. Bazzichetto, C. Cognetti, F. Corbo, V. Scarpa, A. and Milella, M. (2017) Lack of growth inhibitory synergism with combined MAPK/PI3K inhibition in preclinical models of pancreatic cancer. *Annals of Oncology* 28(11), 2896-2898.
- Clausson, C. M. Arngården, L. Ishaq, O. Klaesson, A. Kühnemund, M. Grannas, K. Koos, B. Qian, X. Ranefall, P. Krzywkowski, T. Brismar, H. Nilsson, M. Wählby, C. and Söderberg, O. (2015) Compaction of rolling circle amplification products increases signal integrity and signal-to-noise ratio. *Scientific reports* 5, 12317.
- Collier, M.E. and Ettelaie C. (2011) Regulation of the incorporation of tissue factor into microparticles by serine phosphorylation of the cytoplasmic domain of tissue factor. *Journal of Biological Chemistry* 286(14), 11977-84.
- Collier, M.E. Ettelaie, C., Gault, B.T. Maraveyas, A. and Goodall, A.H. (2017) Investigation of the Filamin A-Dependent Mechanisms of Tissue Factor Incorporation into Microvesicles. *Thrombosis and Haemostasis* 117(11), 2034-2044.
- Collier, M.E. Maraveyas, A. and Ettelaie, C. (2014) Filamin-A is required for the incorporation of tissue factor into cell-derived microvesicles. *Thrombosis and Haemostasis* 111(4), 647-655.
- Coughlin, S.R. (1999) How the protease thrombin talks to cells. *Proceedings of the National Academy of Sciences of the United States of America* 96(20), 11023-7.
- Coughlin, S.R. (2005) Protease-activated receptors in hemostasis, thrombosis and vascular biology. *Journal of Thrombosis and Haemostasis* 3(8), 1800-14.
- Cully, M. You, H. Levine, A.J. and Mak, T.W. (2006) Beyond PTEN mutations: the PI3K pathway as an integrator of multiple inputs during tumorigenesis. *Nature Reviews Cancer* 6, 184-192.

- Cunliffe, H. E. Jiang, Y. Fornace, K. M. Yang, F. and Meltzer, P. S. (2012) PAR6B is required for tight junction formation and activated PKC ζ localization in breast cancer. *American journal of cancer research* 2(5), 478-491.
- Cunningham, M. A., Romas, P., Hutchinson, P., Holdsworth, S. R. & Tipping, P. G. (1999) Tissue factor and factor VIIa receptor/ligand interactions induce proinflammatory effects in macrophages. *Blood* 94(10), 3413-20.
- Dai, J.L. Wang, L. Sahin, A.A. Broemeling, L.D. Schutte, M. and Pan, Y. (2004) NHERF (Na⁺/H⁺ exchanger regulatory factor) gene mutations in human breast cancer. *Oncogene* 23(53), 8681-7.
- Dammacco, F. Vacca, A. Procaccio, P. Ria, R. Marech, I. and Racanelli, V. (2013) Cancer-related coagulopathy (Trousseau's syndrome): review of the literature and experience of a single center of internal medicine. *International Journal of Clinical and Experimental Medicine* 13(2), 85-97.
- Das, S. Dixon, J. E. and Cho, W. (2003) Membrane-binding and activation mechanism of PTEN. *Proceedings of the National Academy of Sciences of the United States of America*, 10(13): 7491–7496.
- D'Asti, E. Anderson, G.M. and Rak, J. (2017) Inhibition of tissue factor signaling in breast tumour xenografts induces widespread changes in the microRNA expression profile. *Biochemical and Biophysical Research Communications* 494(3-4), 700-705.
- Debaize, L. Jakobczyk, H. Rio, A. G. Gandemer, V. and Troadec, M. B. (2017) Optimization of proximity ligation assay (PLA) for detection of protein interactions and fusion proteins in non-adherent cells: application to pre-B lymphocytes. *Molecular cytogenetics* 10, 27.
- Del Conde, I. Shrimpton, C. Thiagarajan, P. and López, J. (2005) Tissue-factor-bearing microvesicles arise from lipid rafts and fuse with activated platelets to initiate coagulation. *Blood* 106(5), 1604-1611.
- Dempsey, D. R. and Cole, P. A. (2018) Protein Chemical Approaches to Understanding PTEN Lipid Phosphatase Regulation. *Methods in enzymology* 607, 405-422.
- Di, Y. and Chen, X. L. (2018) Inhibition of LY294002 in retinal neovascularization via down-regulation the PI3K/AKT-VEGF pathway in vivo and in vitro. *International journal of ophthalmology* 11(8), 1284-1289.
- Diaz, R. Nguewa, P. A. Diaz-Gonzalez, J. A. Hamel, E. Gonzalez-Moreno, O. Catena, R. Serrano, D. Redrado, M. Sherris, D. and Calvo, A. (2009) The novel Akt inhibitor Palomid 529 (P529) enhances the effect of radiotherapy in prostate cancer. *British journal of cancer* 100(6), 932-940.
- Dietzen, D.J. Page, K.L. and Tetzloff, T.A. (2004) Lipid rafts are necessary for tonic inhibition of cellular tissue factor procoagulant activity. *Blood* 103(8), 3038-44.
- Dobrosotskaya, I. Y. Guy, R.K. and James, G.L. (1997) MAGI-1, a membrane-associated guanylate kinase with a unique arrangement of protein-protein interaction domains. *Journal of Biological Chemistry* 272: 31589-31597.

- Dobrosotskaya, I.Y. and James, G.L. (2000) MAGI-1 interacts with beta-catenin and is associated with cell-cell adhesion structures. *Biochemical and Biophysical Research Communications* 270(3), 903-9.
- Dorfleutner, A and Ruf, W. (2003) Regulation of tissue factor cytoplasmic domain phosphorylation by palmitoylation. *Blood* 102(12), 3998-4005.
- Drake, T.A. Morrissey, J.H. and Edgington, T.S. (1989) Selective cellular expression of tissue factor in human tissues. Implications for disorders of hemostasis and thrombosis. *The American Journal of Pathology* 134(5), 1087-97.
- Duning, K. Schurek, E.M. Schlüter, M. Bayer, M. Reinhardt, H.C. Schwab, A. Schaefer, L. Benzing, T. Schermer, B. Saleem, M.A. Huber, T.B. Bachmann, S. Kremerskothen, J. Weide, T. and Pavenstädt, H. (2008) KIBRA modulates directional migration of podocytes. *Journal of the American Society of Nephrology* 19(10), 1891-903.
- Dunn, S. Lombardi, O. Lukoszek, R. and Cowling, V. H. (2019) Oncogenic PIK3CA mutations increase dependency on the mRNA cap methyltransferase, RNMT, in breast cancer cells. *Open biology* 9(4), 190052.
- Dutra-Oliveira, A. Monteiro, R.Q. and Mariano-Oliveira, A. (2012) Protease-activated receptor-2 (PAR2) mediates VEGF production through the ERK1/2 pathway in human glioblastoma cell lines. *Biochemical and Biophysical Research Communications* 421(2), 221-7.
- Egorina, E.M. Sovershaev, M.A. and Osterud, B. (2008) Regulation of tissue factor procoagulant activity by post-translational modifications. *Thrombosis Research* 122(6), 831-7.
- Eisenreich, A. Bolbrinker, J. and Leppert, U. (2016) Tissue Factor: A Conventional or Alternative Target in Cancer Therapy. *Clinical Chemistry* 62(4), 563-70.
- Elewa, H. Elrefai, R. and Barnes, G.D. (2016) Cancer-Associated Venous Thromboembolism. *Current Treatment Options in Cardiovascular Medicine* 18(4), 23.
- ElKeeb, A. M., Collier, M. E., Maraveyas, A. and Ettelaie, C. (2015) Accumulation of tissue factor in endothelial cells induces cell apoptosis, mediated through p38 and p53 activation. *Thrombosis and Haemostasis* 114(2), 364-78.
- Ender, F. Freund, A. Quecke, T. Steidel, C. Zamzow, P. von Bubnoff, N. and Gieseler, F. (2020) Tissue factor activity on microvesicles from cancer patients. *Journal of cancer research and clinical oncology* 146(2), 467-475.
- Enjoji, S. Ohama, T. And Sato, K. (2014) Regulation of epithelial cell tight junctions by protease-activated receptor 2. *The Journal of veterinary medical science* 76(9), 1225-1229.
- Ethaeab, A.M. Mohammad, M.A. Madkhali, Y. Featherby, S. Maraveyas, A. Greenman, J. and Ettelaie, C. (2020) Accumulation of tissue factor in endothelial cells promotes cellular apoptosis through over-activation of Src1 and involves β 1-integrin signalling. *Apoptosis : an international journal on programmed cell death* 25(1-2), 29-41.

- Ettelaie, C. Collier, M. E. Featherby, S. Benelhaj, N. E. Greenman, J. and Maraveyas, A. (2016) Analysis of the potential of cancer cell lines to release tissue factor-containing microvesicles: correlation with tissue factor and PAR2 expression. *Thrombosis Journal*, 14, 2.
- Ettelaie, C. Collier, M.E. Featherby, S. Greenman, J. and Maraveyas, A. (2016) Oligoubiquitination of tissue factor on Lys255 promotes Ser253-dephosphorylation and terminates TF release. *Biochimica et Biophysica Acta* 1863(11), 2846-2857.
- Ettelaie, C. Collier, M.E.W. Featherby, S. Greenman, J. and Maraveyas, A. (2018) Peptidyl-prolyl isomerase 1 (Pin1) preserves the phosphorylation state of tissue factor and prolongs its release within microvesicles. *Biochimica et Biophysica Acta* 1865(1), 12-24.
- Ettelaie, C. Elkeeb, A.M. Maraveyas, A. and Collier, M.E. (2013) p38 α phosphorylates serine 258 within the cytoplasmic domain of tissue factor and prevents its incorporation into cell-derived microparticles. *Biochim Biophys Acta* 1833(3), 613-21.
- Ettelaie, C. Li, C. Collier, M.E. Pradier, A. Frentzou, G.A. Wood, C.G. Chetter, I.C. McCollum, P.T. Bruckdorfer, K.R. and James, N.J. (2007) Differential functions of tissue factor in the trans-activation of cellular signalling pathways. *Atherosclerosis* 194(1), 88-101.
- Facciuto, F. Cavatorta, A.L. Valdano, M.B. Marziali, F. and Gardiol, D. (2012) Differential expression of PDZ domain-containing proteins in human diseases - challenging topics and novel issues. *The FEBS Journal* 279(19), 3538-3548.
- Falanga, A. Russo, L. Milesi, V. and Vignoli, A. (2017) Mechanisms and risk factors of thrombosis in cancer. *Critical Reviews in Oncology / Hematology* 118: 79-83.
- Falkenburger, B. H. Jensen, J. B. Dickson, E. J. Suh, B. C. And Hille, B. (2010) Phosphoinositides: lipid regulators of membrane proteins. *The Journal of physiology* 588(17), 3179-3185.
- Fan, L., Yotov, W. V., Zhu, T., Esmailzadeh, L., Joyal, J. S., Sennlaub, F. Heveker, N. Chemtob, S. and Rivard, G. E. (2005) Tissue factor enhances protease-activated receptor-2-mediated factor VIIa cell proliferative properties. *Journal of Thrombosis and Haemostasis* 3(5), 1056-1063.
- Fang, J. Gu, L. Zhu, N. Tang, H. Alvarado, C.S. and Zhou, M. (2008) Tissue factor/FVIIa activates Bcl-2 and prevents doxorubicin-induced apoptosis in neuroblastoma cells. *BMC Cancer* 8, 69.
- Fang, J. Tang, H. Xia, L.H. Wei, W.N. Hu, Y. and Song, S.J. (2007) Regulation of tissue factor expression by anti-oncogene PTEN in human neuroblastoma cell line. *Zhonghua Xue Ye Xue Za Zhi* 28 (6), 363-6.
- Feilotter, H.E. Coulon, V. McVeigh, J.L. Boag, A.H. Dorion-Bonnet, F. Duboué, B. Latham, W.C. Eng, C. Mulligan, L.M. and Longy, M. (1999) Analysis of the 10q23 chromosomal region and the PTEN gene in human sporadic breast carcinoma. *British Journal of Cancer* 79 (5-6), 718-23.

- Feng, W. Wu, H. Chan, L.N. and Zhang, M. (2008) Par-3-mediated junctional localization of the lipid phosphatase PTEN is required for cell polarity establishment. *Journal of Biological Chemistry* 283, 23440-23449.
- Feng, X. Jia, S. Martin, T.A. and Jiang, W.G. (2014) Regulation and involvement in cancer and pathological conditions of MAGI1, a tight junction protein. *Anticancer Research* 34(7), 3251-6.
- Feoktistova, M. Geserick, P. and Leverkus, M. (2016) Crystal Violet Assay for Determining Viability of Cultured Cells. *Cold Spring Harb Protocol* 2016 (4).
- Flynn, A.N. and Buret, A.G. (2004) Proteinase-activated receptor 1 (PAR-1) and cell apoptosis. *Apoptosis* 9(6), 729-37.
- Fornai, M. Colucci, R. Pellegrini, C. Benvenuti, L. Natale, G. Ryskalin, L. Blandizzi, L and Antonioli, L. (2020) Role of proteinase-activated receptors 1 and 2 in nonsteroidal anti-inflammatory drug enteropathy. *Pharmacological Reports* 72(5), 1347-1357.
- Fresno Vara, J.A. Casado, E. de Castro, J. Cejas, P. Belda-Iniesta, C. and González-Barón, M. (2004) PI3K/Akt signalling pathway and cancer. *Cancer Treatment Reviews* 30(2), 193-204.
- Furie, B. and Furie, B. C. (2006) Cancer-associated thrombosis. *Blood Cells, Molecules, and Diseases* 36 (2), 177-181.
- Gao, Y.L. Liu, C.S. Zhao, R. Wang, L.L. Li, S.S. Liu, M. Zhang, M. Jiang, S.K. Tian, Z.L. Wang, M. (2016) Effects of PI3K/Akt Pathway in Wound Healing Process of Mice Skin. *Fa Yi Xue Za Zhi* 32, 7-12.
- Garnier, D. Magnus, N. Lee, T.H. Bentley, V. Meehan, B. Milsom, C. Montermini, L. Kislinger, T. and Rak, J. (2012) Cancer cells induced to express mesenchymal phenotype release exosome-like extracellular vesicles carrying tissue factor. *Journal of Biological Chemistry* 287(52), 43565-72.
- Garnier, D. Milsom, C. Magnus, N. Meehan, B. Weitz, J. Yu, J. and Rak, J. (2010) Role of the tissue factor pathway in the biology of tumor initiating cells. *Thrombosis Research* 125(2), S44-50.
- Geddings, J. E. Hisada, Y. Boulaftali, Y. Getz, T. M. Whelihan, M. Fuentes, R. Dee, R. Cooley, B.C. Key, N.S. Wolberg, A.S. Bergmeier, W. and Mackman, N. (2016). Tissue Factor-positive Tumor Microvesicles Activate Platelets and Enhance Thrombosis in Mice. *Journal of Thrombosis and Haemostasis* 14(1), 153-166.
- Geddings, J. E. and Mackman, N. (2013) Tumor-derived tissue factor-positive microparticles and venous thrombosis in cancer patients. *Blood* 122(11), 1873–1880.
- Genera, M. Samson, D. Raynal, B. Haouz, A. Baron, B. Simenel, C. Guerois, R. Wolff, N. and Caillet-Saguy, C. (2019) Structural and functional characterization of the PDZ domain of the human phosphatase PTPN3 and its interaction with the human papillomavirus E6 oncoprotein. *Scientific Reports* 9(1), 7438.

- Georgescu, M.M. (2010) PTEN Tumor Suppressor Network in PI3K-Akt Pathway Control. *Genes & Cancer*, 1(12): 1170-1177.
- Georgescu, M.M. Kirsch, K.H. Akagi, T. Shishido, T. and Hanafusa, H. (1999) The tumor-suppressor activity of PTEN is regulated by its carboxyl-terminal region. *Proceedings of the National Academy of Sciences of the United States of America* 96(18),10182-7.
- Gessler, F. Voss, V. Dutzmann, S. Seifert, V. Gerlach, R. And Kogel, D. (2010) Inhibition of tissue factor/protease-activated receptor-2 signaling limits proliferation, migration and invasion of malignant glioma cells. *Neuroscience*, 165(4), 1312-22.
- Gil, A. Rodriguez-Escudero, I. Stumpf, M. Molina, M. Cid, V.J. and Pulido, R. (2015) A functional dissection of PTEN N-terminus: implications in PTEN subcellular targeting and tumor suppressor activity. *PLoS One* 10 (4), e0119287.
- Goel, H.L. Alam, N. Johnson, I.N. and Languino, L.R. (2009) Integrin signaling aberrations in prostate cancer. *American Journal of Translational Research* 1(3), 211-20.
- Goldsmith, Z. and Dhanasekaran, D. (2007) G Protein regulation of MAPK networks. *Oncogene* 26, 3122-3142.
- Goldstein, J. Borowsky, A.D. Goyal, R. Roland, J.T. Arnold, S.A. Gellert, L.L. Clark, P.E. Hameed, O. Giannico, G.A. (2016) MAGI-2 in prostate cancer: an immunohistochemical study. *Human Pathology* 52, 83-91.
- González-Mariscal, L. Betanzos, A. and Avila-Flores, A. (2000) MAGUK proteins: structure and role in the tight junction. *Seminars in Cell & Developmental Biology* 11(4), 315-24.
- Gonzalez-Perez, A. Perez-Llamas, C. Deu-Pons, J. Tamborero, D. Schroeder, M.P. Jene-Sanz, A. Santos, A. and Lopez-Bigas, N. (2013) IntOGen-mutations identifies cancer drivers across tumor types. *Nature methods* 10(11), 1081-2.
- Gregorc U. Ivanova, S. Thomas, M. Guccione, E. Glaunsinger, B. Javier, R. Turk, V. Banks, L. and Turk, B. (2012) Cleavage of MAGI-1, a tight junction PDZ protein, by caspases is an important step for cell-cell detachment in apoptosis. *Apoptosis* 12(2), 343-54.
- Grover, S.P. and Mackman, N. (2018) Tissue Factor: An Essential Mediator of Hemostasis and Trigger of Thrombosis. *Arteriosclerosis, Thrombosis, and Vascular Biology* 38(4), 709-725.
- Grover, S.P. and Mackman, N. (2019) Intrinsic Pathway of Coagulation and Thrombosis. *Arteriosclerosis, Thrombosis, and Vascular Biology* 39(3), 331-338.
- Gu, T. Zhang, Z. Wang, J. Guo, J. Shen W. H. and Yin, Y. (2011) CREB Is a Novel Nuclear Target of PTEN Phosphatase. *Cancer Research* 71(8), 2821-2825.
- Guo, S. T. Chi, M. N. Yang, R. H. Guo, X. Y. Zan, L. K. Wang, C. Y. Xi, Y. F. Jin, L., Croft, A. Tseng, H. Y., Yan, X. G. Farrelly, M. Wang, F. H. Lai, F. Wang, J. F. Li, Y. P. Ackland, S. Scott, R. Agoulnik, I. U. and Hondermarck, H. (2016). INPP4B is an oncogenic regulator in human colon cancer. *Oncogene* 35(23), 3049-3061.
- Hamada, K. Kuratsu, J. Saitoh, Y. Takeshima, H. Nishi, T. and Ushio, Y. (1996) Expression of tissue factor correlates with grade of malignancy in human glioma. *Cancer* 77 (9), 1877-83.

- Hammad, M.M. Dunn, H.A. and Ferguson, S.S.G. (2016) MAGI Proteins Regulate the Trafficking and Signaling of Corticotropin-Releasing Factor Receptor 1 via a Compensatory Mechanism. *Journal of Molecular Signalling* 11:5.
- Hammond, G.R. and Balla, T. (2015) Polyphosphoinositide binding domains: Key to inositol lipid biology. *Biochim Biophys Acta* 1851 (6), 746-58.
- Han, X. Guo, B, Li, Y. and Zhu, B. (2014). Tissue factor in tumor microenvironment: a systematic review. *Journal of Hematology & Oncology* 7, 54.
- Harayama, T. and Riezman, H. (2018) Understanding the diversity of membrane lipid composition. *Nature Reviews Molecular Cell Biology* 19, 281-296
- He, J. Bellini, M. Inuzuka, H. Xu, J. Xiong, Y. Yang, X. Castleberry, A.M. and Hall, R.A. (2006) Proteomic analysis of beta1-adrenergic receptor interactions with PDZ scaffold proteins. *The journal of Biological Chemistry* 281(5), 2820-7.
- Heavner, M.S. Zhang, M. Bast, C.E. Parker, L. and Eyler, R.F. (2017) Thrombolysis for Massive Pulmonary Embolism in Pregnancy. *Pharmacotherapy* 37(11), 1449-1457.
- Heuberger, D. M. and Schuepbach, R. A. (2019) Correction to: protease-activated receptors (PARs): mechanisms of action and potential therapeutic modulators in PAR-driven inflammatory diseases. *Thrombosis journal* 17, 22.
- Hirabayashi, S. Tajima, M. Yao, I. Nishimura, W. Mori, H. and Hata, Y. (2003) JAM4, a junctional cell adhesion molecule interacting with a tight junction protein, MAGI-1. *Molecular and Cell Biology* 23(12), 4267-82.
- Hirao, K. Hata, Y. Ide, N. Takeuchi, M. Irie, M. Yao, I. Deguchi, M. Toyoda, A. Sudhof, T.C. and Takai, Y. (1998) A novel multiple PDZ domain-containing molecule interacting with N-methyl-D-aspartate receptors and neuronal cell adhesion proteins. *The journal of Biological Chemistry* 273(33), 21105-10.
- Hisada, Y. and Mackman, N. (2019) Tissue Factor and Cancer: Regulation, Tumor Growth, and Metastasis. *Seminars in thrombosis and hemostasis* 45(4), 385-395.
- Ho, K. Myatt, S. and Lam, E. (2008) Many forks in the path: cycling with FoxO. *Oncogene* 27, 2300–2311.
- Hoffman, M. and Monroe, D. M. (2001) A cell-based model of hemostasis. *Thrombosis and Haemostasis* 85(6), 958-65.
- Holliday, D.L. and Speirs, V. (2011) Choosing the right cell line for breast cancer research. *Breast Cancer Research* 13(4), 215.
- Holy, E.W. and Tanner, F.C. (2010) Tissue factor in cardiovascular disease pathophysiology and pharmacological intervention. *Advances in Pharmacology* 59, 259-92.
- Holzhausen, M. Spolidorio, L.C. and Vergnolle, N. (2005) Role of protease-activated receptor-2 in inflammation, and its possible implications as a putative mediator of periodontitis. *Memórias do Instituto Oswaldo Cruz* 100 (1):177-80.

- Hopkins, B. D. Hodakoski, C. Barrows, D. Mense, S. and Parsons, R. E. (2014) PTEN function, the long and the short of it. *Trends in Biochemical Sciences* 39(4): 183–190.
- Hu, C. Huang, L. Gest, C. Xi, X. Janin, A. Soria, C. Li, H. and Lu, H. (2012). Opposite regulation by PI3K/Akt and MAPK/ERK pathways of tissue factor expression, cell-associated procoagulant activity and invasiveness in MDA-MB-231 cells. *Journal of Hematology & Oncology* 5, 16.
- Hu, L. Xia, L. Zhou, H. Wu, B. Mu, Y. Wu, Y. and Yan, J. (2013) TF/FVIIa/PAR2 promotes cell proliferation and migration via PKC α and ERK-dependent c-Jun/AP-1 pathway in colon cancer cell line SW620. *Tumour Biology* 34(5), 2573-81.
- Hu, Y. Li, Z. Guo, L. Wang, L. Zhang, L. Cai, X. Zhao, H. and Zha, X. (2007) MAGI-2 Inhibits cell migration and proliferation via PTEN in human hepatocarcinoma cells. *Archives of Biochemistry and Biophysics* 467 (1), 1-9.
- Hui, S. and Bader, G.D. (2010) Proteome scanning to predict PDZ domain interactions using support vector machines. *BMC Bioinformatics* 11, 507.
- Hui, S. Xing, X. and Bader, G.D. (2013) Predicting PDZ domain mediated protein interactions from structure. *BMC Bioinformatics* 14: 27.
- Hung, A.Y. and Sheng, M. (2002) PDZ domains: structural modules for protein complex assembly. *Journal of Biological Chemistry* 277(8), 5699-702.
- Huse, J.T. Brennan. C. Hambarzumyan, D. Wee, B. Pena, J. Rouhanifard, S.H. Sohn-Lee, C. le Sage, C. Agami, R. Tuschl, T. and Holland, E.C. (2009) The PTEN-regulating microRNA miR-26a is amplified in high-grade glioma and facilitates gliomagenesis in vivo. *Genes and Development* 23 (11), 1327-37.
- Iablokov, V. Hirota, C. L. Peplowski, M. A. Ramachandran, R. Mihara, K. Hollenberg, M. D. and MacNaughton, W. K. (2014) Proteinase-activated receptor 2 (PAR2) decreases apoptosis in colonic epithelial cells. *The Journal of biological chemistry* 289(49), 34366-34377.
- Ikushima, S. Ono, R. Fukuda, K. Sakayori, M. Awano, N. and Kondo, K. (2016) Trousseau's syndrome: cancer-associated thrombosis. *Japanese Journal of Clinical Oncology* 46(3), 204-8.
- Ivanova, S. Gregorc, U. Videgar, N. Javier, R. Bredt, D.S. Vandenabeele, P. Pardo, J. Simon, M.M. Turk, V. Banks, L. and Turk, B. (2011) MAGUKs, scaffolding proteins at cell junctions, are substrates of different proteases during apoptosis. *Cell Death & Disease* 2(1), e116.
- Jean-Charles, P.Y. Kaur, S. and Shenoy, S.K. (2017) G Protein-Coupled Receptor Signaling Through β -Arrestin-Dependent Mechanisms. *Journal of Cardiovascular Pharmacology* 70(3), 142-158.
- Jere, S.W. and Houreld, N.N. and Abrahamse, H. (2019) Role of the PI3K/AKT (mTOR and GSK3 β) signalling pathway and photobiomodulation in diabetic wound healing. *Cytokine & Growth Factor Reviews* 50, 52-59.

- Jiang, L. Chen, Y. Luo, L. and Peck, S.C. (2018) Central Roles and Regulatory Mechanisms of Dual-Specificity MAPK Phosphatases in Developmental and Stress Signaling. *Frontiers in Plant Science* 20, 9:1697.
- Jiang, X. Bailly, M.A. Panetti, T.S. Cappello, M. Konigsberg, W.H. and Bromberg, M.E. (2004) Formation of tissue factor-factor VIIa-factor Xa complex promotes cellular signaling and migration of human breast cancer cells. *Journal of Thrombosis and Haemostasis* 2(1), 93-101.
- Jiang, X. Guo, Y.L. and Bromberg, M.E. (2006) Formation of tissue factor: Factor VIIa-factor Xa complex prevents apoptosis in human breast cancer cells. *Thrombosis and Haemostasis* 96 (2), 196-201.
- Kakkar, A.K. Lemoine, N.R. Scully, M.F. and Williamson, R.C. (1995) Tissue factor expression correlates with histological grade in human pancreatic cancer. *The British Journal of Surgery* 82,1101-1104.
- Kanamori, M. Sandy, P. Marzinotto, S. Benetti, R. Kai, C. Hayashizaki, Y. Schneider, C. and Suzuki, H. (2003) The PDZ protein tax-interacting protein-1 inhibits beta-catenin transcriptional activity and growth of colorectal cancer cells. *Journal of Biological Chemistry* 278(40), 38758-64.
- Kasthuri, R. S. Taubman, M. B. and Mackman, N. (2009) Role of tissue factor in cancer. *Journal of clinical oncology : official journal of the American Society of Clinical Oncology* 27(29), 4834- 4838.
- Kato, S. Pinto, M. Carvajal, A. Espinoza, N. Monsó, C. Bravo, L. Villalon, M. Cuello, M. Quest, A.F. Suenaga, A. Brosens, J.J. and Owen, G.I. (2005) Tissue factor is regulated by epidermal growth factor in normal and malignant human endometrial epithelial cells. *Thrombosis and Haemostasis* 94 (2), 444-53.
- Kazan, J. M. El-Saghir, J. Saliba, J. Shaito, A. Jaleddine, N. El-Hajjar, L. Al-Ghadban, S. Yehia, L. Zibara, K. and El-Sabban, M. (2019) Cx43 Expression Correlates with Breast Cancer Metastasis in MDA-MB-231 Cells In Vitro, In a Mouse Xenograft Model and in Human Breast Cancer Tissues. *Cancers* 11(4), 460.
- Khorana, A. A. Ahrendt, S. A. Ryan, C. K. Francis, C. W. Hruban, R. H. Hu, Y. C. Hostetter, G. Harvey, J and Taubman, M. B. (2007) Tissue factor expression, angiogenesis, and thrombosis in pancreatic cancer. *Clinical Cancer Research* 13(10), 2870-5.
- Knights, A.J. Funnell, A.P. Crossley, M. and Pearson, R.C. (2012) Holding Tight: Cell Junctions and Cancer Spread. *Trends in Cancer Research* 8, 61-69.
- Kocatürk, B. and Versteeg, H.H. (2013) Tissue factor-integrin interactions in cancer and thrombosis: every Jack has his Jill. *Journal of Thrombosis and Haemostasis* 11 (1), 285-93.
- Kolmodin, K. and Aqvist, J. (2001) The catalytic mechanism of protein tyrosine phosphatases revisited. *FEBS Lett* 498 (2-3), 208-13.

- Kothari, H. Pendurthi, U. R. and Rao, L. V. (2013) Analysis of tissue factor expression in various cell model systems: cryptic vs. active. *Journal of thrombosis and haemostasis* 11(7), 1353-1363.
- Kurakula, K. Koenis, D.S. Herzik, M.A. Jr. Liu, Y. Craft, J.W. Jr. van Loenen, P.B. Vos, M. Tran, M.K. Versteeg, H.H. Goumans, M.T.H. Ruf, W. de Vries, C.J.M. and Şen, M. (2018) Structural and cellular mechanisms of peptidyl-prolyl isomerase Pin1-mediated enhancement of Tissue Factor gene expression, protein half-life, and pro-coagulant activity. *Haematologica* 103(6), 1073-1082.
- Kurosu, H. Maehama, T. Okada, T. Yamamoto, T. Hoshino, S. Fukui, Y. Ui, M. Hazeki, O. and Katada, T. (1997) Heterodimeric phosphoinositide 3-kinase consisting of p85 and p110 β is synergistically activated by the β gamma subunits of G proteins and phosphotyrosyl peptide. *Journal of Biological Chemistry* 272, 24252-24256.
- Kwon, J. Lee, S.-R. Yang, K.-S. Ahn, Y. Kim, Y. J. Stadtman, E. R. and Rhee, S. G. (2004) Reversible oxidation and inactivation of the tumor suppressor PTEN in cells stimulated with peptide growth factors. *Proceedings of the National Academy of Sciences of the United States of America* 101(47): 16419-16424.
- Lablokov, V. Hirota, C. L. Peplowski, M. A. Ramachandran, R. Mihara, K. Hollenberg, M. D. and MacNaughton, W. K. (2014) Proteinase-activated Receptor 2 (PAR2) Decreases Apoptosis in Colonic Epithelial Cells. *The Journal of Biological Chemistry* 289(49), 34366–34377.
- Lampugnani, M.G (2010) Endothelial adherens junctions and the actin cytoskeleton: an 'infinity net'?. *Journal of Biology* 9, 16.
- Larue, L. and Bellacosa, A. (2005) Epithelial–mesenchymal transition in development and cancer: role of phosphatidylinositol 3' kinase/AKT pathways. *Oncogene* 24, 7443-7454.
- Laura, R.P. Ross, S. Koeppen, H. and Lasky, L.A. (2002) MAGI-1: a widely expressed, alternatively spliced tight junction protein. *Experimental Cell Research* 275(2), 155-70.
- Lee, B.J. Kim, J.H. Woo, S.H. Kim, J.H. Kim, D.H. and Yu, Y.S. (2011) Tissue factor is involved in retinoblastoma cell proliferation via both the Akt and extracellular signal-regulated kinase pathways. *Oncology Reports* 26(3), 665-70.
- Lee, E.R. Kim, J.Y. Kang, Y.J. Ahn, J.Y. Kim, J.H. Kim, B.W. Choi, H.Y. Jeong, M.Y. and Cho, S.G. (2006) Interplay between PI3K/Akt and MAPK signaling pathways in DNA-damaging drug-induced apoptosis. *Biochimica et Biophysica Acta* 1763(9), 958-68.
- Lee, H.J. Lee, H.Y. Lee, J.H. Lee, H.4. Kang, G. Song, J.S. Kang, J. and Kim, J.H. (2014) Prognostic significance of biallelic loss of PTEN in clear cell renal cell carcinoma. *The Journal of Urology* 192 (3), 940-6.
- Lee, S.R. Yang, K.S. Kwon, J. Lee, C. Jeong, W. and Rhee, S.G. (2002) Reversible inactivation of the tumor suppressor PTEN by H₂O₂. *The Journal of Biological Chemistry* 277(23), 20336-42.

- Lee, S. J. Ritter, S. L. Zhang, H. Shim, H. Hall, R. A. and Yun, C. C. (2011) MAGI-3 competes with NHERF-2 to negatively regulate LPA2 receptor signaling in colon cancer cells. *Gastroenterology* 140(3), 924-934.
- Lee, Y. R. Chen, M. and Pandolfi, P. P. (2018) The functions and regulation of the PTEN tumour suppressor: new modes and prospects. *Nature Reviews Molecular Cell Biology* 19(9), 547-562.
- Leech, A. O. Cruz, R. G, Hill, A. D. and Hopkins, A. M. (2015) Paradigms lost-an emerging role for over-expression of tight junction adhesion proteins in cancer pathogenesis. *Annals of translational medicine* 3(13), 184.
- Lewis, C. S. Elnakat Thomas, H. Orr-Asman, M. A. Green, L. C. Boody, R. E. Matiash, K. Karve, A. Hisada, Y. M. Davis, H. W. Qi, X. Mercer, C. A. Lucas, F. V. Aronow, B. J. Mackman, N. Versteeg, H. H. and Bogdanov, V. Y. (2019) mTOR kinase inhibition reduces tissue factor expression and growth of pancreatic neuroendocrine tumors. *Journal of thrombosis and haemostasis* 17(1), 169-182.
- Li, C. Lyu, J. and Meng, Q.H. (2017) MiR-93 Promotes Tumorigenesis and Metastasis of Non-Small Cell Lung Cancer Cells by Activating the PI3K/Akt Pathway via Inhibition of LKB1/PTEN/CDKN1A. *Journal of Cancer* 8 (5), 870-879.
- Li, G. Li, Y.Y. Sun, J.E. Lin, W.H. and Zhou, R.X. (2016) ILK-PI3K/AKT pathway participates in cutaneous wound contraction by regulating fibroblast migration and differentiation to myofibroblast. *Laboratory Investigation* 96, 741-751.
- Li, H.Y. Yu, J.P. Guo, X.Z. Li, J.J. Zhao, J.J. Wang, D. Huo, R. and Xia, Y.T. (2005) Effects of in vitro PTEN transfection on proliferation of human pancreatic cancer ASPC-1 cells. *Zhonghua Nei Ke Za* 44(3), 191-4.
- Li, Z. Y. Li, X. H. Tian, G. W. Zhang, D. Y. Gao, H. and Wang, Z. Y. (2019) MAGI1 Inhibits the Proliferation, Migration and Invasion of Glioma Cells. *OncoTargets and therapy* 12, 11281-11290.
- Lima, L. G. and Monteiro, R. Q. (2013) Activation of blood coagulation in cancer: implications for tumour progression. *Bioscience Reports*, 33 (5), e00064.
- Lima-Fernandes, E. Enslen, H. Camand, E. Kotelevets, L. Boularan, C. Achour, L. Benmerah, A. Gibson, L. C. Baillie, G. S. Pitcher, J. A. Chastre, E. Etienne-Manneville, S. Marullo, S. and Scott, M. G. (2011) Distinct functional outputs of PTEN signalling are controlled by dynamic association with β -arrestins. *The EMBO journal* 30(13), 2557-2568.
- Liu, J. Youn, H. Yang, J. Du, N. Liu, J. Liu, H. and Li, B. (2011) G-protein alpha-s and -12 subunits are involved in androgen-stimulated PI3K activation and androgen receptor transactivation in prostate cancer cells. *Prostate* 71(12), 1276-86.
- Liu, P. Cheng, H. Roberts, T. M. and Zhao, J. J. (2009). Targeting the phosphoinositide 3-kinase pathway in cancer. *Nature reviews. Drug discovery* 8(8), 627-644.
- Liu, W. Zhou, Y. Reske, S.N. and Shen, C (2008) PTEN mutation: many birds with one stone in tumorigenesis. *Anticancer Research* 28(6A), 3613-9.

- Liu, Y. Jiang, P. Capkova, K. Xue, D. Ye, L. Sinha, S.C. Mackman, N. Janda, K.D. and Liu, C. (2011) Tissue factor-activated coagulation cascade in the tumor microenvironment is critical for tumor progression and an effective target for therapy. *Cancer Research* 71(20), 6492-502.
- Liu, Y. and Mueller, B.M. (2006) Protease-activated receptor-2 regulates vascular endothelial growth factor expression in MDA-MB-231 cells via MAPK pathways. *Biochemical and Biophysical Research Communications* 344(4), 1263-70.
- Lobo, G. P. Waite, K. A. Planchon, S. M. Romigh, T. Houghton, J. A. and Eng, C. (2008) ATP modulates PTEN subcellular localization in multiple cancer cell lines. *Human Molecular Genetics*, 17(18): 2877–2885.
- Lodish, H. Berk, A. Zipursky, S.L. Matsudaira, P. Baltimore, D. and Darnell, J. (2000) *Molecular Cell Biology. 4th edition.* New York: W. H. Freeman.
- Lopes-Bezerra, L.M. and Filler, S.G. (2003) Endothelial cells, tissue factor and infectious diseases. *Brazilian Journal of Medical and Biological Research* 36(8), 987-91.
- López-Pedreira, C. Barbarroja, N. Dorado, G. Siendones, E. and Velasco, F. (2006) Tissue factor as an effector of angiogenesis and tumor progression in hematological malignancies. *Leukemia* 20(8), 1331-1340.
- Los, M. Maddika, S. Erb, B. and Schulze-Osthoff, K. (2009) Switching Akt: from survival signaling to deadly response. *Bioessays* 31(5), 492-5.
- Lu, X.X. Cao, L.Y., Chen, X. Xiao, J. Zou, Y. and Chen, Q. (2016). PTEN Inhibits Cell Proliferation, Promotes Cell Apoptosis, and Induces Cell Cycle Arrest via Downregulating the PI3K/AKT/hTERT Pathway in Lung Adenocarcinoma A549 Cells. *BioMed Research International* 2476842.
- Luo, J.D. and Chen, A.F. (2005) Nitric oxide: a newly discovered function on wound healing. *Acta Pharmacologica Sinica* 26(3), 259-264.
- Luongo, F. Colonna, F. Calapà, F. Vitale, S. Fiori, M.E. and De Maria, R. (2019) PTEN Tumor-Suppressor: The Dam of Stemness in Cancer. *Cancers (Basel)* 11(8), 1076.
- Ma, Q. Yang, Y. Feng, D. Zheng, S. Meng, R. Fa, P. Zhao, C. Liu, H. Song, R. Tao, T. Yang, L. Dai, J. Wang, S. Jiang, W.G. and He, J. (2015) MAGI3 negatively regulates Wnt/ β -catenin signaling and suppresses malignant phenotypes of glioma cells. *Oncotarget* 6(34), 35851-65.
- Mackman, N. (2004) Role of Tissue Factor in Hemostasis, *Thrombosis, and Vascular Development. Arteriosclerosis, Thrombosis, and Vascular Biology* 24, 1015-1022.
- Mackman, N. (2009). The role of tissue factor and factor VIIa in hemostasis. *Anesthesia & Analgesia* 108(5), 1447-52.
- Mackman, N. and Luther, T. (2013) Platelet tissue factor: to be or not to be. *Thrombosis Research* 132(1), 3-5.

- Mackman, N. Morrissey, J. H. Fowler, B. and Edgington, T. S. (1989) Complete sequence of the human tissue factor gene, a highly regulated cellular receptor that initiates the coagulation protease cascade. *Biochemistry* 28(4), 1755-62.
- Maddika, S. Kavela, S. Rani, N. Palicharla, V.R. Pokorny, J.L. Sarkaria, J.N. and Chen, J. (2011) WWP2 is an E3 ubiquitin ligase for PTEN. *Nature Cell Biology* 13 (6), 728-33.
- Maehama T. and Dixon J. E. (1998). The tumor suppressor, PTEN/MMAC1, dephosphorylates the lipid second messenger, phosphatidylinositol 3,4,5-trisphosphate. *Journal of Biological chemistry* 273, 13375-13378
- Malaney, P. Pathak, R.R. Xue, B., Uversky, V.N. and Davé, V. (2013) Intrinsic disorder in PTEN and its interactome confers structural plasticity and functional versatility. *Science Reports* 3, 2035.
- Malý, M.A. Tomasov, P. Hájek, P. Blasko, P. Hrachovinová, I. Salaj, P. and Veselka, J. (2007) The role of tissue factor in thrombosis and hemostasis. *Physiological Research* 56 (6), 685-95.
- Mandal, S. Pendurthi, U. and Pendurthi, U. (2006) Cellular localization and trafficking of tissue factor. *Blood* 107(12), 4746-4753.
- Manjunath, G.P. Ramanujam, P.L. and Galande, S. (2018) Structure function relations in PDZ-domain-containing proteins: Implications for protein networks in cellular signalling. *Journal of Bioscience* 43(1), 155-171.
- Manly, D. A. Wang, J. Glover, S. L. Kasthuri, R. Liebman, H. A. Key, N. S. and Mackman, N (2010). Increased microparticle tissue factor activity in cancer patients with Venous Thromboembolism. *Thrombosis research* 125(6), 511-512.
- Mann, K.G. Brummel-Ziedins, K. Orfeo, T. And Butenas, S (2006) "Models of blood coagulation." *Blood Cells, Molecules and Diseases* 36(2), 108-117.
- Manning, B.D. and Toker, A. (2017) AKT/PKB Signaling: Navigating the Network. *Cell* 169 (3), 381-405.
- Marinissen, M.J. and Gutkind, J.S. (2001) G-protein-coupled receptors and signaling networks: emerging paradigms. *Trends in Pharmacological Sciences* 22(7), 368-76.
- Martin-Belmonte, F. Gassama, A. Datta, A. Yu, W. Rescher, U. Gerke, V. and Mostov, K. (2007) PTEN-mediated apical segregation of phosphoinositides controls epithelial morphogenesis through Cdc42. *Cell* 128, 383-397.
- Martin, T.A. and Jiang, W.G. (2009) Loss of tight junction barrier function and its role in cancer metastasis. *Biochimica et Biophysica Acta* 1788(4), 872-91.
- Matsuda, S. and Kitagishi, Y. (2013) MAGI Scaffolding Molecules Involved in Cancer Cell Signaling. *Journal of Carcinogenesis & Mutagenesis* S7:005.
- Matsuoka, T. Yashiro, M. Nishioka, N. Hirakawa, K. Olden, K. and Roberts, J. D. (2012) PI3K/Akt signalling is required for the attachment and spreading, and growth in vivo of metastatic scirrhous gastric carcinoma. *British journal of cancer* 106(9), 1535-1542.

- Mazloumi Gavgani, F. Smith Arnesen, V. Jacobsen, R. G. Krakstad, C. Hoivik, E. A. and Lewis, A. E. (2018) Class I Phosphoinositide 3-Kinase PIK3CA/p110 α and PIK3CB/p110 β Isoforms in Endometrial Cancer. *International journal of molecular sciences* 19(12), 3931.
- McDaniel, W. (2007) Cytoplasmic Signaling Circuitry Programs Many of the Traits of Cancer (Webiste). <https://slideplayer.com/slide/6033449/> accessed 31/01/2020.
- Mihara, K. Ramachandran, R. Saifeddine, M. Hansen, K.K. Renaux, B. Polley, D. Gibson, S. Vanderboor, C. and Hollenberg, M.D. (2016) Thrombin-mediated direct activation of proteinase-activated receptor-2 (PAR2): another target for thrombin signaling. *Molecular Pharmacology* 89(5), 606-14.
- Milella, M. Falcone, I. Conciatori, F. Cesta Incani, U. Del Curatolo, A. Inzerilli, N. Carmen M. A. Nuzzo, C. Vaccaro, V. Vari, S. Cognetti, F. and Ciuffreda, L. (2015) PTEN: Multiple Functions in Human Malignant Tumors. *Frontiers in Oncology* 5, 24.
- Mody, R. S. and Carson, S. D. (1997) "Tissue factor cytoplasmic domain peptide is multiply phosphorylated in vitro," *Biochemistry* 36(25), 7869-7875.
- Molinari, F. and Frattini, M. (2013) Functions and Regulation of the PTEN Gene in Colorectal Cancer. *Frontiers in Oncology* 3, 326.
- Monteiro, R.Q. Lima, L.G. Gonçalves, N.P. DE Souza, M.R. Leal, A.C. Demasi, M.A. Sogayar, M.C. and Carneiro-Lobo, T.C. (2016) Hypoxia regulates the expression of tissue factor pathway signaling elements in a rat glioma model. *Oncology Letters* 12 (1), 315-322.
- Morris, D.R. Ding, Y. Ricks, T.K. Gullapalli, A. Wolfe, B.L. and Trejo, J. (2006) Protease-activated receptor-2 is essential for factor VIIa and Xa-induced signaling, migration, and invasion of breast cancer cells. *Cancer Research*. 66 (1), 307-314.
- Mosessian, S. and Wu, H. (2010) PTEN-associated complexes: An overview. *Current Topics in Biochemical Research* 12 (1), 37-42.
- Mueller, B.M. and Ruf, W. (1998) Requirement for binding of catalytically active factor VIIa in tissue factor-dependent experimental metastasis. *The Journal of Clinical Investigation* 101 (7), 1372-8.
- Mulder, A.B. Smit, J.W. Bom, V.J.J. Blom, N.R. Halie, M.R. and van der Meer, J. (1996) Association of endothelial tissue factor and thrombomodulin with caveolae. *Blood* 88, 3667-3670.
- Müller, M. Flössel, C. Haase, M. Luther, T. Albrecht, S. Nawroth, P.P. and Zhang, Y. (1993) Cellular localization of tissue factor in human breast cancer cell lines. *Virchows archiv. B, Cell pathology including molecular patholog* 64(5), 265-9.
- Murga, C. Laguigne, L. Wetzker, R. Cuadrado, A. and Gutkind, J.S. (1998) Activation of Akt/protein kinase B by G protein-coupled receptors. A role for alpha and beta gamma subunits of heterotrimeric G proteins acting through phosphatidylinositol-3-OH kinasegamma. *Journal of Biological Chemistry* 273, 19080-19085.

- Myers, M.P. Pass, I. Batty, I.H. Van der Kaay, J. Stolarov, J.P. Hemmings, B.A. Wigler, M.H. Downes, C.P. and Tonks, N.K. (1998) The lipid phosphatase activity of PTEN is critical for its tumor suppressor function. *Proceedings of the National Academy of Sciences* 95 (23), 13513-13518.
- Myers, M. P. Stolarov, J. P. Eng, C. Li, J. Wang, S. I. Wigler, M. H. Parsons, R. and Tonks, N. K. (1997) P-TEN, the tumor suppressor from human chromosome 10q23, is a dual-specificity phosphatase. *Proceedings of the National Academy of Sciences of the United States of America* 94 (17), 9052-9057.
- Nagasaka, K. Kawana, K. Osuga, Y. and Fujii, T. (2013) PDZ domains and viral infection: versatile potentials of HPV-PDZ interactions in relation to malignancy. *BioMed Research International* 13, 369712.
- Nagashima, S. Kodaka, M. Iwasa, H. and Hata, Y. (2015) MAGI2/S-SCAM outside brain. *Journal of Biochemistry* 157(4), 177-84.
- Naik, M.U. Naik, T.U. Suckow, A.T. Duncan, M.K. and Naik, U.P. (2008) Attenuation of junctional adhesion molecule-A is a contributing factor for breast cancer cell invasion. *Cancer Research* 68(7), 2194-203.
- Nakasaki, T. Wada, H. Shigemori, C. Miki, C. Gabazza, E.C. Nobori, T. Nakamura, S. and Shiku, H. (2002) Expression of tissue factor and vascular endothelial growth factor is associated with angiogenesis in colorectal cancer. *American Journal of Hematology* 69 (4), 247-54.
- Narahara, N. Enden, T. Wiiger, M. and Prydz, H. (1994) Polar expression of tissue factor in human umbilical vein endothelial cells. *Arterioscler Thrombosis* 14 (11), 1815-1820.
- Neuenschwander, P.F. Bianco-Fisher, E. Rezaie, A.R. and Morrissey, J.H. (1995) Phosphatidylethanolamine augments factor VIIa-tissue factor activity: enhancement of sensitivity to phosphatidylserine. *Biochemistry* 34(43), 13988-93.
- New, D.C. and Wong, Y.H. (2007) Molecular mechanisms mediating the G protein-coupled receptor regulation of cell cycle progression. *Journal of Molecular Signaling* 2-2.
- New, D.C., Wu, K. Kwok, A.W. and Wong, Y.H. (2007) G protein-coupled receptor-induced Akt activity in cellular proliferation and apoptosis. *The FEBS Journal* 274(23), 6025-6036.
- Ngeow, J. and Eng, C. (2020) PTEN in Hereditary and Sporadic Cancer. *Cold Spring Harbor Perspectives in Medicine* 10(4), a036087.
- Ni, T. K. and Kuperwasser, C. (2016) Premature polyadenylation of MAGI3 produces a dominantly-acting oncogene in human breast cancer. *eLife* 5, e14730.
- Nitulescu, G. M. Van De Venter, M. Nitulescu, G. Ungurianu, A. Juzenas, P. Peng, Q. Oлару, O. T. Grădinaru, D. Tsatsakis, A. Tsoukalas, D. Spandidos, D. A. and Margina, D. (2018). The Akt pathway in oncology therapy and beyond (Review). *International journal of oncology* 53(6), 2319-2331.

- Norén, E. Almer, S. and Söderman, J. (2017) Genetic variation and expression levels of tight junction genes identifies association between MAGI3 and inflammatory bowel disease. *BMC Gastroenterol* 17(1), 68.
- Nunès, J,A, and Guittard, G. (2013) An Emerging Role for PI5P in T Cell Biology. *Frontiers in Immunology* 4, 80.
- Nürnberg, B. and Beer-Hammer, S. (2019) Function, Regulation and Biological Roles of PI3Kγ Variants. *Biomolecules* 9(9), 427.
- Odrizola, L. Singh, G. Hoang, T. and Chan, A.M. (2007) Regulation of PTEN activity by its carboxyl-terminal autoinhibitory domain. *Journal of Biological Chemistry* 282(32), 23306-15.
- Okumura, K. Mendoza, M. Bachoo, R.M. DePinho, R.A. Cavenee, W.K. and Furnari, F.B. (2006) PCAF modulates PTEN activity. *The Journal of Biological Chemistry* 281(36): 26562-8.
- Orellana, R. Kato, S. Erices, R. Bravo, M. L. Gonzalez, P. Oliva, B. Cubillos, S. Vadivia, A. Ibañez, C. Brañes, J. Barriga, M.I. Bravo, E. Alonso, C. Bustamente, E. Castellon, E. Hidalgo, P. Trigo, C. Panes, O. Pereira, J. Mezzano, D. Cuello, M.A. and Owen, G. I. (2015). Platelets enhance tissue factor protein and metastasis initiating cell markers, and act as chemoattractants increasing the migration of ovarian cancer cells. *BMC Cancer*, 15, 290.
- Østerud, B. (2010) Tissue factor expression in blood cells. *Thrombosis Ressearch* 125 (1), S31-4.
- Østerud, B. and Bjørklid, E. (2006) Sources of tissue factor. *Seminars in Thrombosis and Hemostasis* 32(1), 11-23.
- Padash Barmchi, M. Samarasekera, G. Gilbert, M. Auld, V.J. and Zhang, B. (2016) Magi Is Associated with the Par Complex and Functions Antagonistically with Bazooka to Regulate the Apical Polarity Complex. *PLoS One* 11(4), e0153259.
- Palta, S. Saroa, R. and Palta, A. (2014) Overview of the coagulation system. *Indian Journal of Anaesthesia* 58 (5), 515–523.
- Papa, A. and Pandolfi, P.P. (2019) The PTEN-PI3K Axis in Cancer. *Biomolecules* 9(4), 153.
- Patrie, K.M. Drescher, A.J. Welihinda, A. Mundel, P. and Margolis, B. (2002) Interaction of two actin-binding proteins, synaptopodin and alpha-actinin-4, with the tight junction protein MAGI-1. *The journal of Biological Chemistry* 277(33), 30183-90.
- Pawar, N.R. Buzza, M.S. and Antalis, T.M. (2019) Membrane-Anchored Serine Proteases and Protease-Activated Receptor-2-Mediated Signaling: Co-Conspirators in Cancer Progression. *Cancer Research* 79(2), 301-310
- Peerapen, P. and Thongboonkerd, V. (2013) p38 MAPK mediates calcium oxalate crystal-induced tight junction disruption in distal renal tubular epithelial cells. *Scientific Reports* 3,1041.

- Peiris, T.H. Ramirez, D. Barghouth, P.G. and Oviedo, N.J. (2016) The Akt signaling pathway is required for tissue maintenance and regeneration in planarians. *BMC Developmental Biology* 16, 7.
- Pendurthi, U. and Rao, L.V. (2002) Factor VIIa/tissue factor-induced signaling: a link between clotting and disease. *Vitamins and Hormones* 64, 323-55.
- Pendurthi, U. and Rao, L. V. (2008) Role of tissue factor disulfides and lipid rafts in signaling. *Thrombosis research* 122 (1), S14–S18.
- Peng, X. D. Xu, P. Z. Chen, M. L. Hahn-Windgassen, A. Skeen, J. Jacobs, J. Sundararajan, D. Chen, W. S. Crawford, S. E. Coleman, K. G. and Hay, N. (2003) Dwarfism, impaired skin development, skeletal muscle atrophy, delayed bone development, and impeded adipogenesis in mice lacking Akt1 and Akt2. *Genes & development* 17(11), 1352-1365.
- Petrocelli, T. and Slingerland, J.M. (2001) PTEN deficiency: a role in mammary carcinogenesis. *Breast Cancer Research* 3, 356.
- Petrovan, R.J. Rapaport, S.I. and Le, D.T. (1999) A novel clotting assay for quantitation of plasma prothrombin (factor II) using Echis multisquamatus venom. *American Journal of Clinical Pathology* 112(5), 705-11.
- Pilarski, R. and Eng, C. (2004) "Will the real Cowden syndrome please stand up (again)? Expanding mutational and clinical spectra of the PTEN hamartoma tumour syndrome". *Journal of Medical Genetics* 41 (5), 323–6.
- Planchon, S.M. Waite, K.A. and Eng, C. (2008) The nuclear affairs of PTEN. *Journal of Cell Biology* 121 (3), 249-53.
- Platre, M. P. and Jaillais, Y. (2017) Anionic lipids and the maintenance of membrane electrostatics in eukaryotes. *Plant signaling & behavior* 12(2), e1282022.
- Porta, C. Paglino, C. and Mosca, A. (2014) Targeting PI3K/Akt/mTOR Signaling in Cancer. *Frontiers in Oncology* 4, 64.
- Poulsen, L.K. Jacobsen, N. Sørensen, B.B. Berghem, N.C. Kelly, J.D. Foster, D.C. Thastrup, O. Ezban, M. and Petersen, L.C. (1998) Signal transduction via the mitogen-activated protein kinase pathway induced by binding of coagulation factor VIIa to tissue factor. *Journal of Biological Chemistry* 273(11), 6228-32.
- Pradier, A. and Ettelaie, C. (2008) The influence of exogenous tissue factor on the regulators of proliferation and apoptosis in endothelial cells. *Journal of Vascular Research* 45(1), 19-32.
- Prior, S. M. Douce, D. Ades, S. Holmes, C. E. Cory, S. Cushman, M. Callas, P. and Butenas, S. (2016) Activated Factors XI and IX and Tissue Factor in Patients with Advanced Cancer. *Blood* 128(22), 4947.
- Provençal, M. Berger-Thibault, N. Labbé, D. Veitch, R. Boivin, D. Rivard, G.E. Gingras, D. and Béliveau, R. (2010) Tissue factor mediates the HGF/Met-induced anti-apoptotic pathway in DAOY medulloblastoma cells. *Journal of neuro-oncology* 97 (3), 365-72.

- Putney, J.W. and Tomita, T. (2012) Phospholipase C signaling and calcium influx. *Advances in Biological Regulation* 52(1), 152-64.
- Rahdar, M. Inoue, T. Meyer, T. Zhang, J. Vazquez, F. and Devreotes, P.N. (2009) A phosphorylation-dependent intramolecular interaction regulates the membrane association and activity of the tumor suppressor PTEN. *Proceedings of the National Academy of Sciences of the United States of America* 106(2), 480-5.
- Rao, L. V. and Pendurthi, U. R. (2005) Tissue factor-factor VIIa signaling. *Arteriosclerosis, thrombosis, and vascular biology* 25(1), 47-56.
- Rao, L. V. and Pendurthi, U. R. (2012) Regulation of tissue factor coagulant activity on cell surfaces. *Journal of thrombosis and haemostasis* 10(11), 2242-2253.
- Regina, S. Valentin, J.B. Lachot, S. Lemarié, E. Rollin, J. and Gruel, Y. (2009) Increased tissue factor expression is associated with reduced survival in non-small cell lung cancer and with mutations of TP53 and PTEN. *Clinical Chemistry* 55 (10), 1834-42.
- Reinhardt, C. von Brühl, M. L. Manukyan, D. Grahl, L. Lorenz, M. Altmann, B. Dlugai, S. Hess, S. Konrad, I. Orschielt, L. Mackman, N. Ruddock, L. Massberg, S. and Engelmann, B. (2008) Protein disulfide isomerase acts as an injury response signal that enhances fibrin generation via tissue factor activation. *The Journal of clinical investigation* 118(3), 1110-1122.
- Rickles, F.R. (2006) Mechanisms of cancer-induced thrombosis in cancer. *Journal of Pathophysiology of Haemostasis and Thrombosis*, 35(1-2), 103-110.
- Rickles, F.R. Hair, G.A. Zeff, R.A. Lee, E. and Bona, R.D. (1995) Tissue factor expression in human leukocytes and tumor cells. *Thrombosis and Haemostasis* 74 (1), 391-5.
- Roberts, H.R. Monroe, D. M. and Hoffman, M. (2006) Molecular biology and biochemistry of the coagulation factors and pathways of hemostasis. *Chapter 106 in: Williams Hematology, Seventh Edition. McGraw-Hill.*
- Rodriguez, V. and Warad, D. (2016) Pediatric Coagulation Disorders. *Pediatric in review* 37(7), 279-91.
- Romero, G von Zastrow, M. and Friedman, P.A. (2011) Role of PDZ proteins in regulating trafficking, signaling, and function of GPCRs: means, motif, and opportunity. *Adv Pharmacol* 62:279-314.
- Rondon, A.M.R. Kroone, C. Kapteijn, M.Y. Versteeg, H.H. and Buijs, J.T. (2019) Role of Tissue Factor in Tumor Progression and Cancer-Associated Thrombosis. *Seminar in Thrombosis and Hemostasis* 45(4), 396-412
- Rong, Y. Belozarov, V. E. Tucker-Burden, C. Chen, G. Durden, D. L. Olson, J. J. Van Meir, E.G. Mackman, N. and Brat, D.J. (2009) Epidermal Growth Factor Receptor and PTEN Modulate Tissue Factor Expression in Glioblastoma through JunD/Activator Protein-1 Transcriptional Activity. *Cancer Research* 69 (6), 2540-2549.

- Rong, Y. Post, D.E. Pieper, R.O. Durden, D.L. Van, Meir, E.G. and Brat, D.J. (2005) PTEN and hypoxia regulate tissue factor expression and plasma coagulation by glioblastoma. *Cancer Research* 65(4), 1406-1413.
- Ross, A.H. and Gericke, A. (2009) Phosphorylation keeps PTEN phosphatase closed for business. *Proceedings of the National Academy of Sciences of the United States of America* 106 (5), 1297-8.
- Rothmeier, A. S. Marchese, P. Petrich, B. G, Furlan-Freguia, C. Ginsberg, M. H. Ruggeri, Z. M. and Ruf, W. (2015) Caspase-1-mediated pathway promotes generation of thromboinflammatory microparticles. *The Journal of clinical investigation* 125(4), 1471-1484.
- Rothmeier, A.S. and Ruf, W. (2012) Protease-activated receptor 2 signaling in inflammation. *Seminars in Immunopathology* 34 (1), 133–149.
- Roy, A. Ansari, S. A. Das, K. Prasad, R. Bhattacharya, A. Mallik, S. Mukherjee, A. and Sen, P. (2017) Coagulation factor VIIa-mediated protease-activated receptor 2 activation leads to β -catenin accumulation via the AKT/GSK3 β pathway and contributes to breast cancer progression. *The Journal of biological chemistry* 292(33), 13688-13701.
- Ruf, W. (2012) Tissue factor and cancer. *Thrombosis Research* 130 (1), S84-7.
- Ruf, W. Disse, J. Carneiro-Lobo, T. C. Yokota, N. and Schaffner, F. (2011). Tissue Factor and Cell Signalling in Cancer Progression and Thrombosis. *Journal of Thrombosis and Haemostasis* 9 (1), 306-315.
- Rydén, L. Grabau, D, Schaffner, F. Jönsson, P. E. Ruf, W. and Belting, M. (2010) Evidence for tissue factor phosphorylation and its correlation with protease-activated receptor expression and the prognosis of primary breast cancer. *International journal of cancer* 126(10), 2330-2340.
- Salmena, L. Carracedo, A. and Pandolfi, P.P. (2008) Tenets of PTEN tumor suppression. *Cell* 133(3), 403-14.
- Salvador, E. Burek, M. and Förster, C.Y. (2016) Tight Junctions and the Tumor Microenvironment. *Current Pathobiology Reports* 4, 135-145.
- Sarrió, D. Palacios, J. Hergueta-Redondo, M. Gómez-López, G. Cano, A. and Moreno-Bueno, G. (2009) Functional characterization of E- and P-cadherin in invasive breast cancer cells. *BMC cancer* 9, 74.
- Schaffner, F. and Ruf, W. (2009). Tissue Factor and PAR2 Signaling in the Tumor Microenvironment. *Arteriosclerosis, Thrombosis, and Vascular Biology* 29(12), 1999-2004.
- Schaffner, F. Versteeg, H. H. Schillert, A. Yokota, N. Petersen, L. C. Mueller, B. M. and Ruf, W. (2010) Cooperation of tissue factor cytoplasmic domain and PAR2 signaling in breast cancer development. *Blood* 116(26), 6106-13.
- Schmidt, B. Ho, L. and Hogg, P.J. (2006) Allosteric disulfide bonds. *Biochemistry* 45(24),7429-7433.

- Schmitz, M. Grignard, G. Margue, C. Dippel, W. Capesius, C. Mossong, J. Nathan, M. Giacchi, S. Scheiden, R. and Kieffer, N. (2007) Complete loss of PTEN expression as a possible early prognostic marker for prostate cancer metastasis. *International Journal of Cancer* 120, 1284-1292.
- Sedda, S. Marafini, I. Caruso, R. Pallone, F. And Monteleone, G. (2014) Proteinase activated-receptors-associated signaling in the control of gastric cancer. *World Journal of Gastroenterology* 20(34), 11977-11984.
- Sen, M. Herzik, M. Craft, J. W. Creath, A. L. Agrawal, S. Ruf, W. and Legge, G. B. (2009) Spectroscopic Characterization of Successive Phosphorylation of the Tissue Factor Cytoplasmic Region. *The open spectroscopy journal* 3, 58-64.
- Sever, R. and Brugge, J. S. (2015) Signal Transduction in Cancer. *Cold Spring Harbor Perspectives in Medicine* 5 (4), a006098.
- Shervington, L. and Patil, H. and Shervington, A. (2015) Could the Anti-Chaperone VER155008 Replace Temozolomide for Glioma Treatment. *Journal of Cancer* 6(8), 786-94.
- Shore, A. N. Chang, C. H. Kwon, O. J. Weston, M. C. Zhang, M. Xin, L. and Rosen, J. M. (2016) PTEN is required to maintain luminal epithelial homeostasis and integrity in the adult mammary gland. *Developmental biology* 409(1), 202-217.
- Sidhu, T. S. French, S. L. and Hamilton, J. R. (2014) Differential signaling by protease-activated receptors: implications for therapeutic targeting. *International journal of molecular sciences* 15(4), 6169-6183.
- Silva, A. Yunes, J.A. Cardoso, B.A. Martins, L.R. Jotta, P.Y. Abecasis, M. Nowill, A.E. Leslie, N.R. Cardoso, A.A. and Barata, J.T. (2008) PTEN posttranslational inactivation and hyperactivation of the PI3K/Akt pathway sustain primary T cell leukemia viability. *Journal of Clinical Investigation* 118(11), 3762-74.
- Silva, D.D. Noronha, J.A. Silva, V.D. and Carvalhal, G.F. (2014) Increased tissue factor expression is an independent predictor of mortality in clear cell carcinoma of the kidney. *International Brazilian Journal of Urology* 40: 499-506.
- Simonson, S.J. Difilippantonio, M.J. and Lambert, P.F. (2005) Two distinct activities contribute to human papillomavirus 16 E6's oncogenic potential. *Cancer Research* 65(18), 8266-73.
- Simonyan, L. Légiot, A. Lascu, I. Durand, G. Giraud, M.F. Gonzalez, C. and Manon, S. (2017) The substitution of Proline 168 favors Bax oligomerization and stimulates its interaction with LUVs and mitochondria. *Biochimica et Biophysica Acta* 1859(6), 1144–1155.
- Snietura, M. Jaworska, M. Mlynarczyk-Liszka, J. Goraj-Zajac, A. Piglowski, W. Lange, D., Wozniak, G. Nowara, E. and Suwinski, R. (2012) PTEN as a prognostic and predictive marker in postoperative radiotherapy for squamous cell cancer of the head and neck. *PloS one* 7(3), e33396.
- Song, M.S. Salmena, L. and Pandolfi, P.P. (2012) The functions and regulation of the PTEN tumour suppressor. *Nature Reviews Molecular Cell Biology* 13(5), 283-96.

- Sorensen, B.B. Freskgard, P-O. Nielsen, L.S. Rao, L.V.M. Ezban, M. and Petersen, L.C. (1999) Factor VIIa-induced p44/42 mitogen-activated kinase activation requires the proteolytic activity of factor VIIa and is independent of the tissue factor cytoplasmic domain. *Journal of Biological Chemistry* 274, 21349-54.
- Sørensen, H.T. Mellekjær, L. Olsen, J.H. and Baron, J.A. (2000) Prognosis of cancers associated with venous thromboembolism. *The New England Journal of Medicine* 343 (25), 1846-50.
- Sotelo, N.S. Schepens, J.T. Valiente, M. Hendriks, W.J. and Pulido, R. (2015) PTEN-PDZ domain interactions: binding of PTEN to PDZ domains of PTPN13. *Methods* 77-78:147-56.
- Squarize, C.H. Castilho, R.M. Bugge, T.H. and Gutkind, J.S. (2010) Accelerated wound healing by mTOR activation in genetically defined mouse models. *PLoS One* 5: e10643.
- Srinivasan, R. Ozhegov, E. van den Berg, Y. W. Aronow, B. J. Franco, R. S. Palascak, M. B. Fallon, J.T. Ruf, W. Versteeg, H. H. and Bogdanov, V. Y. (2011) Splice variants of Tissue Factor promote monocyte-endothelial interactions by triggering the expression of cell adhesion molecules via integrin-mediated signaling. *Journal of Thrombosis and Haemostasis* 9 (10), 2087-2096.
- Steffel, J. Lüscher, T.F. and Tanner, F.C. (2006) Tissue factor in cardiovascular diseases: molecular mechanisms and clinical implications. *Circulation* 113 (5), 722-31.
- Stetak, A. and Hajnal, A. (2011) The *C. elegans* MAGI-1 protein is a novel component of cell junctions that is required for junctional compartmentalization. *Developmental Biology* 350(1), 24-31.
- Su, C.C. Lin, Y.P. Cheng, Y.J. Huang, J.Y. Chuang, W.J. Shan, Y.S. and Yang, B.C. (2007) Phosphatidylinositol 3-kinase/Akt activation by integrin-tumor matrix interaction suppresses Fas-mediated apoptosis in T cells. *Journal of Immunology* 179(7), 4589-97.
- Subbaiah, V.K. Kranjec, C. Thomas, M. and Banks, L. (2011) PDZ domains: the building blocks regulating tumorigenesis. *The Biochemical Journal* 439(2), 195-205.
- Sun, Z., Cao, B. and Wu, J. (2015) Protease-activated receptor 2 enhances renal cell carcinoma cell invasion and migration via PI3K/AKT signaling pathway. *Experimental and Molecular Pathology* 98, 382-389.
- Swat, W. Montgrain, V. Doggett, T. A. Douangpanya, J. Puri, K. Vermi, W. and Diacovo, T. G. (2006) Essential role of PI3K δ and PI3K γ in thymocyte survival. *Blood* 107(6): 2415-2422.
- Tamura, M. Gu, J. Takino, T. and Yamada, K.M. (1999) Tumor suppressor PTEN inhibition of cell invasion, migration, and growth: differential involvement of focal adhesion kinase and p130Cas. *Cancer Research* 59 (2), 442-9.
- Tan, T. (2015) Akt/PKB signaling pathway. *Wikipedia Online* https://en.wikipedia.org/wiki/Akt/PKB_signaling_pathway#/media/File:Akt_Phosphorylation_Substrates_Affecting_Apoptosis.png (Accessed 3 February 2018).

- Tang, K. L. Tang, H. Y. Du, Y. Tian, T. and Xiong, S. J. (2019) PAR-2 promotes cell proliferation, migration, and invasion through activating PI3K/AKT signaling pathway in oral squamous cell carcinoma. *Bioscience reports* 39(7), BSR20182476.
- Tesselaar, M.E. Romijn, F.P. van der Linden, I.K. Bertina, R.M. and Osanto S. (2009) Microparticle-associated tissue factor activity in cancer patients with and without thrombosis. *Journal of Thrombosis and Haemostasis* 7(8): 1421-3.
- Thaler, J. Ay, C. Mackman, N. Bertina, R. M. Kaider, A. Marosi, C. Key, N. S. Barcel, D. A. Scheithauer, W. Kornek, G. Zielinski, C and Pabinger, I. (2012) Microparticle-associated tissue factor activity, venous thromboembolism and mortality in pancreatic, gastric, colorectal and brain cancer patients. *Journal of Thrombosis and Haemostasis* 10(7), 1363-1370.
- Thomas, M. Glaunsinger, B. Pim, D. Javier, R. and Banks, L. (2001) HPV E6 and MAGUK protein interactions: determination of the molecular basis for specific protein recognition and degradation. *Oncogene* 20(39), 5431-5439.
- Thomas, M. Laura, R. Hepner, K. Guccione, E. Sawyers, C. Lasky, L. and Banks L. (2002) Oncogenic human papillomavirus E6 proteins target the MAGI-2 and MAGI-3 proteins for degradation. *Oncogene* 21(33), 5088-96.
- Thorpe, L. M. Yuzugullu, H. and Zhao, J. J. (2015) PI3K in cancer: divergent roles of isoforms, modes of activation, and therapeutic targeting. *Nature Reviews Cancer* 15(1): 724.
- Tibarewal, P. Zilidis, G. Spinelli, L. Schurch, N. Maccario, H. Gray, A. Perera, N.M. Davidson, L. Barton, G.J. and Leslie, N.R. (2012) PTEN protein phosphatase activity correlates with control of gene expression and invasion, a tumor-suppressing phenotype, but not with AKT activity. *Science Signaling* 5(213), ra18.
- Tolkacheva, T. Boddapati, M. Sanfiz, A. Tsuchida, K. Kimmelman, A.C. and Chan, A.M. (2001) Regulation of PTEN binding to MAGI-2 by two putative phosphorylation sites at threonine 382 and 383. *Cancer Research* 61(13), 4985-4989.
- Torres, J. Rodriguez, J. Myers, M.P. Valiente, M. Graves, J.D. Tonks, N.K. and Pulido, R. (2003) Phosphorylation-regulated cleavage of the tumor suppressor PTEN by caspase-3: implications for the control of protein stability and PTEN-protein interactions. *Journal of Biological Chemistry* 278(33), 30652-60.
- Toschi, V. (2011) Blood-born tissue factor in cardiovascular disease: where are we now? *Internal and Emergency Medicine* 6 (1), 3-5.
- Toyoshima, F. Matsumura, S. Morimoto, H. Mitsushima, M. and Nishida, E. (2007) PtdIns(3,4,5)P3 regulates spindle orientation in adherent cells. *Developmental Cell* 13, 796-811.
- Trotman, L. C. Wang, X. Alimonti, A. Chen, Z. Teruya-Feldstein, J. Yang, H. and Pandolfi, P. P. (2007) Ubiquitination regulates PTEN nuclear import and tumor suppression. *Cell* 128(1): 141-156.

- Ueno, T. Toi, M. Koike, M. Nakamura, S. and Tominaga, T. (2000) Tissue factor expression in breast cancer tissues: its correlation with prognosis and plasma concentration. *British Journal of Cancer* 83(2): 164-170.
- Unruh, D. and Horbinski, C. (2020) Beyond thrombosis: the impact of tissue factor signaling in cancer. *Journal of Hematology & Oncology* 13, 93.
- Uren, R.T. Iyer, S. and Kluck, R.M. (2017) Pore formation by dimeric Bak and Bax: an unusual pore? *Philosophical transactions of the Royal Society of London. Series B, Biological sciences* 372(1726), 20160218.
- Van den Berg, Y. W. Osanto, S. Reitsma, P. H. and Versteeg, H. H. (2012). The relationship between tissue factor and cancer progression: insights from bench and bedside. *Blood* 119 (4), 924-932.
- Vanhaesebroeck, B. Guillermet-Guibert, J. Graupera, M. and Bilanges, B. (2010) The emerging mechanisms of isoform-specific PI3K signalling. *Nature Reviews Molecular Cell Biology* 11 (5), 329-41.
- Vazquez, F. Ramaswamy, S. Nakamura, N. and Sellers, W. R. (2000) Phosphorylation of the PTEN Tail Regulates Protein Stability and Function. *Molecular and Cellular Biology* 20(14): 5010–5018.
- Verhagen, P.C. van Duijn, P.W. Hermans, K.G. Looijenga, L.H. van Gorp, R.J. Stoop, H. van der Kwast, T.H. and Trapman, J. (2006) The PTEN gene in locally progressive prostate cancer is preferentially inactivated by bi-allelic gene deletion. *The Journal of Pathology* 208 (5), 699-707.
- Versteeg, H.H. Hoedemaeker, I. Diks, S.H. Stam, J.C. Spaargaren, M. van Bergen En Henegouwen, P.M. van Deventer, S.J. and Peppelenbosch, M.P. (2000) Factor VIIa/tissue factor-induced signaling via activation of Src-like kinases, phosphatidylinositol 3-kinase, and Rac. *Journal of Biological Chemistry* 275, 28750-28756.
- Versteeg, H.H. Schaffner, F. Kerver, M. Petersen, H.H. Ahamed, J. Felding-Habermann, B. Takada, Y. Mueller, B.M. and Ruf, W. (2008) Inhibition of tissue factor signaling suppresses tumor growth. *Blood* 111(1), 190-9.
- Versteeg, H. H. Spek, C. A. Peppelenbosch, M. P. and Richel, D. J. (2004) Tissue Factor and Cancer Metastasis: The Role of Intracellular and Extracellular Signaling Pathways. *Molecular Medicine* 10 (1-6), 6–11.
- Vrana, J. A. Stang, M. T. Grande, J. P. and Getz, M. J. (1995) Expression of tissue factor in tumor stroma correlates with progression to invasive human breast cancer: paracrine regulation by carcinoma cell-derived members of the transforming growth factor beta family. *Cancer Research* 56 (21), 5063-70.
- Wang, J. Zhu, H.H. Chu, M. Liu, Y. Zhang, C. Liu, G. Yang, X. Yang, R. and Gao, W.Q. (2014) Symmetrical and asymmetrical division analysis provides evidence for a hierarchy of prostate epithelial cell lineages *Nature Communications* 5, 4758.

- Wang, P. and DeFea, K.A. (2006) Protease-activated receptor-2 simultaneously directs beta-arrestin-1-dependent inhibition and G α q-dependent activation of phosphatidylinositol 3-kinase. *Biochemistry* 45(31), 9374-85.
- Wang, X. Trotman, L. C. Koppie, T. Alimonti, A. Chen, Z. Gao, Z. Wang, J. Erdjument-Bromage, H. Tempst, P. Cordon-Cardo, C. Pandolfi, P. P. and Jiang, X. (2007) NEDD4-1 is a proto-oncogenic ubiquitin ligase for PTEN. *Cell* 128(1), 129-139.
- Wang, X. Wang, E. Kavanagh, J. J. and Freedman, R. S. (2005) Ovarian cancer, the coagulation pathway, and inflammation. *Journal of translational medicine* 3, 25.
- Wegmann, F. Ebnet, K. Du Pasquier, L. Vestweber, D. and Butz, S. (2004) Endothelial adhesion molecule ESAM binds directly to the multidomain adaptor MAGI-1 and recruits it to cell contacts. *Experimental Cell Research* 300(1),121-33.
- Weng, Z. Shang, Y. Ji, Z. Ye, F. Lin, L. Zhang, R. and Zhu, J. (2018) Structural Basis of Highly Specific Interaction between Nephrin and MAGI1 in Slit Diaphragm Assembly and Signaling. *Journal of the American Society of Nephrology* 29(9), 2362-2371.
- Winter, M.C. Shasby, S.S. Ries, D.R. and Shasby, D.M. (2006) PAR2 activation interrupts E-cadherin adhesion and compromises the airway epithelial barrier: protective effect of beta-agonists. *The American Journal of Physiology-Lung Cellular and Molecular Physiology*. 291, L628–35.
- Wojtukiewicz, M. Sierko, S. Zimnoch, L. Thorpe, P. Brekken, R.A. and Kisiel, W. (2005) Expression of Vascular Endothelial Growth Factor (VEGF) Associated with Its Receptor (VEGFR) in Relation to Tissue Factor (TF) in Human Breast Cancer Tissue. *Blood* 2106 (11), 4024.
- Wolberg, A.S. Kon, R.H. Monroe, D.M. Ezban, M. Roberts, H.R. and Hoffman, M. (2000) Deencryption of cellular tissue factor is independent of its cytoplasmic domain. *Biochemical and Biophysical Research Communications* 272, 332-6.
- Wu, B. Zhou, H. Hu, L. Mu, Y. and Wu Y. (2013) Involvement of PKC α activation in TF/VIIa/PAR2-induced proliferation, migration, and survival of colon cancer cell SW620. *Tumour Biology* 34(2), 837-846.
- Wu, J. Xie, N. Zhao, X. Nice, E.C. and Huang, C. (2012) Dissection of aberrant GPCR signaling in tumorigenesis a systems biology approach. *Cancer Genomics Proteomics*. 9(1), 37-50.
- Wu, X. Hepner, K. Castelino-Prabhu, S. Do, D. Kaye, M.B. Yuan, X.J. Wood, J. Ross, C. Sawyers, C.L. and Whang, Y.E. (2000) Evidence for regulation of the PTEN tumor suppressor by a membrane-localized multi-PDZ domain containing scaffold protein MAGI-2. *Proceedings of the National Academy of Sciences* 97 (8), 4233-8.
- Wu, Y. Dowbenko, D. Spencer, S. Laura, R. Lee, J. Gu, Q. and Lasky, L.A. (2000) Interaction of the tumor suppressor PTEN/MMAC with a PDZ domain of MAGI3, a novel membrane-associated guanylate kinase. *Journal of Biological Chemistry* 275 (28), 21477-85.

Xu, J. Paquet, M. Lau, A.G. Wood, J.D. Ross, C.A. and Hall, R.A. (2001) beta 1-adrenergic receptor association with the synaptic scaffolding protein membrane-associated guanylate kinase inverted-2 (MAGI-2). Differential regulation of receptor internalization by MAGI-2 and PSD-95. *The Journal of Biological Chemistry* 276(44), 41310-7.

Xu, W. Yang, Z. Zhou, S.F. and Lu, N. (2014) Posttranslational regulation of phosphatase and tensin homolog (PTEN) and its functional impact on cancer behaviors. *Drug Design, Development and Therapy* 8: 1745-51.

Yanagawa, N. Leduc, C. Kohler, D. Saieg, M.A. John, T. Sykes, J. Yoshimoto, M. Pintilie, M. Squire, J. Shepherd, F.A. and Ming-Sound, T. (2012) Loss of phosphatase and tensin homolog protein expression is an independent poor prognostic marker in lung adenocarcinoma. *Journal of Thoracic Oncology* 7, 1513-1521.

Yang, L. and Karin, M. (2014) Roles of tumor suppressors in regulating tumor-associated inflammation. *Cell death and differentiation*, 21(11), 1677-1686.

Yang, X. Zheng, J. Xiong, Y. Shen, H. Sun, L. Huang, Y. Sun, C. Li, Y. and He, J. (2010) Beta-2 adrenergic receptor mediated ERK activation is regulated by interaction with MAGI-3. *FEBS Letters* 584(11), 2207-12.

Yang, Y. Lee, M. and Fairn, G. D. (2018). Phospholipid subcellular localization and dynamics. *The Journal of biological chemistry* 293(17), 6230-6240.

Yang, Z. Xie, C. Xu, W. Liu, G. Cao, X. Li, W., Chen, J. Zhu, Y. Luo, S. Luo, Z and Lu, N. (2015) Phosphorylation and inactivation of PTEN at residues Ser380/Thr382/383 induced by *Helicobacter pylori* promotes gastric epithelial cell survival through PI3K/Akt pathway. *Oncotarget* 6(31), 31916–31926.

Yang, Z. Yuan, X.G. Chen, J. Luo, S.W. Luo, Z.J. and Lu, N.H. (2013) Reduced expression of PTEN and increased PTEN phosphorylation at residue Ser380 in gastric cancer tissues: a novel mechanism of PTEN inactivation. *Clinics and Research in Hepatology and Gastroenterology* 37(1), 72-9.

Yau, J. W. Teoh, H. and Verma, S. (2015) Endothelial cell control of thrombosis. *BMC Cardiovascular Disorders* 15, 130.

Ye, F. and Zhang, M. (2013) Structures and target recognition modes of PDZ domains: recurring themes and emerging pictures. *The Biochemical Journal* 455(1), 1-14.

Yehia, L. and Eng, C. (2018) 65 YEARS OF THE DOUBLE HELIX: One gene, many endocrine and metabolic syndromes: PTEN-opathies and precision medicine. *Endocrine-Related Cancer*, 25(8).

Yim, E.K. Peng, G. Dai, H. Hu, R.Z. Li, K.Y. Lu, W. Mills, G.B. MericBernstam, F. Hennessy, B.T. Craven, R.J. and Lin, S.Y. (2009) Rak functions as a tumor suppressor by regulating pten protein stability and function. *Cancer Cell* 15 (4), 304-14.

Yin, Y. and Shen, W.H. (2008) PTEN: a new guardian of the genome. *Oncogene* 27, 5443-5453.

- Yoneyama, K. Ishibashi, O. Kawase, R. Kurose, K. and Takeshita, T. (2015) miR-200a, miR-200b and miR-429 are onco-miRs that target the PTEN gene in endometrioid endometrial carcinoma. *Anticancer Research* 35 (3), 1401-10.
- Yu, J.L. May, L. Lhotak, V. Shahrzad, S. Shirasawa, S. Weitz, J.I. Coomber, B.L. Mackman, N. and Rak, J.W. (2005) Oncogenic events regulate tissue factor expression in colorectal cancer cells: implications for tumor progression and angiogenesis. *Blood* 105 (4), 1734-41.
- Yu, M. Liu, W. Li, J. Lu, J. Lu, H. Jia, W. and Liu, F. (2020) Exosomes derived from atorvastatin-pretreated MSC accelerate diabetic wound repair by enhancing angiogenesis via AKT/eNOS pathway. *Stem Cell Research and Therapy* 11(1), 350.
- Yu, Y. Li, S. Wang, K. and Wan, X. (2019) A PDZ Protein MDA-9/Syntenin: As a Target for Cancer Therapy. *Computational and structural biotechnology journal* 17, 136-141.
- Yuan, L. Lv, Y. Li, H. Gao, H. Song, S. Zhang, Y. Xing, G. Kong, X. Wang, L. Li, Y. Zhou, T. Gao, D. Xiao, Z.X. Yin, Y. Wei, W. He, F. and Zhang L. (2015) Deubiquitylase OTUD3 regulates PTEN stability and suppresses tumorigenesis. *Nature Cell Biology* 17(9), 1169-81.
- Zaessinger, S. Zhou, Y. Bray, S. J. Tapon, N. and Djiane, A. (2015) Drosophila MAGI interacts with RASSF8 to regulate E-Cadherin-based adherens junctions in the developing eye. *Development* 142(6), 1102-1112.
- Zaric, J. Joseph, J.M. Tercier, S. Sengstag, T. Ponsonnet, L. Delorenzi, M. and Rüegg, C. (2012) Identification of MAGI1 as a tumor-suppressor protein induced by cyclooxygenase-2 inhibitors in colorectal cancer cells. *Oncogene* 31(1), 48-59.
- Zeller, K.S. (2012) integrin signalling in cell adhesion and mechanotransduction: regulation of PI3K, AKT and ROS. *Acta Universitatis Upsaliensis. Faculty of Medicine* 750, 46.
- Zhang, E. Gao, B. Yang, L. Wu, X. and Wang Z. (2016) Notoginsenoside Ft1 Promotes Fibroblast Proliferation via PI3K/Akt/mTOR Signaling Pathway and Benefits Wound Healing in Genetically Diabetic Mice. *Journal of Pharmacology and Experimental Therapeutics* 356(2), 324-332.
- Zhang, G. and Wang, Z. (2011) MAGI1 inhibits cancer cell migration and invasion of hepatocellular carcinoma via regulating PTEN. *Zhong Nan Da Xue Xue Bao Yi Xue Ban* 36(5), 381-5.
- Zhang, H. Wang, D. Sun, H. Hall, R. A. and Yun, C. C. (2007) MAGI-3 regulates LPA-induced activation of Erk and RhoA. *Cellular signalling* 19(2), 261-268.
- Zhang, J. Ding, J. Zhang, X. Shao, X. and Hao, Z. (2005) Regulation of vascular endothelial growth factor (VEGF) production and angiogenesis by tissue Factor (TF) in SGC-7901 gastric cancer cells. *Cancer Biology & Therapy* 4(7), 769-72.
- Zhang, X. C. Piccini, A. Myers, M. P. Van Aelst, L. and Tonks, N. K. (2012) Functional analysis of the protein phosphatase activity of PTEN. *Biochemical Journal*, 444 (3), 457-464.
- Zhang, X. Tang, N. Hadden, T.J. and Rishi, A.K. (2011) Akt, FoxO and regulation of apoptosis. *Biochimica et Biophysica Acta* 1813(11), 1978-86.

- Zhang, Y. Liu, N.M. Wang, Y. Youn, J.Y. and Cai, H. (2017) Endothelial cell calpain as a critical modulator of angiogenesis. *Biochimica et Biophysica Acta* 1863(6), 1326-1335.
- Zhao, M. (2007) PTEN: a promising pharmacological target to enhance epithelial wound healing. *British Journal of Pharmacology* 152(8), 1141-4.
- Zhao, P. Lieu, T. Barlow, N. Sostegni, S. Haerteis, S. Korbmacher, C. Liedtke, W. Jimenez-Vargas, N. N. Vanner, S. J. and Bunnett, N. W. (2015) Neutrophil Elastase Activates Protease-activated Receptor-2 (PAR2) and Transient Receptor Potential Vanilloid 4 (TRPV4) to Cause Inflammation and Pain. *The Journal of biological chemistry* 290(22), 13875-13887.
- Zhou, B.1. Zhou, H. Ling, S. Guo, D. Yan, Y. Zhou, F. and Wu, Y. (2011) Activation of PAR2 or/and TLR4 promotes SW620 cell proliferation and migration via phosphorylation of ERK1/2. *Oncology Reports* 25(2), 503-11.
- Zhu, J. Shang, Y. Chen, J. and Zhang, M. (2012) Structure and function of the guanylate kinase-like domain of the MAGUK family scaffold proteins. *Frontiers in Biology* 7(5), 379-396.
- Zhu, J. Shang, Y. Xia, C. Wang, W. Wen, W. and Zhang, M. (2011) Guanylate kinase domains of the MAGUK family scaffold proteins as specific phospho-protein-binding modules. *The EMBO journal* 30(24), 4986-4997.
- Zhu, J. Shang, Y. and Zhang, M. (2016) Mechanistic basis of MAGUK-organized complexes in synaptic development and signalling. *Nature Reviews Neuroscience* 17:209-223.
- Zihni, C. Mills, C. Matter, K. and Balda, M. S. (2016) Tight junctions: from simple barriers to multifunctional molecular gates. *Nature reviews Molecular cell biology* 17(9), 564-580.
- Zioncheck, T.F. Roy, S. and Vehar, G.A. (1992) The cytoplasmic domain of tissue factor is phosphorylated by a protein kinase C-dependent mechanism. *Journal of Biological Chemistry* 267(6):3561-3564.
- Zmajkovicova, K. Jesenberger, V. Catalanotti, F. Baumgartner, C. Reyes, G. and Baccarini, M. (2013) MEK1 is required for PTEN membrane recruitment, AKT regulation, and the maintenance of peripheral tolerance. *Molecular cell* 50(1), 43-55.
- Zwicker, J.I. Trenor, C.C. Furie, B.C. and Furie, B. (2011) Tissue factor-bearing microparticles and thrombus formation. *Arteriosclerosis, Thrombosis, and Vascular Biology* 31 (4), 728-33.